STALL FLUTTER OF GRAPHITE/EPOXY WINGS
WITH BENDING-TORSION COUPLING

by

PETER EARL DUNN

B.S., Massachusetts Institute of Technology
(1985)

SUBMITTED TO THE DEPARTMENT OF
AERONAUTICS AND ASTRONAUTICS
IN PARTIAL FULFILLMENT OF THE
REQUIREMENTS FOR THE DEGREE OF

MASTER OF SCIENCE
IN AERONAUTICS AND ASTRONAUTICS

at the

MASSACHUSETTS INSTITUTE OF TECHNOLOGY
May 1989

© Massachusetts Institute of Technology 1989

Signature of Author_____
Department of Aeronautics and Astronautics
May 4, 1989

Certified by_____
Professor John Dugundji
Thesis Supervisor

Accepted by_____
Professor Harold Y. Wachman
Chairman, Departmental Committee on Graduate Students
Department of Aeronautics and Astronautics

To my parents

and

to my angels: Dés, Clára, Tasha, Alison, and Mimi.

STALL FLUTTER OF GRAPHITE/EPOXY WINGS
WITH BENDING-TORSION COUPLING

by

PETER EARL DUNN

Submitted to the Department of Aeronautics and Astronautics on May 4, 1989, in partial fulfillment of the requirements for the degree of Master of Science in Aeronautics and Astronautics.

ABSTRACT

The nonlinear, stalled, aeroelastic behavior of rectangular, graphite/epoxy, cantilevered plates with varying amount of bending-torsion stiffness coupling and with NACA-0012 styrofoam airfoil shapes is investigated for low Reynold's number flow (<200,000). A general, 5-mode Rayleigh-Ritz formulation is used to calculate point load static deflections, and static vibration frequencies and mode shapes. Nonlinear, lift and moment aerodynamics are used in the context of the Rayleigh-Ritz formulation to calculate static airload deflections. The nonlinear, stalled ONERA model initially developed by Tran & Petot is compared against experimental, low Reynold's number, 2-dimensional lift and moment hysteresis loops. Low angle of attack, linear flutter calculations are done using the U-g method. Nonlinear flutter calculations are done by applying Fourier analysis to extract the harmonics from the ONERA-calculated, 3-dimensional aerodynamics, then applying a harmonic balance method and a Newton-Raphson solver to the resulting nonlinear, Rayleigh-Ritz aeroelastic formulation.

Test wings were constructed and subjected to static, vibration, and wind tunnel tests. Static tests indicated good agreement between theory and experiment for bending and torsion stiffnesses. Vibrations tests indicated good agreement between theory and experiment for bending and torsion frequencies and mode shapes. 2-dimensional application of the ONERA model indicated good agreement with experimental lift hysteresis loops, but poor agreement with experimental moment hysteresis loops. Wind tunnel tests showed good agreement between theory and experiment for static deflections, for linear flutter and divergence, and for stalled, nonlinear, bending and torsion flutter limit cycles. The current nonlinear analysis shows a transition from divergence to stalled bending flutter, which linear analyses are unable to predict.

Thesis Supervisor: John Dugundji

Title: Professor of Aeronautics and Astronautics

ACKNOWLEDGEMENTS

First and foremost I would like to thank Professor John Dugundji for his guidance, wisdom, and patience - for always helping to see the "big picture" when short-sighted solutions seemed the most convenient problem solvers.

Special thanks to my undergraduate helpers, Christine Chen, Darrin Tebon, Ali Zandieh, and Chakko Kovoor for tireless work in accumulating and reducing experimental data; to Al Supple and Carl Varnerin for help in manufacturing and instrumenting the test specimens; to Don Weiner and Earl Wassmouth for help in assembling the test setup; to Al Shaw for never-ending aid in all phases of wind tunnel testing; to Professor Paul Lagace and Ping Lee for taking care of all the bureaucratic details and for nudging me to completion.

I would also like to thank all those invaluable people who helped with always-welcome suggestions for my analysis: the past and present TELAC denizens of 41-219c and 41-317 who are too numerous to list here; the "Spinheads" of Friday afternoon rotor lunches, in particular Eric Ducharme, Kenneth Hall, and Professor Ed Crawley; and my roomates Cathy Mavriplis, Earl Renaud, Wolfgang, and Aga Goodsell who also provided support and respite during the tougher times.

Lastly I would like to acknowledge those who provided the incentive to keep the fires burning: to Mom and Dad who supported all my decisions without question or qualm - thanks for that first Sopwith Camel; to Dés, David, Mihir, *et al* - this work will forever be referred to as the "Tweety Bird" method; to *The Tech* for providing an escape from classwork; and to Michelle Perry for being a good friend in trying times.

TABLE OF CONTENTS

LIST OF TABLES

LIST OF FIGURES

LIST OF SYMBOLS

a_{ij} coefficients of polynomial series for i-th region of the aerodynamic force curve

a_{oz} linear slope of the general aerodynamic force coefficient $\equiv dC_{z\ell}/d\alpha$

$a_{oL},\ a_{oM}$ linear slopes of lift and moment coefficient curves

A   wing area

[A]   matrix of combined mass and complex aerodynamic components used in linear U-g flutter method

A_{ij} components of combined complex mass-aerodynamic matrix used in linear U-g flutter method

AR   aspect ratio $\equiv 2\ell/c$

b   semi-chord $\equiv c/2$

b_{im} power series summation in Fourier analysis of the nonlinear aerodynamics, defined by equation (2-51)

B_{ij} coefficients of i-th torsional mode shape

c   chord length

C(k)   Theodorsen function

$C_D,\ C_L,\ C_M$ drag, lift, and moment coefficients

C_{D_o} profile drag coefficient

$C_{L\alpha}$ slope of linear lift coefficient $\equiv dC_{L\ell}/d\alpha$

C_{L2D} 2-dimensional lift coefficient

C_{L3D} 3-dimensional lift coefficient

C_{M2D} 2-dimensional moment coefficient

C_{M3D} 3-dimensional moment coefficient

C_z general aerodynamic force coefficient

$C_{z\ell}$ static, linear component of general aero-dynamic force coefficient

C_{zs} static general aerodynamic force coefficient

C_{z1} total linear contribution to the general aerodynamic force coefficient

C_{z2} nonlinear contribution to the general aerodynamic force coefficient

$C_{z\gamma}$ linear, circulatory contribution to the general aerodynamic force coefficient

C_{zo}, C_{zs}, C_{zc} mean, sine, and cosine components of the general aerodynamic force coefficient

C_{z1o}, C_{z1s}, C_{z1c} mean, sine, and cosine components of the total linear contribution to the general aerodynamic force coefficient

C_{z2o}, C_{z2s}, C_{z2c} mean, sine, and cosine components of the non-linear contribution to the general aerodynamic force coefficient

$C_{z\gamma o}$, $C_{z\gamma s}$, $C_{z\gamma c}$ mean, sine, and cosine components of the linear, circulatory contribution to the general aerodynamic force coefficient

d	damping coefficient of ONERA non-linear aerodynamic differential equation (2-27d)
D_{ij}	flexural modulus components
e	phase lag of ONERA non-linear aerodynamic differential equation (2-27d)
e	eccentricity of center of pressure from elastic axis
E_L	longitudinal modulus
E_T	transverse modulus
f	residual vector in Newton-Raphson scheme
f, f_1, f_2	cosh and sinh parameters of torsional mode shapes
$F(k)$	real part of Theodorsen function
g	structural damping used in linear U-g flutter method
g, g_1, g_2	cosine and sine parameters of torsional mode shapes
G_{LT}	shear modulus
GJ	single-mode torsional stiffness
$G(k)$	imaginary part of Theodorsen function
h	1/4-chord tip deflection
$\bar{h}$	non-dimensional 1/4-chord deflection
$\bar{h}_o$, $\bar{h}_s$, $\bar{h}_c$	mean, sine, and cosine components of the non-dimensional 1/4-chord deflection

I_1, I_2	modulus invariants
I_{11}, I_{12}, I_{22}	mode shape integrals corrected for spanwise effects, used in linear U-g flutter method
I_{im}	sinusoidal integrals in Fourier analysis of the nonlinear aerodynamics, defined by equation (2-52)
J_i	maximum power of the polynomial series for the i-th region of the aerodynamic force curve
k	reduced frequency $\equiv \omega b/U$
k_{vz}	second apparent mass coefficient
k_{vL}, k_{vM}	lift and moment second apparent mass coefficients
$[K]$	stiffness matrix
K_1, K_2, K_3, K_4	intermediate variables of the harmonic balance approximation applied to the non-linear ONERA differential equation
K_{ij}	components of the stiffness matrix
K_{ij}^s	styrofoam contribution to the components of the stiffness matrix
K_{22}^L, K_{22}^C	linear and cubic coefficients of the 1st torsional stiffness component
ℓ	semi-span, laminate length
L_1, L_2, L_3, L_4	components of complex lift used in linear U-g flutter method

L_s, L_c intermediate variables of the harmonic balance approximation applied to the ONERA linear differential equation

m mass per unit area

$[M]$ mass matrix

M_1, M_2, M_3, M_4 components of complex moment used in linear U-g flutter method

M_{ij} components of the mass matrix

M_{ij}^s styrofoam contribution to the components of the mass matrix

n number of mode shapes

q_i i-th modal amplitude

q_{io}, q_{is}, q_{ic} mean, sine, and cosine components of the i-th modal amplitude

$\{q_o\}$, $\{q_s\}$, $\{q_c\}$ vectors of the means, sines, and cosines of the modal amplitudes

$\tilde{q}$ frequency domain modal amplitude, used for free vibration analysis and linear flutter analysis

$\tilde{Q}$ non-dimensional dynamic pressure

Q_i i-th modal force

Q_{io}, Q_{is}, Q_{ic} mean, sine, and cosine components of the i-th modal force

$\{Q_o\}$, $\{Q_s\}$, $\{Q_c\}$ vectors of the means, sines, and cosines of the modal forces

Q_{ij} unidirectional modulus components

$Q_{ij}^{(\theta)}$	rotated modulus components
R_1, R_2	modulus invariants
s_z	first apparent mass coefficient
s_L, s_M	lift and moment first apparent mass coefficients
t	real time
$t_{G/E}$	thickness of graphite/epoxy plate
t_{max}	maximum thickness of styrofoam NACA airfoil shape
T	kinetic energy
U	free stream velocity
V	strain energy
w	out-of-plane deflection
w	undamped, non-dimensional frequency of ONERA nonlinear equation (2-27d)
x	spanwise cartesian coordinate
$\mathbf{x}$	state vector in Newton-Raphson scheme
x_s	spanwise location that first experiences stall
y	chordwise cartesian coordinate
z	out-of-plane cartesian coordinate
z_k	distance from mid-plane to upper surface of k-th ply

z	complex eigenvalue of linear U-g flutter equation
α	effective angle of attack
α_o, α_s, α_c	mean, sine, and cosine components of the effective angle of attack
α_c	angle of attack corrected for 3-dimensional finite span effects
α_i	angle delineating the beginning of the i-th polynomial region of the approximation to the aerodynamic force curve
α_L, α_M	lift and moment phase lags of ONERA linear aerodynamic differential equation
α_R	root angle of attack, same as θ_R
α_v	oscillatory amplitude of the effective angle of attack $\equiv \sqrt{\alpha_s^2 + \alpha_c^2}$
α_z	phase lag of the ONERA linear aerodynamic differential equation (2-27c)
α_1, α_2	sinh and sine coefficients of the 1st and 2nd beam bending mode shapes
α_Δ	stall angle for single break point model
β	non-dimensional bending-torsion stiffness ratio
γ_i	i-th mode shape
ΔC_z	deviation of the non-linear aerodynamic force curve from the linear approximation

ΔC_{zo}, ΔC_{zs}, ΔC_{zc} mean, sine, and cosine components of the deviation of the non-linear aerodynamic force curve from the linear approximation

ΔC_{zv} oscillatory amplitude of the deviation of the non-linear aerodynamic force curve from the linear approximation $\equiv \sqrt{\Delta C_{zs}^2 + \Delta C_{zc}^2}$

ε_1, ε_2 parameters of 1st and 2nd beam bending mode shapes

θ ply angle referenced to free stream

θ instantaneous angle of attack

θ_o, θ_s, θ_c mean, sine, and cosine components of the instantaneous angle of attack

θ_R root angle of attack, same as α_R

λ_z lag of ONERA linear aerodynamic differential equation (2-27c)

λ_L, λ_M lift and moment lags of ONERA linear aerodynamic differential equation

ν_{LT} Poisson's ratio

ξ phase of effective angle of attack $\equiv \sin^{-1}(\alpha_c/\alpha_v)$

ρ free stream density

ρ_S styrofoam density

σ_z linear phase lag used in equation (2-27c)

σ_z, σ_z lift and moment linear phase lags

τ non-dimensional time $\equiv Ut/b$

ϕ_i spanwise variation of i-th mode shape

ψ_i chordwise variation of i-th mode shape

ω real frequency

φ_i non-dimensional phase delineating the beginning of the i-th polynomial region of the approximation to the aerodynamic force curve

CHAPTER I
INTRODUCTION

The development and ever increasing use of advanced composite materials in the aeronautics field lends another dimension to the aircraft designer's list of design tools. In designing for desired aeroelastic response - most often maximization of flutter and divergence speeds - the aircraft designer's ability to control the anisotropy of advanced composite materials through selective lamination makes these materials attractive for aeroelastic tailoring.

The present research is part of a continuing investigation into the aeroelastic flutter and divergence behavior of forward-swept, graphite/epoxy composite wing aircraft. The specific objectives of the current investigation are to investigate experimentally and analytically, the roles of nonlinear structures and nonlinear aerodynamics in large amplitude, high angle-of-attack stall flutter of aeroelastically tailored wings.

In previous investigations at the Technology Laboratory for Advanced Composites (TELAC) at MIT, the aeroelastic flutter and divergence behavior of cantilevered, unswept and swept, graphite/epoxy wings was investigated in a small, low-speed wind tunnel. The wings were six-ply, graphite/epoxy plates with strong bending-torsion coupling. Experiments were conducted to determine the flutter boundaries of these wings both at low and high angles of attack, stall flutter often

being observed in the latter. The divergence and flutter results at low angles of attack correlated well with linear, unsteady theory, indicating some beneficial effects of ply orientation in aeroelastic behavior [Refs. 1, 2, and 3]. Steady, nonlinear aerodynamics correlated reasonably before the onset of flutter, but no unsteady, nonlinear flutter analyses were attempted for higher root angles of attack.

Recently, Tran & Petot [Ref. 5] and Dat & Tran [Ref. 6] of *Office National d'Etudes et de Recherches Aerospatiales* have developed a semi-empirical, unsteady, nonlinear model (called the ONERA model) for determining 2-dimensional aerodynamic forces on an airfoil oscillating in pitch only, which experiences dynamic stall. This model incorporates a single lag term operating on the linear part of the airfoil's static force curve, thus analogous to the Theodorsen function for linear, flat-plate theory, and a two lag term operating on the nonlinear (i.e. stalling) part of the airfoil's static force curve. The semi-empirical coefficients of the nonlinear aerodynamics for the ONERA model were determined for various airfoils and the model, using a numerical time-marching scheme, applied as comparison against experiment by Dat, Tran, and Petot. Further analysis of the model was done by Peters [Ref. 11] to differentiate the roles of angle-of-attack due to pitching (θ) and effective angle-of-attack due to plunging ($\dot{h}/U$), and by Petot & Dat [Ref. 12] to reformulate the differential force equations so that they reduce to the Theodorsen function in the case of a flat plate in the

linear domain. In addition, Petot & Loiseau [Ref. 13] have contributed corrections to the ONERA model for low Reynold's number flows, in the regime of the current investigation. Generally, however, little work has been done in implementing the ONERA model in a nonlinear, aeroelastic flutter analysis.

The ultimate objectives of the current investigation were to develop an analytic aeroelastic model, using the ONERA model as the basis for the aerodynamics, to predict characteristics of 3-dimensional, stalled, flutter limit cycles, while concurrently developing an experimental base of both small amplitude and large amplitude flutter data for a variety of composite laminate wings with a wide range of bending-torsion characteristics. To reach these analytic and experimental objectives, intermediate goals were to conduct experimental static tests, vibration tests, static aeroelastic tests, and linear, small-amplitude flutter tests, and to accurately predict the results of these tests using those portions of the final analytic model which were applicable to each.

CHAPTER II

THEORY

2.1 Anisotropic Plate Flexural Stiffness

The flexural modulus components of a laminated, graphite/epoxy plate depends on both the fiber orientations and stacking sequence of the individual plies. Only laminated plates with mid-plane symmetric stacking sequences were constructed in this study. The ply angles (θ) follow the sign convention in Figure 1.

The in-plane, unidirectional modulus components (Q_{ij}) were obtained from the orthotropic engineering constants for Hercules AS4/3501-6 graphite/epoxy, from which the test specimens were fabricated. These engineering constants take on different values depending on whether they are obtained from out-of-plane bending or in-plane stretching tests. Engineering constants obtained from each type of test appear in Appendix A. The Q_{ij} terms are defined in terms of the engineering constants as,

$$Q_{11} = \frac{E_L}{1 - \nu_{LT}\nu_{TL}} \tag{2-1a}$$

$$Q_{22} = \frac{E_T}{1 - \nu_{LT}\nu_{TL}} \tag{2-1b}$$

$$Q_{12} = Q_{21} = \frac{\nu_{LT}E_T}{1 - \nu_{LT}\nu_{TL}} \tag{2-1c}$$

$$Q_{66} = G_{LT} \tag{2-1d}$$
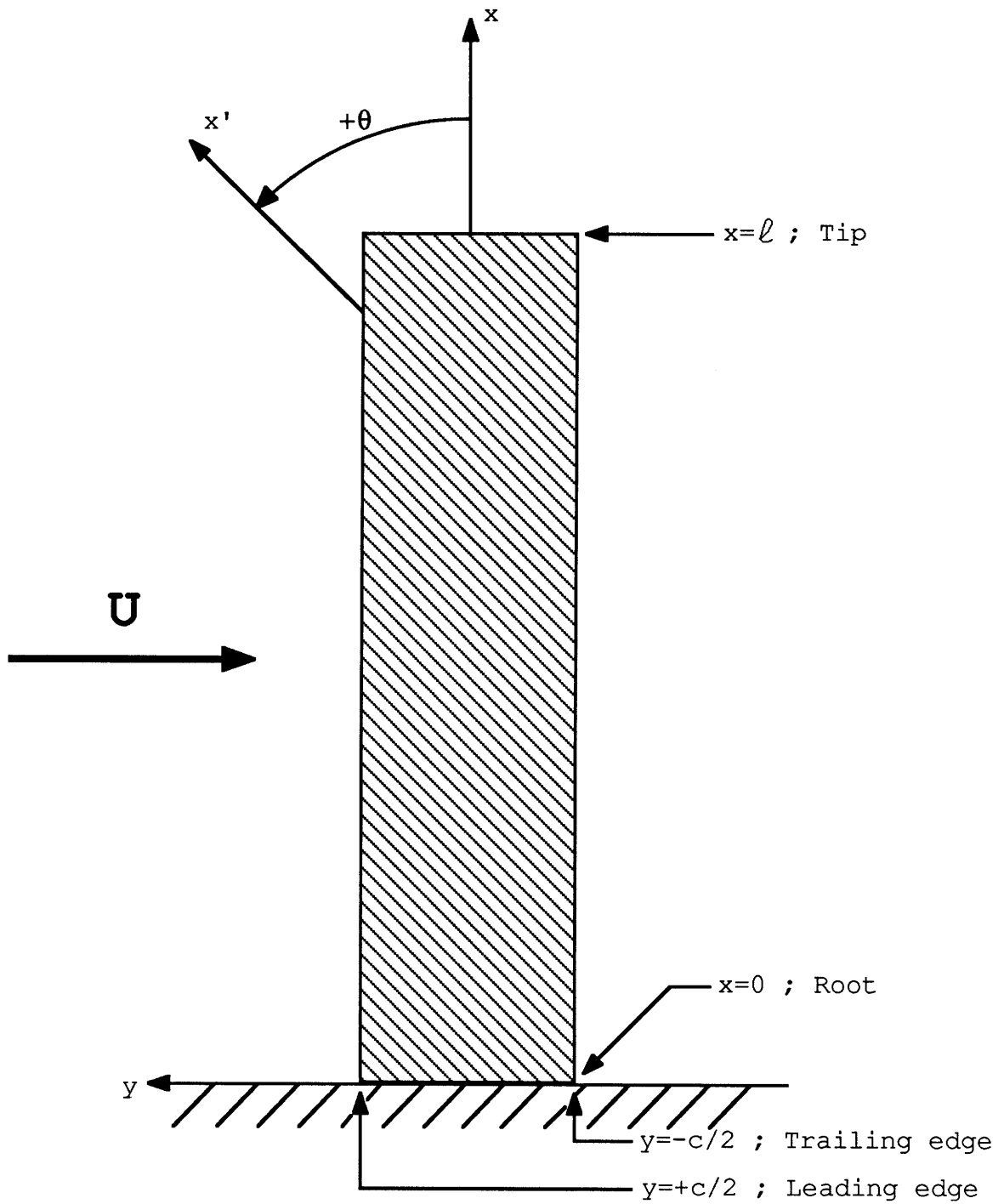
Figure 1. Sign convention for ply angles and axes

where,

$$v_{TL} = \frac{E_T}{E_L} \, v_{LT} \qquad\qquad (2\text{-}1e)$$

The in-plane, rotated modulus components were obtained by first defining a set of invariants,

$$I_1 = \frac{1}{4} \, [Q_{11} + Q_{22} + 2Q_{12}] \qquad\qquad (2\text{-}2a)$$

$$I_2 = \frac{1}{8} \, [Q_{11} + Q_{22} - 2Q_{12} + 4Q_{66}] \qquad\qquad (2\text{-}2b)$$

$$R_1 = \frac{1}{2} \, [Q_{11} - Q_{22}] \qquad\qquad (2\text{-}2c)$$

$$R_2 = \frac{1}{8} \, [Q_{11} + Q_{22} - 2Q_{12} - 4Q_{66}] \qquad\qquad (2\text{-}2d)$$

The invariants are transformed to the rotated modulus components using the relations:

$$Q_{11}^{(\theta)} = I_1 + I_2 + R_1 \cos 2\theta + R_2 \cos 4\theta \qquad\qquad (2\text{-}3a)$$

$$Q_{22}^{(\theta)} = I_1 + I_2 - R_1 \cos 2\theta + R_2 \cos 4\theta \qquad\qquad (2\text{-}3b)$$

$$Q_{12}^{(\theta)} = I_1 - I_2 - R_2 \cos 4\theta \qquad\qquad (2\text{-}3c)$$

$$Q_{66}^{(\theta)} = I_2 - R_2 \cos 4\theta \qquad\qquad (2\text{-}3d)$$

$$Q_{16}^{(\theta)} = \frac{1}{2} \, R_1 \sin 2\theta + R_2 \sin 4\theta \qquad\qquad (2\text{-}3e)$$

$$Q_{26}^{(\theta)} = \frac{1}{2} \, R_1 \sin 2\theta - R_2 \sin 4\theta \qquad\qquad (2\text{-}3f)$$

where θ is the ply angle.

The flexural modulus components, D_{ij}, for an n-ply laminate with arbitrary ply angle orientation are obtained from,

$$D_{ij} = \sum_{k=1}^{n} Q_{ij}^{(\theta)} \frac{z_k^3 - z_{k-1}^3}{3} \quad i,j = 1,2,6 \tag{2-4}$$

where,

θ_k = ply angle of the k-th ply

z_k = distance from the mid-plane to the upper surface of the k-th ply (positive above mid-plane, negative below mid-plane)

z_{k-1} = distance from the mid-plane to the lower surface of the k-th ply

2.2 Generalized Rayleigh-Ritz Problem

The direct Rayleigh-Ritz energy method is a relatively simple, straightforward approximation for the plate deflections, as required for the static deflection, free vibration, and flutter analyses in this study. The Rayleigh-Ritz method also has the advantage of showing the effect of the individual variables on the solution more clearly than other more accurate methods, such as finite element analysis. The "wing" is idealized by a rectangular, cantilevered, graphite/epoxy flat plate of uniform thickness, with styrofoam fairings covering the entire chord but only part of the entire span. The styrofoam fairings have chordwise variation because of their aerodynamic shape, and the calculation of their contribution to the wing mass and stiffness is described by the equations in section 2.4.

The Rayleigh-Ritz analysis begins by assuming a deflection shape for the structure. If only lateral deflections,

w, are allowed, the single deflection equation, written in generalized coordinates, is,

$$w = \sum_{i=1}^{n} \gamma_i(x,y)\, q_i(t) \qquad (2\text{-}5)$$

where $\gamma_i(x,y)$ is the non-dimensional deflection, or mode shape, of the i-th mode; $q_i(t)$ is the generalized displacement, or modal amplitude, of the i-th mode; and n is the number of mode shapes.

For simplicity, it is further assumed that the mode shapes are separable in the chordwise and spanwise directions, x and y, namely that the mode shapes can be written in the form,

$$\gamma_i(x,y) = \phi_i(x)\, \psi_i(y) \qquad (2\text{-}6)$$

The symmetric stiffness coefficients, K_{ij}, and the symmetric mass coefficients, M_{ij}, are defined as,

$$K_{ij} = \iint\limits_{A} \{ D_{11}\gamma_{i,xx}\gamma_{j,xx} + D_{22}\gamma_{i,yy}\gamma_{j,yy} + 4D_{66}\gamma_{i,xy}\gamma_{j,xy} +$$
$$D_{12}[\gamma_{i,xx}\gamma_{j,yy} + \gamma_{i,yy}\gamma_{j,xx}] + 2D_{16}[\gamma_{i,xx}\gamma_{j,xy} + \gamma_{i,xy}\gamma_{j,xx}] +$$
$$2D_{26}[\gamma_{i,yy}\gamma_{j,xy} + \gamma_{i,xy}\gamma_{j,yy}]\} \, dA \qquad (2\text{-}7)$$

$$M_{ij} = \iint\limits_{A} m\gamma_i\gamma_j \, dA \qquad (2\text{-}8)$$

where m is the mass per unit area and the subscripts following the commas denote partial differentiation with respect to the spatial coordinates, x and y. Since the styrofoam fairings only cover the last 5/6 of the wing span, therefore the m and D_{ij} terms are not uniform along the span, necessitating

a numerical integration scheme to evaluate the K_{ij} and M_{ij} terms. A 12-point Gaussian quadrature scheme was used to evaluate the above integrals. The strain energy, V, and kinetic energy, T, under the assumed modes are then given as,

$$V = \frac{1}{2} \sum_{i} \sum_{j} K_{ij} q_i q_j \qquad (2\text{-}9)$$

$$T = \frac{1}{2} \sum_{i} \sum_{j} M_{ij} \dot{q}_i \dot{q}_j \qquad (2\text{-}10)$$

The modal forces, Q_i, represent how much the distributed, applied load, $f(x,y)$, affects each mode shape. The Q_i are defined as,

$$Q_i = \iint_A f(x,y)\, \gamma_i(x,y)\, dA = \iint_A f(x,y)\, \phi_i(x)\, \psi_i(y)\, dA \qquad (2\text{-}11)$$

Lagrange's equations of motion for conservative linear systems [Ref. 8] yield the following differential equation, relating the modal amplitudes to the modal forces [Ref. 9],

$$\sum_{j=1}^{n} M_{ij} \ddot{q}_j + \sum_{j=1}^{n} K_{ij} q_j = Q_i \qquad i = 1, \ldots, n \qquad (2\text{-}12a)$$

or, in matrix form,

$$[M]\{\ddot{q}\} + [K]\{q\} = \{Q\} \qquad (2\text{-}12b)$$

To increase the accuracy of the structural model, an empirical cubic stiffening factor was added to the stiffness of the first torsional mode. The motivation for adding this factor was based solely on the experimentally observed results of the static bending tests. So, the stiffening factor for the first torsional mode is given by,

-28-

$$K_{22} = K_{22}^L + K_{22}^C q_2^2 \qquad\qquad (2\text{-}13)$$

where K_{22}^L is the linear stiffness of the flat plate given by equation (2-7) and K_{22}^C is the empirically determined cubic stiffening factor. Values of K_{22}^C for different layups are listed in Appendix B.

2.3 Selection of Modes

To sufficiently describe the deflection of the wing in the static bending, free vibration, and flutter tests, five mode shapes were chosen. As in previous studies [Refs. 3 and 4] these included two cantilever beam bending modes, two beam torsion modes, and a chordwise bending mode. Previous studies used simplified, sinusoidal torsional mode shapes [Refs. 3 and 4] that did not meet the cantilevered root conditions, but with a torsional stiffness correction which accounted for the effect of root warping stiffness [Ref. 9]. Vibrations tests, where the modal amplitudes were very small and the modal forces identically zero, showed that this torsional stiffness correction sufficed to accurately predict the natural frequencies and modes of vibration of the wings.

However, static bending tests and low speed, steady deflection, wind tunnel tests conducted in this study, where the modal amplitudes and modal forces were no longer insignificant, showed that the use of mode shapes which did not meet the cantilevered root condition adversely affected the Rayleigh-Ritz prediction of modal deflections. Therefore, the more complex torsional modes, with similar spanwise

form as the beam bending modes, were used instead of the simplified sinusoidal mode shapes. These five mode shapes are,

mode	$\phi_i(x)$	$\psi_i(y)$	
1	$\cosh(\epsilon_1\frac{x}{\ell}) - \cos(\epsilon_1\frac{x}{\ell}) -$ $\alpha_1[\sinh(\epsilon_1\frac{x}{\ell}) - \sin(\epsilon_1\frac{x}{\ell})]$	1	(2-14a)
2	$B_{11}\cos(g_1\frac{x}{\ell}) + B_{12}\sin(g_1\frac{x}{\ell}) +$ $+B_{13}\cosh(f_1\frac{x}{\ell}) + B_{14}\sinh(f_1\frac{x}{\ell})$	$\frac{y}{c}$	(2-14b)
3	$\cosh(\epsilon_2\frac{x}{\ell}) - \cos(\epsilon_2\frac{x}{\ell}) -$ $\alpha_2[\sinh(\epsilon_2\frac{x}{\ell}) - \sin(\epsilon_2\frac{x}{\ell})]$	1	(2-14c)
4	$B_{21}\cos(g_2\frac{x}{\ell}) + B_{22}\sin(g_2\frac{x}{\ell}) +$ $+B_{23}\cosh(f_2\frac{x}{\ell}) + B_{24}\sinh(f_2\frac{x}{\ell})$	$\frac{y}{c}$	(2-14b)
5	$\frac{x}{\ell}(1-\frac{x}{\ell})$	$\frac{4y^2}{c^2} - \frac{1}{3}$	(2-14e)

where the parameters of the two beam bending modes (1 and 3) are,

$$\epsilon_1 = 1.875104 \ , \ \alpha_1 = 0.734096$$

$$\epsilon_2 = 4.694091 \ , \ \alpha_2 = 1.018466$$

The parameters of the two beam torsion modes (2 and 4) are derived from the definition of β and the relationship between f and g,

$$\beta = \frac{D_{11}c^2}{48D_{66}\ell^2} \tag{2-15}$$

$$f^2 = g^2 + \frac{1}{\beta} \qquad (2\text{-}16)$$

and by solving the coupled equations which ensure that the mode shape meets the plate boundary conditions at the root and tip. For the assumed torsional mode shapes, the equations that describe the boundary condition that must be met can be written in matrix form as [Ref. 10],

$$\begin{bmatrix} 1 & 0 & 1 & 0 \\ 0 & g & 0 & f \\ -g^2\cos g & -g^2\sin g & f^2\cosh f & f^2\sinh f \\ gf^2\sin g & gf^2\cos g & g^2 f\sinh f & g^2 f\cosh f \end{bmatrix} \begin{bmatrix} B_{i1} \\ B_{i2} \\ B_{i3} \\ B_{i4} \end{bmatrix} = \begin{bmatrix} 0 \\ 0 \\ 0 \\ 0 \end{bmatrix} \qquad (2\text{-}17)$$

The first two lines of the matrix equation (2-17) ensure that the deflection and slope at the plate root are zero. The last two lines of the matrix equation ensure that the internal forces at the plate tip are also zero.

Since f and g are related through equation (2-16), the non-trivial solution to the eigenvalue problem is found by setting the determinant of the matrix in equation (2-17) to zero. The values for f and g can be found by a simple Newton solver scheme. Once the f and g values are found, the B_{ij} coefficients are determined through the following matrix equation,

$$\begin{bmatrix} 1 & 0 & 1 & 0 \\ 0 & g & 0 & f \\ -g^2\cos g & -g^2\sin g & f^2\cosh f & f^2\sinh f \\ \cos g & \sin g & \cosh f & \sinh f \end{bmatrix} \begin{bmatrix} B_{i1} \\ B_{i2} \\ B_{i3} \\ B_{i4} \end{bmatrix} = \begin{bmatrix} 0 \\ 0 \\ 0 \\ 1 \end{bmatrix} \qquad (2\text{-}18)$$

The fourth line in equation (2-18), which normalizes the modal tip deflection to one, replaces the fourth line of

equation (2-17), which becomes redundant when f and g are solved so as to make the matrix singular.

It is clear from equation (2-18) that B_{i1} and B_{i3} are equal in magnitude but opposite in sign. It is also generally found that f is order of magnitude 10, so that the cosh(f) and sinh(f) terms dominate the third line of the matrix equation, making B_{i3} and B_{i4} opposite in sign and almost equal in magnitude. It is important to note for purposes of calculating the tip deflection that B_{i3} and B_{i4} are not exactly equal in magnitude, since this difference is magnified exponentially by the cosh and sinh terms near $x/\ell=1$. Values of β, f, g, and B_{ij} for the layups used in this study are listed in Appendix B.

2.4 Styrofoam Mass and Stiffness Properties

The contributions to the stiffness matrix in equation (2-7) from the styrofoam fairing are governed by its flexural modulus components, which are calculated in the same manner as for the graphite/epoxy plies in equation (2-4). The isotropic engineering constants for Styrofoam HD-300, from which the fairings were constructed, appear in Appendix A. However, unlike the graphite/epoxy plies, the styrofoam fairing does not have a uniform thickness along the chord. Instead, the upper and lower distances from the mid-plane follow the standard NACA formula for symmetric airfoils [Ref. 7],

$$z = \pm \frac{t_{max}}{.20} \left[.2969 \sqrt{\frac{y}{c}} - .126 \frac{y}{c} - .3516 \left(\frac{y}{c}\right)^2 + .2843 \left(\frac{y}{c}\right)^3 - .1015 \left(\frac{y}{c}\right)^4 \right] \quad (2\text{-}19)$$

where y represents the chordwise location referenced from the airfoil leading edge, and t_{max} represents the maximum thickness of the airfoil (for example, for a NACA-0012 airfoil, the non-dimensional thickness, t_{max}/c, would be 0.12). As in equation (2-4) for the graphite/epoxy plies, z represents the distance from the midplane to the outer surfaces of each styrofoam fairing. The inner surface of each fairing is assumed to be at half the thickness of the graphite/epoxy flat plate, so that when the graphite/epoxy and styrofoam are combined they form the desired airfoil shape.

The contributions to the mass matrix in equation (2-8) can be calculated directly using the known thickness of the styrofoam in equation (2-19) and the chosen mode shapes in equation (2-14).

$$M_{11}^s = \int_{\ell/6}^{\ell} \int_{-c/2}^{c/2} m \, (\phi_1)^2 \, dx \, dy = \int_{-c/2}^{c/2} \rho_s \, (2z - t_{G/E}) \, dy \int_{\ell/6}^{\ell} (\phi_1)^2 \, dx$$

$$= \rho_s c \, (0.685 t_{max} - t_{G/E}) \int_{\ell/6}^{\ell} (\phi_1)^2 \, dx \quad (2\text{-}20a)$$

$$M_{22}^s = \int_{\ell/6}^{\ell} \int_{-c/2}^{c/2} m \left(\frac{y}{c} \phi_2\right)^2 dx \, dy = \int_{-c/2}^{c/2} \rho_s \left(\frac{y}{c}\right)^2 (2z - t_{G/E}) \, dy \int_{\ell/6}^{\ell} (\phi_2)^2 \, dx$$

$$= \rho_s \frac{c}{12} \, (0.506 t_{max} - t_{G/E}) \int_{\ell/6}^{\ell} (\phi_2)^2 \, dx \quad (2\text{-}20b)$$

$$M_{12}^s = \int_{\ell/6}^{\ell} \int_{-c/2}^{c/2} m\phi_1\left(\frac{y}{c}\phi_2\right) dx\, dy = \int_{-c/2}^{c/2} \rho_s \frac{y}{c} (2z - t_{G/E})\, dy \int_{\ell/6}^{\ell} \phi_1\phi_2 dx$$

$$= -.0545\rho_s c t_{max} \int_{\ell/6}^{\ell} \phi_1\phi_2 dx \qquad (2\text{-}20c)$$

M_{33}^s and M_{13}^s follow the same form as equation (2-20a) since $\psi_1(y) = \psi_3(y)$. Likewise, M_{44}^s and M_{24}^s follow the same form as equation (2-20b) since $\psi_2(y) = \psi_4(y)$. Finally, M_{14}^s, M_{23}^s, and M_{34}^s follow the same form as equation (2-20c). The calculations of the contributions to the mass matrix from the fifth mode (chordwise bending) are more cumbersome because of the complicated chordwise variation of the mode shape. Therefore, for those components of the mass matrix involving the fifth mode, the styrofoam thickness is assumed to be uniformly half the maximum thickness, t_{max}, as might be suggested by equation (2-20b).

In the same manner, the contributions of the styrofoam to the stiffness matrix can be calculated by inserting equation (2-19) into the flexural stiffness formula, equation (2-4), then directly carrying out the integration for the stiffnesses K_{ij} in equation (2-7). These give,

$$K_{11}^s = 2cQ_{11}^s \frac{\left(\frac{.779t_{max}}{2}\right)^3 - \left(\frac{t_{G/E}}{2}\right)^3}{3} \int_{\ell/6}^{\ell} (\phi_{1,xx})^2 dx \qquad (2\text{-}21a)$$

$$K_{22}^s = 2c\frac{Q_{11}^s}{24}\frac{\left(\frac{.824t_{max}}{2}\right)^3 - \left(\frac{t_{G/E}}{2}\right)^3}{3}\int_{\ell/6}^{\ell}(\phi_{2,xx})^2\,dx \;+$$

$$+\; 8cQ_{66}^s\frac{\left(\frac{.779t_{max}}{2}\right)^3 - \left(\frac{t_{G/E}}{2}\right)^3}{3}\int_{\ell/6}^{\ell}\left(\frac{\phi_{2,x}}{c}\right)^2\,dx \qquad (2\text{-}21b)$$

$$K_{12}^s = -.01585cQ_{11}^s t_{max}^3\int_{\ell/6}^{\ell}\phi_{1,xx}\phi_{2,xx}\,dx \qquad (2\text{-}21c)$$

where Q_{11}^s and Q_{66}^s are the styrofoam engineering constants, defined in the same manner as for the graphite/epoxy in equation (2-1), as listed in Appendix A.

K_{33}^s and K_{13}^s follow the same form as equation (2-21a) since $\psi_1(y)=\psi_3(y)$. Likewise, K_{44}^s and K_{24}^s follow the same form as equation (2-21b) since $\psi_2(y)=\psi_4(y)$. Finally, K_{14}^s, K_{23}^s, and K_{34}^s follow the same form as equation (2-21c). Again, the calculations involving the fifth mode are quite cumbersome, so for these purposes the styrofoam is assumed to be uniformly 80% its maximum thickness, as might be suggested by equations (2-21a) and (2-21b).

2.5 Static Deflection Problem

The static deflection problem is formulated as an analytical model of the experimental deflection tests described in Chapter III. For a pure force test, the cantilevered plate or wing is subjected to a concentrated load at the specimen tip $(x=\ell)$, at the elastic axis $(y=0)$. For a pure

moment test, the cantilevered plate or wing is subjected to equal and opposite concentrated loads at the specimen tip $(x=\ell)$, at the leading and trailing edges $(y=\pm c/2)$. The accelerations are zero for static deflection, and the real forces are point loads, so equation (2-12a) for a pure force reduces to,

$$\sum_{j=1}^{n} K_{ij}q_j = Q_i = F\phi_i(\ell)\psi_i(0) \qquad i=1,\ldots,n \qquad (2-22)$$

where F is the concentrated load applied at the wing tip. Similarly for a pure moment, where M is the moment applied to the wing tip, equation (2-12a) reduces to,

$$\sum_{j=1}^{n} K_{ij}q_j = Q_i = \frac{M}{c}\phi_i(\ell)\left[\psi_i(+\tfrac{c}{2}) - \psi_i(-\tfrac{c}{2})\right] \qquad (2-23)$$

Since the stiffness matrix contains a cubic stiffening term which depends on the amplitude of the first torsional mode, these equations are not purely linear and are therefore not directly solvable by a matrix inversion scheme, such as Gaussian elimination. However, since this cubic term only introduces a nonlinearity in one entry of the matrix equation, a simple Newton-Raphson technique (Appendix F) quickly converges to the desired solution.

2.6 Free Vibration Problem

The free vibration problem is formulated as an analytical model of the experimental vibration tests described in Chapter III. The problem is formulated by setting the modal

forces, Q_i, equal to zero in equations (2-12a) and (2-12b).
The equations of motion are reduced from differential form to
algebraic form by assuming harmonic (sinusoidal) motion. The
modal amplitudes can be expressed as,

$$q = \tilde{q}e^{i\omega t} \qquad \ddot{q} = -\omega^2 \tilde{q}e^{i\omega t} \qquad\qquad (2\text{-}24)$$

where ω is the frequency. These assumptions are substituted
into the differential equations of motion, (2-12a), to obtain
the sinusoidal equations of motion,

$$\sum_{j=1}^{n} (-\omega^2 M_{ij} + K_{ij})\tilde{q}_j = 0 \qquad i = 1, ..., n \qquad\qquad (2\text{-}25a)$$

or, in matrix form,

$$\left[-\omega^2 [M] + [K]\right]\{\tilde{q}\} = \{0\} \qquad\qquad (2\text{-}25b)$$

Equations (2-25a) and (2-25b) describe an eigenvalue
problem which can be solved in two manners. First, one can
set the determinant of the coefficient matrix equal to zero
and analytically solve for the eigenvalues, ω^2, and the
eigenvectors, $\{\tilde{q}\}$, corresponding to the natural frequencies
and natural modes of the plate or wing. This first method is
typically used for linear problems. Second, one can search
for a non-trivial solution by fixing one of the modal ampli-
tudes to be non-zero and solving for the remaining modal
amplitudes and the unknown frequency via a Newton-Raphson
scheme, as described in Appendix F. This second method is
typically used for nonlinear problems.

The latter method was chosen since it corresponds
closely to the Newton-Raphson scheme later used to solve the

flutter problem (for the flutter problem, harmonic motion is also assumed but the modal forces are no longer zero), thus enabling the use of the same solution technique for two problems. In addition, use of the second method allows for investigation of the nonlinear effects of amplitude of oscillation on the characteristics of the free vibration.

The Newton-Raphson scheme requires a fairly good initial guess, especially for an eigenvalue problem where the numeric scheme may converge to one of several valid solutions. This was resolved by looking more closely at the physical and mathematical makeup of the problem. The mode shapes are specifically chosen so that they are almost uncoupled [Ref. 10], hence *apriori* it is already known that the individual eigenvectors are close to the individual modes themselves. Therefore a good initial guess for the i-th natural mode shape is a non-zero entry in the $\{\tilde{q}\}$ vector for the i-th mode, and zero entries for all the other modes. In addition, since the modes are almost uncoupled, the mass and stiffness matrices are almost diagonal, so that a good initial guess for the natural frequency corresponding to the i-th mode is,

$$\omega_i^2 \approx \frac{K_{ii}}{M_{ii}} \tag{2-26}$$

The Newton-Raphson scheme quickly converges to the individual natural modes and frequencies with these initial guesses, and these results are compared in Chapter IV with the experimentally obtained results.

2.7 General Aerodynamic Model

The aerodynamic model used for this study was initially developed at *Office National d'Etudes et de Recherches Aérospatiales* by Tran and Petot [Ref. 5] and by Dat and Tran [Ref. 6]. This ONERA model is a semi-empirical, unsteady, nonlinear model which uses quasi-linear, small amplitude of oscillation, experimental data to predict aerodynamic forces on an oscillating airfoil which experiences dynamic stall. The model incorporates a single lag term operating on the linear part of the airfoil's static force curve, thus analogous to the Theodorsen function for linear theory, and a two lag term operating on the nonlinear (i.e. stalling) portion of the airfoil's static force curve.

The ONERA model was later investigated by Peters [Ref. 11] who differentiated the roles of angle of attack due to pitching (θ) and angle of attack due to plunging ($\dot{h}/U$). The final form of the ONERA model used for this study incorporates all terms needed such that it fits the theoretical Theodorsen and Kussner coefficients within the linear domain of operation [Ref. 12],

$$C_z = C_{z1} + C_{z2} \tag{2-27a}$$

$$C_{z1} = s_z \overset{*}{\alpha} + k_{vz} \overset{**}{\theta} + C_{z\gamma} \tag{2-27b}$$

$$\overset{*}{C}_{z\gamma} + \lambda_z C_{z\gamma} = \lambda_z [a_{oz}\alpha + \sigma_z \overset{*}{\theta}] + \alpha_z [a_{oz}\overset{*}{\alpha} + \sigma_z \overset{**}{\theta}] \tag{2-27c}$$

$$\overset{**}{C}_{z2} + 2dw\overset{*}{C}_{z2} + w^2(1+d^2)C_{z2} =$$
$$= -w^2(1+d^2)\left[\Delta C_z\Big|_\alpha + e\frac{\Delta C_z}{\partial\tau}\Big|_\alpha\right] \qquad (2\text{-}27\text{d})$$

where,

$$\alpha = \theta - \overset{*}{\bar{h}} \qquad (2\text{-}27\text{e})$$

$$(\overset{*}{}) \equiv \frac{\partial(\ )}{\partial\tau} \quad ; \quad \tau \equiv \frac{Ut}{b} \qquad (2\text{-}27\text{f})$$

and,

θ = instantaneous angle of attack

h = instantaneous deflection of 1/4-chord

$\bar{h} \equiv \dfrac{h}{b}$ = non-dimensional deflection

α = effective angle of attack

C_z represents any of the three relevant non-dimensional force coefficients: C_L, the coefficient of lift, or C_D, the coefficient of drag, or C_M, the moment coefficient. a_{oz} is the slope of the linear part of the static force curve, ΔC_z is the nonlinear deviation from the extended linear force curve, and s_z, k_{vz}, λ_z, σ_z, α_z, w, d, and e are the coefficients associated with the appropriate force coefficient, determined empirically by parameter identification. These force coefficients are listed in Appendix D.

Equations (2-27b) and (2-27c) describes that part of the force coefficient associated with the linear model C_{z1}, and are similar in form to the description of unsteady, linear theory with a first order lag for the Theodorsen function. $C_{z\gamma}$ is the linear circulatory contribution, while C_{z1} is the

total linear contribution, also incorporating the apparent mass terms. Equation (2-27d) describes that part of the force coefficient associated with the nonlinear model C_{z2}, and is dependent on the deviation of the actual static curve from the linear static curve, ΔC_z, as shown in Figure 2. It also includes a second order lag for C_{z2}. Equation (2-27a) combines these linear and nonlinear terms of the force coefficient into the total coefficient C_z.

For implementation of the ONERA aerodynamic model, it is necessary to describe the static aerodynamic force curves in terms of the linear domain, described by the linear slope a_{oz}, and the nonlinear domain, described by the deviation from the linear curve ΔC_z. The deviation ΔC_z is defined as positive for a decrease in the aerodynamic force, as shown in Figure 2. The general description of the static aerodynamic force curve is then given by,

$$C_{zs}(\alpha) = a_{oz}\alpha - \Delta C_z(\alpha) \qquad (2-28a)$$

where,

$$a_{oz} = \frac{dC_{z\ell}}{d\alpha} = \text{linear aerodynamic force slope} \qquad (2-28b)$$

In general, the deviation ΔC_z can be described in any manner desired. In the current study, the deviation ΔC_z was described by simple straight line fits between discrete points (see Appendix C). More generally, the ΔC_z could be described by polynomials in several regions of the aerodynamic force curve. Polynomials of order J_i are used for ease

$C_{ZS}(\alpha)$

extension of linear
static curve, $C_z\ell$

ΔC_z

non-linear
static curve

α
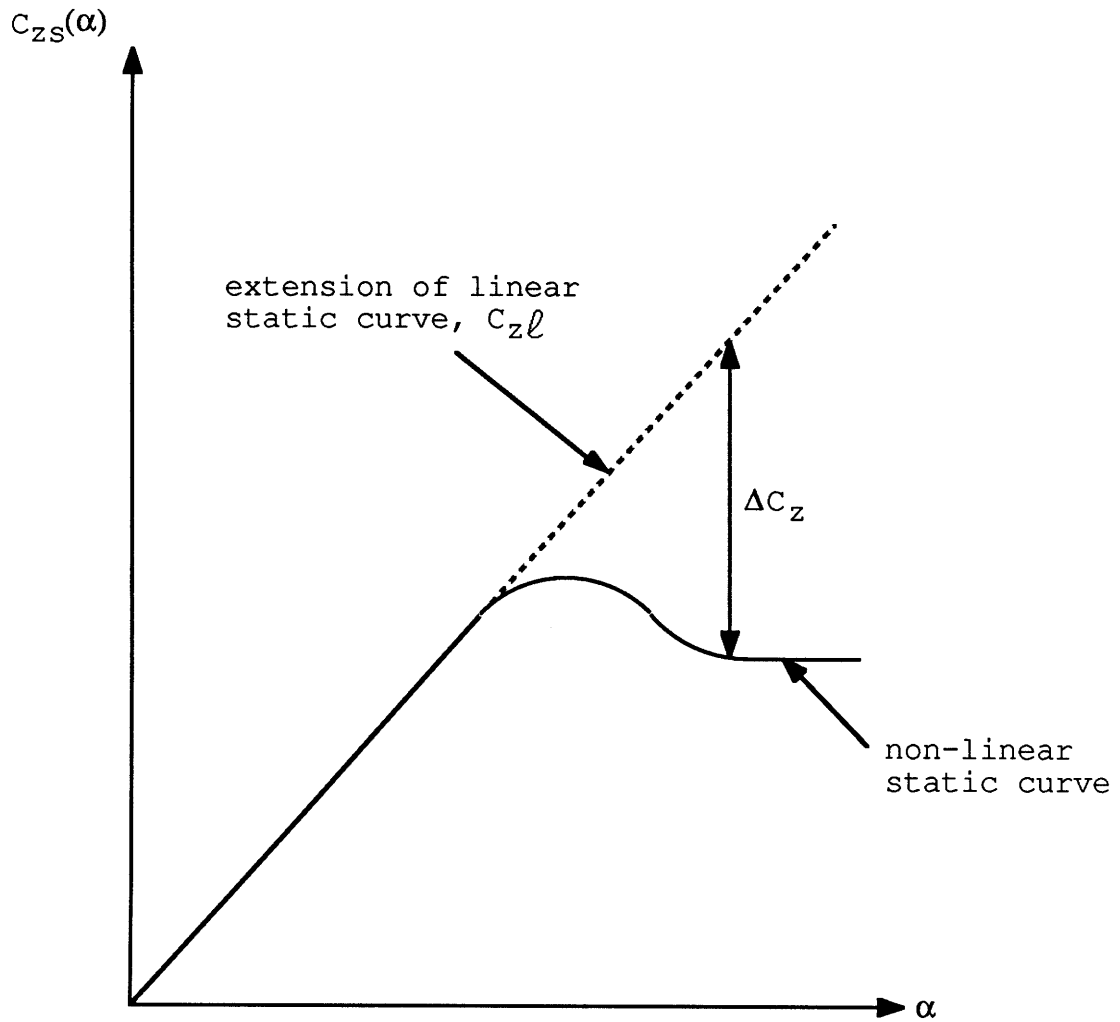
Figure 2. Description of static curve

of algebraic manipulations in the Fourier analysis, described later in section 2.9.

The general formula for the deviation ΔC_z in the i-th region can then be expressed as,

$$\Delta C_z(\alpha) = \sum_{j=0}^{J_i} a_{ij}(\alpha - \alpha_i)^j \; ; \; \alpha_i \leq \alpha \leq \alpha_{i+1} \qquad (2\text{-}29\text{a})$$

where,

$$a_{io} \equiv \Delta C_z(\alpha_i) \qquad (2\text{-}29\text{b})$$

$$\Delta C_z(\alpha = \alpha_1) \equiv 0 \qquad (2\text{-}29\text{c})$$

Equation (2-29b) ensures that the description of the aerodynamic force curve is continuous at the juncture of the describing domains. Equation (2-29c) ensures that the deviation ΔC_z is identically zero in the linear region before stall. The description of the aerodynamic force coefficients used in the current study is more fully described in Appendix C.

Once the aerodynamic force coefficients are determined, they are inserted into equation (2-11) to give the modal forces,

$$Q_i = \frac{1}{2}\rho U^2 \int_0^\ell \{c[C_L(x)\cos\theta_R + C_D(x)\sin\theta_R]\psi_i(+\frac{c}{4}) \;\; +$$

$$+ \; c^2 C_M(x)\psi_{i,y}(+\frac{c}{4})\}\phi_i(x)\,dx \qquad (2\text{-}30)$$

2.8 Linear Aeroelastic U-g Method

As a starting point from which to investigate the full, nonlinear flutter problem, it is useful to look at the linear, small-amplitude, zero root-angle-of-attack flutter and divergence problem, which can typically be solved using what is called the U-g method. Since this analysis is only intended as a rough starting point for the full, nonlinear analysis, the derivation is carried out for only two Rayleigh-Ritz modes for simplicity.

First, because the problem is linear, the steady problem is completely uncoupled from the unsteady problem, and the two can be considered separately. So, for the unsteady problem, sinusoidal motion is first assumed,

$$q_1 = \tilde{q}_1 e^{i\omega t} \quad ; \quad q_2 = \tilde{q}_2 e^{i\omega t} \tag{2-31}$$

After some algebraic manipulation, it is derived that the aerodynamic modal forces are given by,

$$Q_1 = \omega^2 s_L \rho b^3 \left\{ \frac{[L_1 + iL_2]\ell I_{11}}{b} \tilde{q}_1 + \frac{[L_3 + iL_4]\ell I_{12}}{c} \tilde{q}_2 \right\} e^{i\omega t} \tag{2-32a}$$

$$Q_2 = \omega^2 s_L \rho b^4 \left\{ \frac{[M_1 + iM_2]\ell I_{12}}{bc} \tilde{q}_1 + \frac{[M_3 + iM_4]\ell I_{22}}{c^2} \tilde{q}_2 \right\} e^{i\omega t} \tag{2-32b}$$

where,

$$[L_1 + iL_2] = 1 - \frac{2i}{k} \frac{a_{oL}}{2s_L} C(k) \tag{2-33a}$$

$$[L_3 + iL_4] = \frac{1}{2} - \frac{k_{vL}}{s_L} + \frac{2C(k)}{k^2}\frac{a_{oL}}{2s_L} + \frac{i}{k}\left\{1 + \left[\frac{\sigma_L}{s_L} - \frac{a_{oL}}{2s_L}\right]C(k)\right\} \qquad (2\text{-}33b)$$

$$[M_1 + iM_2] = \frac{1}{2} + \frac{2s_M}{s_L} - \frac{i}{k}\frac{a_{oL}}{2s_L}C(k) \qquad (2\text{-}33c)$$

$$[M_3 + iM_4] = \frac{1}{4} - \frac{k_{vL}}{2s_L} + \frac{s_M}{s_L} - \frac{2k_{vM}}{s_L} + \frac{C(k)}{k^2}\frac{a_{oL}}{2s_L} +$$

$$+ \frac{i}{k}\left\{\frac{1}{2} + \frac{2s_M}{s_L} + \frac{2\sigma_M}{s_L} + \frac{1}{2}\left[\frac{\sigma_L}{s_L} - \frac{a_{oL}}{2s_L}\right]C(k)\right\} \qquad (2\text{-}33d)$$

and where the approximation to the Theodorsen function and the mode shape integrals corrected for spanwise effects are given by,

$$C(k) = \frac{\lambda_L + \alpha_L ik}{\lambda_L + ik} \qquad (2\text{-}34)$$

$$I_{11} = \frac{1}{1 + \dfrac{a_{oL}}{\pi AR}}\frac{1}{\ell}\int_0^\ell 1.11\left[1 - (\tfrac{x}{\ell})^9\right](\phi_1)^2\,dx \qquad (2\text{-}35a)$$

$$I_{12} = \frac{1}{1 + \dfrac{a_{oL}}{\pi AR}}\frac{1}{\ell}\int_0^\ell 1.11\left[1 - (\tfrac{x}{\ell})^9\right]\phi_1\phi_2\,dx \qquad (2\text{-}35b)$$

$$I_{22} = \frac{1}{1 + \dfrac{a_{oL}}{\pi AR}}\frac{1}{\ell}\int_0^\ell 1.11\left[1 - (\tfrac{x}{\ell})^9\right](\phi_2)^2\,dx \qquad (2\text{-}35c)$$

One must note at this point that if the linearly derived coefficients are inserted into equations (2-33a) to (2-33d) $[a_{oL}=2\pi;\ s_L=\pi;\ k_{vL}=\pi/2;\ \sigma_L=2\pi;\ s_M=-\pi/4;\ k_{vM}=-3\pi/16;\ \sigma_M=-\pi/4]$, then the typical 2-dimensional, linear relations, as shown in Refs. 1 and 3, are recovered.

Inserting these into the equations of motion and canceling the $e^{i\omega t}$, yields the following form of the equations of motion, written in contracted matrix form,

$$\left[[K] - \omega^2 [A] \right] \{\tilde{q}\} = 0 \tag{2-36}$$

where,

$$A_{11} = M_{11} + s_L \rho \ell b^2 I_{11} [L_1 + iL_2] \tag{2-37a}$$

$$A_{12} = M_{12} + s_L \rho \frac{\ell b^3}{c} I_{12} [L_3 + iL_4] \tag{2-37b}$$

$$A_{21} = M_{21} + s_L \rho \frac{\ell b^3}{c} I_{12} [M_1 + iM_2] \tag{2-37c}$$

$$A_{22} = M_{22} + s_L \rho \frac{\ell b^4}{c^2} I_{22} [M_3 + iM_4] \tag{2-37d}$$

Structural damping is then introduced into equation (2-36) by multiplying the $[K]$ matrix by $(1+ig)$. Introducing the complex eigenvalue Z, equation (2-36) then becomes,

$$\left[[A] - [K]Z \right] \{\tilde{q}\} = 0 \tag{2-38}$$

where,

$$Z \equiv \frac{1 + ig}{\omega^2} \tag{2-39}$$

The solution method is to pick a value of reduced frequency, and solve equation (2-38) for all the corresponding complex eigenvalues Z_i. Then, for each Z, the associated frequency, structural damping, and velocity are given by,

$$\omega = \frac{1}{\sqrt{\text{Re}\{Z\}}} \quad ; \quad g = \frac{\text{Im}\{Z\}}{\text{Re}\{Z\}} \quad ; \quad U = \frac{\omega b}{k} \tag{2-40a,b,c}$$

The procedure is repeated for several values of the reduced frequency k, until enough values have been generated to plot a smooth U-g diagram. The divergence points are those locations where the structural damping and frequency simultaneously go to zero. The flutter points are those other locations where the structural damping goes to zero but the frequency is non-zero.

2.9 Fourier Analysis of the Nonlinear Aerodynamics

For later use in the Harmonic Balance Method, it is necessary to be able to evaluate the lowest order frequency components of the nonlinear aerodynamic force coefficients when given a harmonic input. First, harmonic motion is assumed for the angle of attack and the non-dimensional, 1/4-chord deflection,

$$\theta(\tau) = \theta_o + \theta_s \sin(k\tau) + \theta_c \cos(k\tau) \qquad (2-41a)$$

$$\bar{h}(\tau) = \bar{h}_o + \bar{h}_s \sin(k\tau) + \bar{h}_c \cos(k\tau) \qquad (2-41b)$$

where,

$$k = \text{reduced frequency} = \frac{\omega b}{U}$$
$$\tau = \text{non-dimensional time} = \frac{Ut}{b}$$

The effective angle of attack, α, which combines both the instantaneous angle of attack and the angle of attack due to the velocity of the 1/4-chord deflection, is given by,

$$\alpha(\tau) = \alpha_o + \alpha_s \sin(k\tau) + \alpha_c \cos(k\tau) \qquad (2-42a)$$

where equation (2-27e) gives,

$$\alpha_o = \theta_o \qquad (2\text{-}42b)$$

$$\alpha_s = \theta_s + k\bar{h}_c \qquad (2\text{-}42c)$$

$$\alpha_c = \theta_c - k\bar{h}_s \qquad (2\text{-}42d)$$

Manipulations of the formulas are further simplified if the angle of attack is put in the form where it is purely sinusoidal,

$$\alpha(\tau) = \alpha_o + \alpha_v \sin(k\tau + \xi) = \alpha_o + \alpha_v \sin\varphi \qquad (2\text{-}43a)$$

where,

$$\alpha_v = \sqrt{\alpha_s^2 + \alpha_c^2} \qquad (2\text{-}43b)$$

$$\xi = \sin^{-1}\frac{\alpha_c}{\alpha_v} \qquad (2\text{-}43c)$$

$$\varphi = k\tau + \xi \qquad (2\text{-}43d)$$

Equation (2-43a) is then substituted into equation (2-29a) to give,

$$\Delta C_z(\tau) = \sum_{j=0}^{J_i} a_{ij}(\alpha_o + \alpha_v \sin\varphi - \alpha_i)^j \qquad (2\text{-}44a)$$

for $\varphi_i \leq \varphi \leq \varphi_{i+1}$

where,

$$\varphi_i = \sin^{-1}\left(\frac{\alpha_i - \alpha_o}{\alpha_v}\right) \qquad (2\text{-}44b)$$

$$\varphi_i = \begin{cases} +\pi/2 & \text{if } \alpha_o + \alpha_v < \alpha_i \quad \text{i.e.,} \quad \alpha_i - \alpha_o > \alpha_v \\ -\pi/2 & \text{if } \alpha_o - \alpha_v > \alpha_i \quad \text{i.e.,} \quad \alpha_i - \alpha_o < -\alpha_v \end{cases} \qquad (2\text{-}44c)$$

Equation (2-44a) is only valid within the i-th region, as shown in the example in Figure 3 for a nonlinear curve described by only two regions. Since the effective angle of attack is a function of the non-dimensional time, for each angle of attack deliniating the i-th region, α_i, there is therefore an associated non-dimensional time, designated φ_i. As shown by the relationship in Figure 3, and diagrammed in the time domain in Figure 4, the relationship between the deliniating angle of attack, α_i, and the associated non-dimensional time, φ_i, is given by equation (2-44b).

For those regions where φ_i is undetermined, φ_i takes on the values $\pm\pi/2$, as described in equation (2-44c). These values are arbitrarily set so that the limits of integration are correct in the Fourier analysis in equation (2-48).

Substituting the power expansion relationship into the polynomial in equation (2-44a) gives,

$$\Delta C_z(\tau) = \sum_{j=0}^{J_i} a_{ij}\left\{\alpha_v^j \sum_{m=0}^{j}\binom{j}{m}\left(\frac{\alpha_o - \alpha_i}{\alpha_v}\right)^{j-m} \sin^m\varphi\right\} \qquad (2\text{-}45)$$

where the binomial coefficients are defined as,

$$\binom{j}{m} = \frac{j!}{m!\,(j-m)!}$$

Next, assume harmonic motion for ΔC_z as well,

$$\Delta C_z(\tau) = \Delta C_{zo} + \Delta C_{zv}\sin\varphi + \text{H.H.T.} \qquad (2\text{-}46)$$
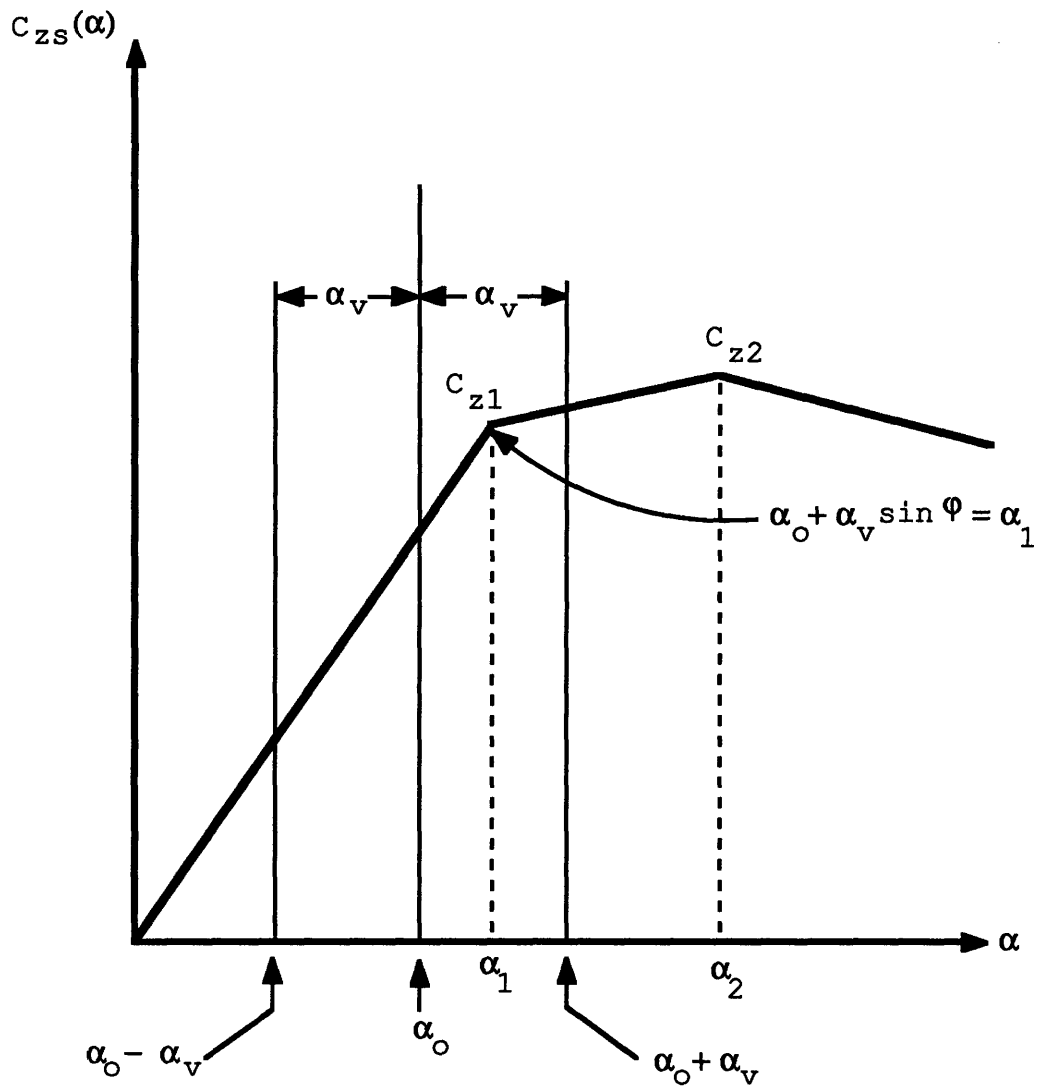
Figure 3. Example of oscillation straddling
stall angle on aerodynamic force curve
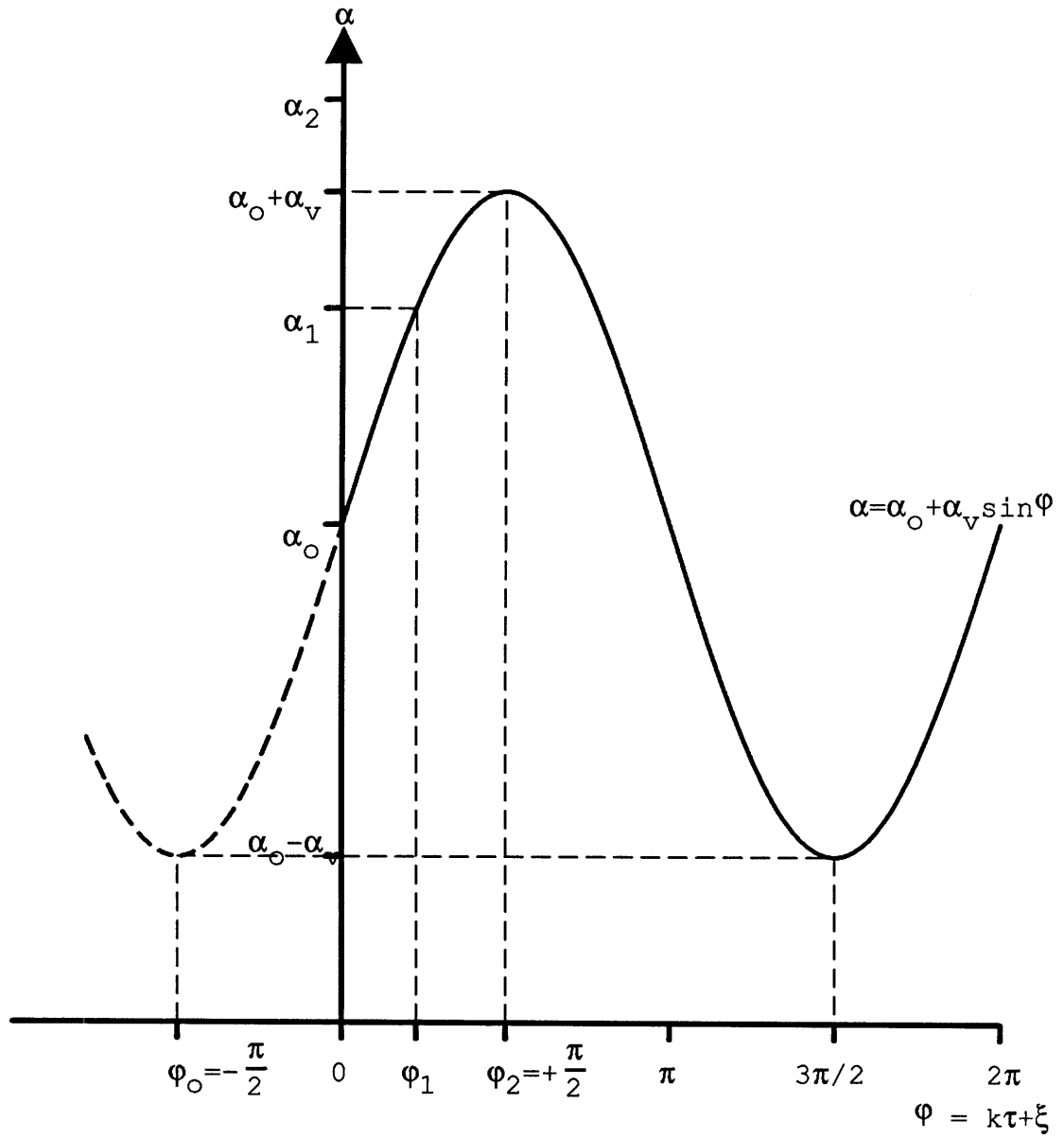
Figure 4. Example of oscillation straddling
stall angle in non-dimensional time domain

Since ΔC_z is a single-valued function of α, the two functions are always in phase with each other, and therefore there is no $\cos\varphi$ term in equation (2-46). Fourier analysis then gives the relations for ΔC_{zo} and ΔC_{zv},

$$\Delta C_{zo} = \frac{1}{2\pi}\int_{-\pi}^{+\pi}\Delta C_z(\tau)\,d\varphi = \frac{1}{\pi}\int_{-\frac{\pi}{2}}^{+\frac{\pi}{2}}\Delta C_z(\tau)\,d\varphi \qquad (2\text{-}47a)$$

$$\Delta C_{zv} = \frac{2}{\pi}\int_{-\frac{\pi}{2}}^{+\frac{\pi}{2}}\Delta C_z(\tau)\sin\varphi\,d\varphi \qquad (2\text{-}47b)$$

Substituting equation (2-45) into equation (2-47a) gives,

$$\Delta C_{zo} = \frac{1}{\pi}\sum_i\left[\sum_{j=0}^{J_i}a_{ij}\alpha_v^j\sum_{m=0}^{j}\binom{j}{m}\left(\frac{\alpha_o-\alpha_i}{\alpha_v}\right)^{j-m}\int_{\varphi_i}^{\varphi_{i+1}}\sin^m\varphi\,d\varphi\right] \qquad (2\text{-}48)$$

Interchanging the j and m summations in equation (2-48) gives,

$$\Delta C_{zo} = \frac{1}{\pi}\sum_i\left[\sum_{m=0}^{J_i}\sum_{j=m}^{J_i}a_{ij}\alpha_v^j\binom{j}{m}\left(\frac{\alpha_o-\alpha_i}{\alpha_v}\right)^{j-m}\int_{\varphi_i}^{\varphi_{i+1}}\sin^m\varphi\,d\varphi\right] \qquad (2\text{-}49)$$

For ease of calculation, the summation in equation (2-49) is separated into two terms: those that are dependent on a summation over the j's, the powers of the polynomial approximation, and those that are independent of j. The new equations are in essence no different than equation (2-49), and no physical significance is implied in this particular

separation of terms, but computationally the evaluation of equation (2-49) is made more simple.

$$\Delta C_{zo} = \frac{1}{\pi} \sum_i \sum_{m=o}^{J_i} b_{im} I_{im} \tag{2-50}$$

where the b_{im}'s are the j dependent terms, and the I_{im}'s are the j independent terms. These terms are given by,

$$b_{im} = \sum_{j=m}^{J_i} \binom{j}{m} a_{ij} \alpha_v^j \left(\frac{\alpha_o - \alpha_i}{\alpha_v} \right)^{j-m} \tag{2-51}$$

$$I_{im} = \int_{\varphi_i}^{\varphi_{i+1}} \sin^m\varphi \, d\varphi = \frac{-\sin^{m-1}\varphi \cos\varphi}{m} \Big|_{\varphi_i}^{\varphi_{i+1}} + \frac{m-1}{m} I_{i,m-2} \tag{2-52}$$

where the first two values required for the recursive formula in equation (2-52) are given by,

$$I_{i0} = \int_{\varphi_i}^{\varphi_{i+1}} d\varphi = \varphi_{i+1} - \varphi_i \tag{2-53a}$$

$$I_{i1} = \int_{\varphi_i}^{\varphi_{i+1}} \sin\varphi \, d\varphi = \cos\varphi_i - \cos\varphi_{i+1} \tag{2-53b}$$

Similarly, using the same calculated b_{ij} and I_{ij} values, the first harmonic term is given by,

$$\Delta C_{zv} = \frac{2}{\pi} \sum_i \sum_{m=o}^{J_i} b_{im} I_{i,m+1} \tag{2-54}$$

Equation (2-46) is then placed back into the usual sine and cosine harmonic form by setting $\varphi = k\tau + \xi$,

$$\Delta C_z(\tau) = \Delta C_{zo} + \Delta C_{zs}\sin(k\tau) + \Delta C_{zc}\cos(k\tau) \tag{2-55a}$$

where,

$$\Delta C_{zs} = \Delta C_{zv}\cos\xi = \Delta C_{zv}\frac{\alpha_s}{\sqrt{\alpha_s^2 + \alpha_c^2}} \qquad (2-55b)$$

$$\Delta C_{zc} = \Delta C_{zv}\sin\xi = \Delta C_{zv}\frac{\alpha_c}{\sqrt{\alpha_s^2 + \alpha_c^2}} \qquad (2-55c)$$

and where ΔC_{zo} and ΔC_{zv} are given by equations (2-50) and (2-54), and where α_s and α_c are given by equations (2-42c) and (2-42d).

It is unnecessary to also carry out the full Fourier analysis for the time derivative of ΔC_z because of the mathematical identity that the Fourier expansion of the derivative of a function is equal to the derivative of the Fourier expansion. Hence, equation (2-55a) gives,

$$\frac{\Delta C_z(\tau)}{\partial\tau} = -k\Delta C_{zc}\sin(k\tau) + k\Delta C_{zs}\cos(k\tau) \qquad (2-56)$$

where ΔC_{zs} and ΔC_{zc} are again given by equations (2-55b) and (2-55c). Simple examples for a force curve with only one and two break points is given in Appendix E.

2.10 The Harmonic Balance Method

All the components of the flutter problem have been stated in differential form and now it remains to reduce the problem to an algebraic form so that it is more easily solved computationally. The general form of the differential equation describing the motion of the wing is given by equation (2-12). The left hand side of equation (2-12) contains the structural information of the problem and is described by the

-54-

definitions of the stiffness and mass matrices given in equations (2-7) and (2-8). The right hand side of equation (2-12) contains the aerodynamic information of the problem, in the form of the modal forces, and is described by equation (2-30).

In general the aeroelastic problem is reduced from differential form to algebraic form by assuming harmonic motion in the same manner as for the free vibration problem in section 2.6. This method is acceptable for the linear flutter problem where the steady part of the solution is uncoupled from the unsteady part of the solution. However, for the nonlinear flutter problem, these two are no longer uncoupled and both must be considered at once.

First, the modal amplitudes are put into harmonic form,

$$q_i(\tau) = q_{io} + q_{is}\sin(k\tau) + q_{ic}\cos(k\tau) \qquad (2-57)$$

From the modal amplitudes, the angle of attack and 1/4-chord deflection at each spanwise location are also put into harmonic form,

$$\bar{h}(x,\tau) = \bar{h}_o(x) + \bar{h}_s(x)\sin(k\tau) + \bar{h}_c(x)\cos(k\tau) \qquad (2-58)$$

$$\theta(x,\tau) = \theta_o(x) + \theta_s(x)\sin(k\tau) + \theta_c(x)\cos(k\tau) \qquad (2-59)$$

where,

$$\bar{h}_o(x) = \sum_{i=1}^{n} \frac{q_{io}}{b}\,\phi_i(x)\,\psi_i(+c/4) \qquad (2-60a)$$

$$\bar{h}_s(x) = \sum_{i=1}^{n} \frac{q_{is}}{b}\,\phi_i(x)\,\psi_i(+c/4) \qquad (2-60b)$$

$$\overline{h}_c(x) = \sum_{i=1}^{n} \frac{q_{ic}}{b} \phi_i(x) \psi_i(+c/4) \qquad (2\text{-}60c)$$

and,

$$\theta_o(x) = \theta_{root} + \sum_{i=1}^{n} q_{io} \phi_i(x) \psi_{i,y}(+c/4) \qquad (2\text{-}61a)$$

$$\theta_s(x) = \sum_{i=1}^{n} q_{is} \phi_i(x) \psi_{i,y}(+c/4) \qquad (2\text{-}61b)$$

$$\theta_c(x) = \sum_{i=1}^{n} q_{ic} \phi_i(x) \psi_{i,y}(+c/4) \qquad (2\text{-}61c)$$

Substituting equations (2-58) and (2-59) into the formula for the linear aerodynamics, equation (2-27c), gives,

$$C_{z\gamma}(x,\tau) = C_{z\gamma 0}(x) + C_{z\gamma s}(x)\sin(k\tau) + C_{z\gamma c}(x)\cos(k\tau) \qquad (2\text{-}62)$$

where,

$$C_{z\gamma o}(x) = a_{oz}\theta_o(x) \qquad (2\text{-}63a)$$

$$C_{z\gamma s}(x) = F(k)L_s(x) - G(k)L_c(x) \qquad (2\text{-}63b)$$

$$C_{z\gamma c}(x) = G(k)L_s(x) + F(k)L_c(x) \qquad (2\text{-}63c)$$

where, in the present analysis, the F and G functions are the resulting single lag approximations to the Theodorsen function, $C(k) = F(k)+iG(k)$, namely,

$$F(k) = \frac{\lambda_z^2 + \alpha_z k^2}{\lambda_z^2 + k^2} \qquad (2\text{-}64a)$$

$$G(k) = -\frac{\lambda_z k(1-\alpha_z)}{\lambda_z^2 + k^2} \qquad (2\text{-}64b)$$

and where the other intermediate variables are,

$$L_s(x) = a_{oz}\left[\theta_s(x) + k\overline{h}_c(x)\right] - \sigma_z k\theta_c(x) \tag{2-64c}$$

$$L_c(x) = a_{oz}\left[\theta_c(x) - k\overline{h}_s(x)\right] + \sigma_z k\theta_s(x) \tag{2-64d}$$

Finally, the apparent mass terms are added to give the usual harmonic form of the linear aerodynamics derived from equation (2-27b),

$$C_{z1o}(x) = C_{z\gamma_o}(x) \tag{2-65a}$$

$$C_{z1s}(x) = C_{z\gamma_s}(x) - s_z[k\theta_c(x) - k^2\overline{h}_s(x)] - k_{vz}k^2\theta_s(x) \tag{2-65b}$$

$$C_{z1c}(x) = C_{z\gamma_c}(x) + s_z[k\theta_s(x) + k^2\overline{h}_c(x)] - k_{vz}k^2\theta_c(x) \tag{2-65c}$$

Substituting the harmonic form of the nonlinear aerodynamics, equation (2-55a), into the nonlinear aerodynamic differential formula, equation (2-27d), gives,

$$C_{z2}(x,\tau) = C_{z2o}(x) + C_{z2s}(x)\sin(k\tau) + C_{z2c}(x)\cos(k\tau) \tag{2-66}$$

where,

$$C_{z2o}(x) = -\Delta C_{zo}(x) \tag{2-67a}$$

$$C_{z2s}(x) = \frac{K_1 K_3 + K_2 K_4}{K_1^2 + K_2^2} \tag{2-67b}$$

$$C_{z2c}(x) = \frac{K_1 K_4 - K_2 K_3}{K_1^2 + K_2^2} \tag{2-67c}$$

and the intermediate variables are given by,

$$K_1 = 1 + d^2 - \left(\frac{k}{w}\right)^2 \tag{2-68a}$$

$$K_2 = 2d\frac{k}{w} \tag{2-68b}$$

$$K_3 = -(1+d^2)\left[\Delta C_{zs}(x) - ek\Delta C_{zc}(x)\right] \tag{2-68c}$$

$$K_4 = -(1+d^2)\left[\Delta C_{zc}(x) + ek\Delta C_{zs}(x)\right] \tag{2-68d}$$

The harmonic forms of the linear and nonlinear force components, given by equations (2-65) and (2-66), are then placed into the combined force formula, equation (2-27a), to give,

$$C_z(x,\tau) = C_{zo}(x) + C_{zs}(x)\sin(k\tau) + C_{zc}(x)\cos(k\tau) \tag{2-69}$$

where,

$$C_{zo}(x) = C_{z10}(x) + C_{z20}(x) \tag{2-70a}$$

$$C_{zs}(x) = C_{z1s}(x) + C_{z2s}(x) \tag{2-70b}$$

$$C_{zc}(x) = C_{z1c}(x) + C_{z2c}(x) \tag{2-70c}$$

The harmonic form of the aerodynamic forces is then placed into equation (2-30) to give the harmonic form of the modal forces,

$$Q_i(\tau) = Q_{io} + Q_{is}\sin(k\tau) + Q_{ic}\cos(k\tau) \tag{2-71}$$

where,

$$Q_{io} = \frac{1}{2}\rho U^2 \int_0^\ell \left\{ c\,[C_{L0}(x)\cos\theta_R + C_{D0}(x)\sin\theta_R]\,\psi_i\left(+\frac{c}{4}\right) \right.$$
$$\left. + c^2 C_{M0}(x)\,\psi_{i,y}\left(+\frac{c}{4}\right) \right\}\phi_i(x)\,dx \tag{2-72a}$$

$$Q_{is} = \frac{1}{2}\rho U^2 \int_0^\ell \left\{ c\,[C_{Ls}(x)\cos\theta_R + C_{Ds}(x)\sin\theta_R]\,\psi_i\left(+\frac{c}{4}\right) \right.$$
$$\left. + c^2 C_{Ms}(x)\,\psi_{i,y}\left(+\frac{c}{4}\right) \right\}\phi_i(x)\,dx \tag{2-72b}$$

$$Q_{ic} = \frac{1}{2}\rho U^2 \int_0^\ell \left\{ c\,[C_{Lc}(x)\cos\theta_R + C_{Dc}(x)\sin\theta_R]\,\psi_i\,(+\tfrac{c}{4}) \right. +$$

$$\left. + c^2 C_{Mc}(x)\,\psi_{i,y}\,(+\tfrac{c}{4}) \right\}\,\phi_i(x)\,dx \qquad (2\text{-}72\text{c})$$

The general equations of motion, described in matrix form in equation (2-12b), are converted into the final harmonic form by substituting the harmonic forms of the modal amplitudes and modal forces from equations (2-57) and (2-71),

$$\begin{bmatrix} [K] & 0 & 0 \\ 0 & -\omega^2[M]+[K] & 0 \\ 0 & 0 & -\omega^2[M]+[K] \end{bmatrix} \begin{bmatrix} \{q_o\} \\ \{q_s\} \\ \{q_c\} \end{bmatrix} = \begin{bmatrix} \{Q_o\} \\ \{Q_s\} \\ \{Q_c\} \end{bmatrix} \qquad (2\text{-}73)$$

2.11 Nonlinear Divergence

The steady deflection problem is solved by setting the sinusoidal terms in equation (2-73), $\{q_s\}$, $\{q_c\}$, $\{Q_s\}$, $\{Q_c\}$, and ω, to zero. The resulting n by n reduced set of non-linear equations can then be solved using the same numerical solver as for the full flutter problem.

Because the problem now contains nonlinear stalling effects in the aerodynamics, the analytic solution will no longer have a divergence velocity in the classical sense: once the wing begins to diverge, part of the wing span will begin to exceed the stall angle, thus reducing the lift and at some point preventing the angle of attack from further increasing. However, the linear divergence velocity can give insight into the full nonlinear behavior of the wing, as can be demonstrated by the following simple model.

A simplified nonlinear divergence problem can be set up using the same Rayleigh-Ritz method as for the full flutter problem, with the simplification that we now only consider one spanwise, linearly varying, torsional mode, and the lift remains at $C_{L_{max}}$ after stalling occurs. This would then give the spanwise variation of the angle of attack as,

$$\alpha(x) = \alpha_R + \frac{x}{\ell} q_2 \tag{2-74}$$

where α_R is the root angle of attack and q_2 is the torsional modal amplitude. (The notation q_2 is used so as to more closely resemble the notation for the torsional mode used in the full analysis.)

The potential energy and work terms are then given by,

$$Q_2 = \frac{1}{2} \rho U^2 \int_0^\ell \frac{x}{\ell} ce\, C_L(\alpha(x))\, dx$$

$$= \frac{1}{2} \rho U^2 \left[\int_0^{x_s} \frac{x}{\ell} C_{L_\alpha} (\alpha_R + \frac{x}{\ell} q_2)\, dx + \int_{x_s}^\ell \frac{x}{\ell} C_{L_\alpha} \alpha_s\, dx \right] \tag{2-75}$$

$$V = \frac{1}{2} \int_0^\ell GJ \left(\frac{d\alpha}{dx} \right)^2 dx = \frac{1}{2} \frac{GJ}{\ell} q_2^2 \tag{2-76}$$

where x_s, the spanwise location beyond which the wing is experiencing stall, is related to the stall angle α_s by the relation,

$$x_s = \frac{\alpha_s - \alpha_R}{q_2} \ell \qquad \text{if less than } \ell$$

$$\tag{2-77}$$

$$= \ell \qquad \text{otherwise}$$

Note that equation (2-77) is valid for both positive and negative stall angles, α_s. Putting equations (2-75) to (2-77) into the equation of motion, $dV/dq_2 = Q_2$, we get the implicit linear and cubic equations,

$$q_2 = \frac{3}{2}\frac{\tilde{Q}}{1-\tilde{Q}} \qquad \text{for } \frac{q_2}{\alpha_s - \alpha_R} < 1 \qquad (2\text{-}78a)$$

$$q_2^3 - \frac{3}{2}\tilde{Q}\alpha_s q_2^2 + \frac{1}{2}\tilde{Q}[\alpha_s - \alpha_R]^3 = 0 \qquad \text{for } \frac{q_2}{\alpha_s - \alpha_R} > 1 \qquad (2\text{-}78b)$$

where the non-dimensional dynamic pressure is given by,

$$\tilde{Q} = \frac{\frac{1}{2}\rho U^2 Ae\ell C_{L_\alpha}}{3GJ} \qquad (2\text{-}79)$$

Figure 5 shows solutions for various values of root angle of attack α_R, with an arbitrary stall angle $\alpha_s = 8^\circ$. This figure is in many ways insightful in its relationship to the classical divergence problem.

First, for root angle of attack $\alpha_R = 0^\circ$, divergence does not occur in the classical sense that at the divergence speed the amplitude of deflection grows to infinity. However, at and above the classical divergence speed ($\tilde{Q}=1$), equations (2-78a) and (2-78b) yield three possible solutions. One of these solution is the trivial solution, $q_2 = 0$, and is unstable – a small perturbation in q_2 will generate an aerodynamic force that cannot be restored by the torsional stiffness of the wing. Therefore, the amplitude continues to increase until it reaches one of the two non-zero values. So, although nonlinear divergence does not indicate an infinitely
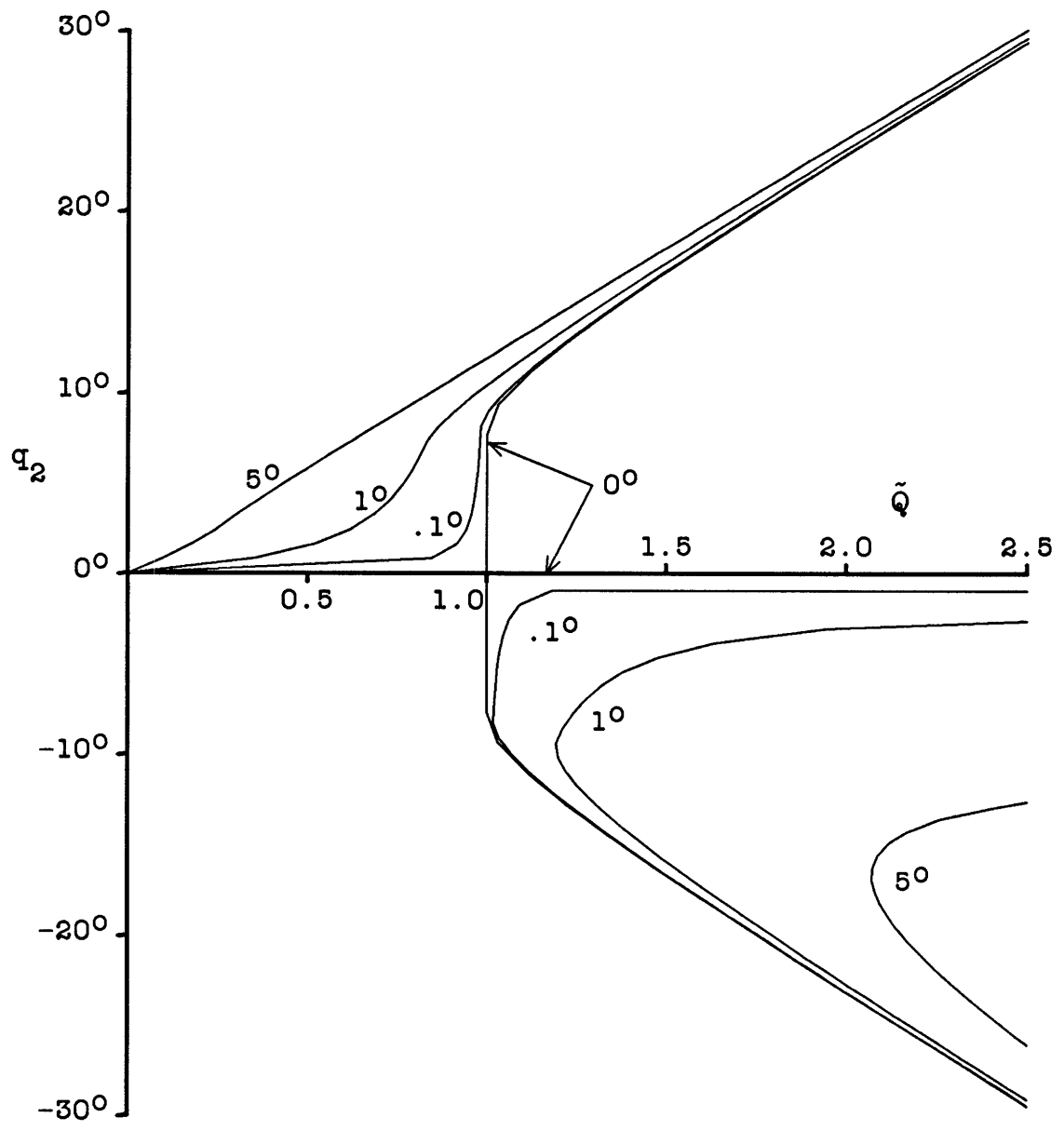
Figure 5. Analytic example of nonlinear divergence.

growing amplitude, it does indicate non-zero amplitude for zero angle of attack.

One also notes from Figure 5 the asymptotic behavior as $\tilde{Q}$ and q_2 grow large. For these values, the q_2^3 and $\alpha_s q_2^2$ terms are much larger than the $(a_s - a_R)^3$ term, thus leaving an equation which is independent of the root angle of attack a_R,

$$q_2^3 - \frac{3}{2}\tilde{Q}\alpha_s q_2^2 \approx 0 \qquad \text{for } \frac{q_2}{\alpha_s - \alpha_R} \gg 1 \qquad (2\text{-}80)$$

which leads to the asymptotic solution $q_2 = \frac{3}{2}\tilde{Q}\alpha_s$.

The full nonlinear divergence problem must be carried out numerically because of the complexity of those effects which were ignored in the simplified model. In the full model, the lift coefficient curve is less straightforward, and drag, moment, and three-dimensional spanwise effects are also included. The addition of more modes and bending-torsion coupling terms also add to the complexity. However, with this simple model we see what to expect from, and how to interpret, the results from the full nonlinear model.

CHAPTER III

EXPERIMENT

3.1 Test Specimen Preparation

The test specimens were constructed from Hercules AS4/3501-6 graphite/epoxy prepreg tape from Lot No. 4021-2, Spool Nos. 53A and 38A, using the standard TELAC manufacturing procedure [Ref. 18]. The laminates and curing materials were arranged on an aluminium curing plate as shown in Figure 6 and cured in a Baron model BAC-35 autoclave using the standard TELAC curing cycle described by Figure 7. After curing, the laminates were post-cured in a forced air circulation oven at 350° F for eight hours. After post-curing, rectangular test specimens 330 mm (13 in) long and 76 mm (3 in) wide were cut from the laminates using a diamond-coated cutting wheel mounted on an automatic feed, milling machine.

The plate was weighed to determine its density, and the thickness and width measured at several locations and averaged. These average measurements for each specimen appear in Appendix G, along with the nominal values. The laminates were also weighed on an electronic balance, from which the material density (ρ) for each specimen was calculated.

Loading tabs 76.2 mm (3 in) x 25.4 mm (1 in) were machined from 3.2 mm (1/8 in) aluminum plate and bonded to the base of each test specimen with FM-123-2 film adhesive, cured using the standard TELAC bond curing cycle. The loading tabs were intended to aid in aligning the test specimen in the

Vacuum Bag

Porous
Teflon

Aluminum
Top Plate

Fiberglass
Air Breather

Paper Bleeder

Specimen

Nonporous Teflon

Aluminum Cure Plate
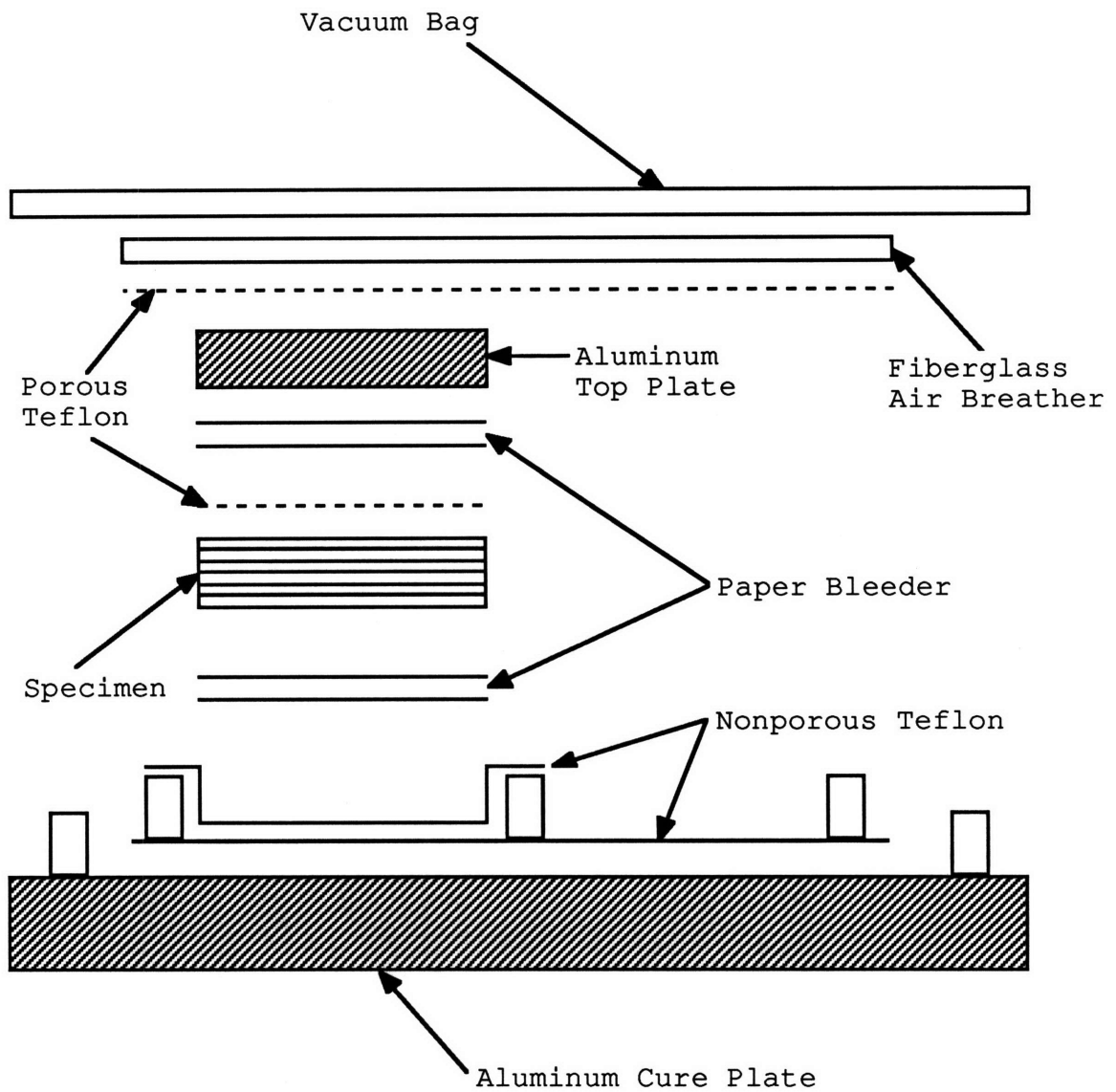
Figure 6. Cross-section of symmetric curing assembly
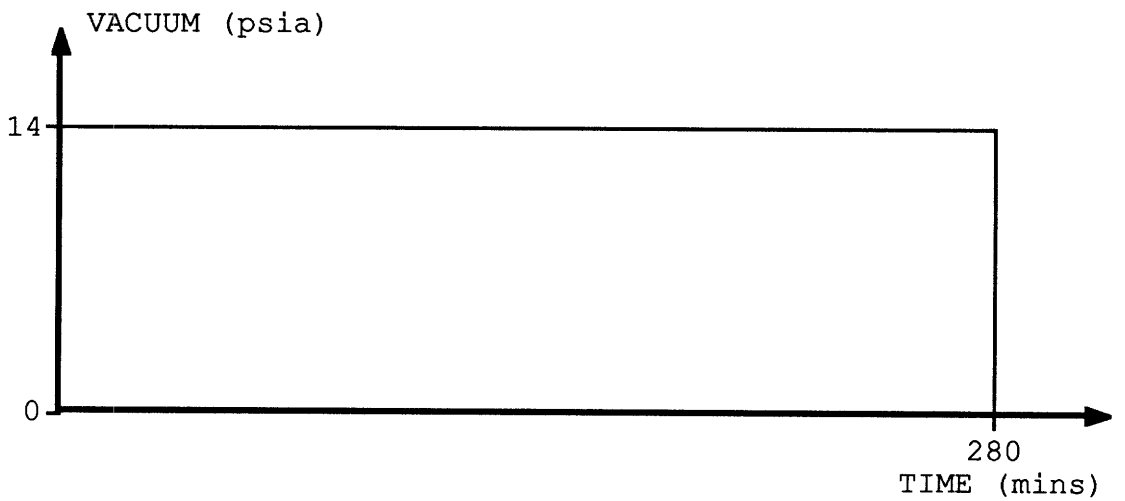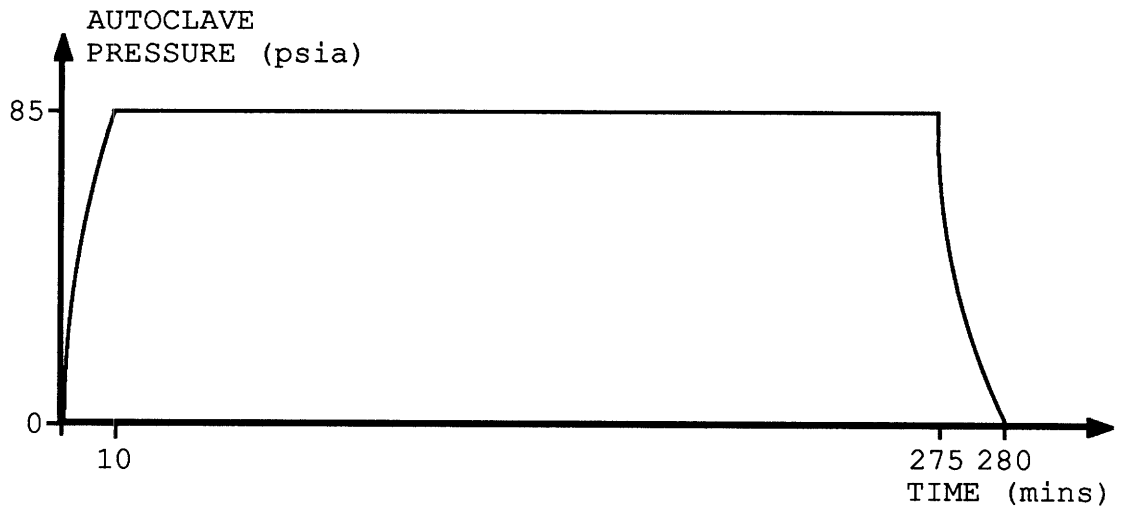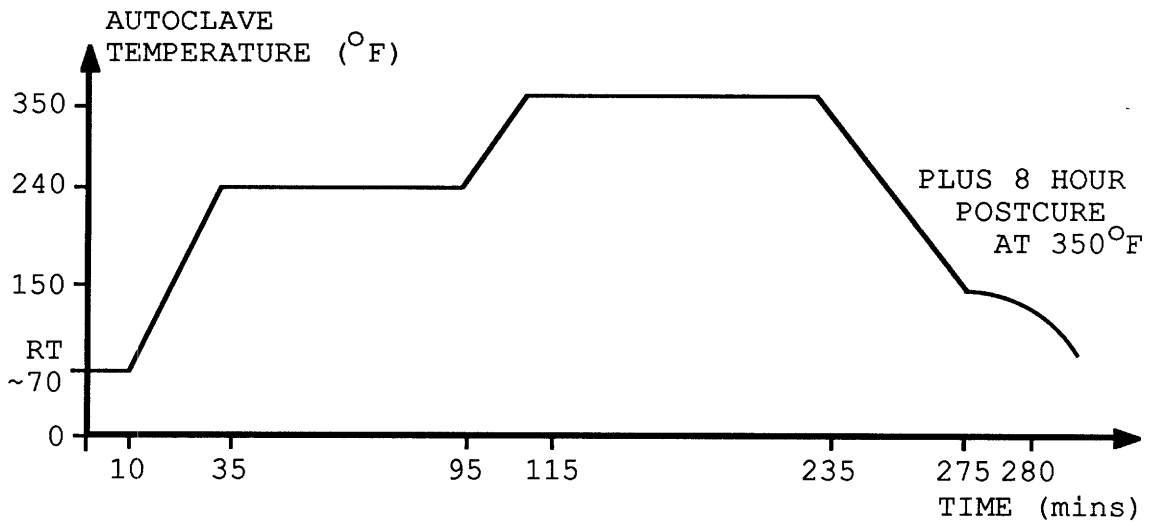
Figure 7. TELAC cure cycle

clamping fixture and to prevent damage to the plate surface fibers.

To get an indication of the lateral deflections, strain gauges were attached to the base of each test specimen at the midchord, as shown in Figure 8. Two Micro-Measurement EA-06-125AD-120 strain gauges, from Lot No. R-A38AD297 with a gauge factor of 2.055, were attached to both sides of each specimen to measure bending strain. Two Micro-Measurement EA-06-250TK-120 strain gauges, from Lot No. R-A38AD286 with a gauge factor of 2.02, were attached to both sides of each specimen to measure torsion strain. The two bending gauges were wired together as a two-arm bridge circuit with three external lead wires. The two torsion gauges were wired together as a four-arm bridge circuit with four external lead wires. Wiring the strain gauges in this manner provided automatic temperature compensation. Finally, the gauges and exposed wiring were coated with Micro-Measurement M-Coat A, an air-drying polyurethane.

The NACA-0012 fairings were cut from 254 mm (10 in) blocks of styrofoam using a hot wire cutter running over an aluminum template. The fairings were then epoxied to the top and bottom of the graphite/epoxy plates and slit chordwise at 63.5 mm (2.5 in) intervals to relieve some of the bending and torsion stiffness.

STYROFOAM FAIRINGS

GRAPHITE/EPOXY
6 PLY LAMINATE

ALUMINIUM LOADING TABS

$2\frac{1}{4}$"

$1\frac{1}{2}$"

3 "

$1\frac{1}{2}$"

10 "

1 "

13 "
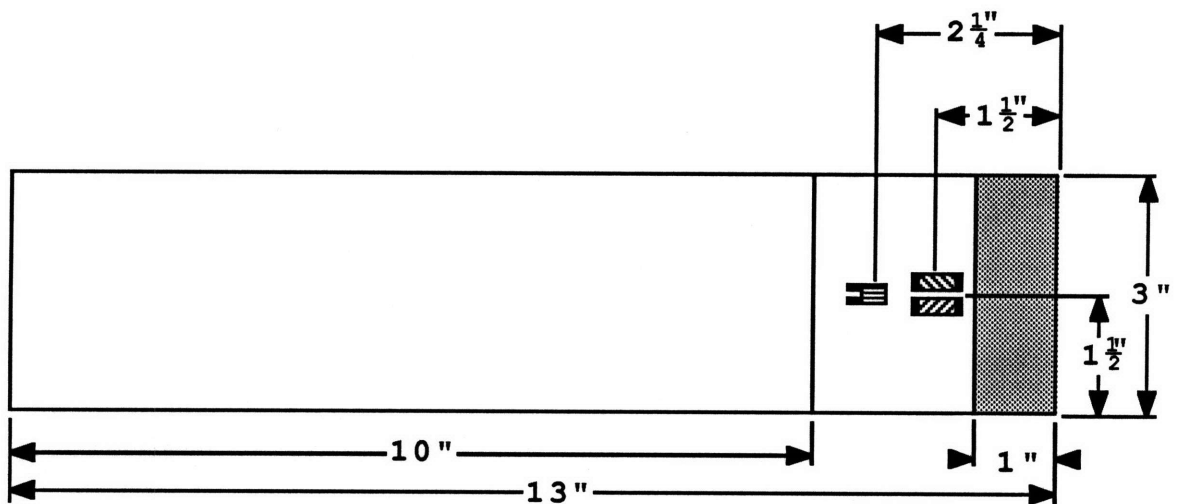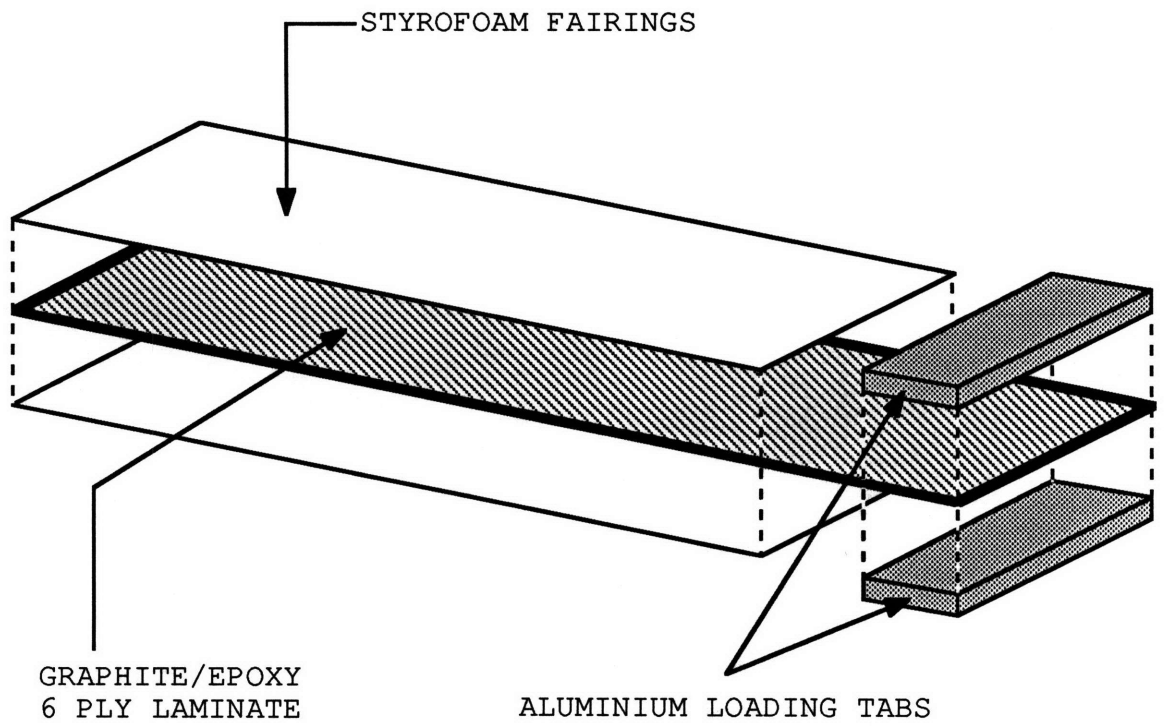
Figure 8. Wing construction and specimen dimensions

3.2 Static Deflection Tests

The static deflection test setup is shown in Figure 9.
It consisted of a clamping device bolted to a large aluminum
table (the "optics bench" at M.I.T.'s Facility for Experimen-
tal Structural Dynamics). Two low friction pulleys were at-
tached to vertical rods such that a force or moment could be
applied to the test specimen at its tip. Rulers, graduated
in millimeters, were attached to Dexion angle-iron to facili-
tate measuring the test specimens' tip deflections. A de-
flection indicator, consisting of wooden dowels and thin
spring-steel for pointers, was constructed. Threads, routed
over the pulleys and attached to weights, could be attached
at any point along the wooden dowels so as to transfer either
a force or a moment to the test specimen.

The deflection indicator was aligned with the tip of the
test specimen and the test specimen clamped in the vise. For
the tip force test, the pulleys were aligned with the plate
midchord and threads from the center of the wooden dowels
were routed over the pulleys. Weights in increments of
5 grams were successively attached to the threads, first to
give positive deflections, then to give negative deflections.
As each weight was attached, the readings from both pointers
were recorded, along with the applied weight and the measured
bending and torsion strains.

Next, the pulleys were aligned with the leading and
trailing edge of the plate tip and the threads routed from

LOW
FRICTION
PULLEY

TIP
MEASURING
RULER

MASS

CANTILEVERED
GR/EP SPECIMEN
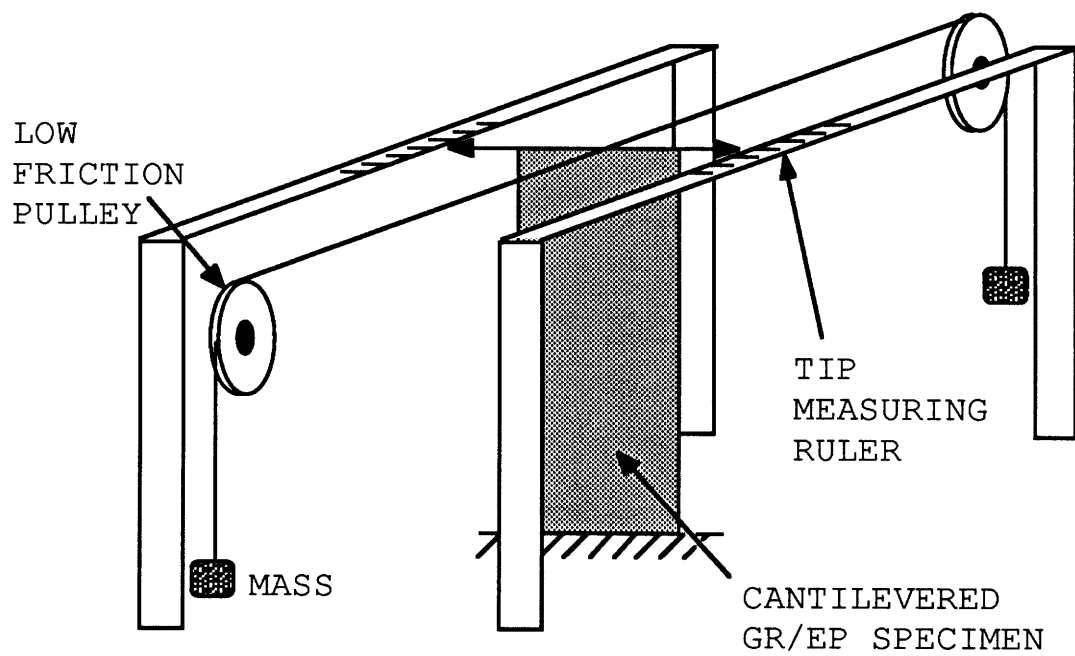
Figure 9. Static deflection test setup

the plate corners over the pulleys, so as to produce a positive moment when equal weights were attached. Weights of 5 gram increments were successively attached to each thread of the couple, and readings from the pointers and the strain gauges were again recorded along with the applied weights. The pulleys were then switched to diagonal opposites of the plate so that negative moments could be applied, and the same procedure applied.

For each data point, the lateral deflection of the elastic axis and the rotation about the elastic axis were calculated from the pointer measurements. The lateral and angular deflections were plotted versus applied tip force for each test specimen, and compared against the 5-mode Rayleigh-Ritz with cubic stiffening. Similarly, the lateral and angular deflections were plotted versus applied tip moment for each test specimen, and compared against the same analysis. Linearized fits between lateral deflection and bending strain, and between angular deflection and torsion strain, were conducted so that a linear relation could be later applied to the flutter tests. The results of the static deflection tests are discussed in section 4.2.

3.3 Free Vibration Tests

The free vibration test setup, shown in Figure 10, used the same clamping device as the static deflection tests. The oscillating force was applied to the test specimen by first attaching a small 0.5" x 0.5" steel strip near the root of

the test specimen using double-sided adhesive tape. A magnetic probe was then placed near the steel strip. The oscillating signal was generated by a Wavetek Model 132 Signal Generator, and amplified to the magnetic probe using a General Radio Company Unit Amplifier Type 1206-B, thus producing the necessary oscillating force. In addition, the input signal was sent to a Tektronix 2213 dual beam oscilloscope to be compared with the measured deflection. The deflection was measured by first attaching a small 0.5" x 0.5" strip of adhesive aluminum tape to the opposite side of the test specimen, near the plate tip. A proximity probe was then placed near the aluminum tape. The signal from the proximity probe was passed through a 7200 11mm transducer, an AP Variable Frequency Filter to eliminate any noise in the signal, and finally to the Tektronix 2213 oscilloscope so as to be compared against the original input signal.

Each test began with the signal generator set below 5 Hz. The frequency was slowly increased until the first bending mode was excited, i.e. when the vibration amplitude peaked and the output signal was observed to be 90° out of phase with the input signal. The frequency was recorded and the node lines recorded using a "chatter" test: the tip of a pencil was moved along the surface of the plate and a node point observed when the pencil no longer chattered against the vibrating plate. This procedure was repeated for the second bending and first torsion vibration modes.
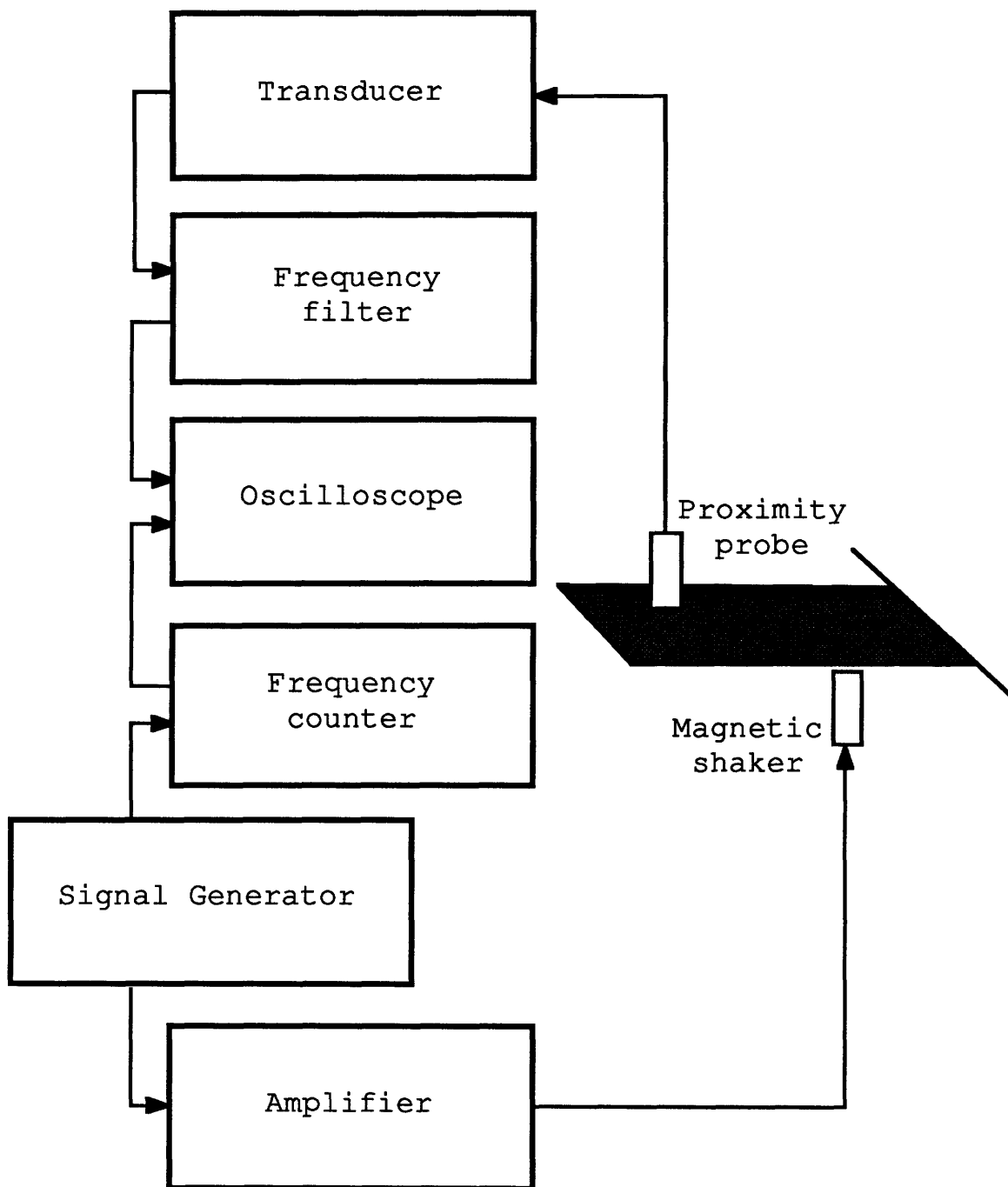
Figure 10. Free vibration instrumentation setup

In addition, "pluck" tests were also conducted to verify the free vibration frequencies of the wings. The wings would either be sharply tapped or given a brief, sharp torsional force, hopefully exciting several of the lower bending and torsion modes. The strain gauge readings were recorded on a Nicolet digital oscilloscope, and passed through a Fourier analyzer so as to decompose the frequency content of the signal. The results of the free vibration tests are discussed in Section 4.3.

3.4 Wind Tunnel Tests

All wind tunnel tests were conducted in the M.I.T. Department of Aeronautics and Astronautics acoustic wind tunnel. The acoustic wind tunnel is a continuous flow tunnel with a 1.5 m (5 ft) x 2.3 m (7.5 ft) free jet test section 2.3 m (7.5 ft) long. The tunnel was powered by a 100 HP motor giving it a continuously variable velocity range of 0 m/s to 30 m/s (0 ft/sec to 105 ft/sec). The tunnel control panel was located outside the chamber and the velocity was controlled by two levers (coarse and fine speed control). The coarse lever controlled the motor field current and was variable in fixed step increments only; the fine lever controlled the motor shunt current and was continuously variable. There was a 400 amp current limitation on the motor, which was protected by circuit breakers. The tunnel velocity was read from an alcohol manometer, calibrated in inches of alcohol, located at the control panel. This manometer was

connected to a pitot tube located slightly forward of the test section.

The test setup, shown in Figures 11 and 12, consisted of a turntable machined from aluminum, mounted on a 914 mm (36 in) tall, cylindrical pedestal made of 51 mm (2 in) thick steel pipe, 305 mm (24 in) in diameter. The pedestal was mounted to the floor of the wind tunnel section. A wooden cover disk 762 mm (30 in) in diameter was used to ensure the pedestal did not affect the flow over the test specimen, and thus provided smooth airflow past the test specimen. A pointer attached to the free rotating portion of the turntable, and an angle indicator attached to the fixed base of the turntable, provided a consistent means of reading the angle of attack of the test specimen.

The bending and torsion strain gauges were wired to a terminal strip attached to the fixed pedestal, which was in turn wired to 2120 Strain Gauge Amplifiers. The amplifiers had a two-arm D.C. bridge installed in channel 1 for the bending gauges and a four-arm D.C. bridge installed in channel 2 for the torsion gauges. The bending and torsion outputs from the Strain Gauge Amplifiers were fed to a Nicolet Digital Oscilloscope where the signals could be recorded on floppy disk. Visual data was recorded by placing a mirror at a 45° angle above the test setup, and recording on videotape the overhead view of the tip deflections. For sinusoidal flutter motion, a strobe light was used to help visualize the oscillations.

TEST SPECIMEN

GROUND PLANE

ROTATING
SPECIMEN STAND

NON-ROTATING
TEST STAND
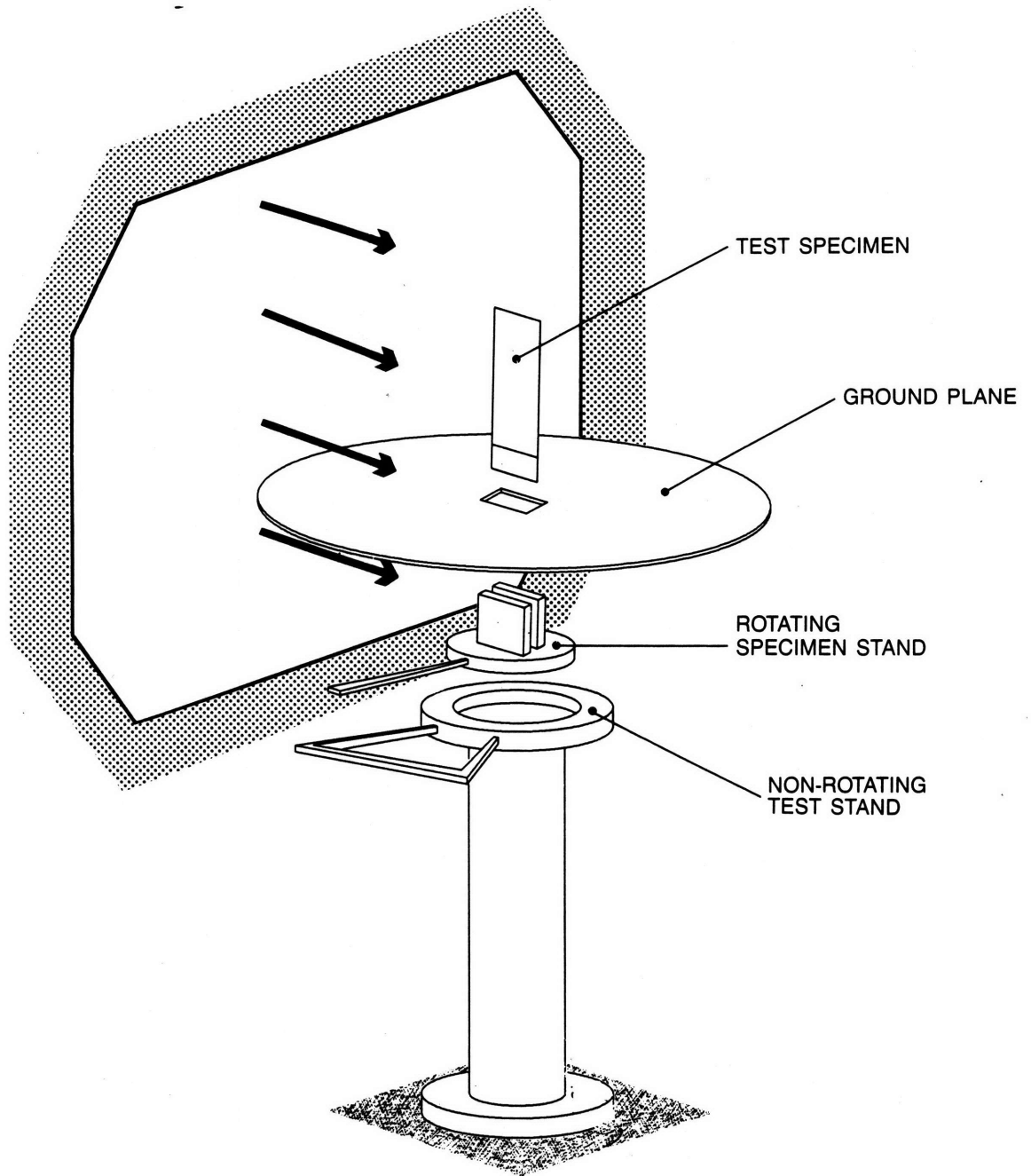
Figure 11. Wind tunnel test stand
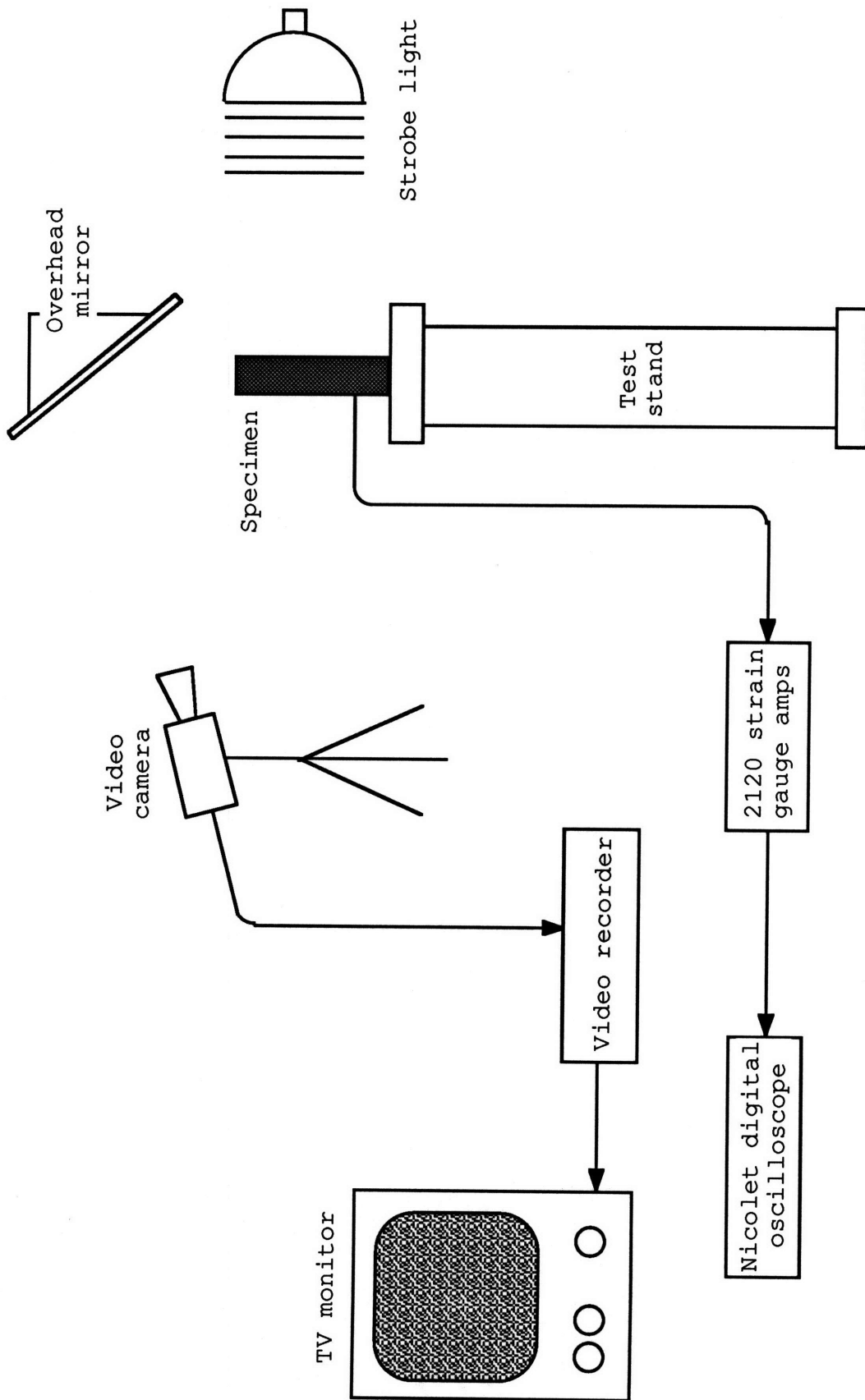
Figure 12. Wind tunnel instrumentation setup

CHAPTER IV
RESULTS & DISCUSSION

4.1 Computer Implementation

The theory described in Chapter 2 was implemented using Fortran code on the MicroVax facility at the Facility for Experimental Structural Dynamics at the Aeronautics and Astronautics Department of M.I.T. The listing of the principal Fortran programs and subroutines is given in Appendix H. A flowchart briefly describing the functions of each of these programs is given in Figure 13.

4.2 Static Deflections

The experimental results of the static deflection tests for the $[0_2/90]_s$, $[90/0_2]_s$, $[+15_2/0]_s$, and $[-30_2/0]_s$ flat plates are compared in Figures 14a to 14d with the 5-mode Rayleigh-Ritz analysis described in Section 2.5. The results for the $[-15_2/0]_s$ flat plate are not presented because they reflect the same results as for the $[+15_2/0]_s$ flat plate, except with the signs of the moment-deflection and force-twist coupling terms changed. The experimental results for the same laminates with NACA-0012 styrofoam fairings are likewise compared to analysis in Figures 15a to 15c. Deflection tests were not conducted for the $[-30_2/0]_s$ wing. Symbols indicate experimental data, solid lines indicate analysis with cubic stiffening, dashed lines without cubic stiffening.

These figures show excellent agreement between experiment and analysis. Note that the figures also indicate a slight asymmetry in the experimental bending characteristics. This may be due, in part, to small errors in manufacturing, which cause some initial warping of the flat plates. Finally, it is noticed that the styrofoam fairing stiffens the wings in torsion, but comparatively little in bending.
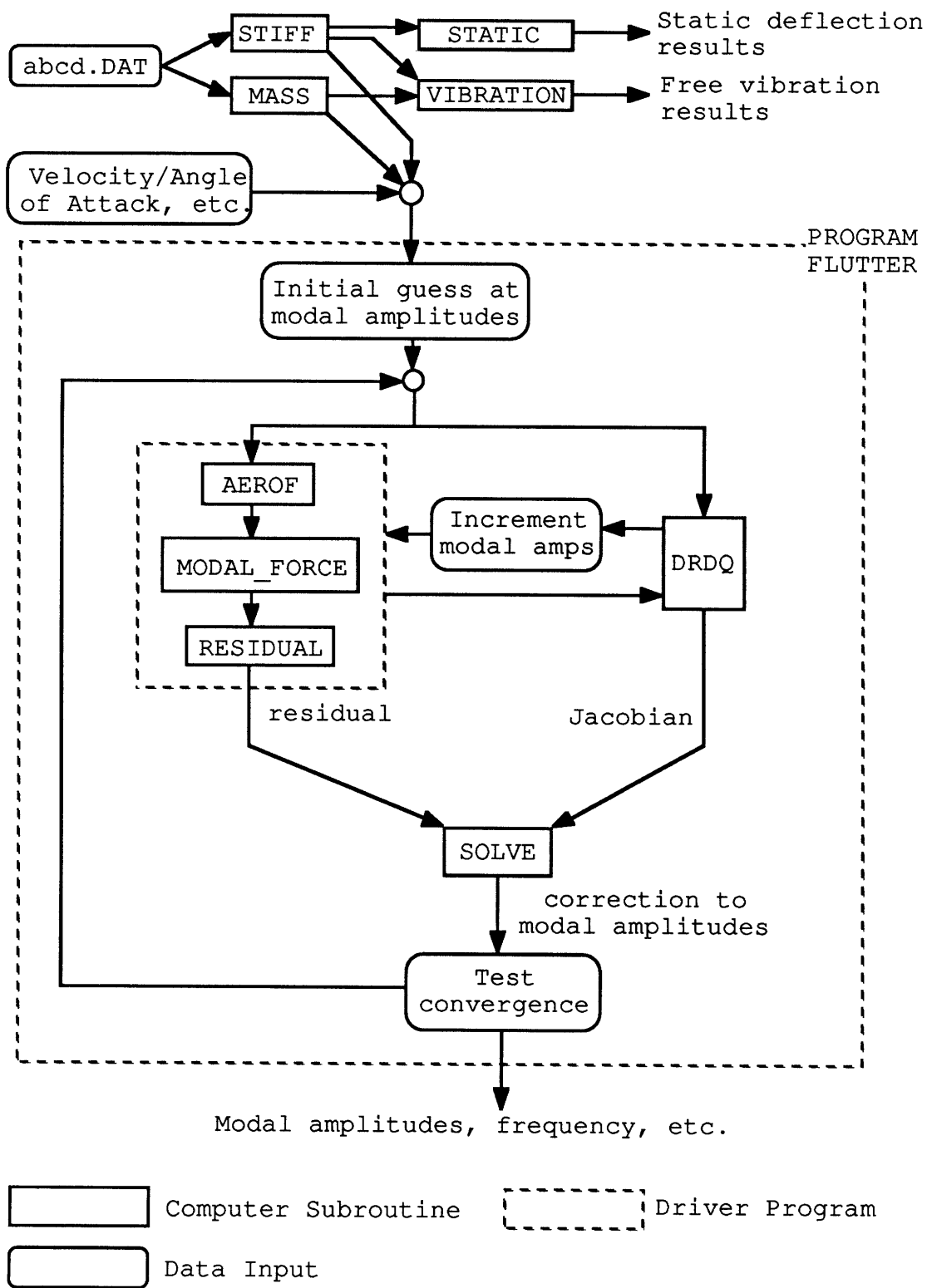
Figure 13. Flow chart of computer programs

Short Definition of Programs

Subroutine STIFF   – calculates stiffness matrix for bare plates and wings

Subroutine MASS   – calculates mass matrix for bare plates and wings

Subroutine STATIC   – calculates analytic static deflection results

Subroutine VIBRATION   – calculates analytic free vibration results

Subroutine AEROF   – calculates 2-dimensional, nonlinear aerodynamics for oscillating angle of attack and 1/4-chord deflection

Subroutine MODAL_FORCE – spanwise integrates 2-dimensional aerodynamic forces to give oscillating modal forces

Subroutine RESIDUAL   – combines aerodynamic modal forces with structural terms to give residuals for Newton-Raphson solver

Subroutine DRDQ   – calculates Jacobian matrix required for Newton-Raphson solver by numerically evaluating derivatives in each direction of state vector

Subroutine SOLVE   – calculates required step in Newton-Raphson solver to drive the residual to zero

Program FLUTTER   – driver program to take inputs from STIFF and MASS subroutines, with desired experiment characteristics (velocity, angle of attack, etc.), and solve nonlinear flutter problem

Figure 13 (cont'd). Description of computer programs

-81-
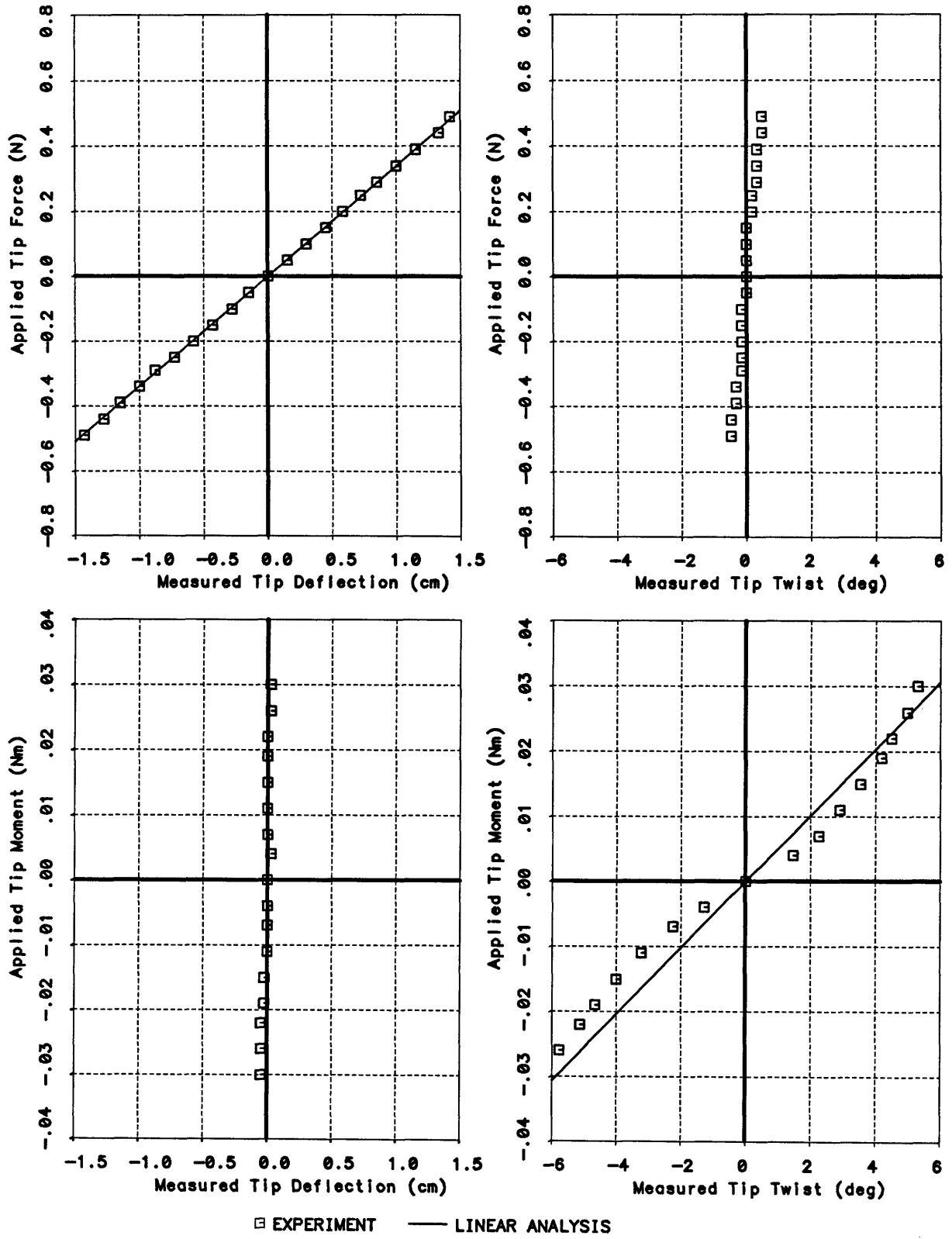
Figure 14a. Static deflection results for $[0_2/90]_s$ plate
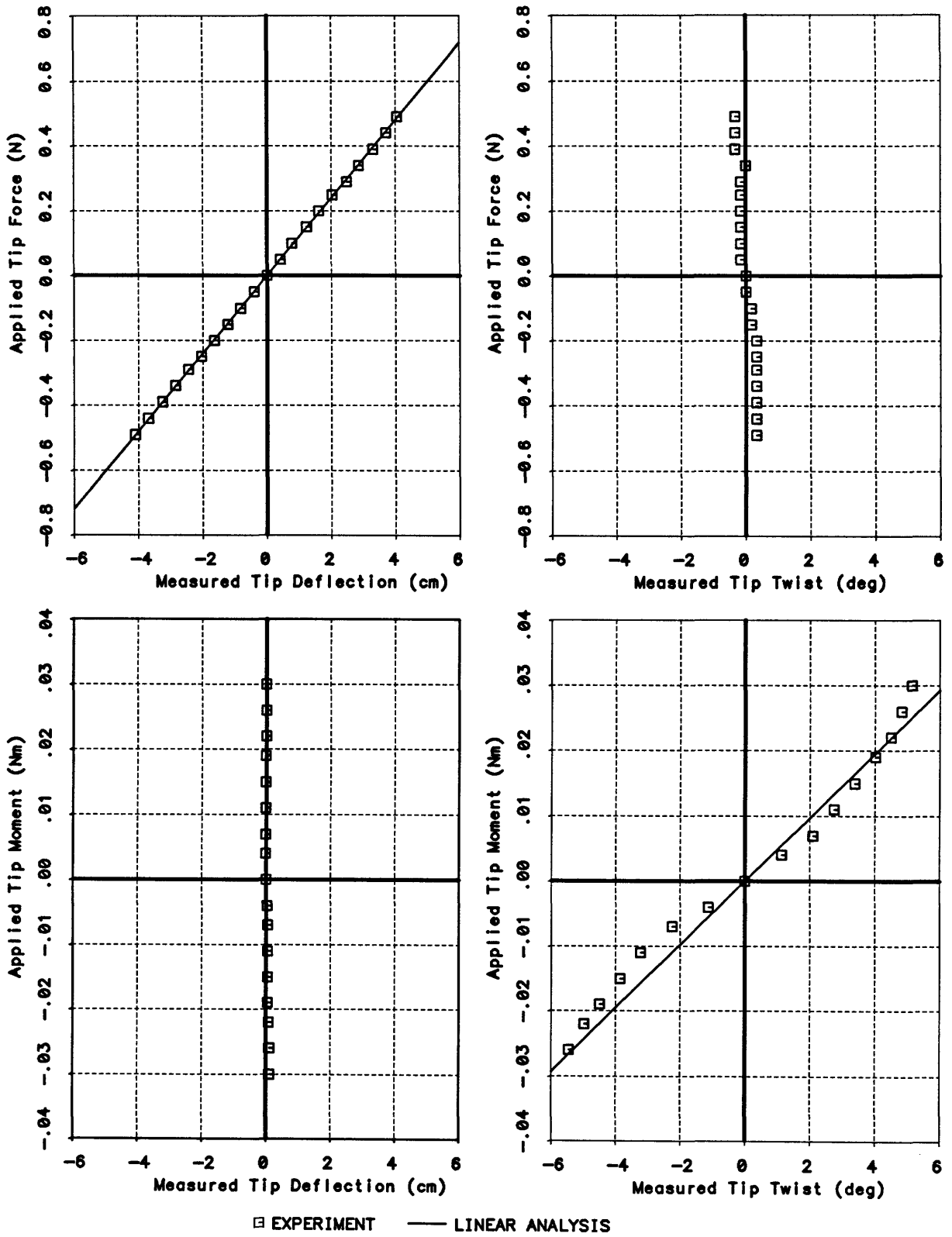
Figure 14b. Static deflection results for $[90/0_2]_s$ plate
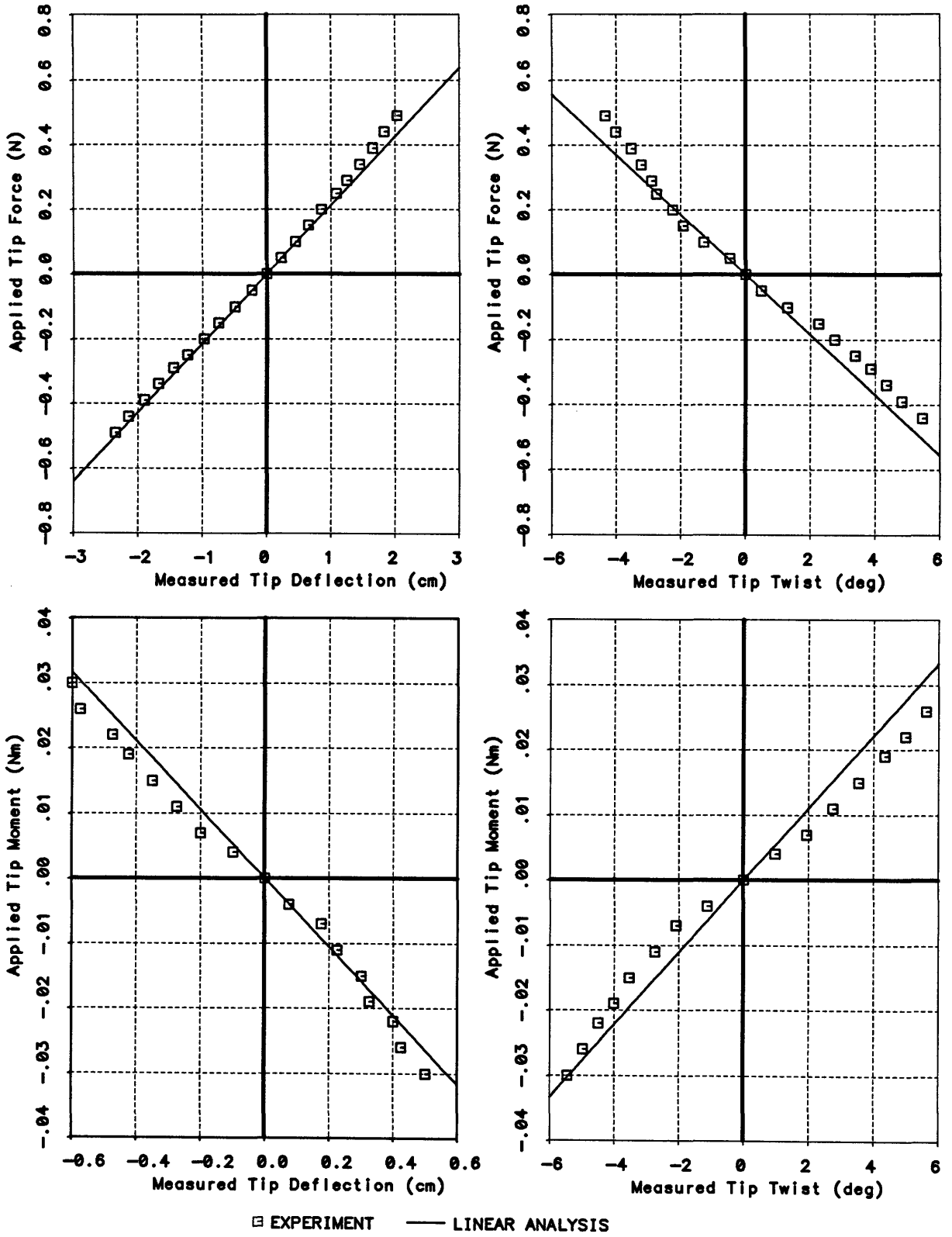
Figure 14c. Static deflection results for $[+15_2/0]_s$ plate
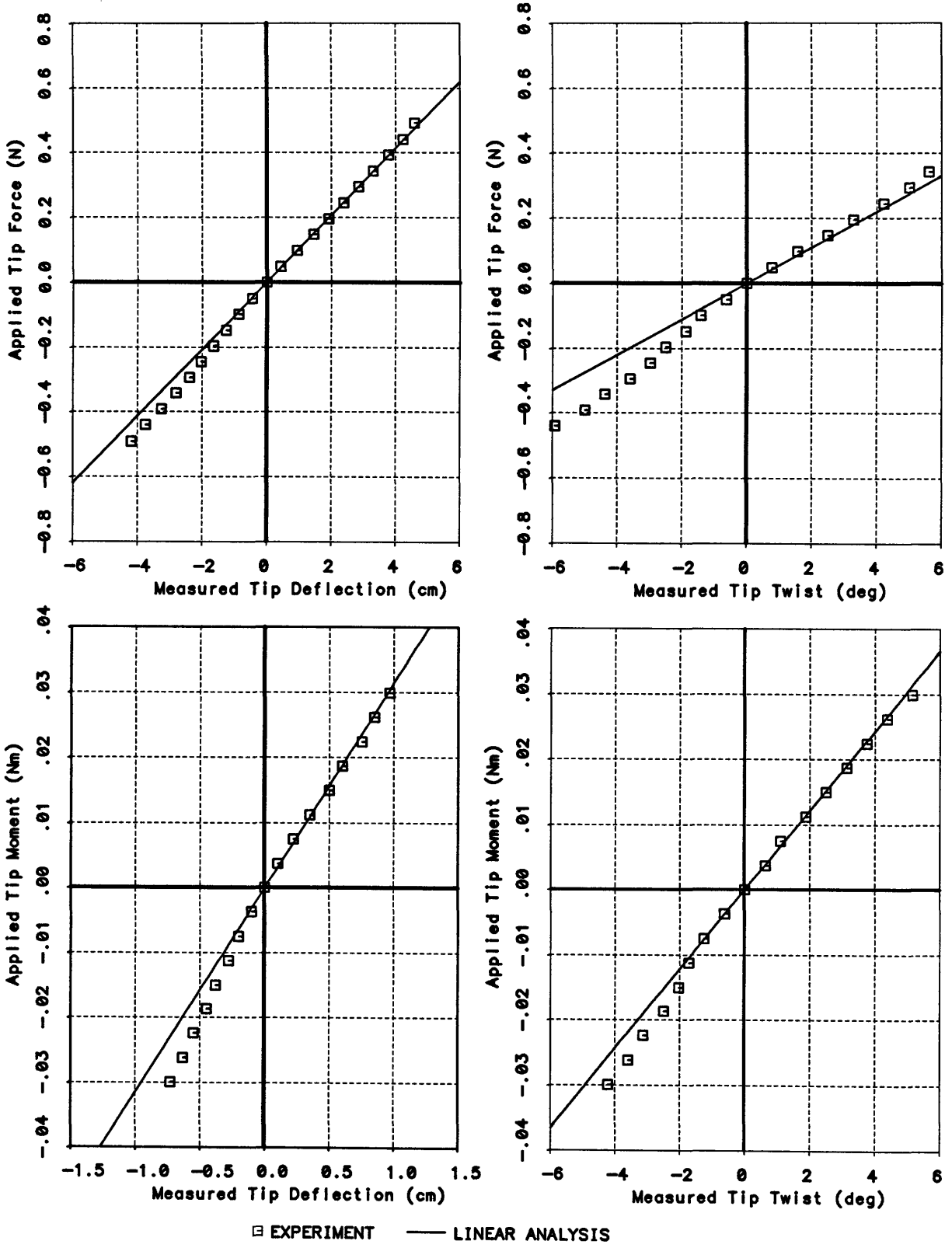
Figure 14d. Static deflection results for $[-30_2/0]_s$ plate
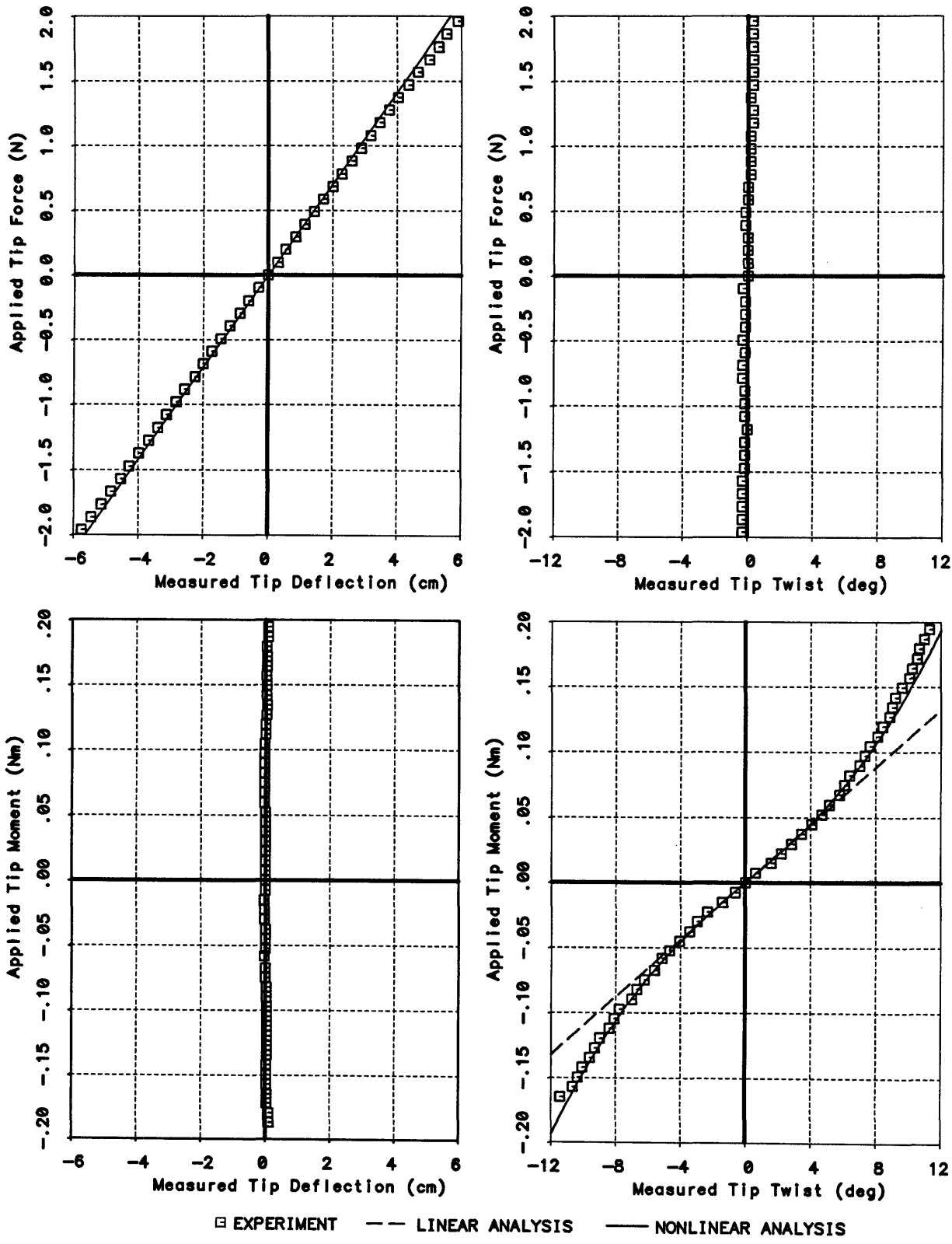
Figure 15a. Static deflection results for $[0_2/90]_s$ wing
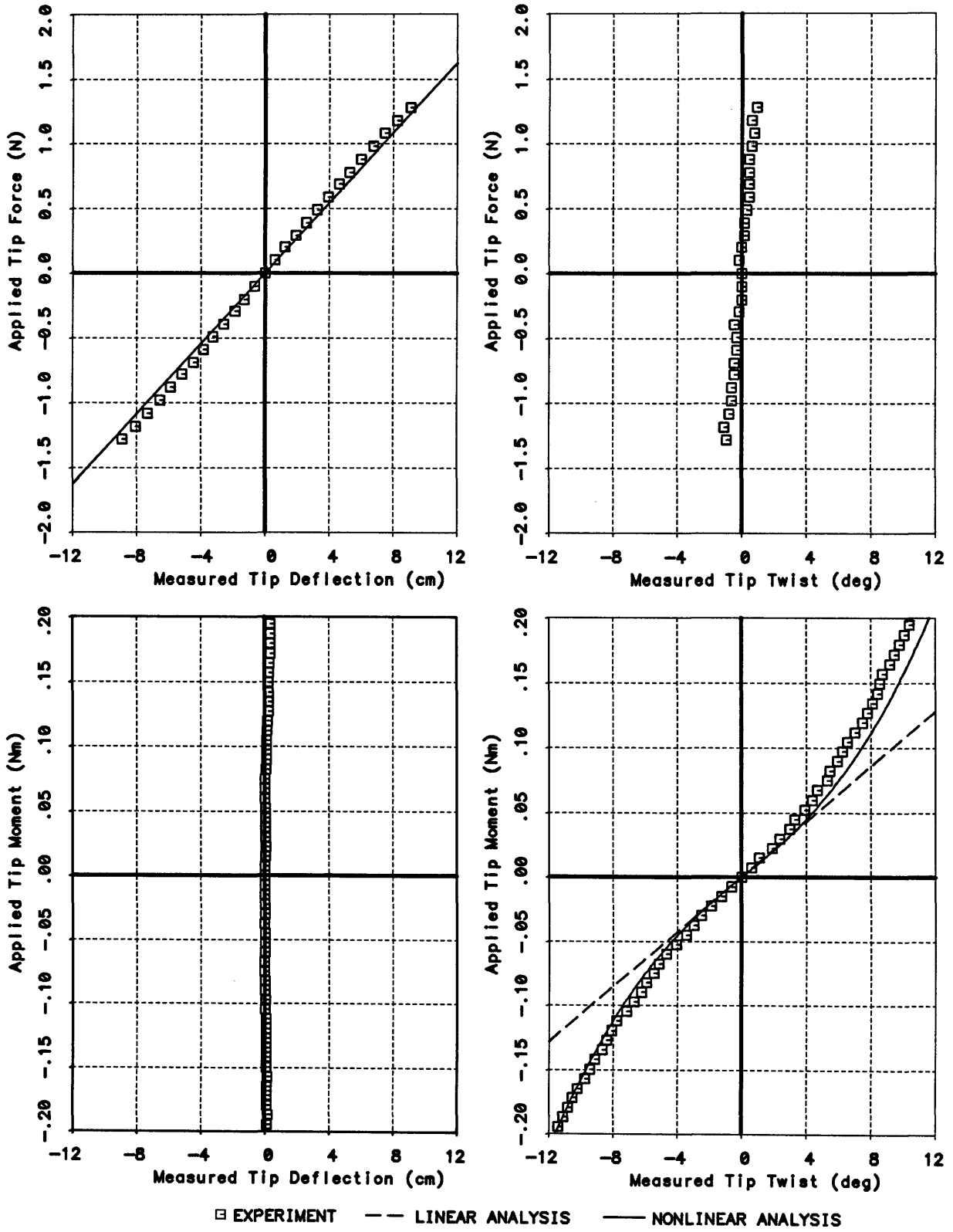
Figure 15b. Static deflection results for $[90/0_2]_s$ wing
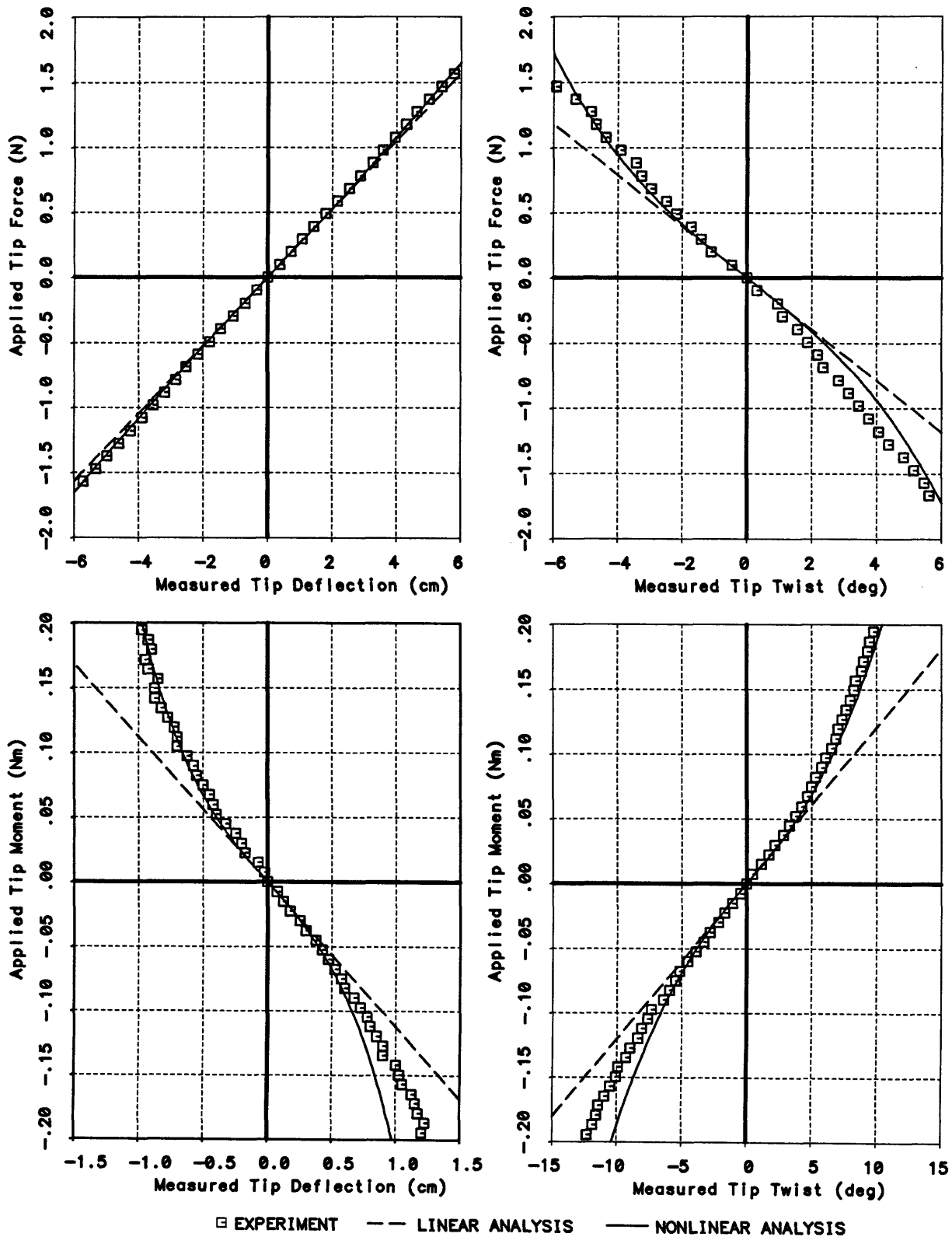
Figure 15c. Static deflection results for $[+15_2/0]_s$ wing

4.3 Free Vibration Frequencies and Modes

Natural vibration frequencies for the flat plates and the NACA-0012 wings were determined both experimentally and analytically, and are tabulated in Table 1. Although these are listed as 1st bending (1B), 1st torsion (1T), and 2nd bending (2B), with highly coupled laminates this distinction becomes much less meaningful because of the high bending-torsion coupling. The coupling of these modes is more evident by comparing the mode shapes of the coupled laminates with those of the uncoupled laminates.

The mode shapes for natural vibration were also determined experimentally and analytically for the flat plates. The resulting experimental and analytic node lines are plotted in Figures 16a to 16d. The node line of the first bending mode is not presented since it simply runs along the root of the laminate.

Both the experimental frequencies and mode shapes show excellent agreement with the analysis for the bending modes and the first torsional mode. The higher modes are less well predicted by the analysis, but they are less important in the final analysis since they are only intended as corrections to the more important lower modes. As with the static deflections results, the vibration results also indicate that the styrofoam fairing stiffens the wings in torsion, but comparatively little in bending. In fact, the bending frequencies are lowered because of the added weight of the styrofoam.

FLAT PLATES					
	Experiment			Analysis		
	1B	1T	2B	1B	1T	2B
$[0_2/90]_s$	11.0	35.0	67.7	11.0	38.7	69.1
$[90/0_2]_s$	6.6	36.0	40.6	6.6	35.8	41.1
$[+15_2/0]_s$	8.8	41.6	61.6	8.9	42.7	64.3
$[-15_2/0]_s$	8.8	41.8	63.6	8.9	42.7	64.3
$[-30_2/0]_s$	6.4	57.7	36.3	6.2	58.0	39.9

NACA-0012 WINGS					
	Experiment			Analysis		
	1B	1T	2B	1B	1T	2B
$[0_2/90]_s$	9.9	50.1	63.2	10.5	51.2	66.1
$[90/0_2]_s$	6.3	45.9	40.5	6.4	47.9	41.4
$[+15_2/0]_s$	8.8	52.8	61.9	9.1	52.4	65.1
$[-15_2/0]_s$	8.6	52.1	61.4	9.1	52.4	65.1
$[-30_2/0]_s$	6.3	63.0	43.5	6.7	66.4	44.6

Table 1. Free vibration frequencies (all values in Hz)

1ST TORSION MODE ; EXPERIMENT = 35.0 Hz ; ANALYSIS =38.7 Hz

2ND BENDING MODE ; EXPERIMENT = 67.7 Hz ; ANALYSIS = 69.1 Hz

2ND TORSION MODE ; EXPERIMENT = 118.4 Hz ; ANALYSIS = 130.7 Hz

-------- EXPERIMENT ——————— 5-MODE RAYLEIGH-RITZ ANALYSIS
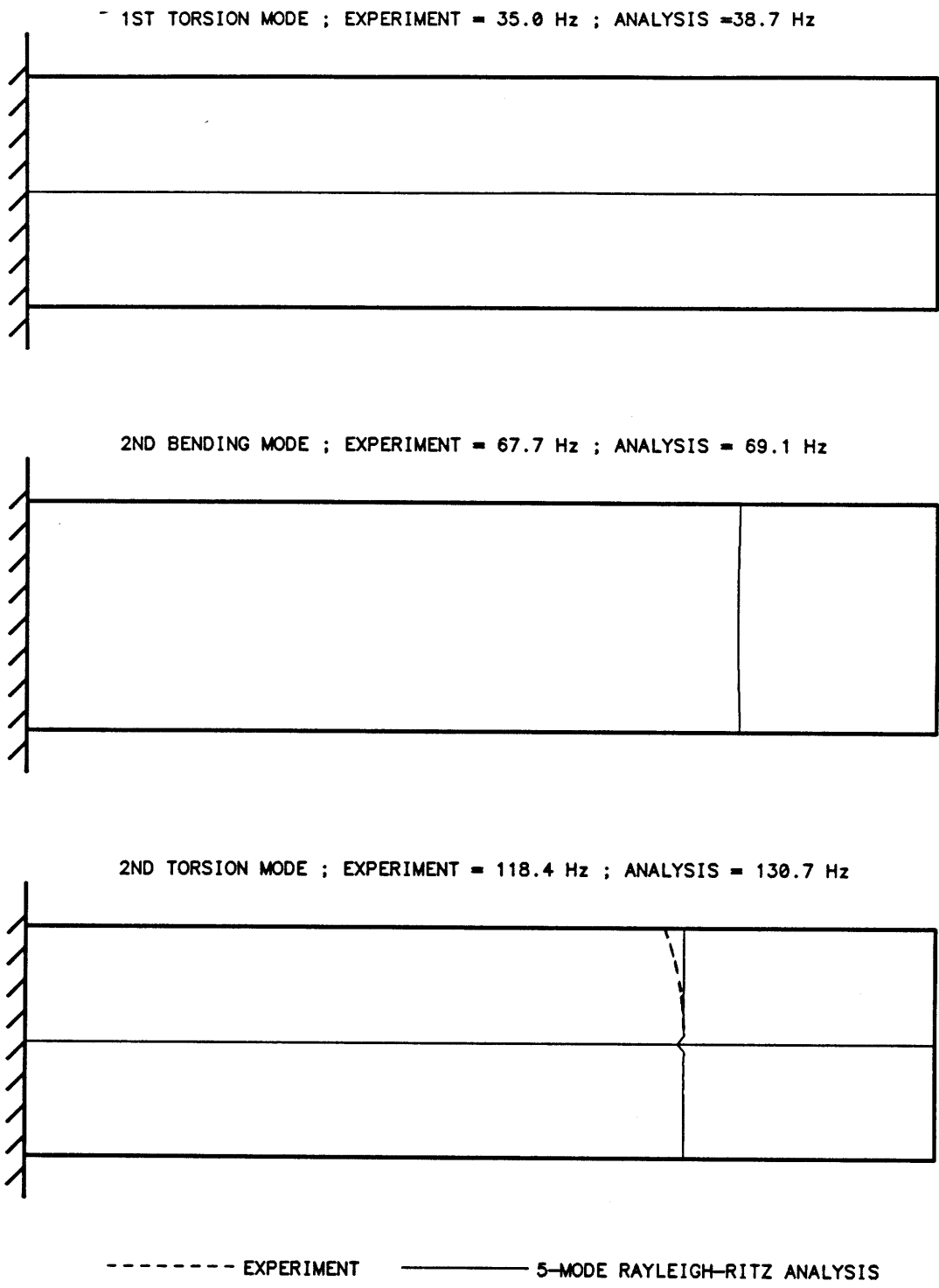
Figure 16a. Free vibration mode shapes for $[0_2/90]_s$ plate

1ST TORSION MODE ; EXPERIMENT = 36.0 Hz ; ANALYSIS = 35.8 Hz

2ND BENDING MODE ; EXPERIMENT = 40.6 Hz ; ANALYSIS = 41.1 Hz

2ND TORSION MODE ; EXPERIMENT = 106.0 Hz ; ANALYSIS = 114.0 Hz

- - - - - - - EXPERIMENT   ——————— 5–MODE RAYLEIGH–RITZ ANALYSIS
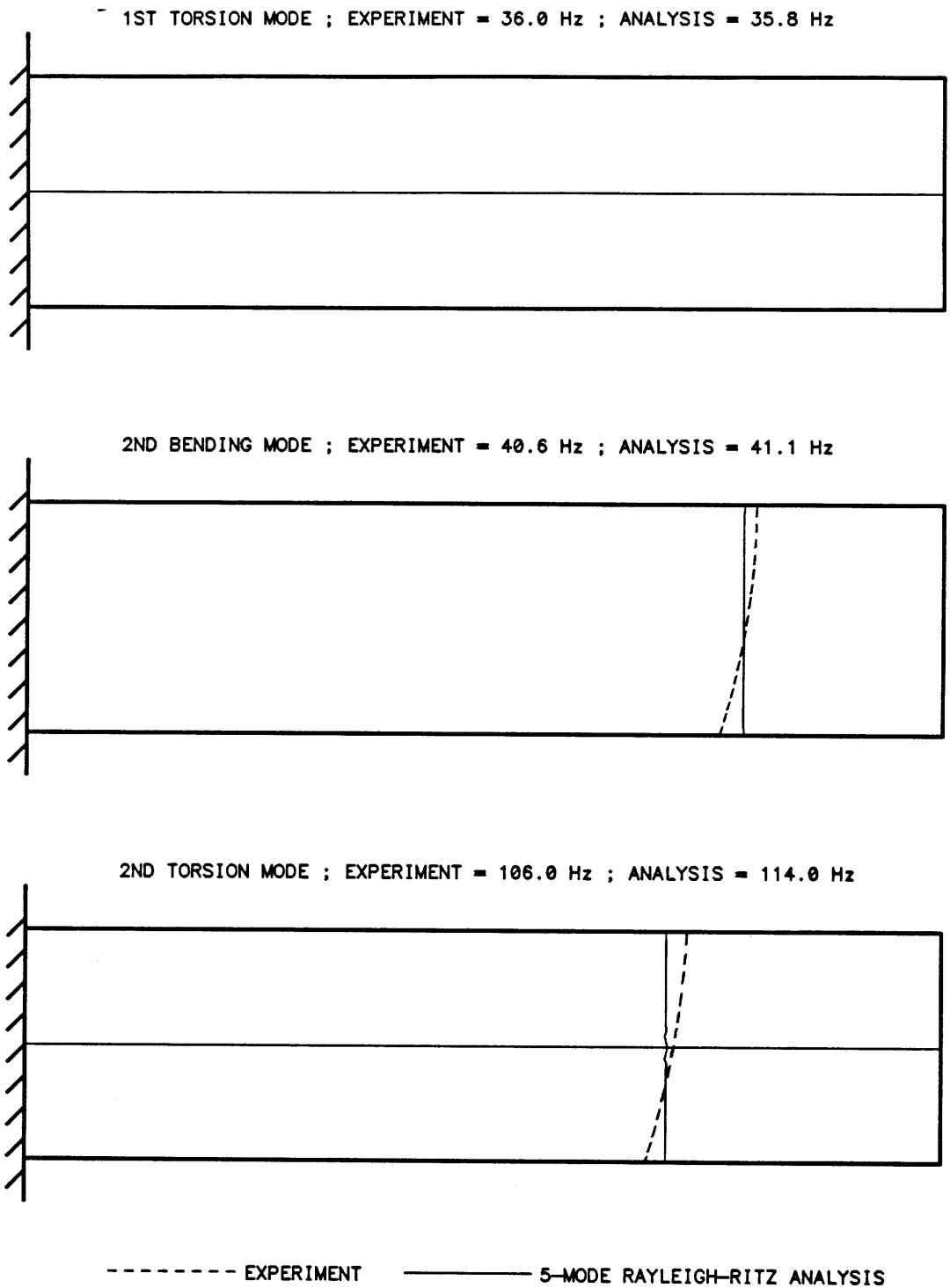
Figure 16b. Free vibration mode shapes for $[90/0_2]_s$ plate

1ST TORSION MODE ; EXPERIMENT = 41.6 Hz ; ANALYSIS = 42.7 Hz

2ND BENDING MODE ; EXPERIMENT = 61.6 Hz ; ANALYSIS = 64.3 Hz

2ND TORSION MODE ; EXPERIMENT = 113.8 Hz ; ANALYSIS = 163.8 Hz

-------- EXPERIMENT ——————— 5-MODE RAYLEIGH-RITZ ANALYSIS
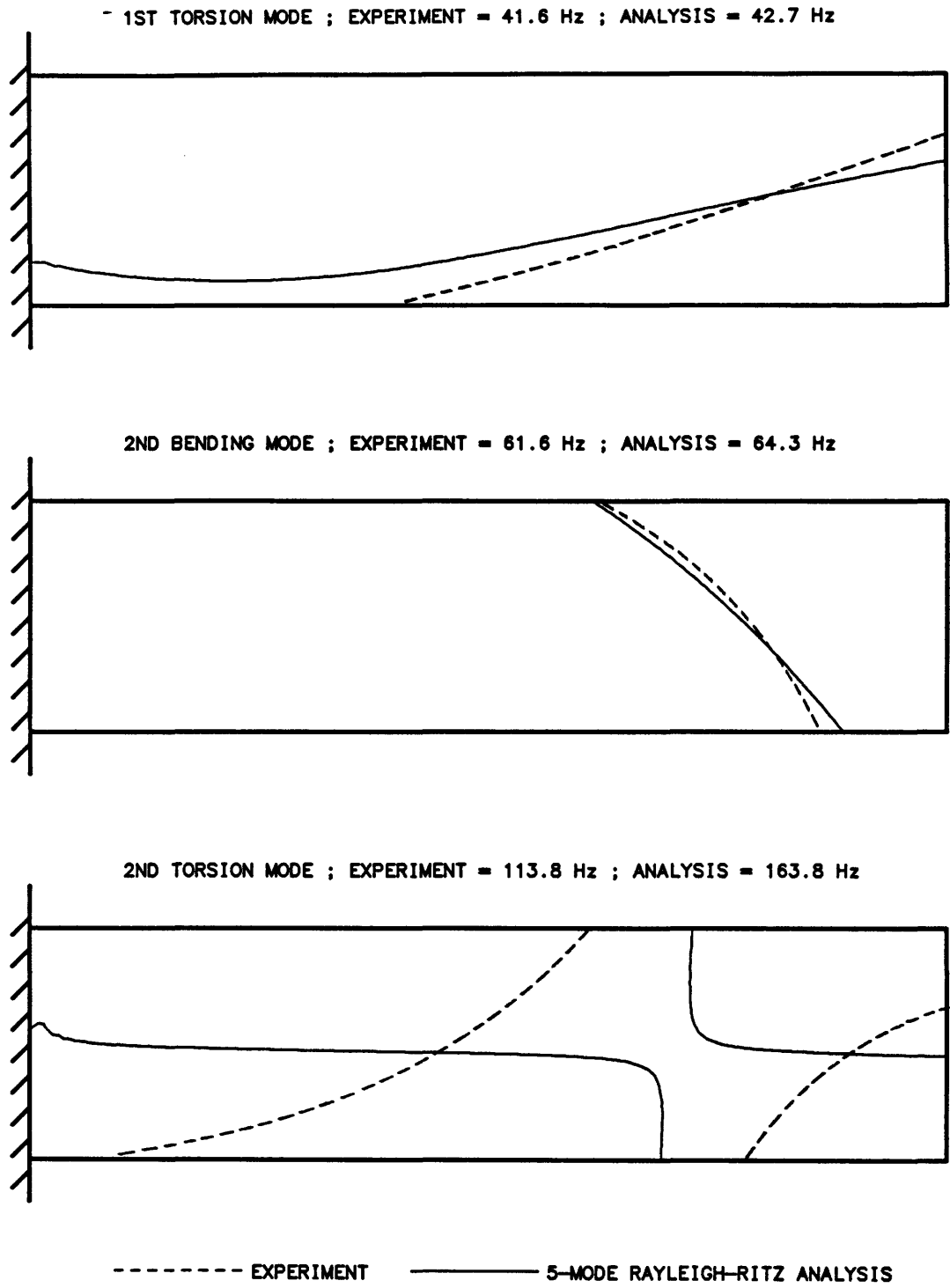
Figure 16c. Free vibration mode shapes for $[+15_2/0]_s$ plate

_ 1ST TORSION MODE ; EXPERIMENT = 57.7 Hz ; ANALYSIS = 58.0 Hz
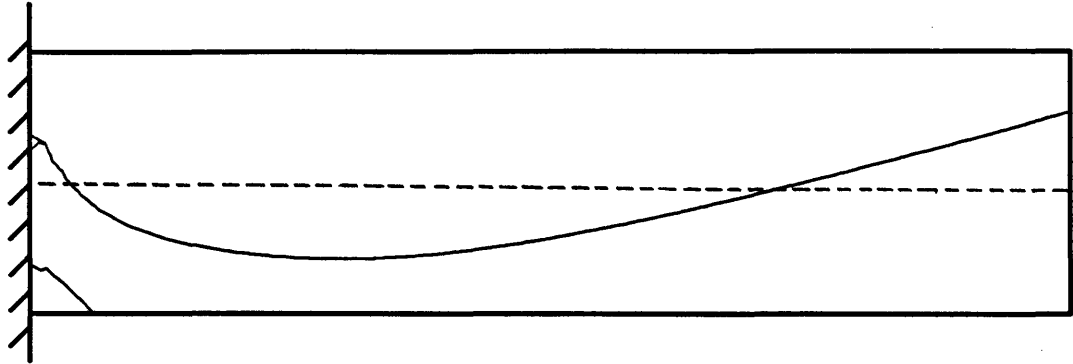
2ND BENDING MODE ; EXPERIMENT = 36.3 Hz ; ANALYSIS = 39.9 Hz
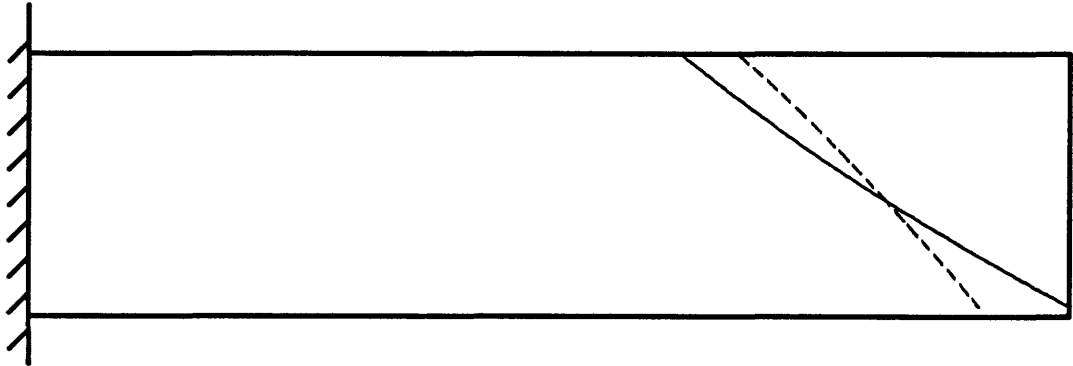
2ND TORSION MODE ; EXPERIMENT = 165.7 Hz ; ANALYSIS = 202.5 Hz
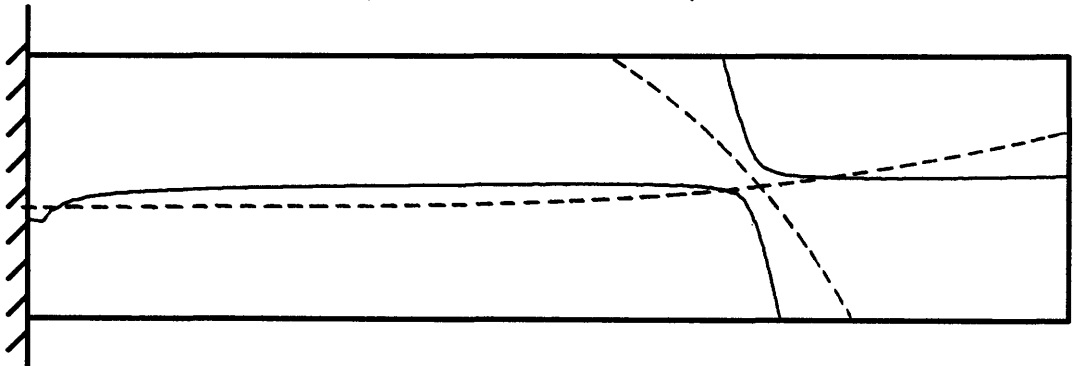
-------- EXPERIMENT ———————— 5-MODE RAYLEIGH-RITZ ANALYSIS

Figure 16d. Free vibration mode shapes for $[-30_2/0]_s$ plate

4.4 Two-Dimensional Aerodynamics

Experimental results of two-dimensional lift coefficient and moment coefficient hysteresis loops from Ref. 16 for a NACA-0012 airfoil in low Reynold's number flow are compared against analysis in Figures 17a and 17b. This analysis employs the Fourier analysis described in Section 2.9 and the two-dimensional static and unsteady aerodynamics described in Appendices C and D. For a gauge of the influence of lag and hysteresis, these figures may be compared with the 2-dimensional lift and moment curves given in Figure 27 in Appendix C.

The second harmonic of the Fourier analysis is also included in producing the analytic hysteresis loops, so as to show a closer match with the high order frequency components of the experimental data. However, this second harmonic is not used in any later part of the nonlinear flutter analysis, as only the lowest order harmonic is required in the harmonic balance method used here.

The lift hysteresis loops show good agreement between experiment and theory while the moment hysteresis loops seem to show poor agreement. However, these discrepancies in the moment loops may be overlooked in future analysis for several reasons: (i) it is clear from the experimental moment data that the moment hysteresis loops contain a larger component of higher frequencies than do the lift hysteresis loops, making it more difficult to easily compare the lowest har-

monic component with the analysis, (ii) the semi-empirical coefficients of the analytic model are principally derived for the lift coefficient, and for much higher Reynold's numbers, leading one to expect poor agreement for the moment coefficient at low Reynold's numbers, and (iii) because the elastic axis of the wings is very near the midchord, in the final flutter analysis it is likely that the moment around the midchord will play a greater role than the moment around the aerodynamically significant 1/4-chord, thus making the moment generated by the 1/4-chord lift offset from the midchord more important than the 1/4-chord moment, since it is on average an order of magnitude larger.
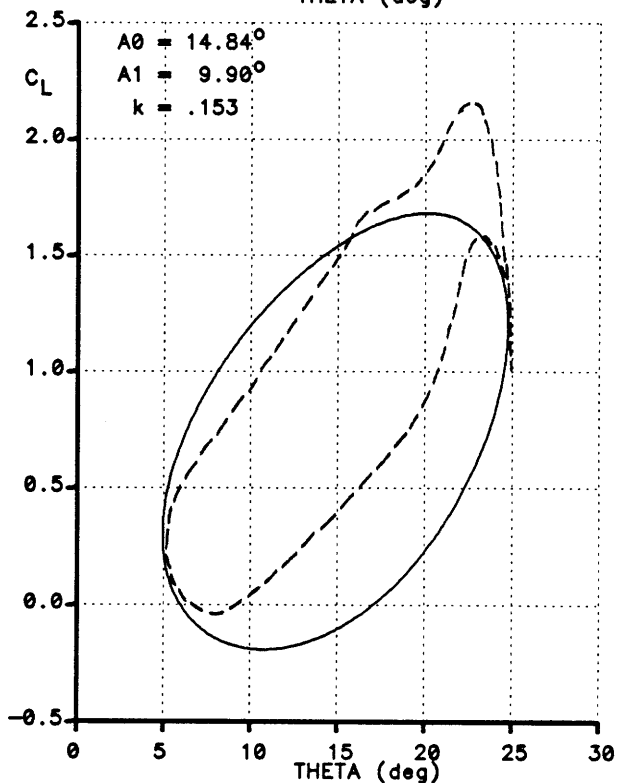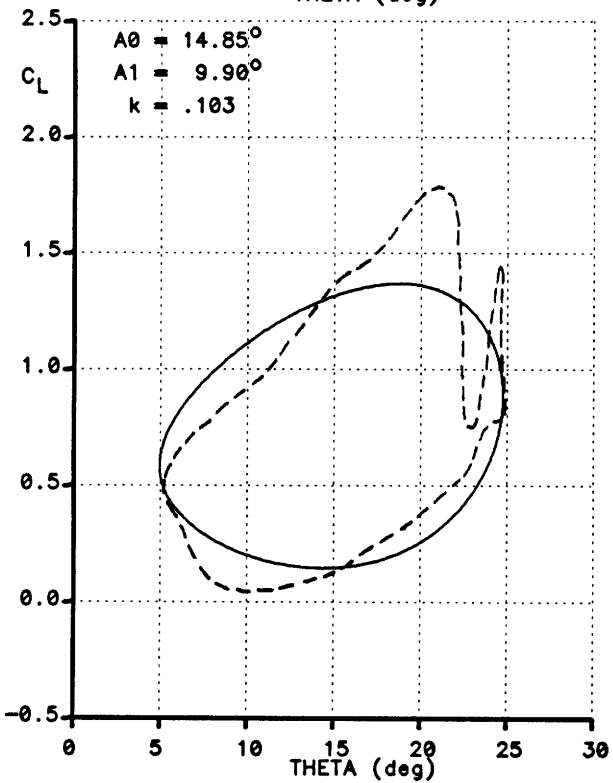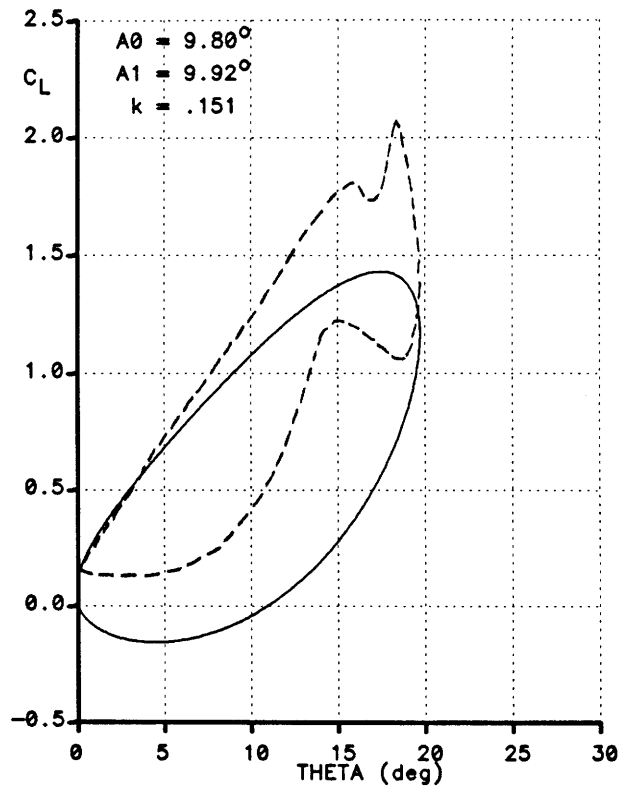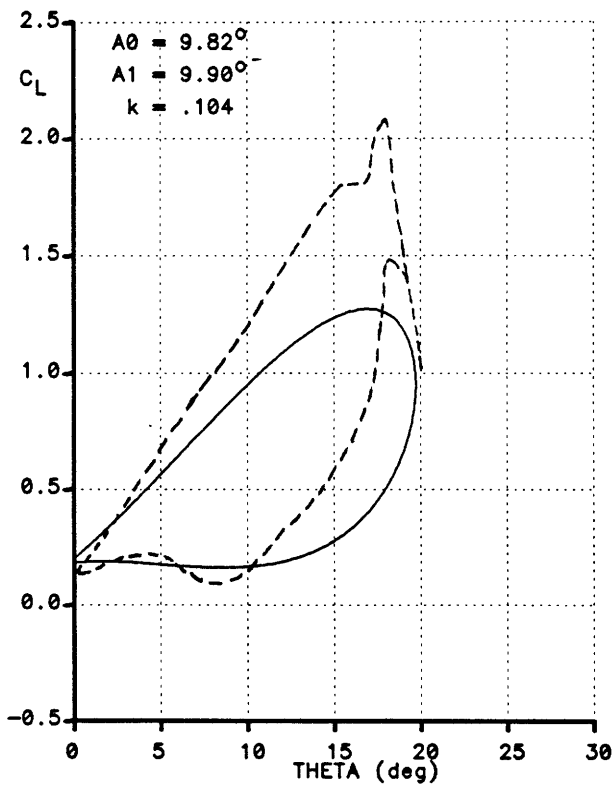
Figure 17a. 2-dimensional lift coefficient hysteresis loops versus angle of attack, NACA-0012 airfoil, Re = 0.49×10^6 (corrected for wind tunnel effects), compared against Ref. 16
———— Analysis   ———— Experiment
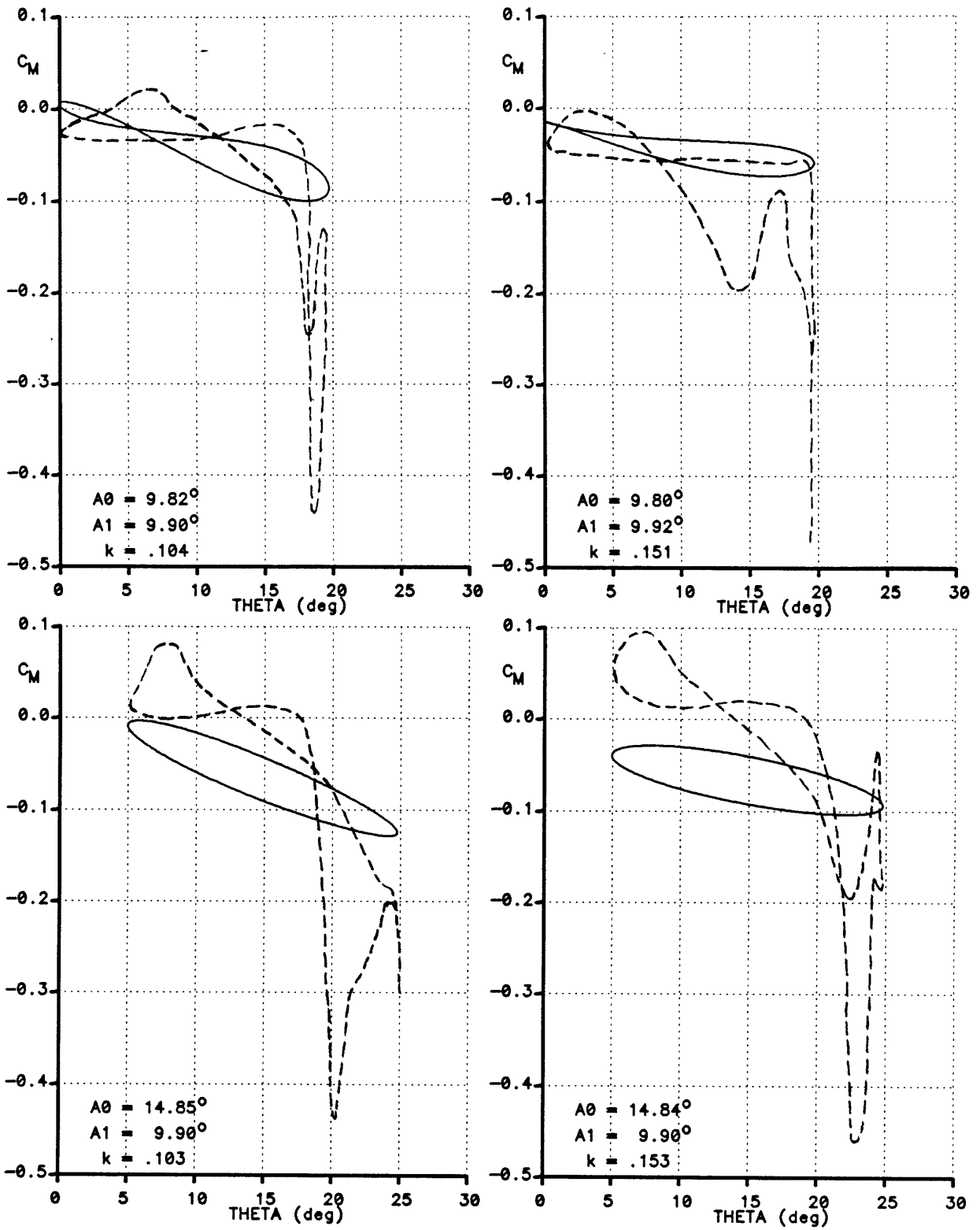
Figure 17b. 2-dimensional moment coefficient hysteresis loops versus angle of attack, NACA-0012 airfoil, Re = 0.49×10^6 (corrected for wind tunnel effects), compared against Ref. 16

———— Analysis   ———— Experiment

4.5 Wind Tunnel Tests

4.5.1 Steady Deflections

The steady aerodynamic deflections were determined analytically for the wings of interest, that is, the deflections that the wings would experience if all unsteady motion were suppressed. These results are presented in terms of midchord tip deflection and tip twist in Figures 18a to 18g for lines of constant velocity. The analysis and experiment are presented in this form because it was in this manner that the actual experiments were conducted (the wind tunnel was brought to a fixed speed, and the root angle-of-attack varied with that speed held fixed). Later graphs will be plotted for the more conventional lines of constant root angle-of-attack. For these figures, the cubic stiffening was included in the structural part of the analysis and only two mode shapes (1st bending and 1st torsion) were used.

The analysis is compared to the mean experimental aerodynamic deflections, that is, the steady deflections if no oscillation is present or the time average deflections if they are unsteady. To distinguish the two, the steady experimental values are plotted as hollow symbols in Figures 18a to 18g, while the time-averaged unsteady deflections are represented as solid symbols. The steady analytic values are plotted as solid lines. Tests were also conducted with flat plates, and the analysis is capable of determining steady

deflections for these, but for brevity only the NACA-0012 wings are presented.

For clarity, these graphs are presented with intervals of 4 m/s, thereby necessitating more than one graph for laminates for which a large number velocities were investigated. These graphs show good agreement between experiment and analysis up to the point where unsteadiness is experienced experimentally. At this point, the time-averaged unsteady deflections show a consistent trend away from the predicted analytic steady values, which is more closely discussed in Section 4.5.5. Only the $[-15_2/0]_s$ wing shows poorer agreement between analysis and experiments, and here only for the tip twist. Still, even with poor agreement, both analysis and experiment show the same trends. The discrepancy is likely explained because the $[-15_2/0]_s$ wing experiences divergence very early on, so that the nonlinear structural and aerodynamic effects are more pronounced.
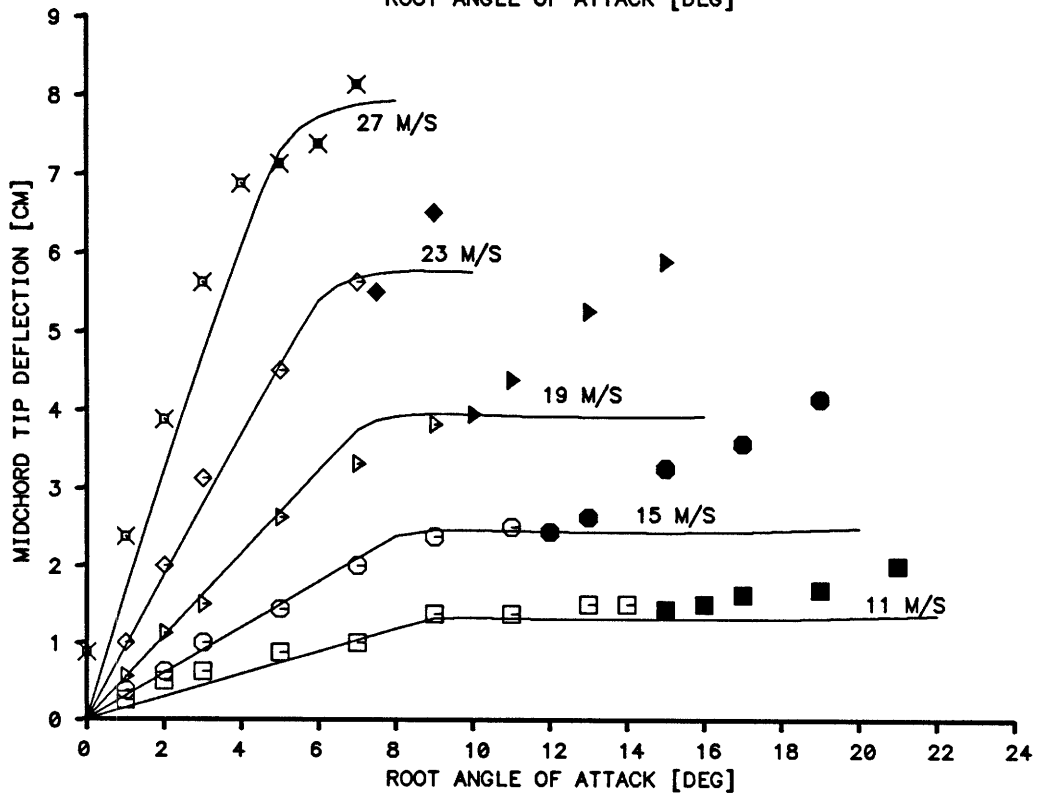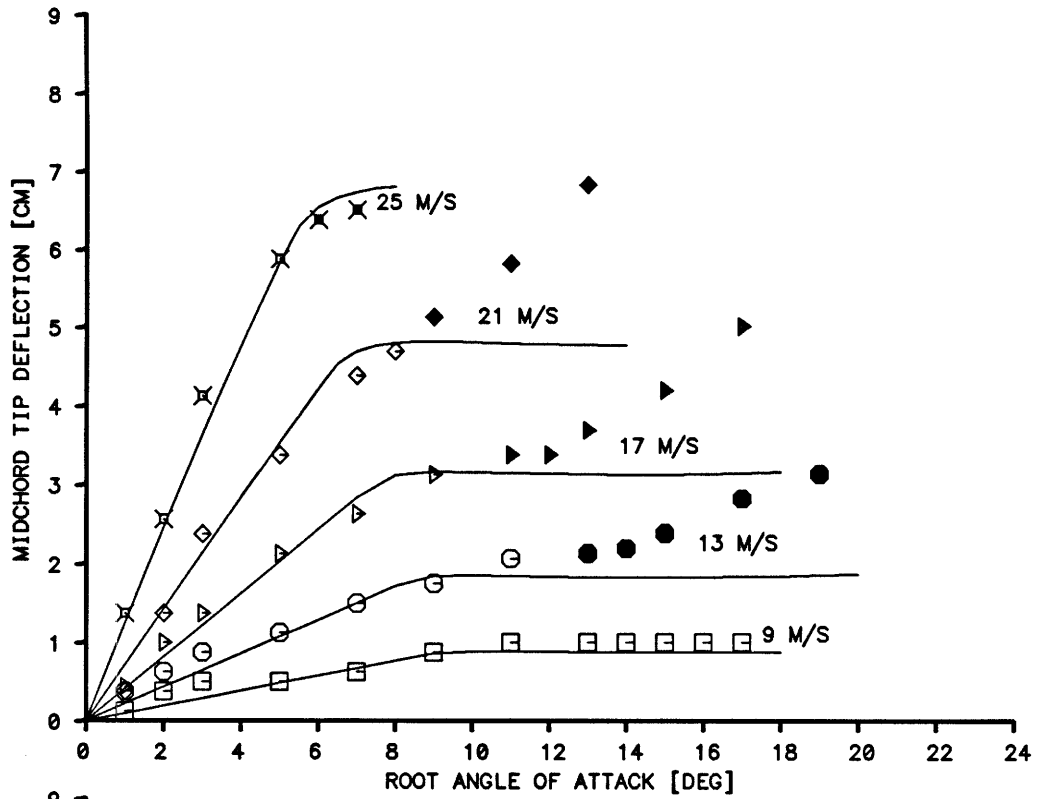
Figure 18a. [0₂/90]ₛ averaged midchord tip
deflections, lines of constant velocity
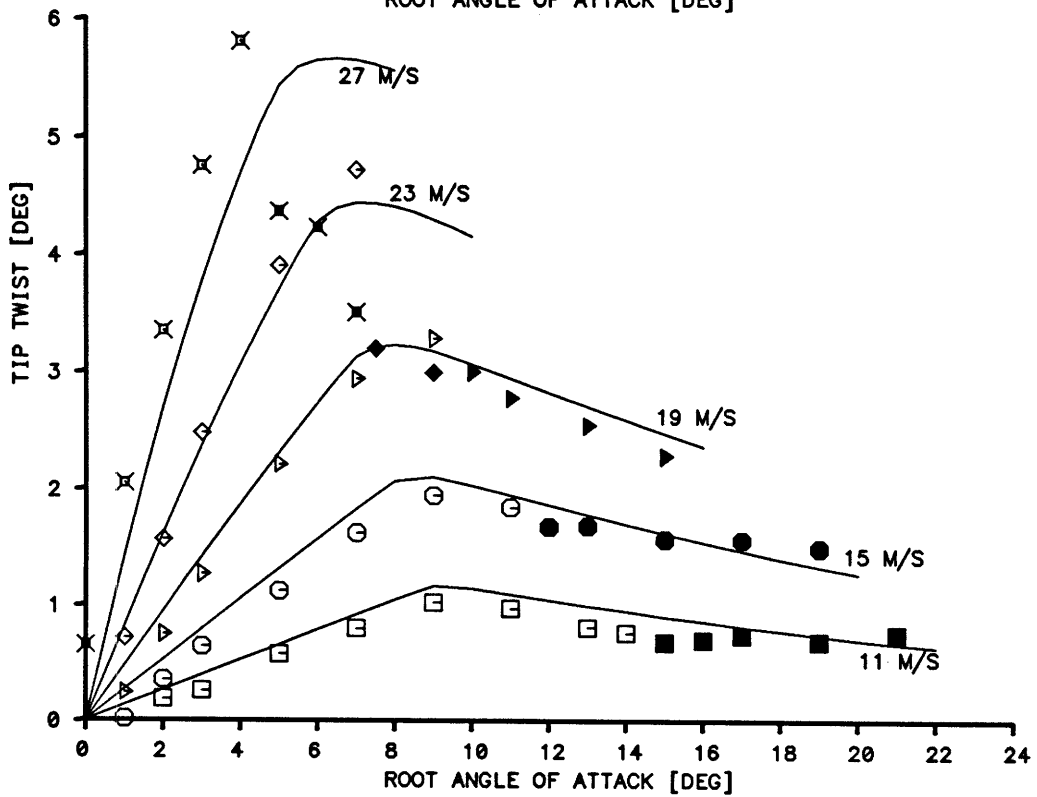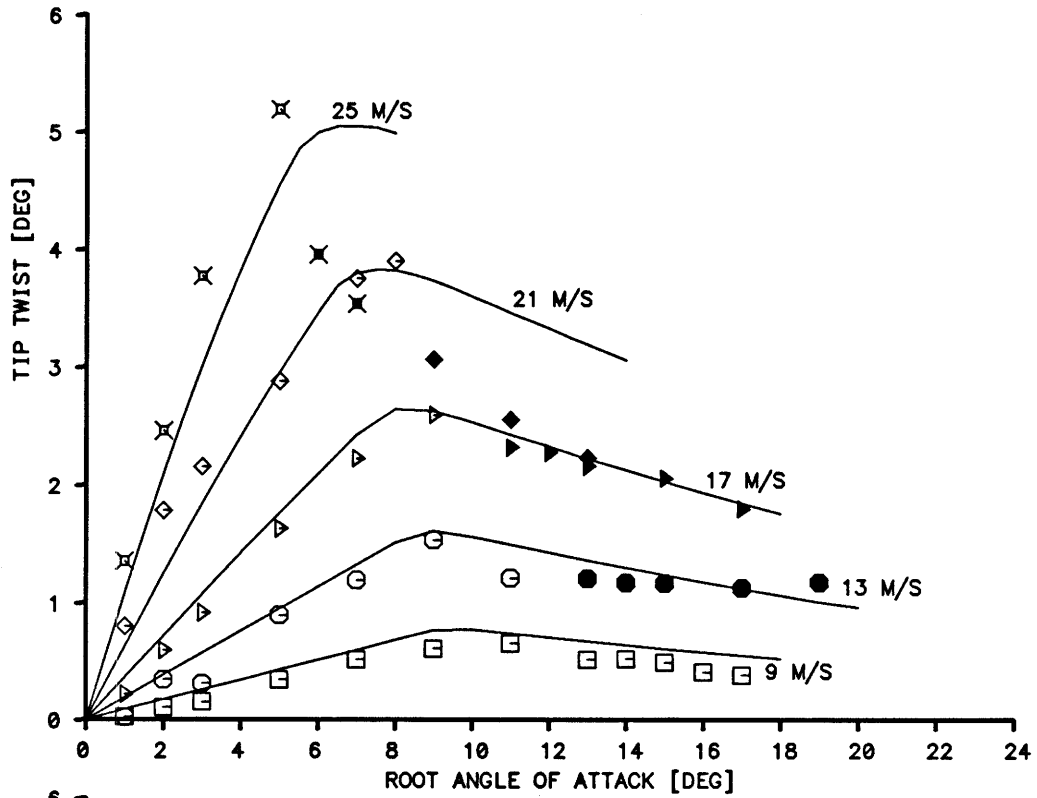
Figure 18b. $[0_2/90]_s$ averaged tip twists, lines of constant velocity
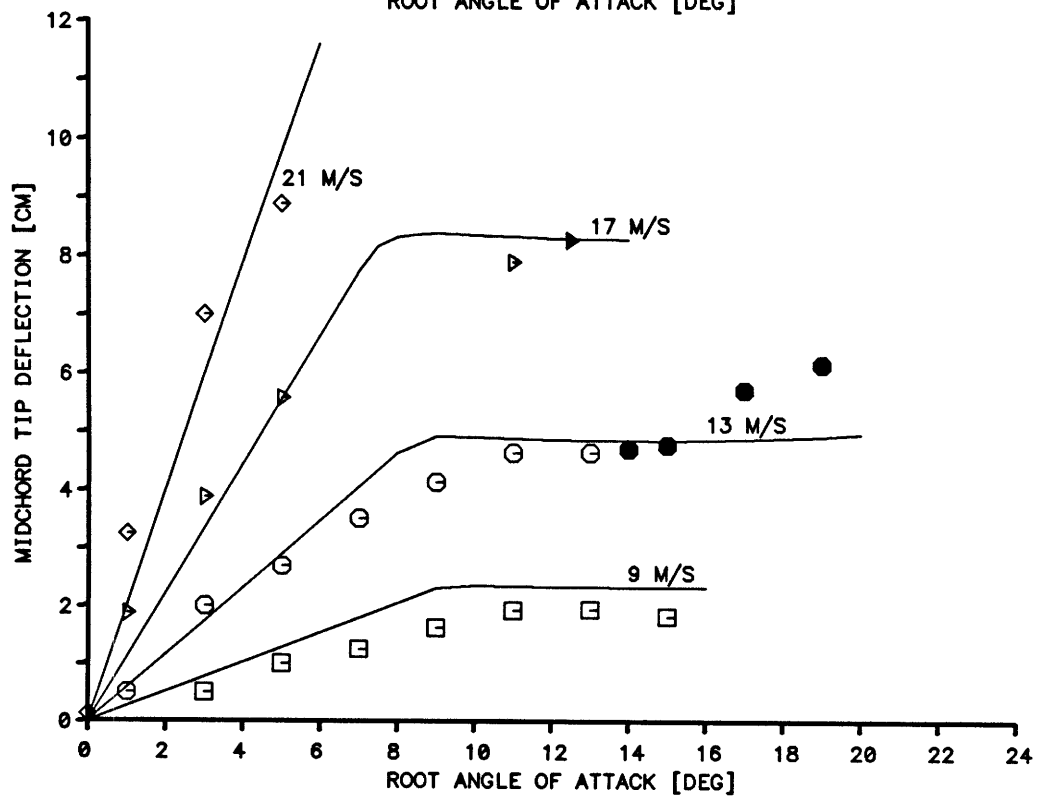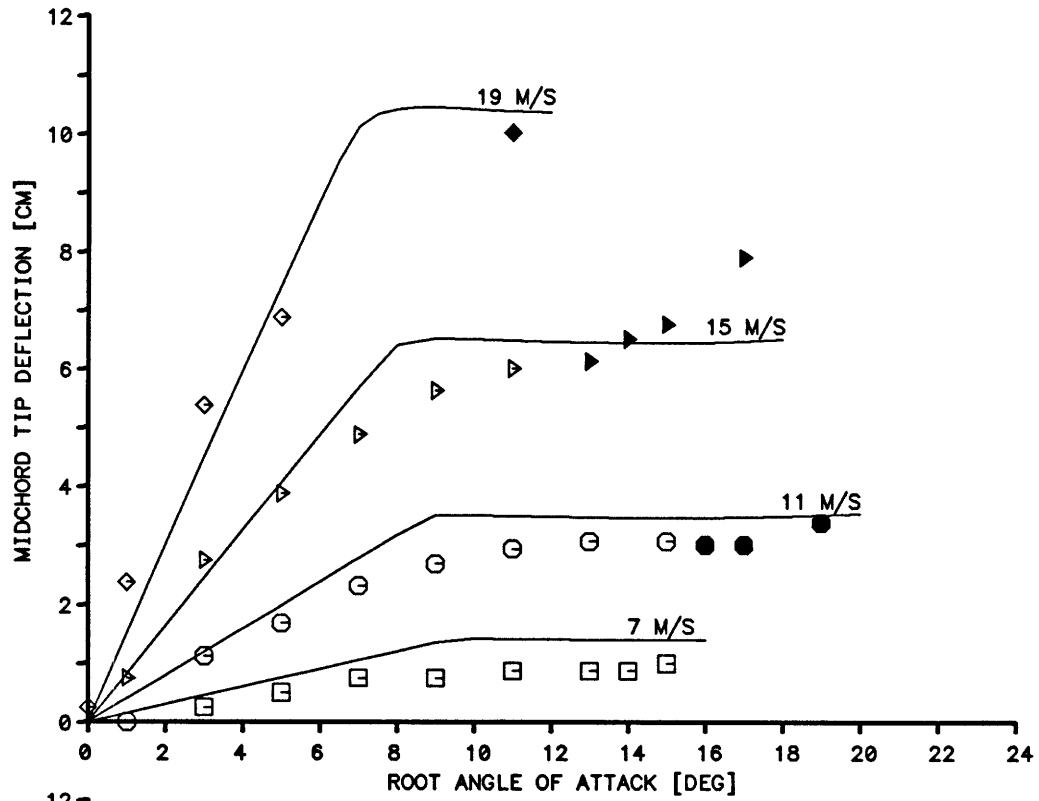
Figure 18c. $[90/0_2]_s$ averaged midchord tip
deflections, lines of constant velocity
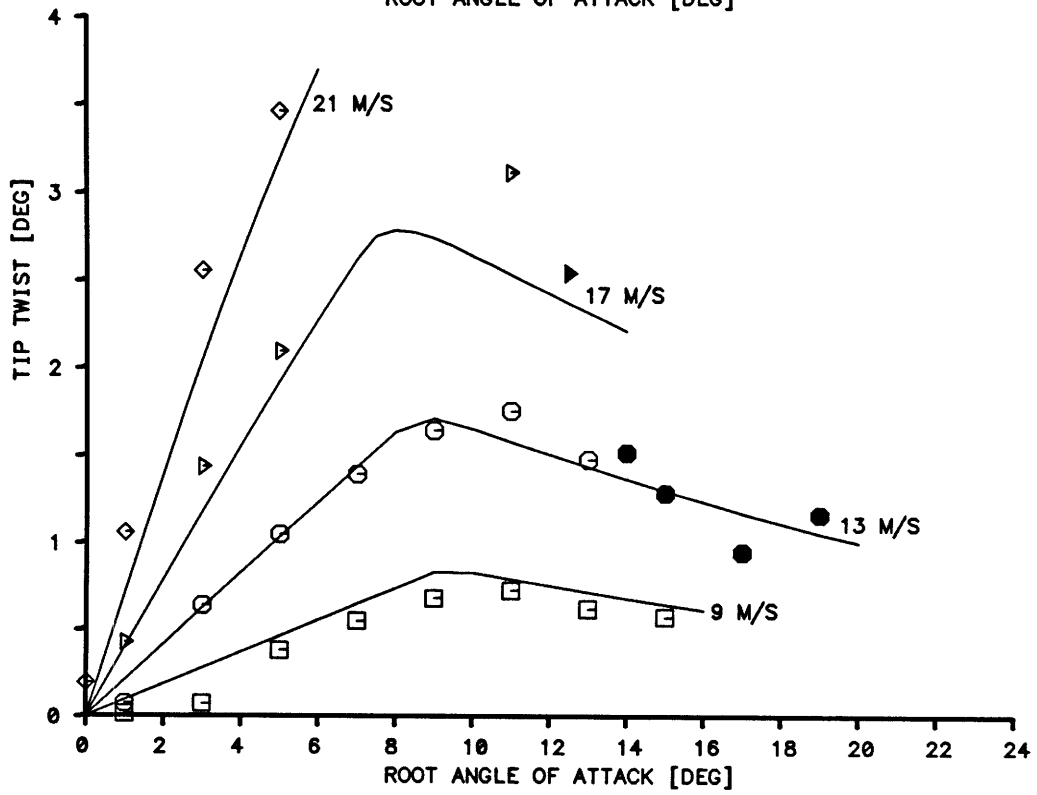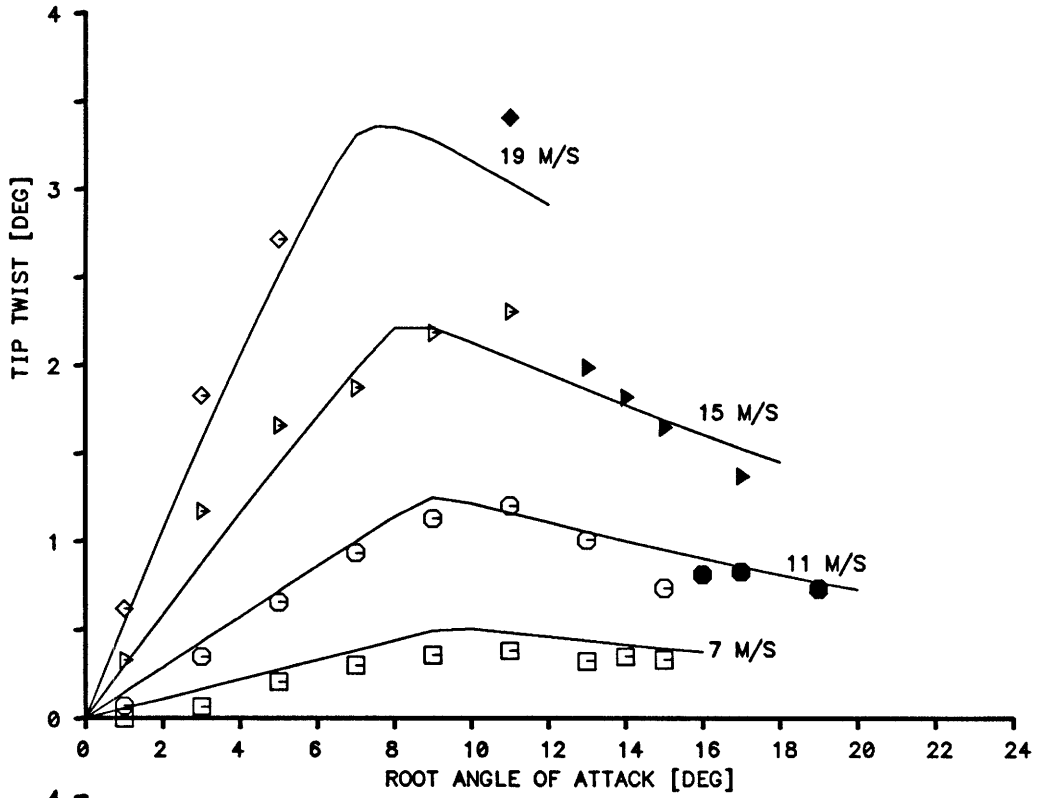
Figure 18d. $[90/0_2]_s$ averaged tip twists, lines of constant velocity
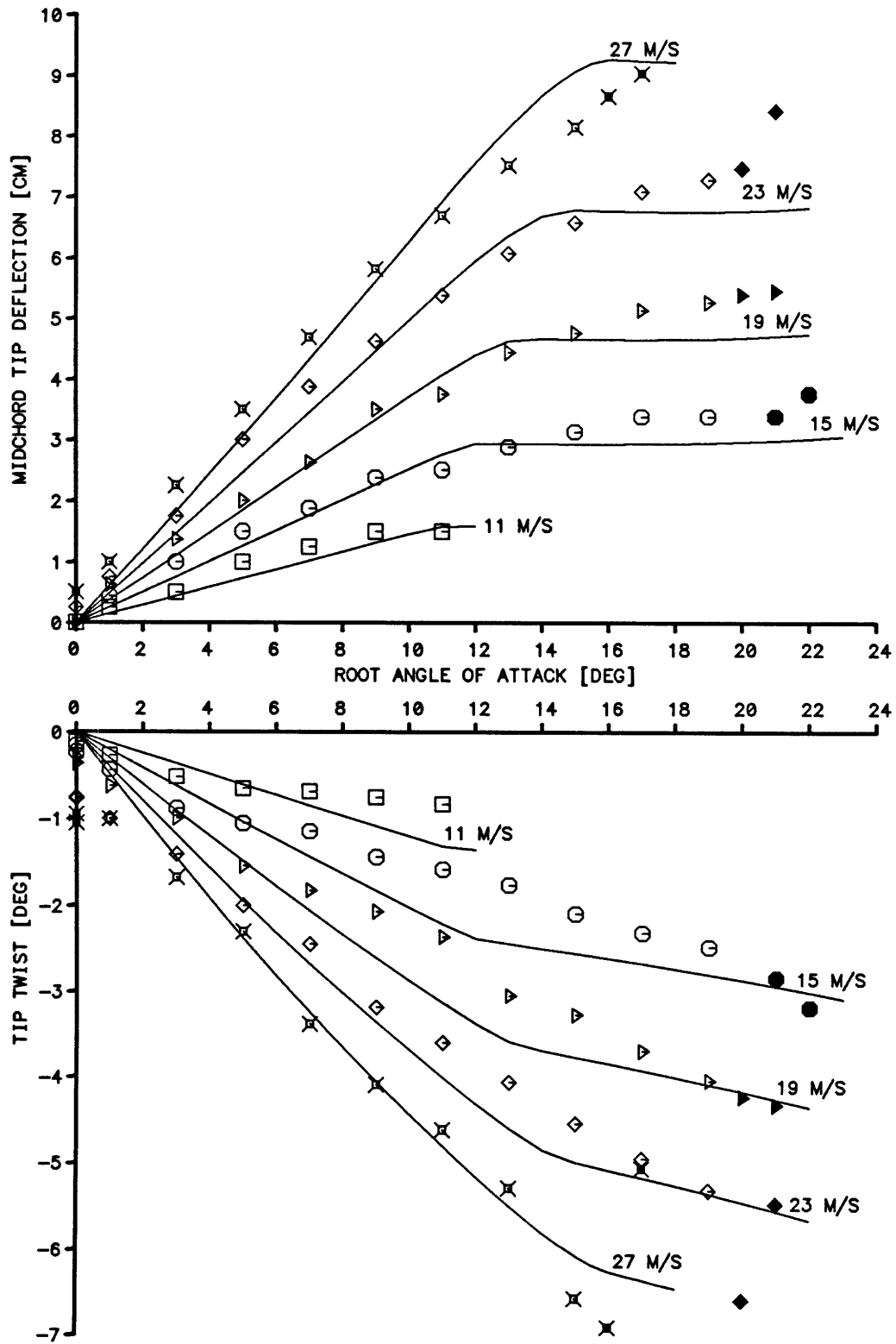
Figure 18e. $[+15_2/0]_s$ averaged midchord tip deflections and tip twists, lines of constant velocity
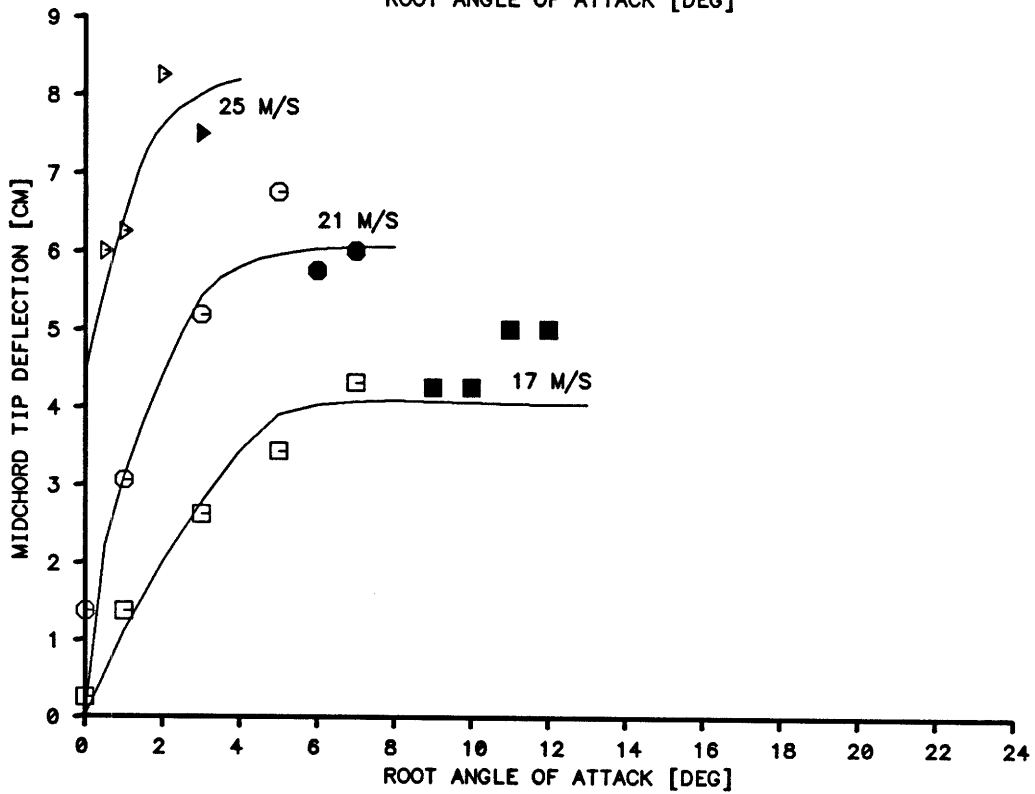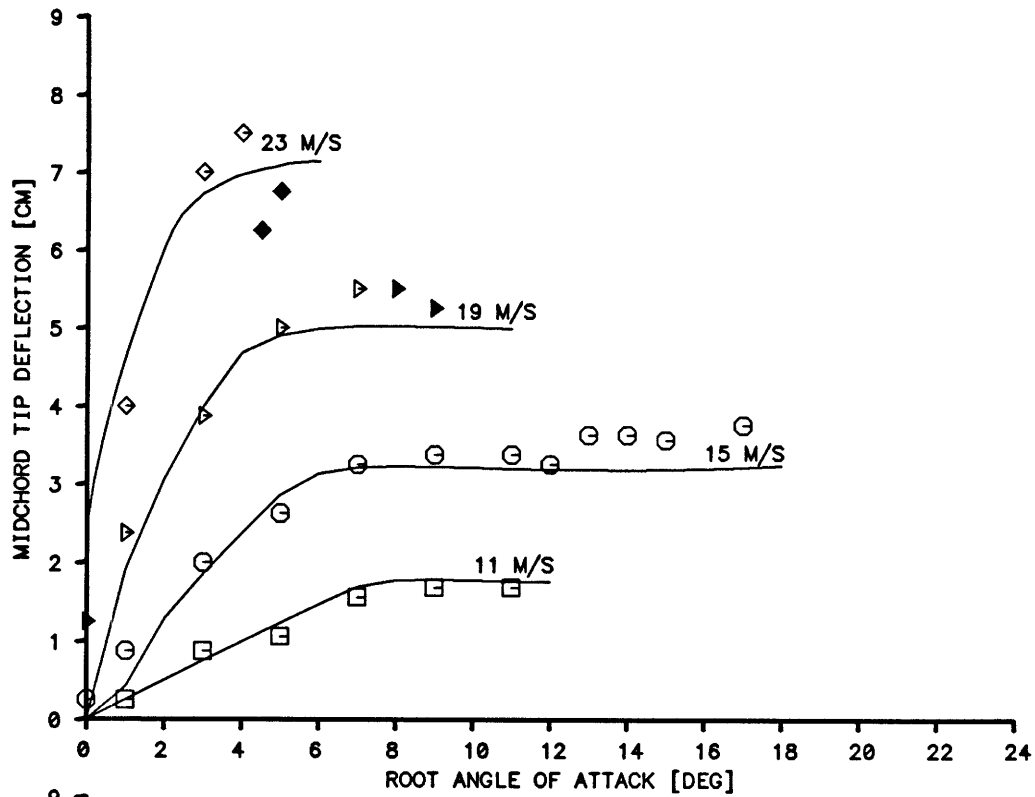
Figure 18f. $[-15_2/0]_s$ averaged midchord tip
deflections, lines of constant velocity
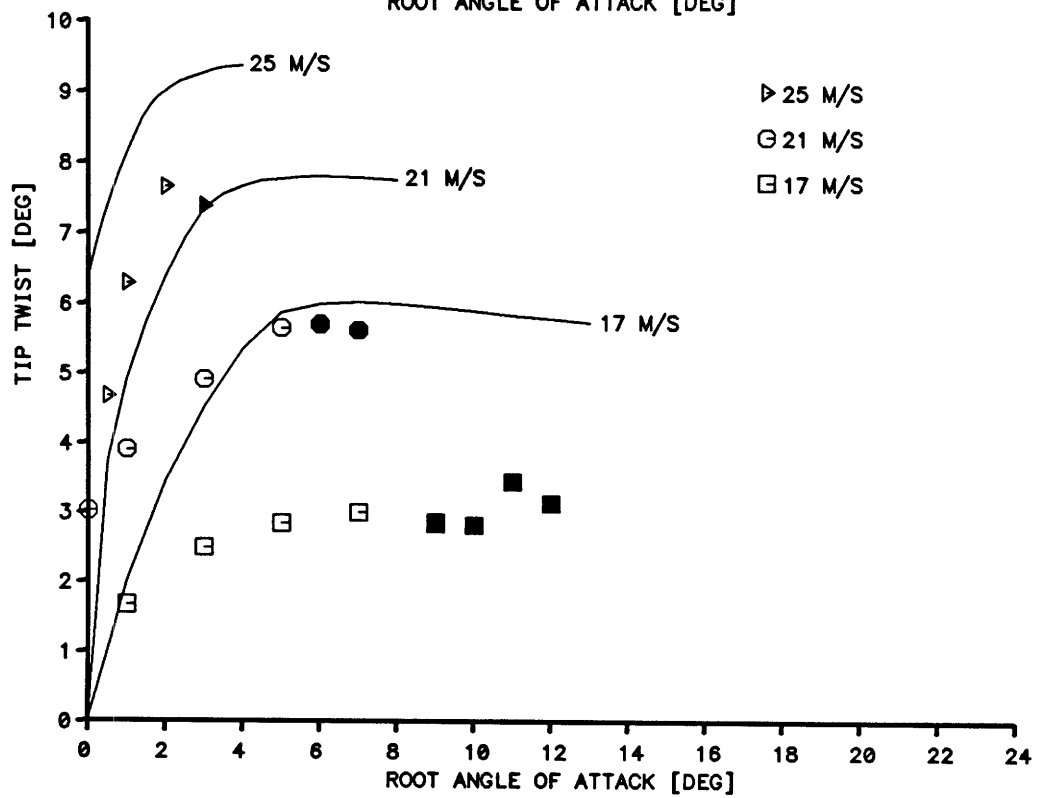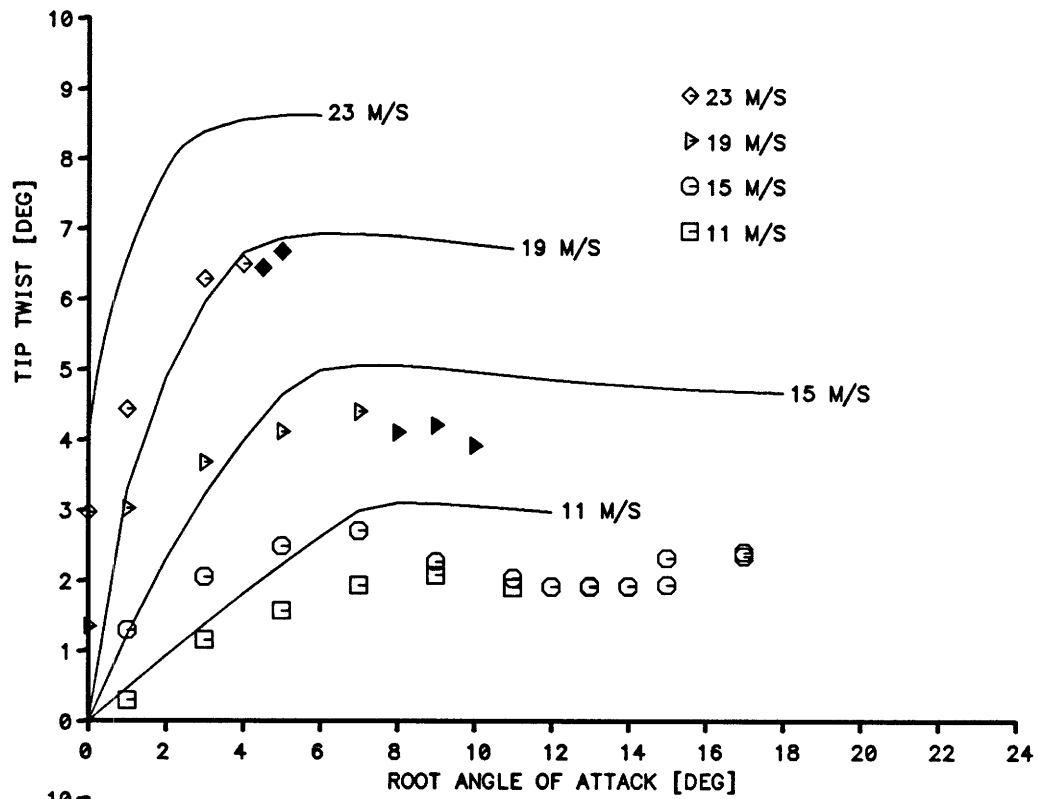
Figure 18g. $[-15_2/0]_s$ averaged tip
twists, lines of constant velocity

4.5.2 Linear Divergence and Flutter

The analytic results for linear divergence and flutter are presented in Table 2 for the laminates of interest using the three-dimensional, linear aeroelastic analysis described in Section 2.8. The U-g plots from which these values are generated are shown in Figures 19a to 19d. As expected, the $[0_2/90]_s$ and $[90/0_2]_s$ wings have torsional flutter velocities very near their divergence velocities, the $[+15_2/0]_s$ wing has a torsional flutter velocity just above those of the $[0_2/90]_s$ and $[90/0_2]_s$ wings and does not experience divergence at all, and the $[-15_2/0]_s$ wing has a divergence velocity well below its torsional flutter velocity.

Figure 19e is simply a reproduction of Figure 19a for the $[0_2/90]_s$ wing, but over a larger velocity range, to show the full trend of the U-g diagram. It is important to note in passing that another flutter velocity occurs somewhere between 200 m/s and 250 m/s, when the torsional branch once again crosses the damping coefficient zero axis. It is also noteworthy that by this point the torsional branch has in fact dropped to a frequency much closer to the natural first bending frequency. These observations are important for later use in the full flutter analysis, since often it was observed in applying the Newton-Raphson solver to the non-linear analysis, that if the initial conditions of the solver were chosen poorly, the scheme would converge to this high-velocity, low-frequency solution.

NACA-0012 WINGS		
Divergence Vel (m/s)	Flutter Vel (m/s)	Flutter Freq (Hz)
$[0_2/90]_s$ 38.14	36.39	25.78
$[90/0_2]_s$ 35.99	33.98	22.34
$[+15_2/0]_s$ > 50	37.27	27.28
$[-15_2/0]_s$ 21.55	48.84	29.73

Table 2. Linear divergence and flutter characteristics
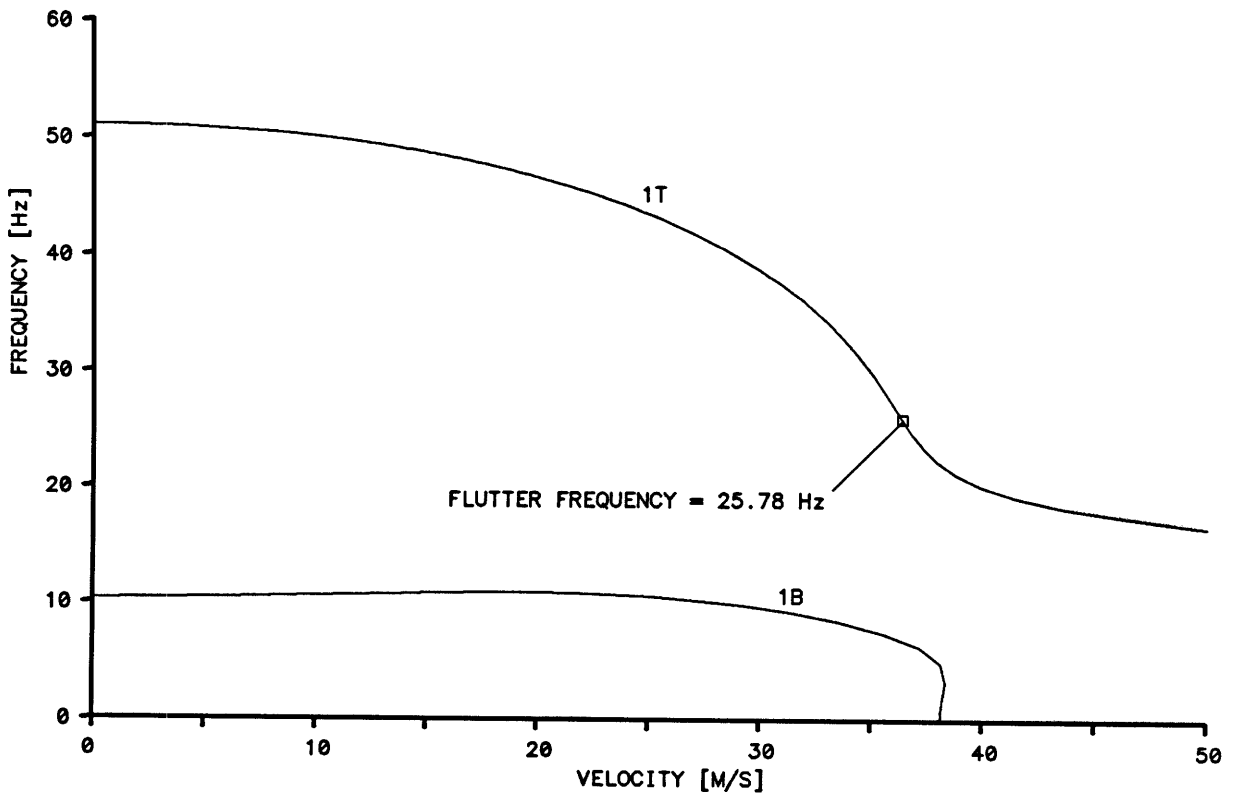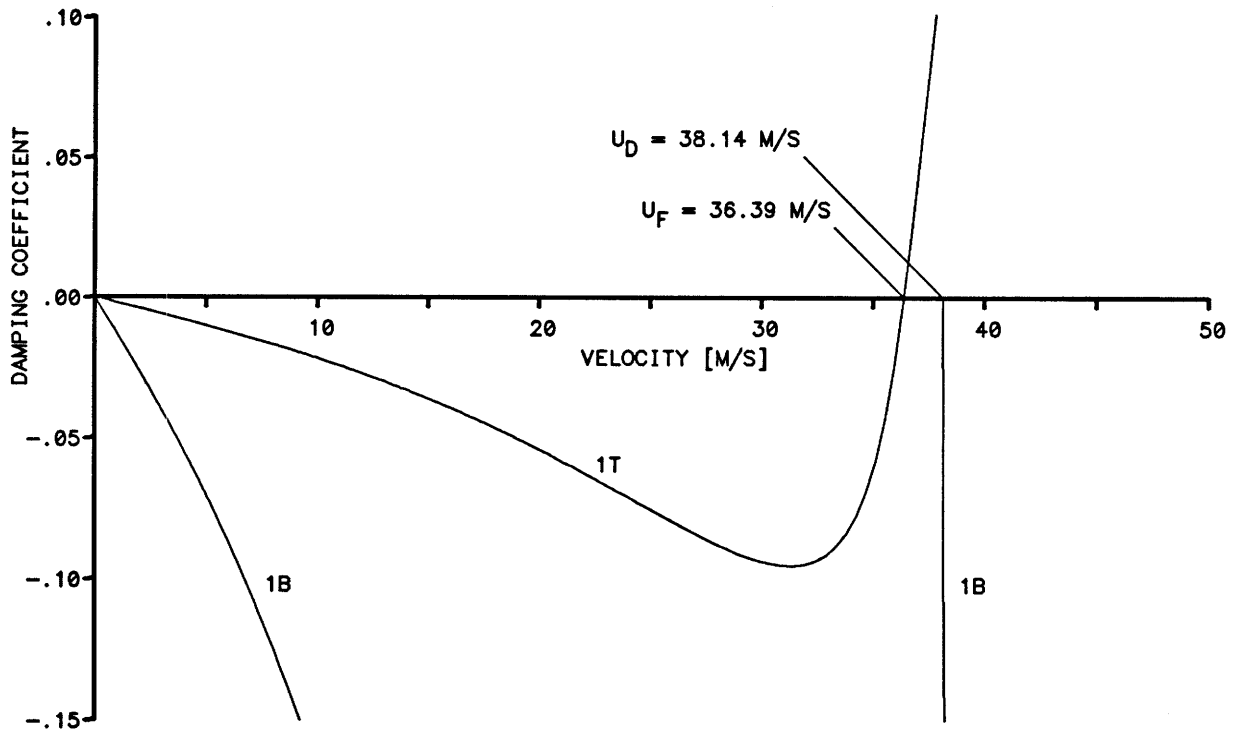
Figure 19a. $[0_2/90]_s$ U-g diagram
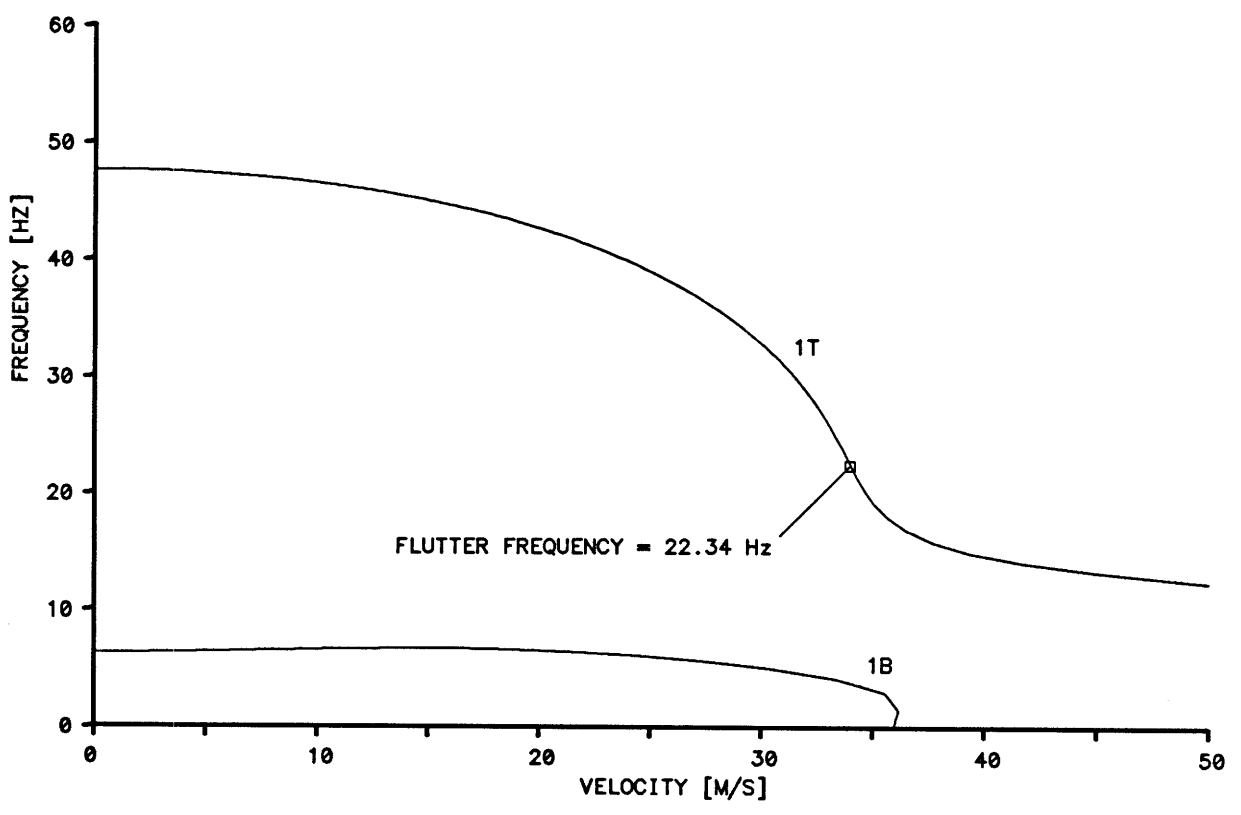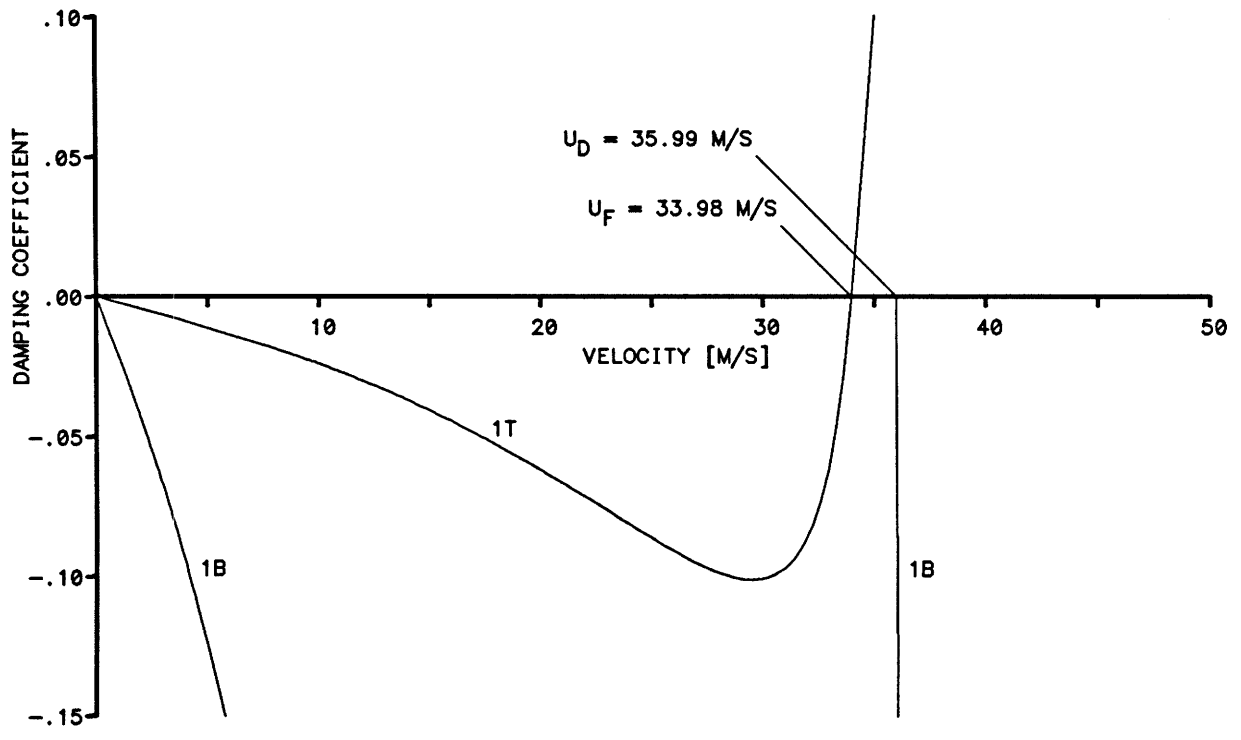
Figure 19b. $[90/0_2]_s$ U-g diagram
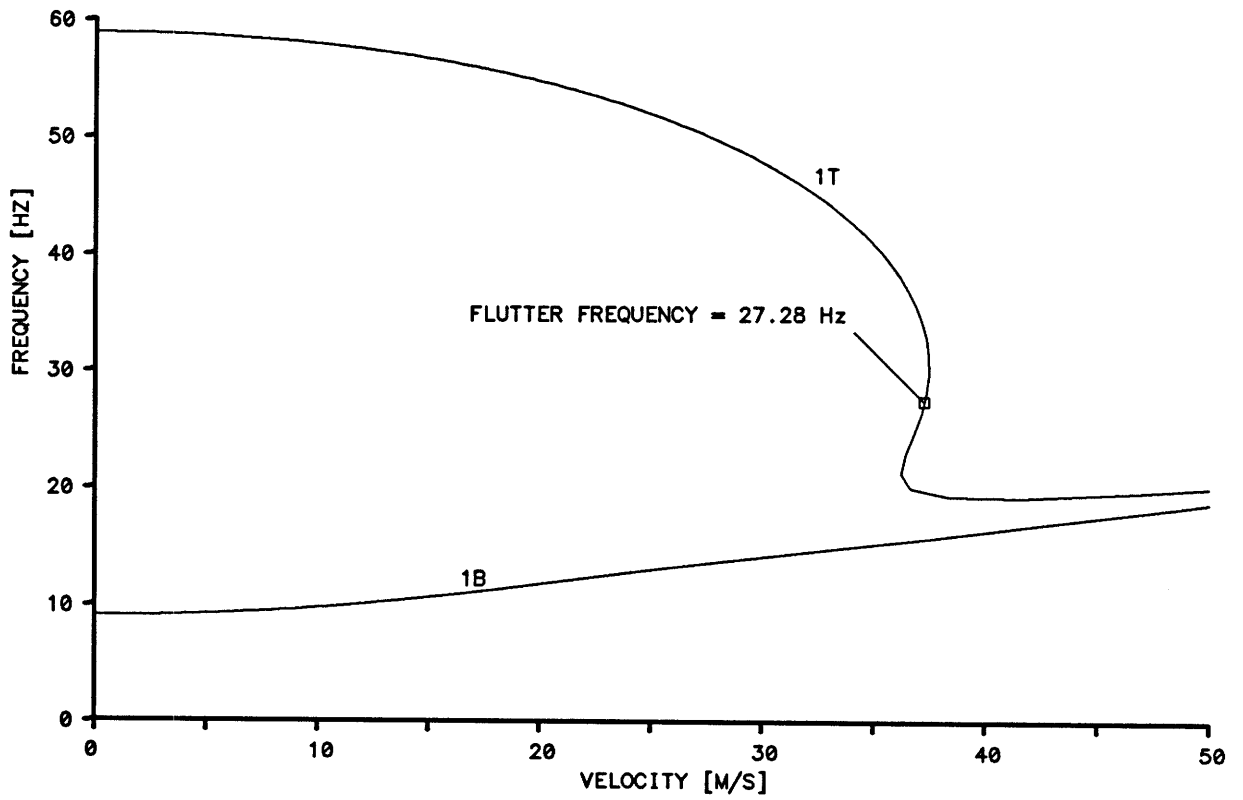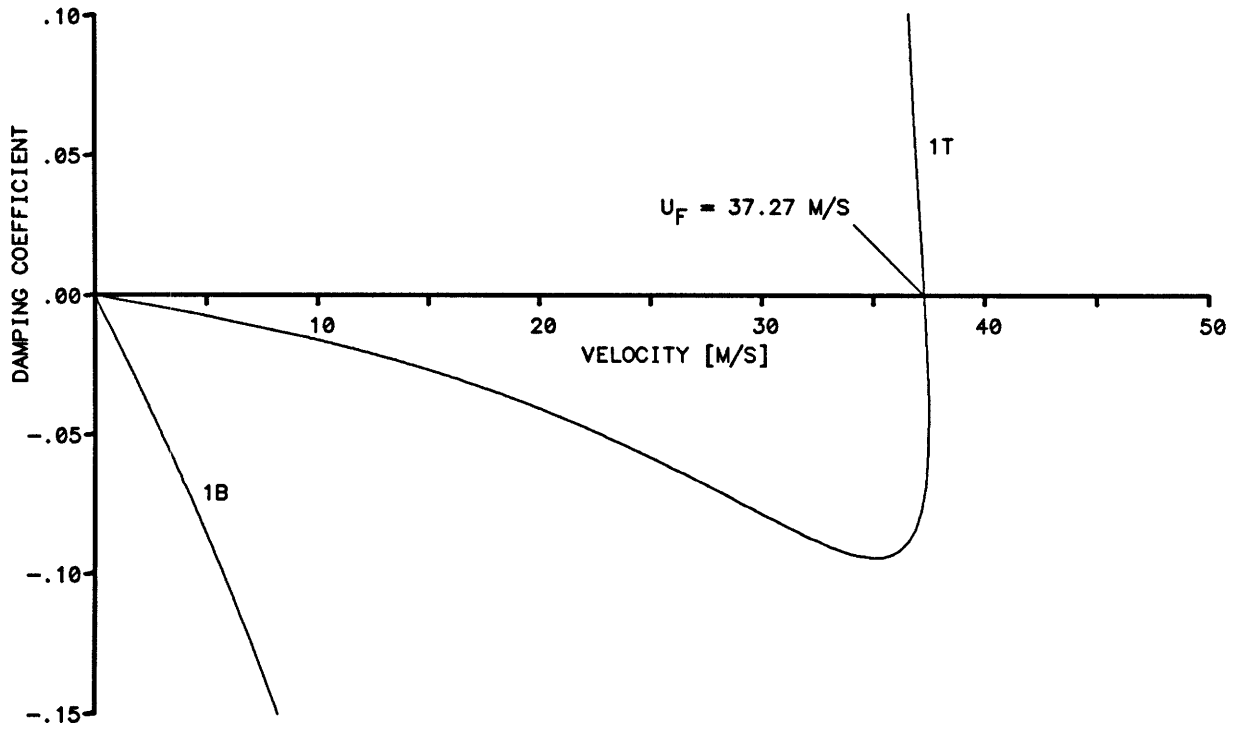
Figure 19c. $[+15_2/0]_s$ U-g diagram
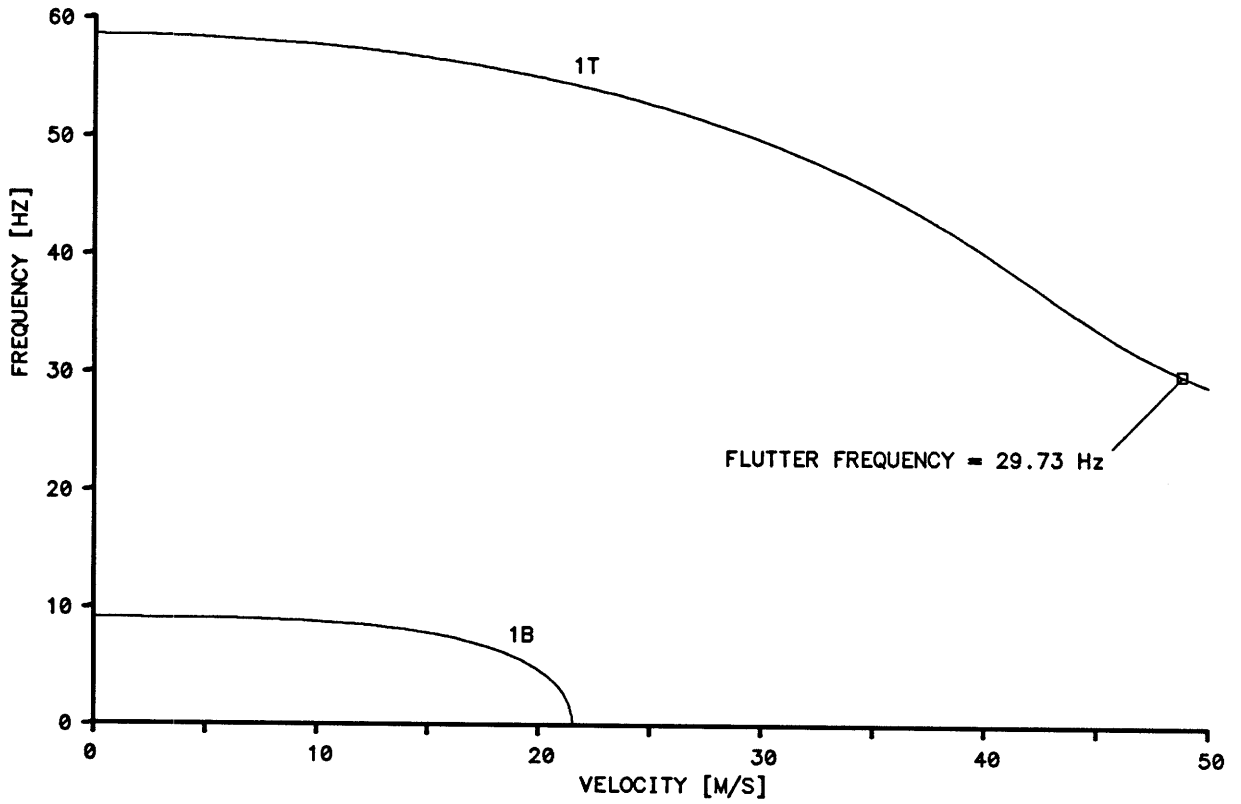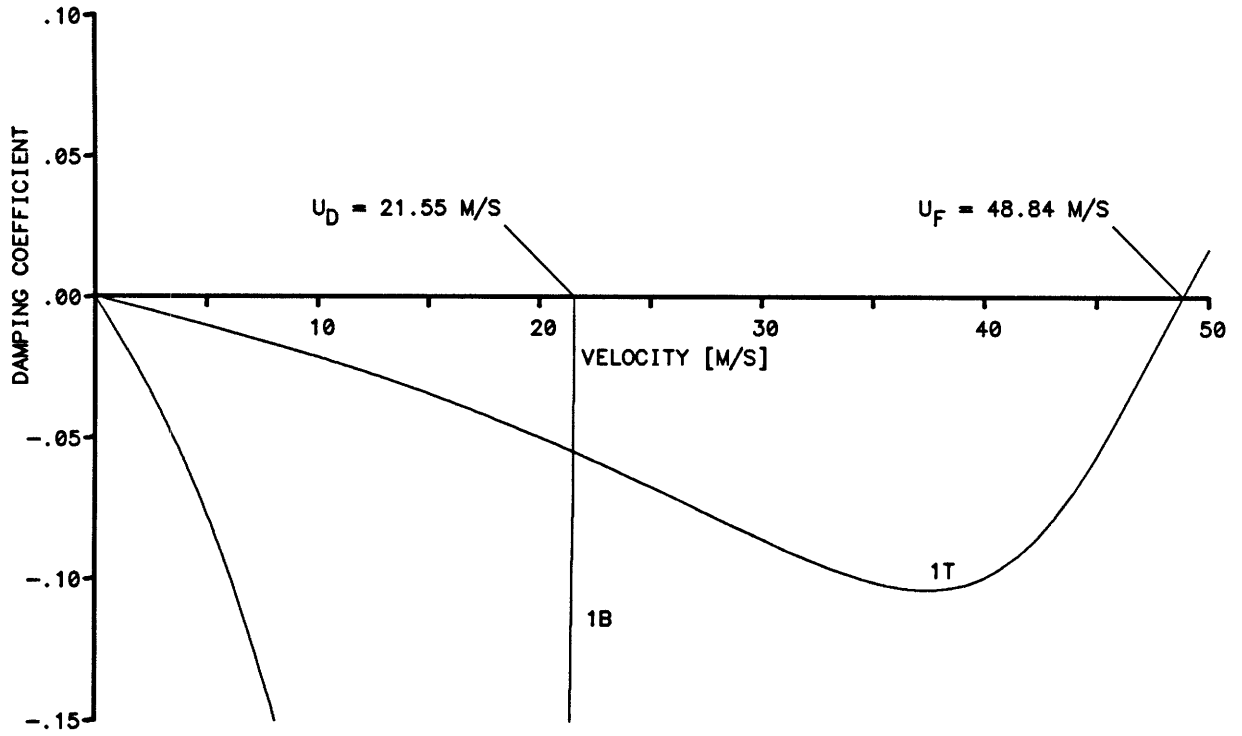
Figure 19d. $[-15_2/0]_s$ U-g diagram
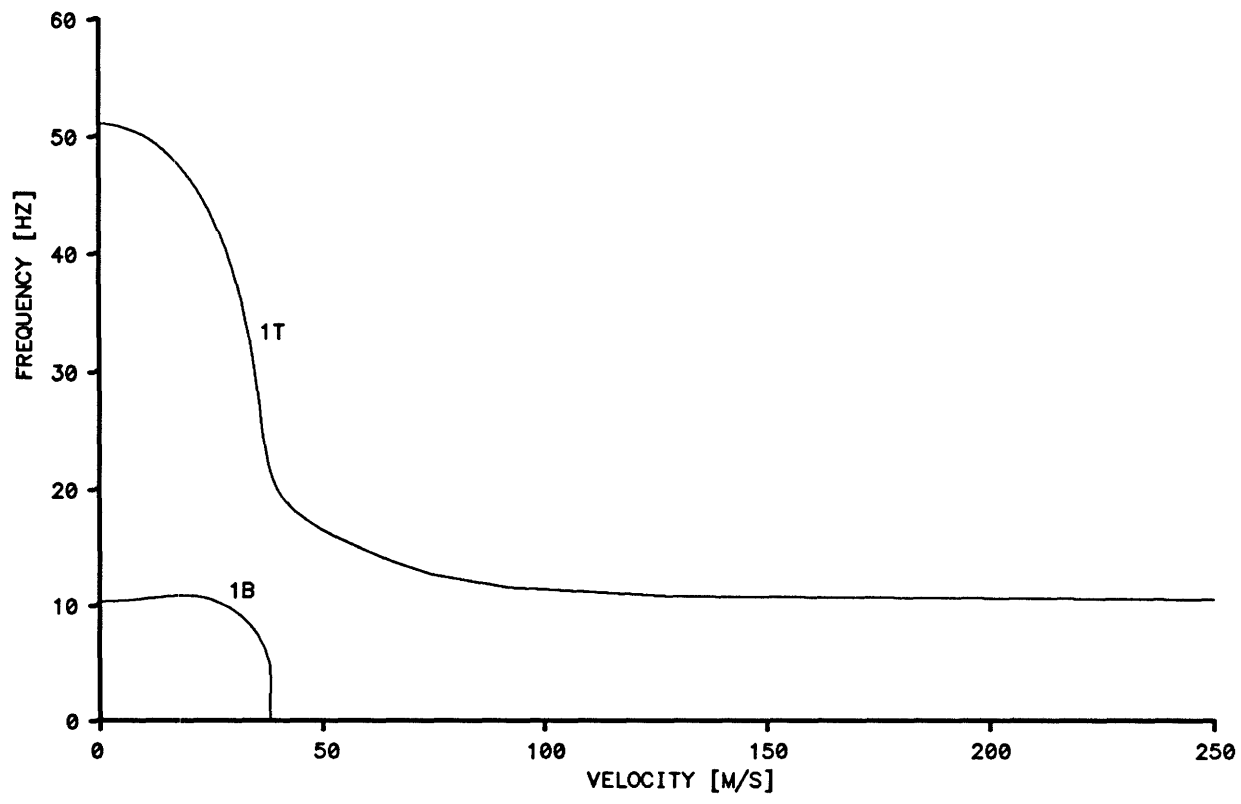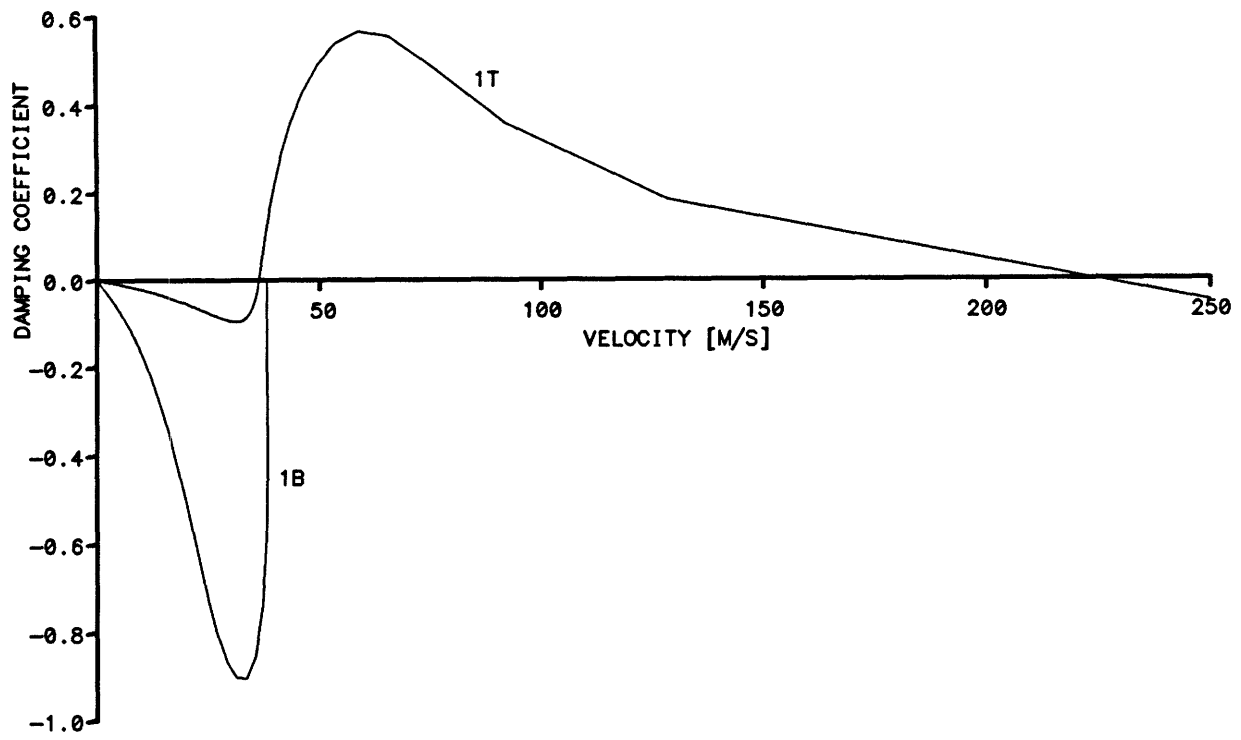
Figure 19e. $[0_2/90]_s$ U-g diagram, max vel = 250 m/s

4.5.3 Flutter Boundaries for Given Root Angles

The experimental and analytic flutter boundaries (i.e. for very small amplitude oscillation) are presented in Figures 20a to 20d for given root angles of attack, with no cubic stiffening included in the structural part of the analysis. The divergence speeds for each laminate, as shown in Section 4.5.2 and listed in Table 2, are also marked on each graph. Each graph demonstrates the expected trends for each laminate type (similar trends of decreasing flutter velocity with increasing root angle-of-attack were also observed by Rainey [Ref. 20]).

Figures 20a and 20b for the $[0_2/90]_s$ and $[90/0_2]_s$ laminates show a very short range of linear behavior (where the flutter velocity and flutter frequency remain constant) - this region is very short because the divergence velocity is near the linear flutter velocity, thus driving the wing very quickly into the nonlinear, stall range - after which point an increase in the root angle-of-attack α_R causes the flutter velocity to drop and the flutter motion to become more purely torsional (denoted by a frequency closer to the first-torsion free vibration frequency and a decrease in the bending amplitude). Figure 20c for the $[+15_2/0]_s$ laminate shows a more extended range of linear behavior (because the divergence velocity is very high and the tip twist is negative) and a very sharp change in the flutter behavior once it goes into the nonlinear stall region. Figure 20d for the

$[-15_2/0]_s$ laminate indicates a much different trend where the flutter is characterized by a low, first-bending frequency and immediate nonlinear, bending stall flutter in the range of the divergence velocity - there is no portion of the flutter graph here which could have been predicted by a linear analysis.

The nonlinear analysis in Figures 20a and 20b for the $[0_2/90]_s$ and $[90/0_2]_s$ laminates compares well against the experimental flutter boundaries and flutter frequencies. The nonlinear analysis in Figure 20c for the $[+15_2/0]_s$ laminate also compares well against experiment, although the upper limit on the wind tunnel velocity (30 m/s), which is below the linear flutter velocity of the $[+15_2/0]_s$ laminate, did not allow for an experimental investigation into the phenomenon of sharp drop from linear to nonlinear behavior. The nonlinear analysis in Figure 20d for the $[-15_2/0]_s$ laminate compares reasonably with experiment when considered in the light of three factors: (i) the analysis and experiment both indicate a bending flutter frequency (note that the frequency scale in Figure 20d is magnified as compared to Figures 20a, 20b, and 20c), (ii) the analysis and experiment display the same trend for flutter velocity, only shifted by a few meters/second, and (iii) more discrepancy is expected for the $[-15_2/0]_s$ laminate since it reaches the nonlinear regime more quickly.
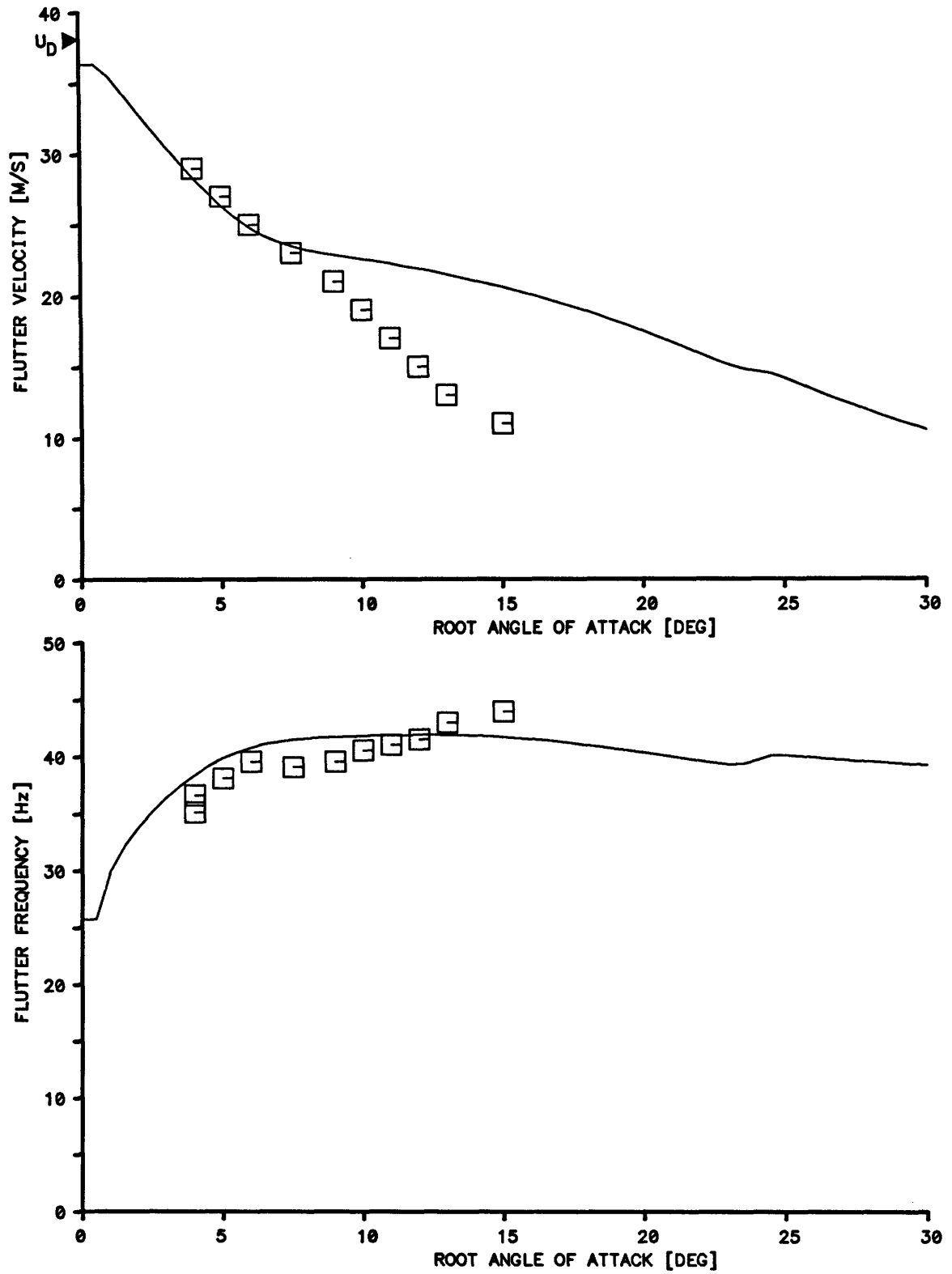
Figure 20a. $[0_2/90]_s$ flutter boundary and frequency variation
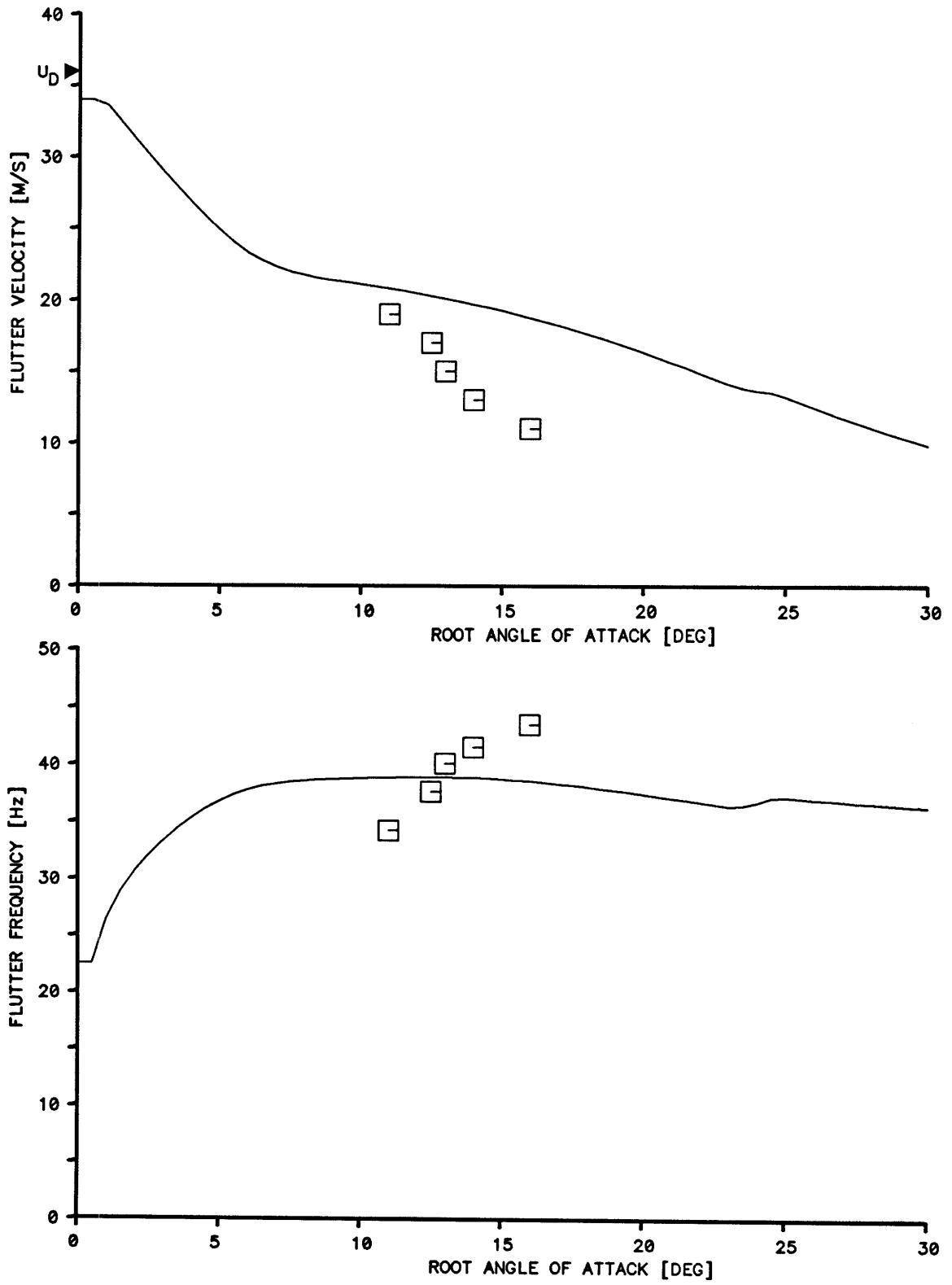
Figure 20b. $[90/0_2]_s$ flutter boundary and frequency variation
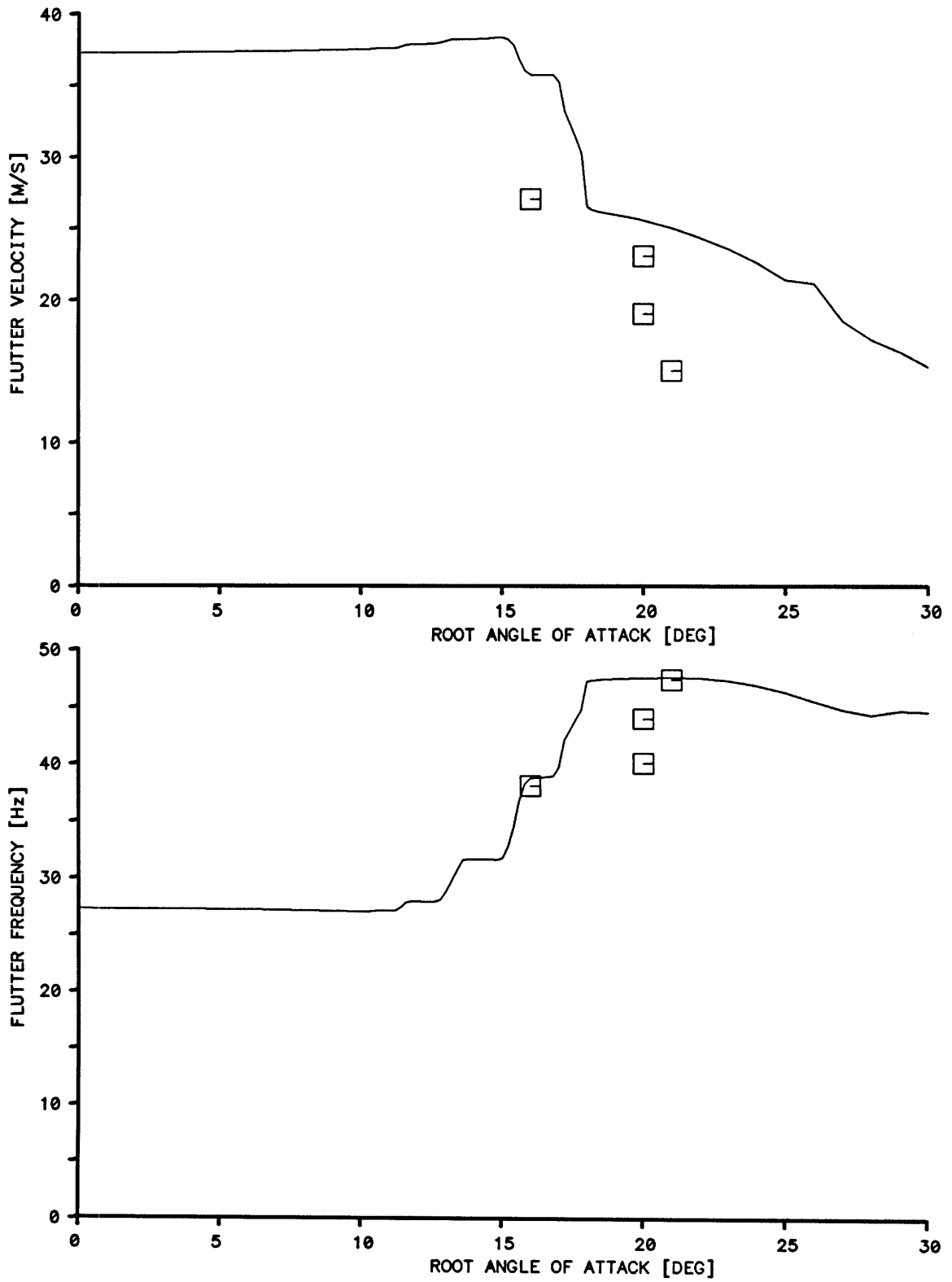
Figure 20c. $[+15_2/0]_s$ flutter boundary and frequency variation
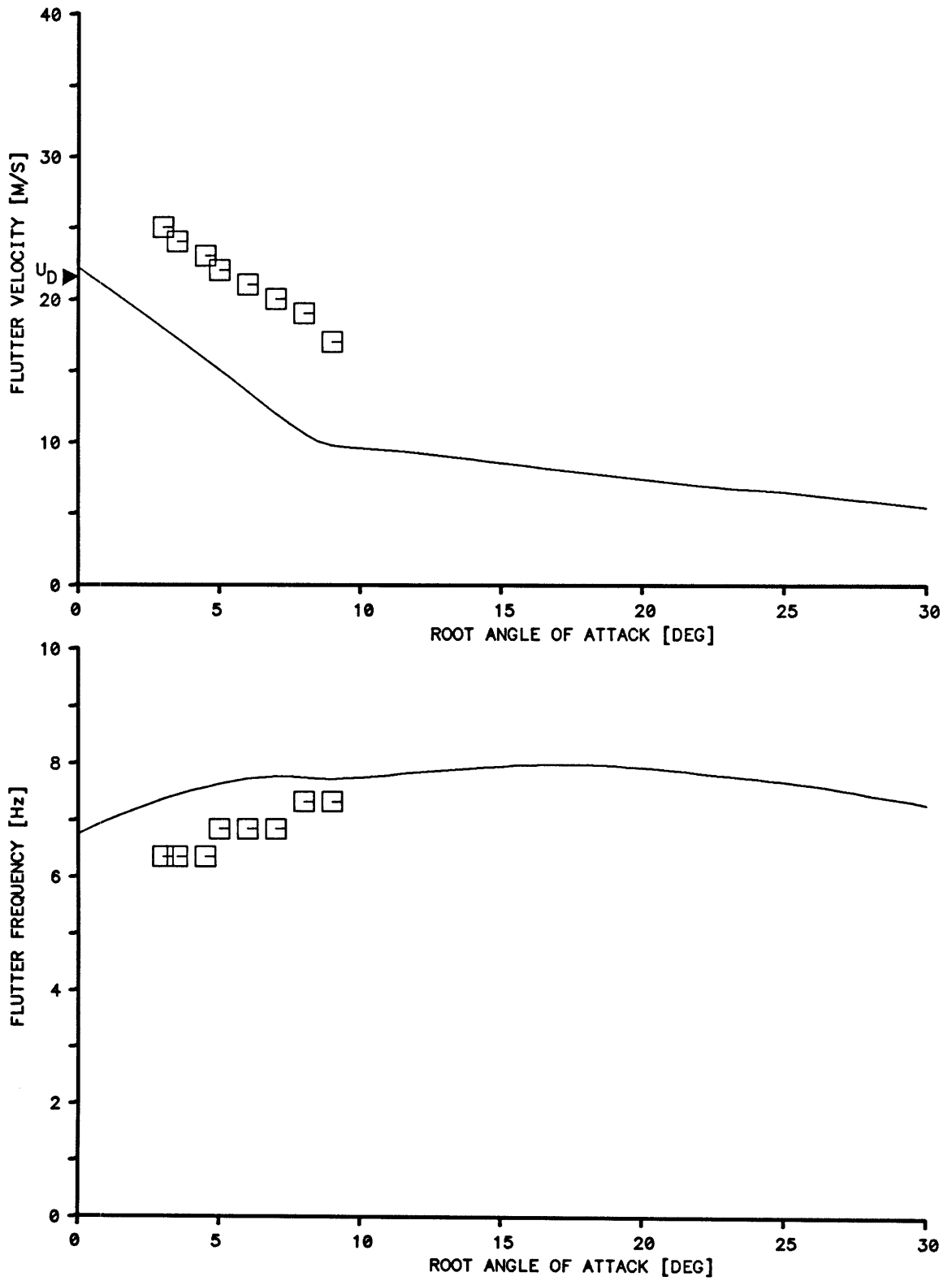
Figure 20d. $[-15_2/0]_s$ flutter boundary and frequency variation

4.5.4 Large-Amplitude, Nonlinear Flutter
without Cubic Stiffening

The experimental and analytic flutter characteristics for increasing amplitudes of oscillation are presented in Figures 21 to 24. Each set of figures contains (a) the graph of the variation of time-averaged midchord tip deflection with increasing velocity for lines of constant root angle-of-attack, (b) the graph of the variation of time-averaged total tip angle (the sum of the root angle-of-attack and the tip twist) with increasing velocity for lines of constant root angle-of-attack, and (c) the graphs of variation of midchord tip deflection and tip twist amplitudes of oscillation. For each line of constant root angle-of-attack, both the steady, static analysis (unsteady terms suppressed; solid lines) and the nonlinear, unsteady flutter analysis (dotted lines) are presented, so as to show where the two meet (equivalent to the flutter boundary) and how each diverges from the other. Likewise, both the steady, static experimental data (hollow symbols) and the unsteady, flutter experimental data (filled-in symbols) are presented. The linear divergence speeds, as shown in Section 4.5.2 and listed in Table 2, are also marked for comparison. For these cases the cubic stiffening was not included in the structural part of the analysis and only two mode shapes (1st bending and first torsion) were used.

Figures 21 and 22 for the $[0_2/90]_s$ and $[90/0_2]_s$ laminates show the same trends in analysis: both the midchord tip deflection and total tip angle show a sharp decrease when the

velocity is increased past the flutter boundary. Although it is not clearly evident in the graphs of midchord tip deflection (but is more clear in Figures 18a and 18c), the experimental trend for midchord tip deflection actually increases. However, the experimental trend for tip angle does decrease in accordance with the analytic trend - this is deemed more significant since the angle plays a larger role in the governing aerodynamics than does the deflection. As expected, Figures 21c and 22c demonstrate the high torsional content of this flutter. Figure 23 for the $[+15_2/0]_s$ laminate shows an analytic softening trend in the flutter characteristic: that is, once past the flutter boundary, a decrease in velocity will increase the flutter amplitude. Again, the upper limit on the velocity of the wind tunnel precluded investigating any of this phenomenon experimentally. Figure 24 for the $[-15_2/0]_s$ laminate shows a more gentle deviation from the steady analysis, as compared to the sharp change in character demonstrated by the $[0_2/90]_s$ and $[90/0_2]_s$ laminates in Figures 21 and 22. Figure 24c, showing the amplitude of oscillation of the bending and torsion components, displays a much higher bending component, as would be expected for this predominantly bending stall flutter. Again, as with the flutter boundary for the $[-15_2/0]_s$ laminate, analysis and experiment show similar trends.
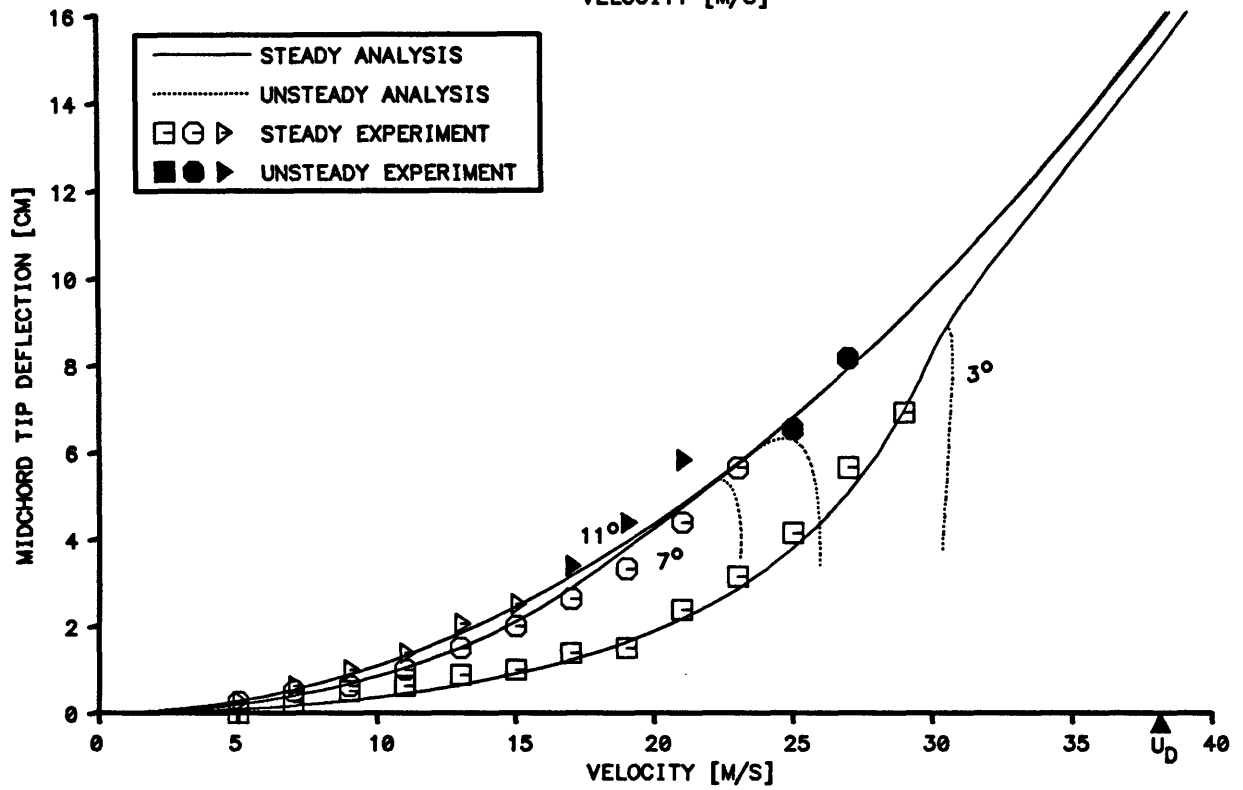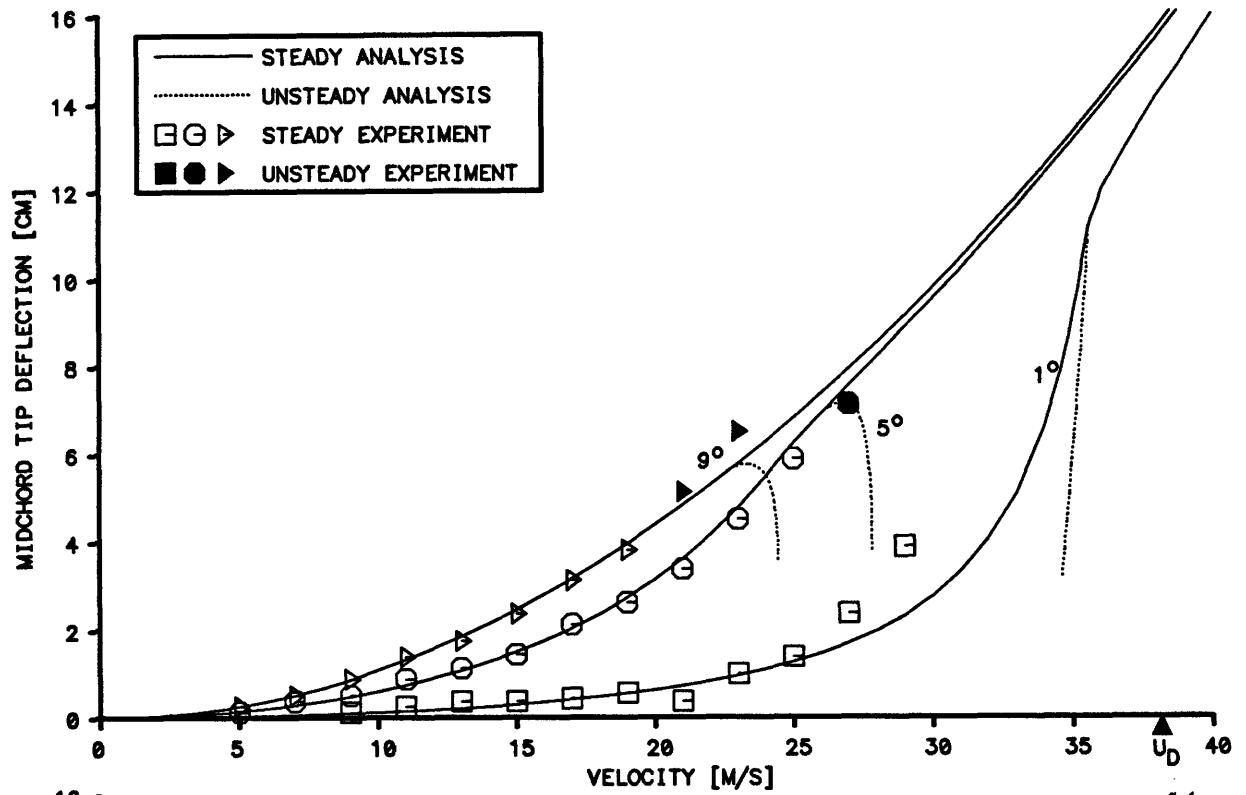
Figure 21a. $[0_2/90]_s$ averaged midchord tip deflections, compared against nonlinear flutter analysis
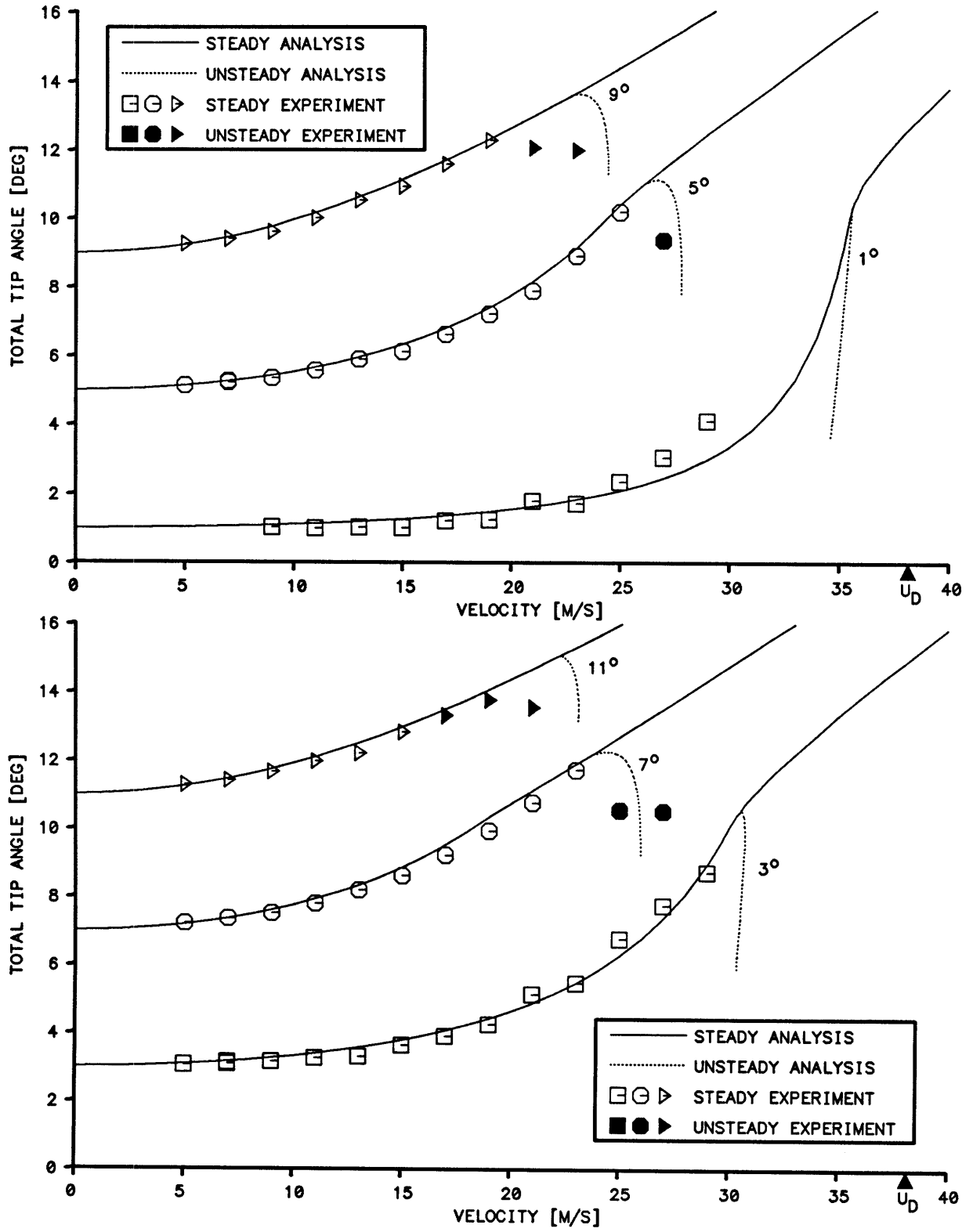
Figure 21b. [0₂/90]ₛ averaged total tip angle, compared against nonlinear flutter analysis
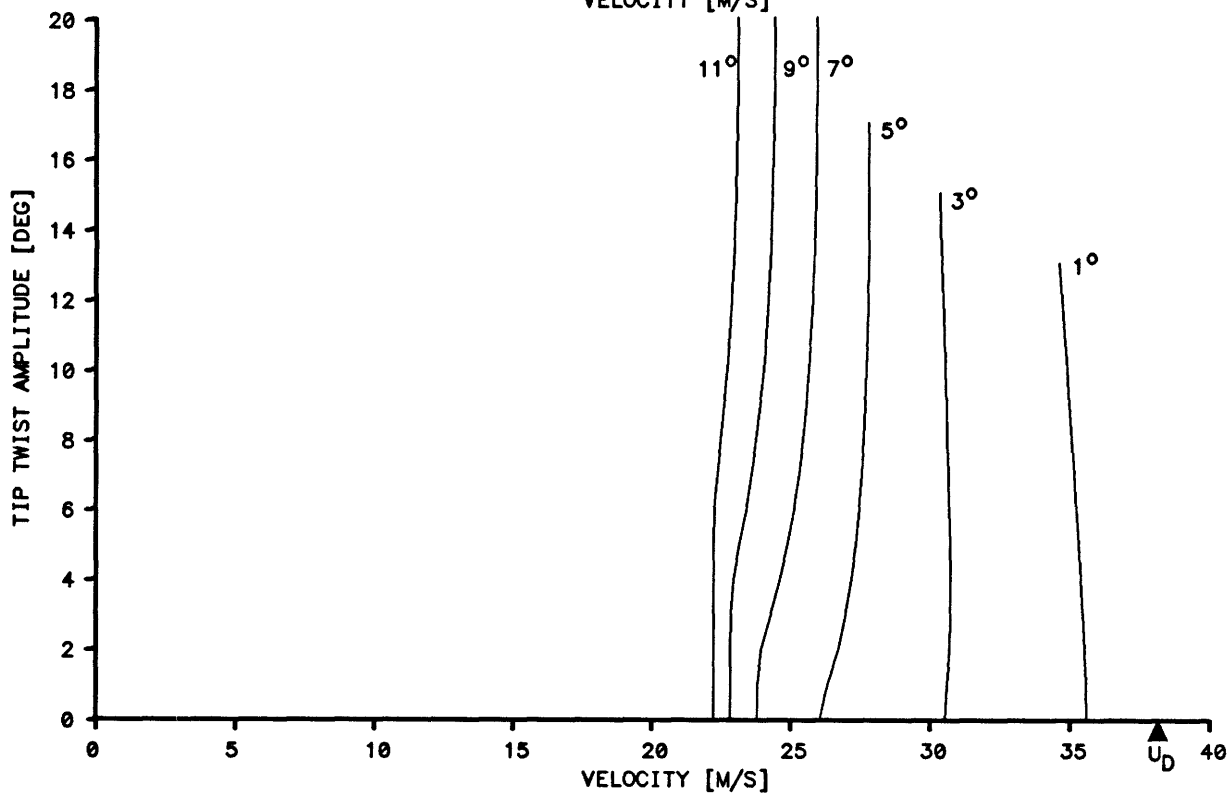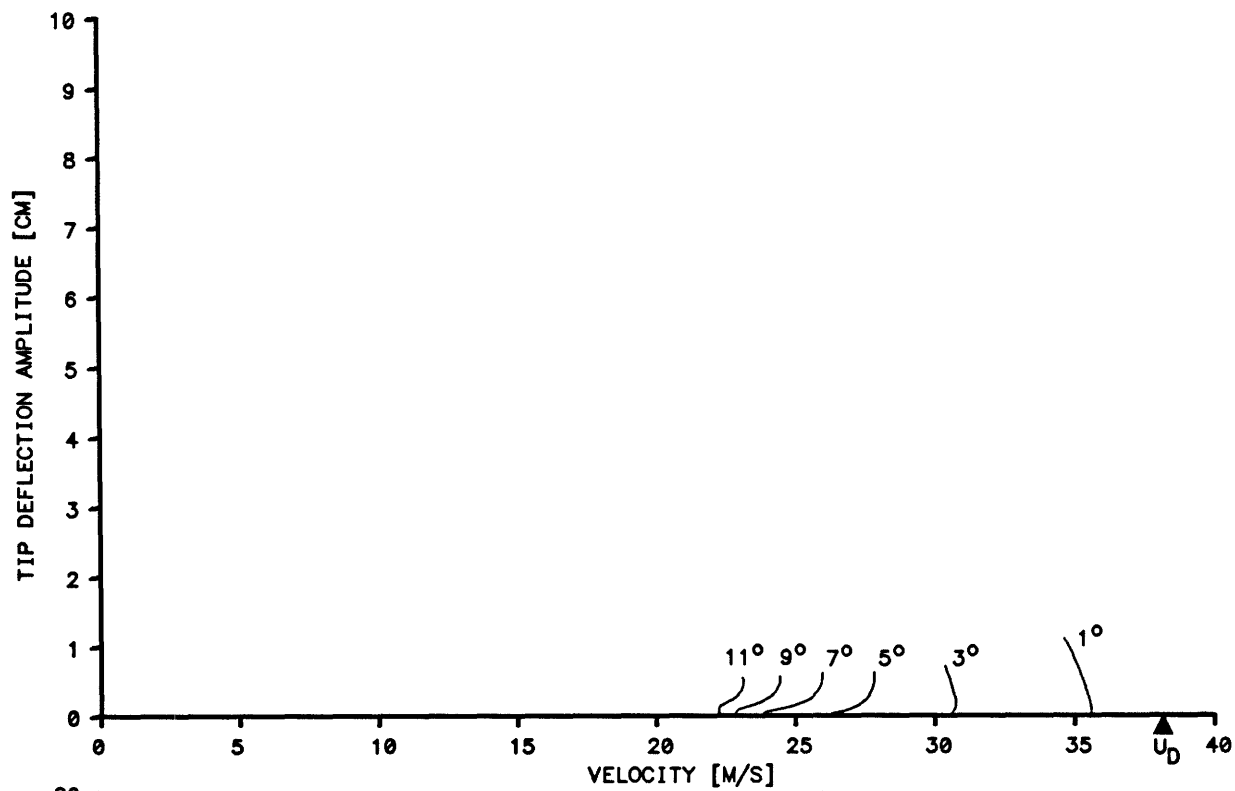
Figure 21c. $[0_2/90]_s$ deflection oscillation amplitudes
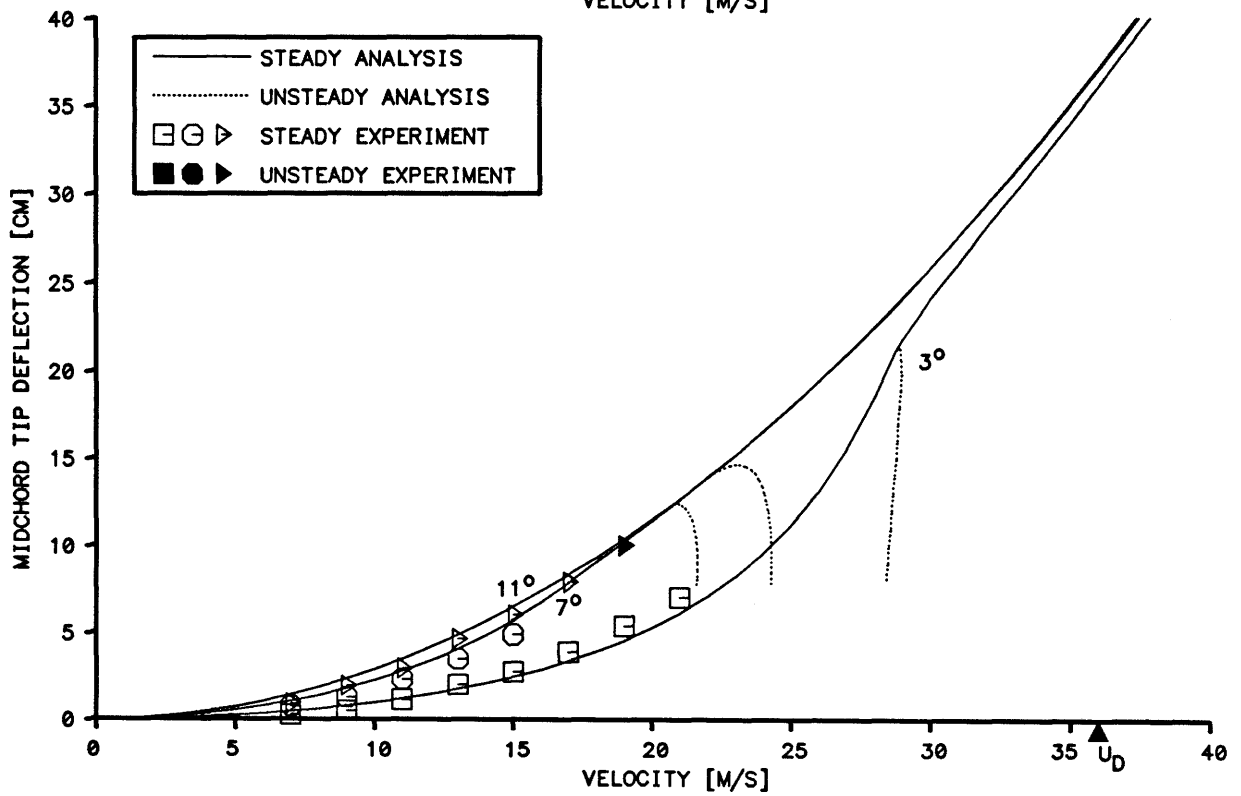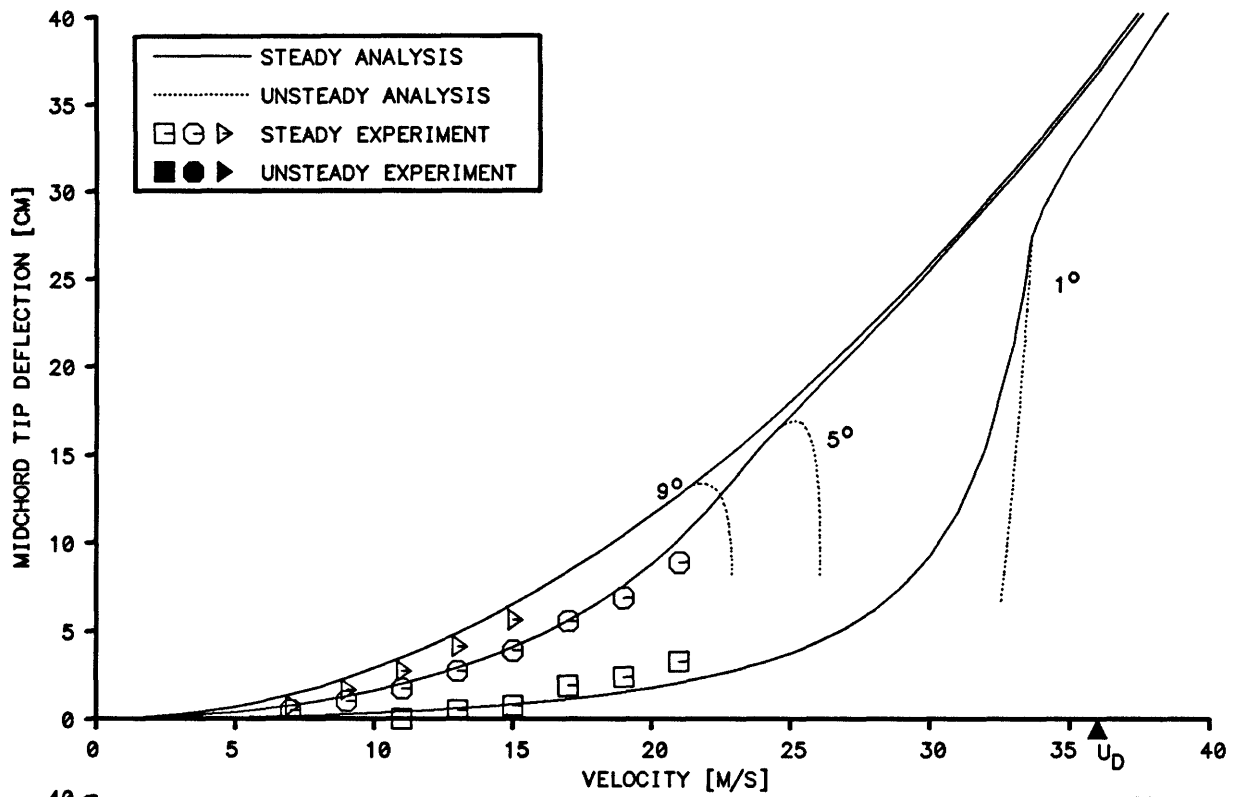
Figure 22a. $[90/0_2]_s$ averaged midchord tip deflections, compared against nonlinear flutter analysis
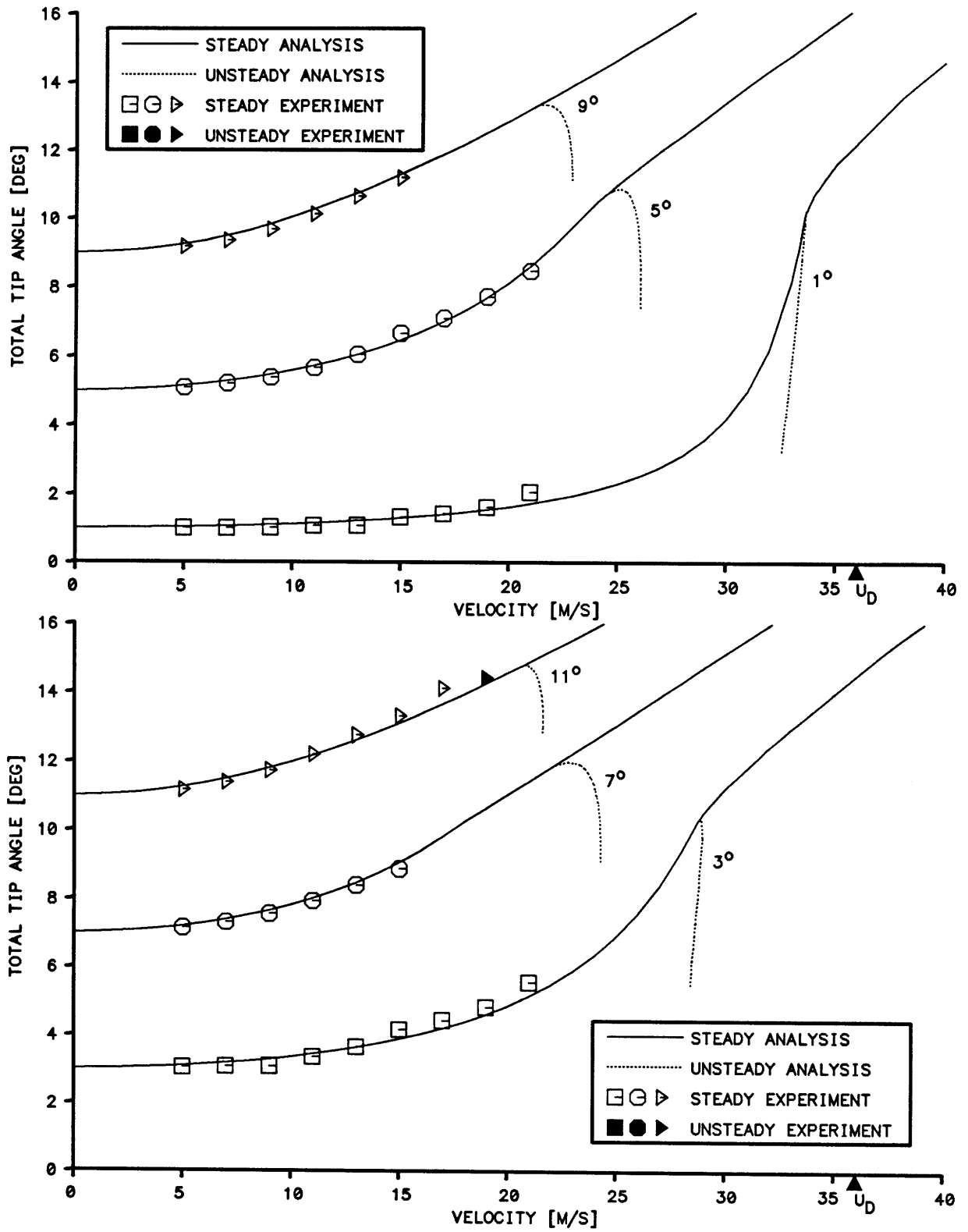
Figure 22b. $[90/0_2]_s$ averaged total tip angle, compared against nonlinear flutter analysis
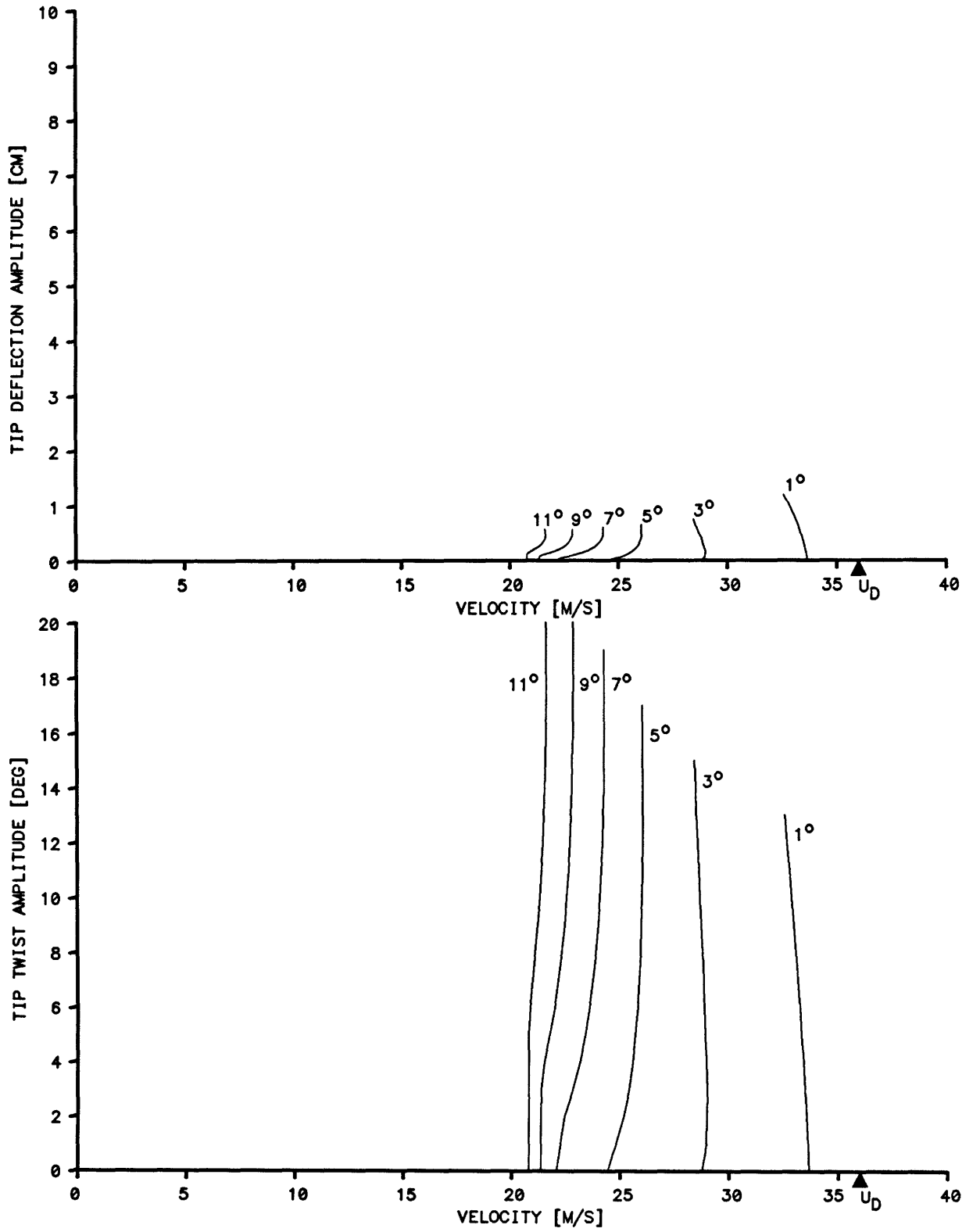
Figure 22c. [90/0₂]ₛ deflection oscillation amplitudes
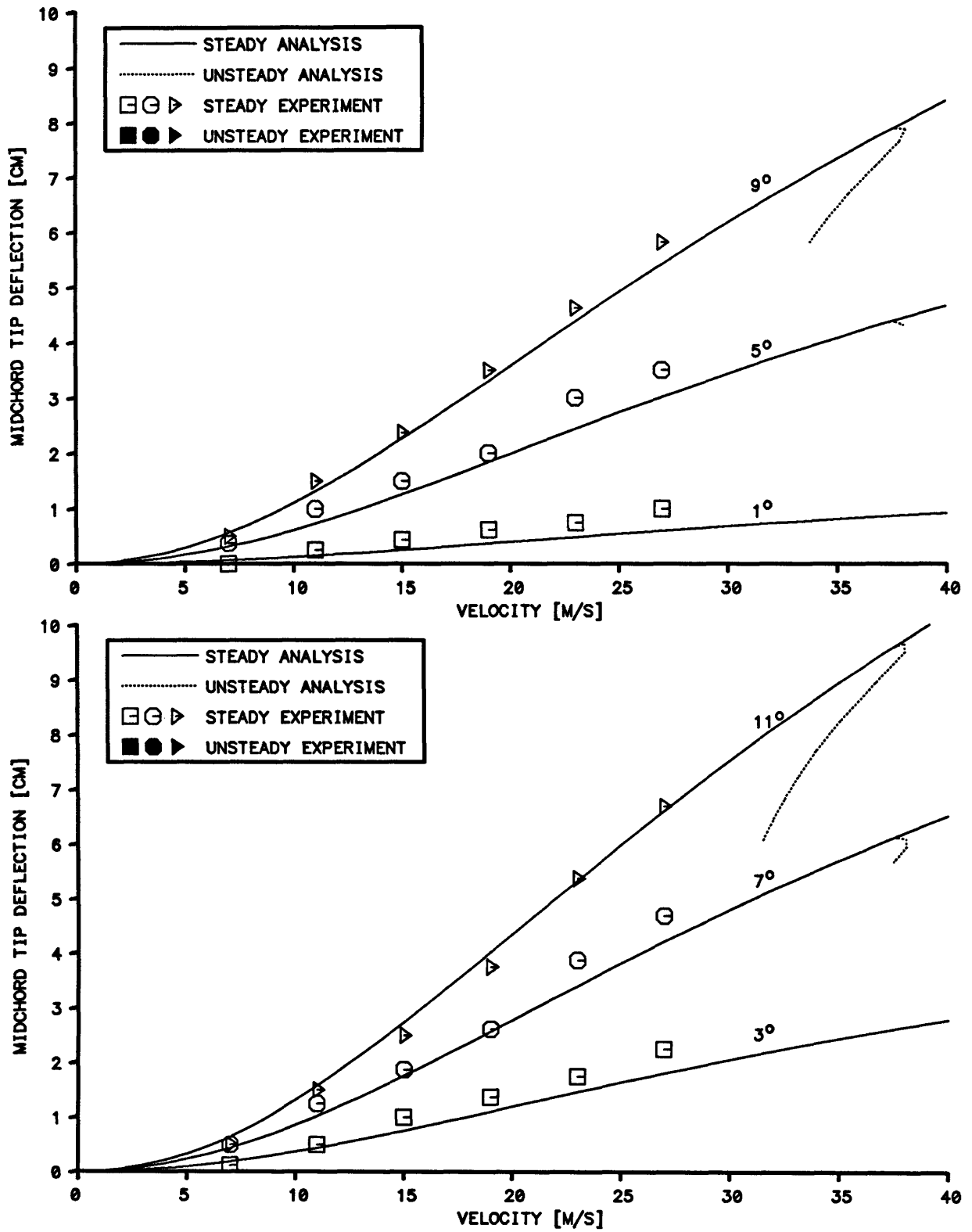
Figure 23a. $[+15_2/0]_s$ averaged midchord tip deflections, compared against nonlinear flutter analysis
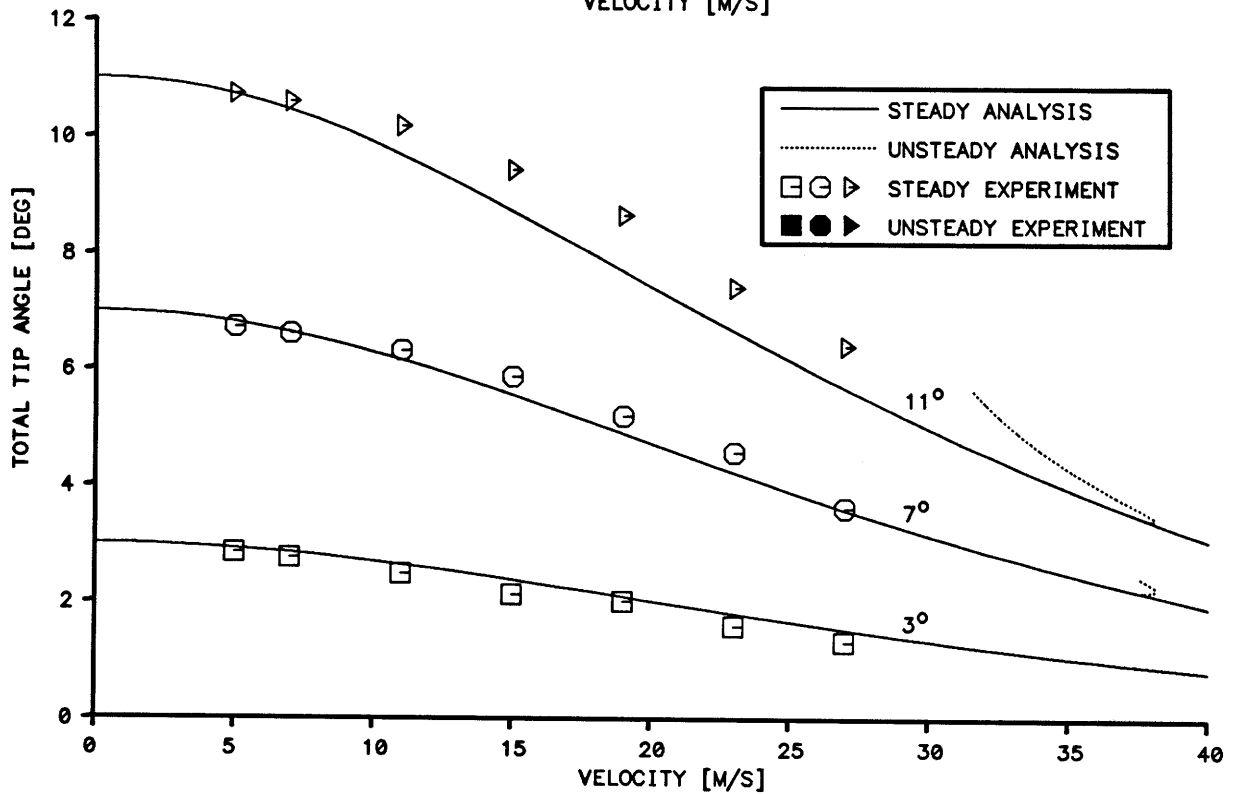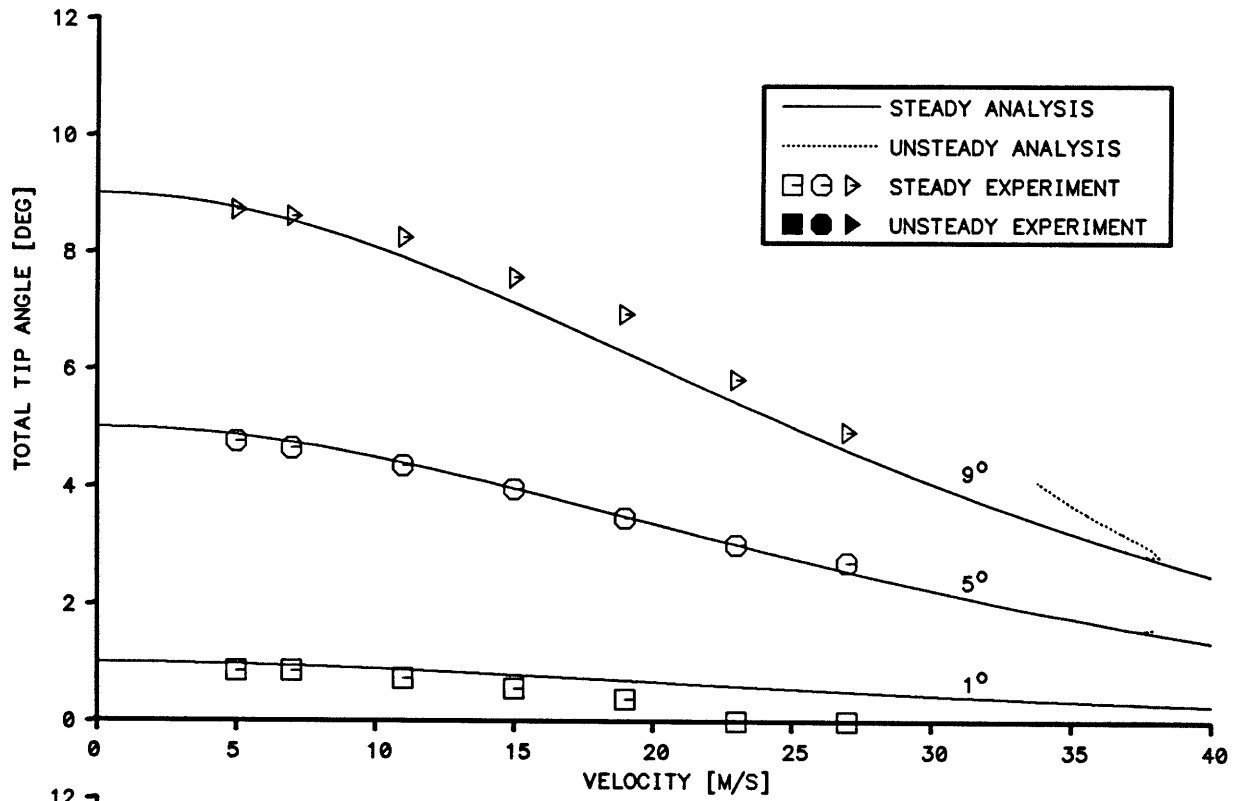
Figure 23b. $[+15_2/0]_s$ averaged total tip angle, compared against nonlinear flutter analysis
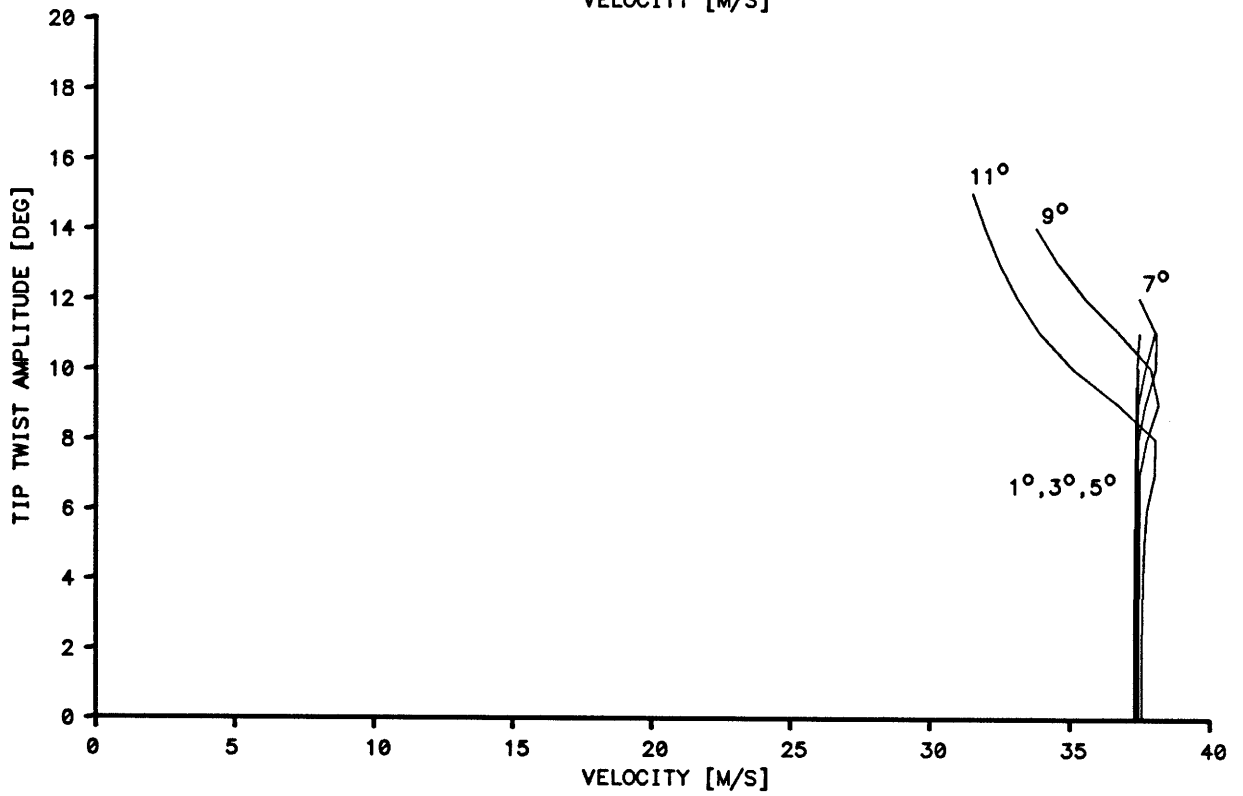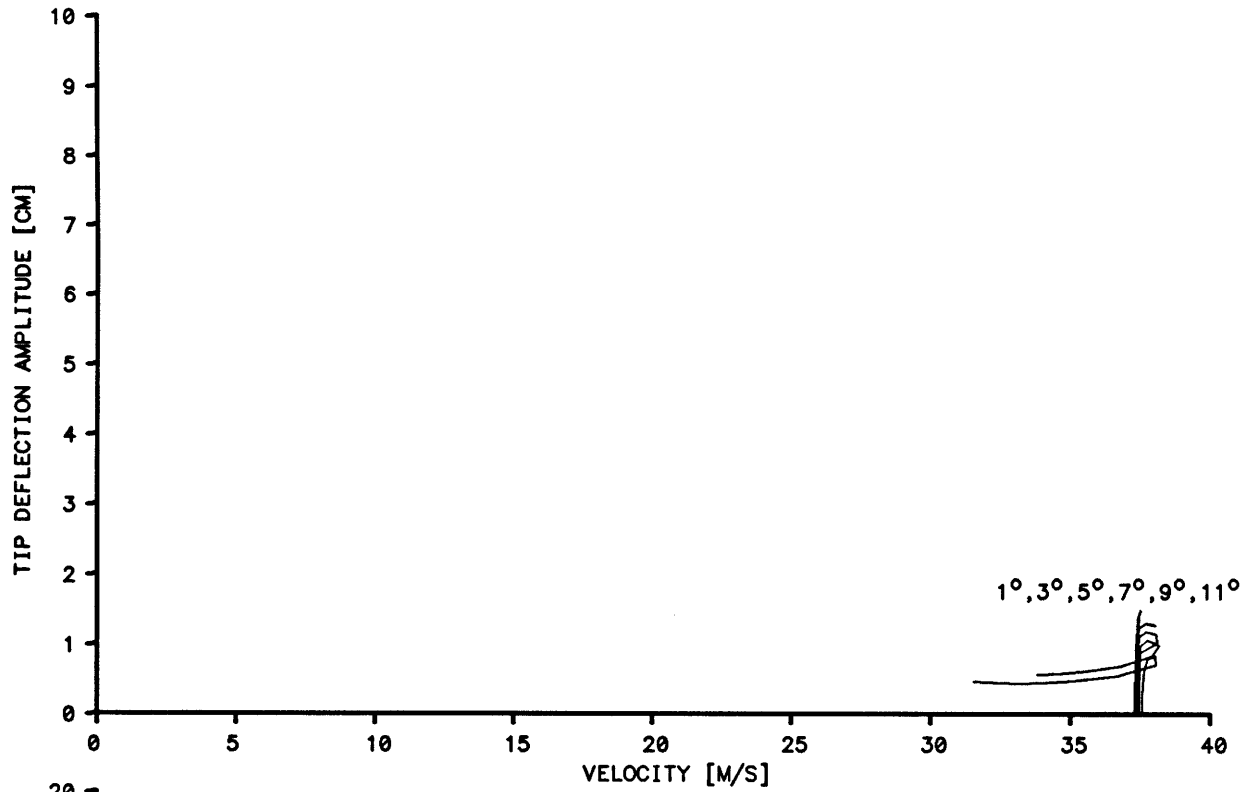
Figure 23c. $[+15_2/0]_s$ deflection oscillation amplitudes
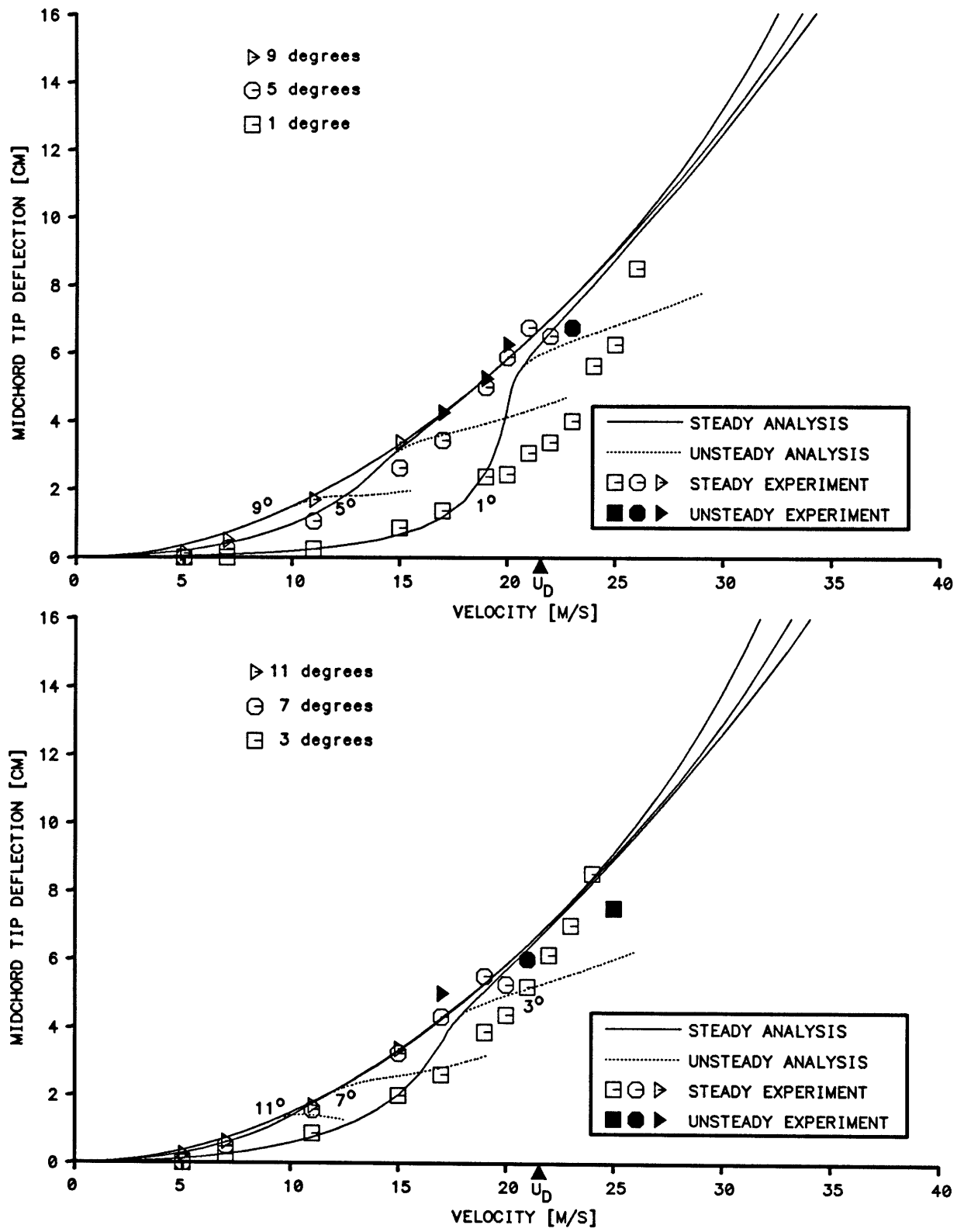
Figure 24a. $[-15_2/0]_s$ averaged midchord tip deflections, compared against nonlinear flutter analysis
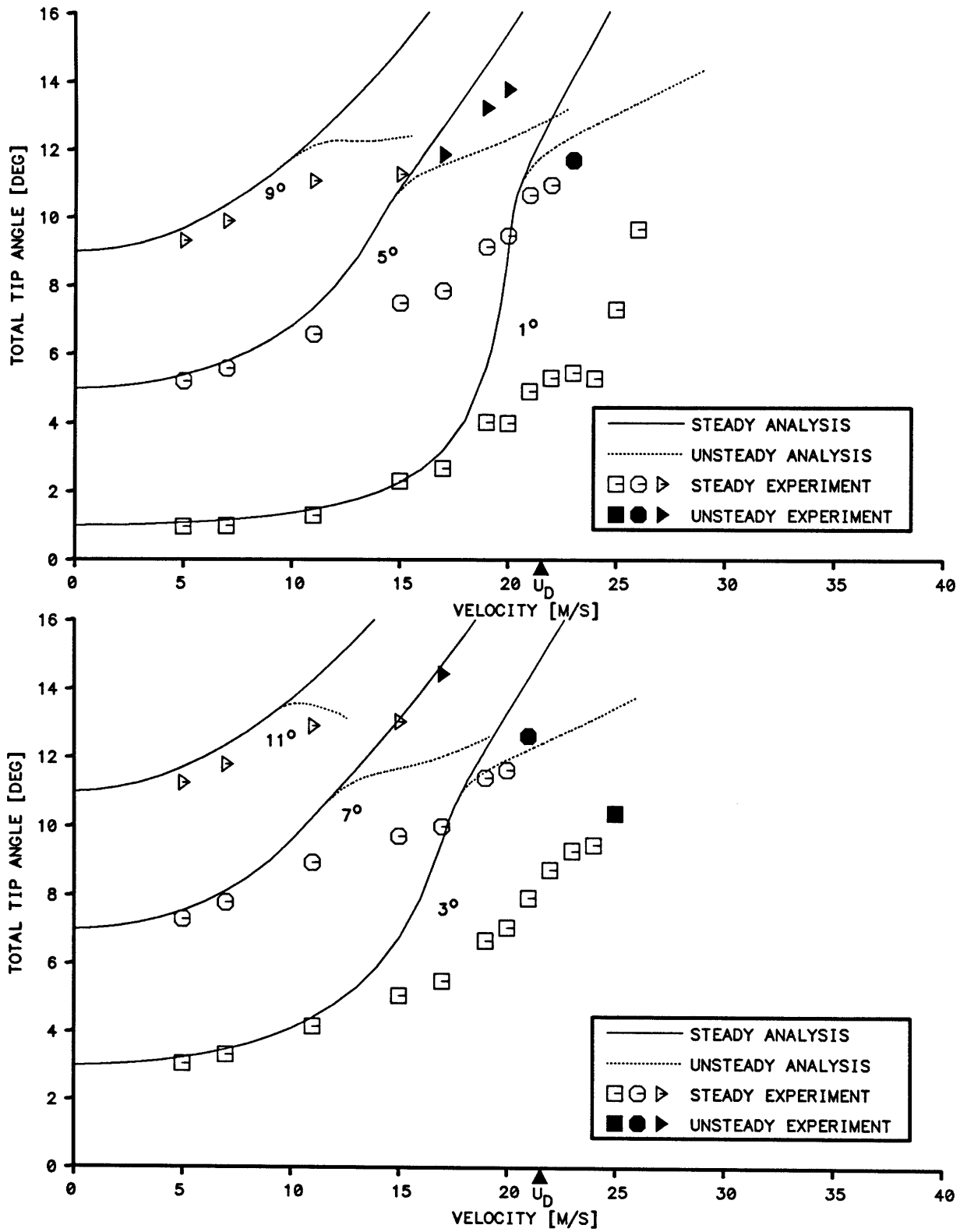
Figure 24b. $[-15_2/0]_s$ averaged total tip angle, compared against nonlinear flutter analysis
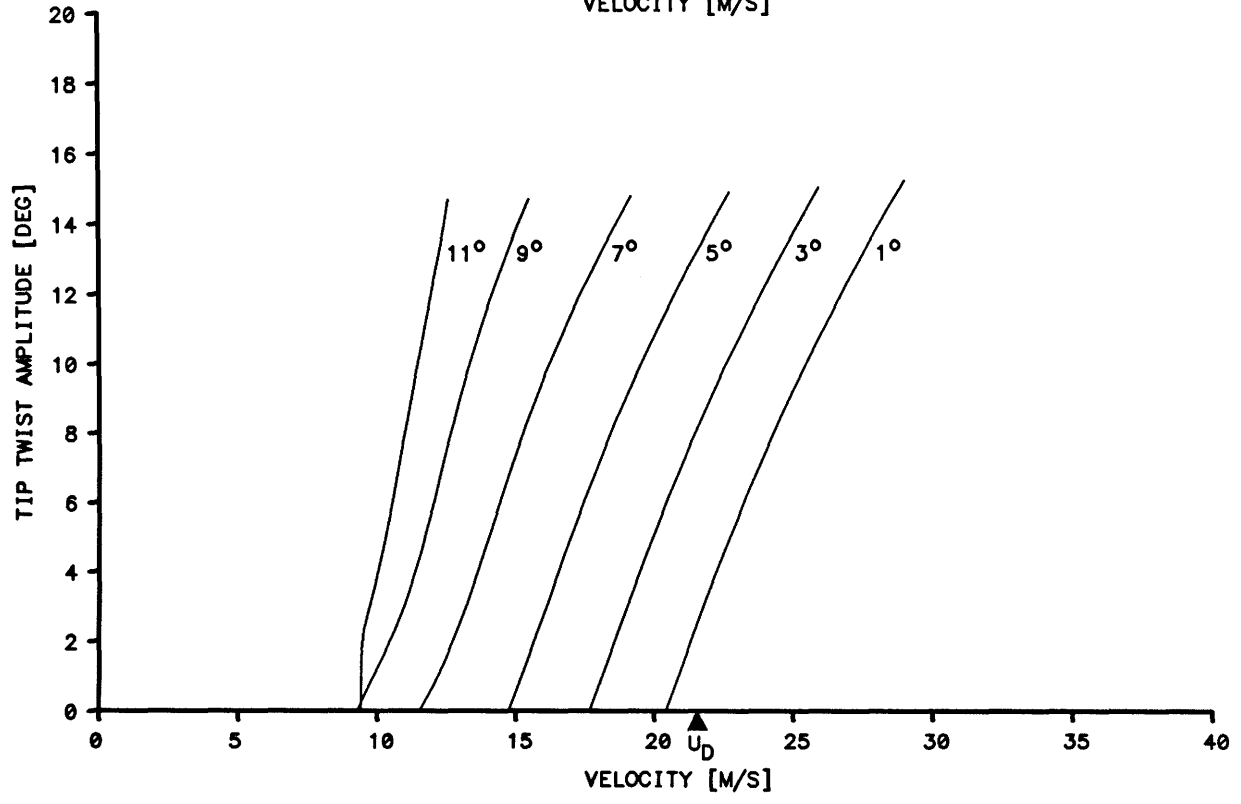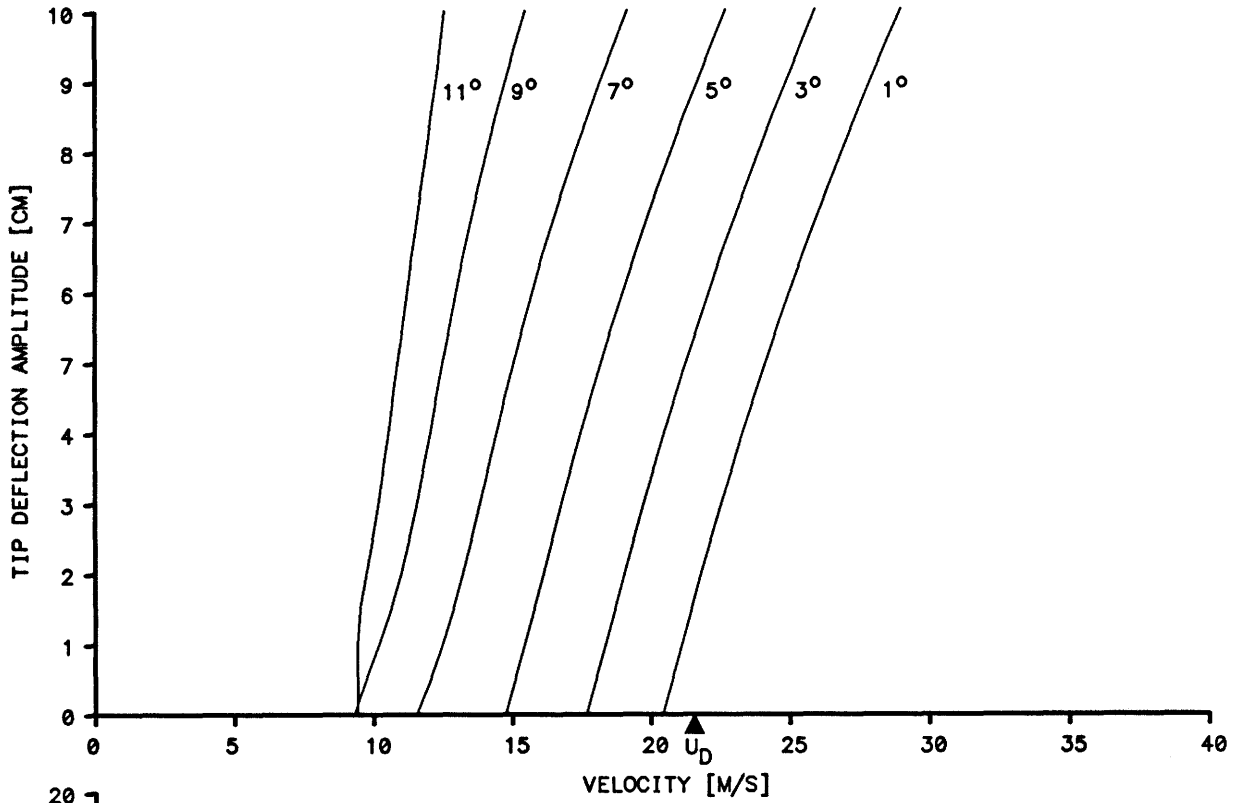
Figure 24c. $[-15_2/0]_s$ deflection oscillation amplitudes

4.5.5 Large-Amplitude, Nonlinear Flutter
with Cubic Stiffening

Figures 25 and 26 show the same results as for Sections
4.5.3 and 4.5.4 for the $[0_2/90]_s$ wing, but with the cubic
stiffening effects now included in the structural analysis.
Figure 25 shows that the flutter boundary follows a similar
trend as in Figure 20a, except that the nonlinear structures
push the flutter velocity into the nonlinear region above the
divergence velocity for very low root angles-of-attack   This
indicates two viable solutions at low root angle-of-attack:
the first below the divergence velocity where the tip angle
operates in the linear region of the cubic torsional stiff-
ness curve, the second above the divergence velocity where
the tip angle operates in the highly nonlinear region of the
cubic torsional stiffness curve.   This phenomenon occurs
because the tip angles become large, thus operating on a
steeper portion of the torsional stiffness curve, and there-
fore resulting in higher torsional frequency and correspond-
ing higher flutter velocity.   The analysis shows a reversal
in trend for the flutter frequency: with the cubic stiffening
included, the flutter frequency decreases with increasing
root angle of attack, while it had previously increased with
increasing root angle of attack in Figure 20a.   This occurs
because the average angle-of-attack decreases as the root
angle-of-attack increases, thus operating on a less steep
portion of the torsional stiffness curve, therefore resulting
in decreasing torsional frequency.   Both these trends show a

strong influence from the nonlinear structures when the flutter velocity is near the divergence velocity.

Figures 26a to 26c demonstrate more reasonable results for the large amplitude, nonlinear stall behavior than those presented in Section 4.5.4. Figures 21, 22, and 23 demonstrated softening effects from the nonlinear aerodynamics, that is, increasing amplitudes of oscillation could be analytically achieved by reducing the free stream velocity, and correspondingly no analytic solution exists above the flutter velocity. This trend seems both counter-intuitive and runs counter to the experimental results, where the amplitudes of oscillation increased with increasing free stream velocity. However, as seen in Figures 26a to 26c, with the cubic stiffening included in the structural analysis, the amplitude of oscillation now increases with increasing velocity, while the general trends of decreased midchord tip deflection and tip angle still reflect the same trends seen in Section 4.5.4. These figures demonstrate the governing roles of the two nonlinearities: the nonlinear aerodynamics contribute primarily to the coupling between the steady and unsteady terms in the aeroelastic problem, while the nonlinear structures contribute primarily to the overall stiffening and large amplitude behavior of the aeroelastic problem.

While the nonlinear structures give the expected, intuitive results that compare well against experimental trends for increasing velocity, Figures 25 and 26 still show some room for refinement. Notably, the increase in flutter veloc-

ities and the change in trend of the flutter frequencies indicate that the magnitude of the cubic stiffening term may have been overestimated. This discrepancy might be accounted for by two factors: (i) the cubic stiffening factor was determined for a 5-mode Rayleigh-Ritz analysis applied to the static deflection tests, while the analysis in this section uses only two modes, and (ii) the coupling effects between large amplitude deflection in the 1st bending mode and torsional stiffening has not been investigated at all. Cursory investigation has shown that reducing the number of modes from five to two increases the effect of the cubic stiffening, i.e. reduction to two modes without appropriate compensation to the cubic stiffening results in an over-estimation of the cubic stiffening term by a factor of approximately two. The effect of large deflections in the first bending mode are yet to be investigated.
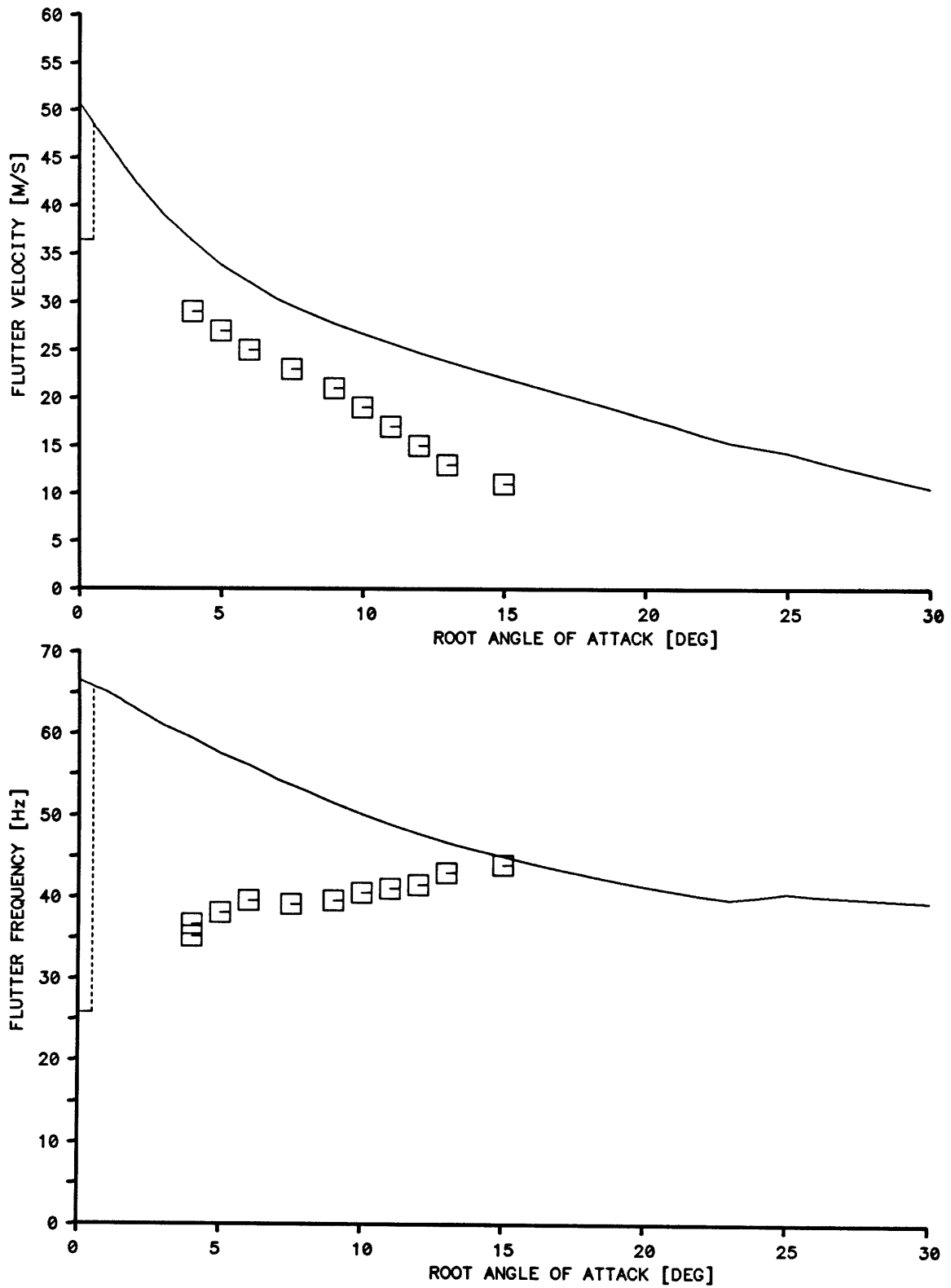
Figure 25. $[0_2/90]_s$ flutter boundary and frequency variation with cubic stiffening included
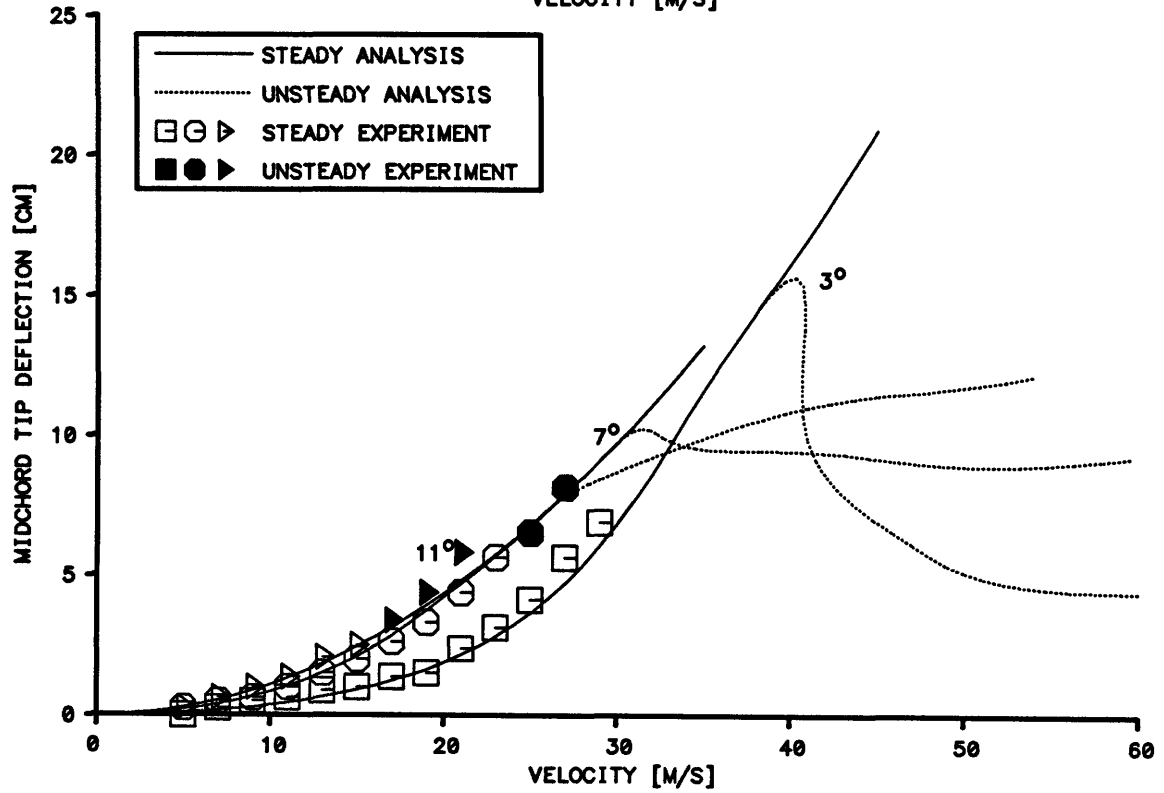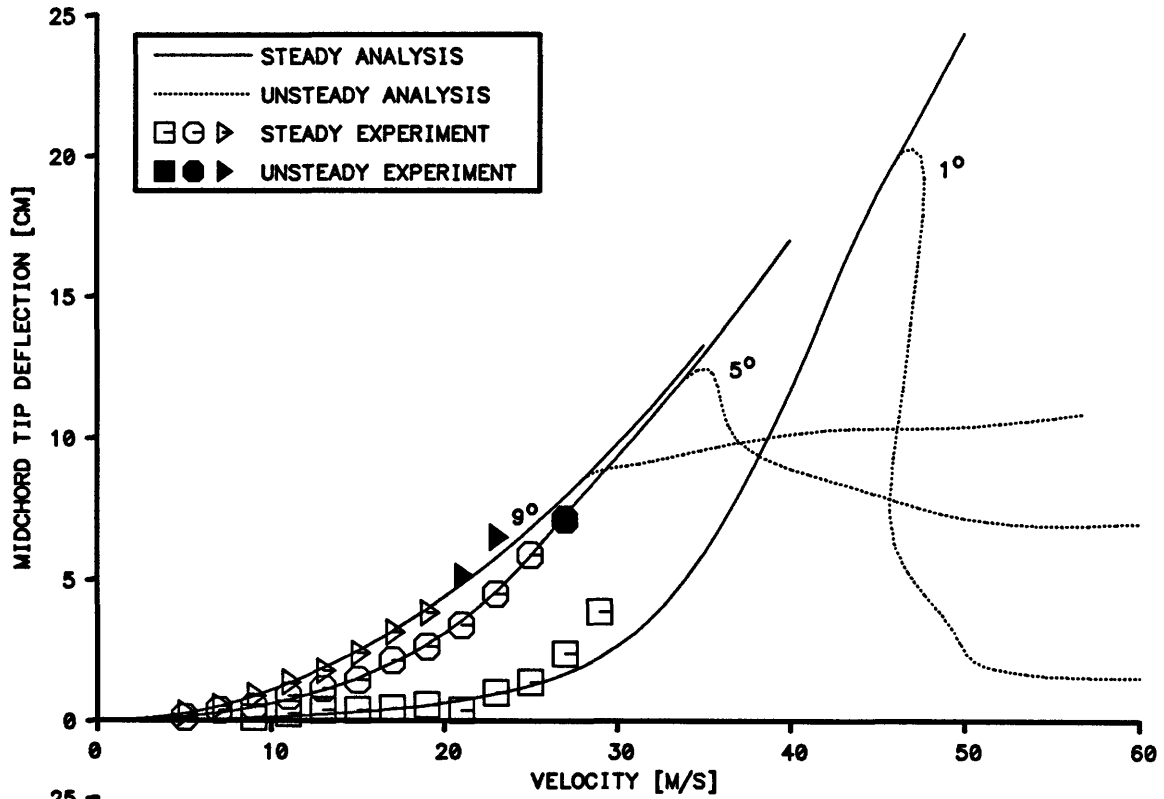
Figure 26a. $[0_2/90]_s$ averaged midchord tip deflections
vs. nonlinear flutter analysis with cubic stiffening
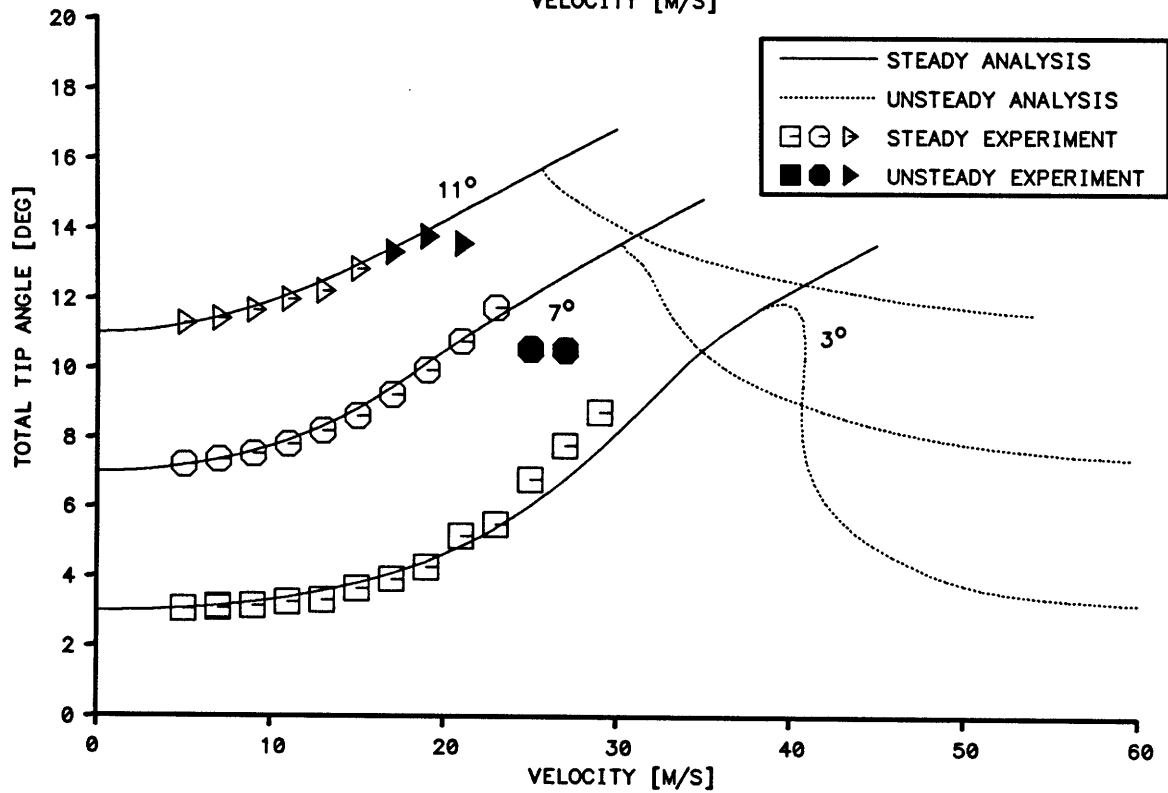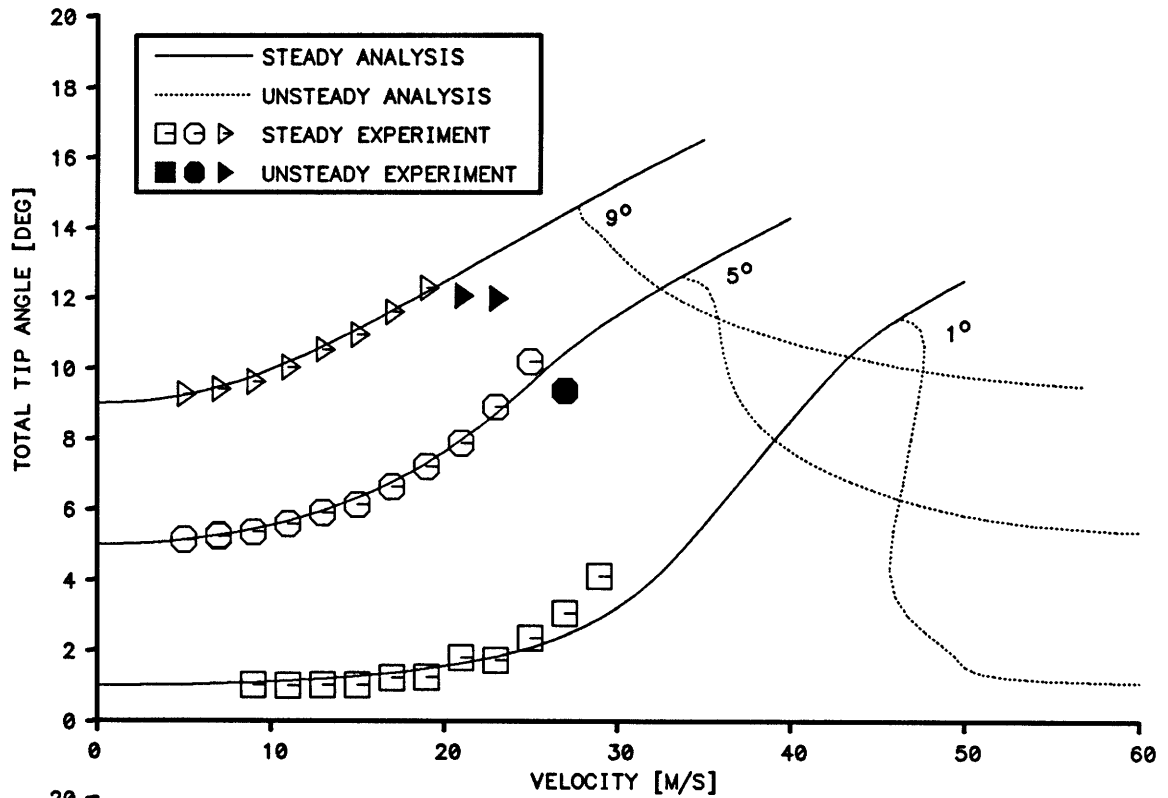
Figure 26b. $[0_2/90]_s$ averaged total tip angle
vs. nonlinear flutter analysis with cubic stiffening
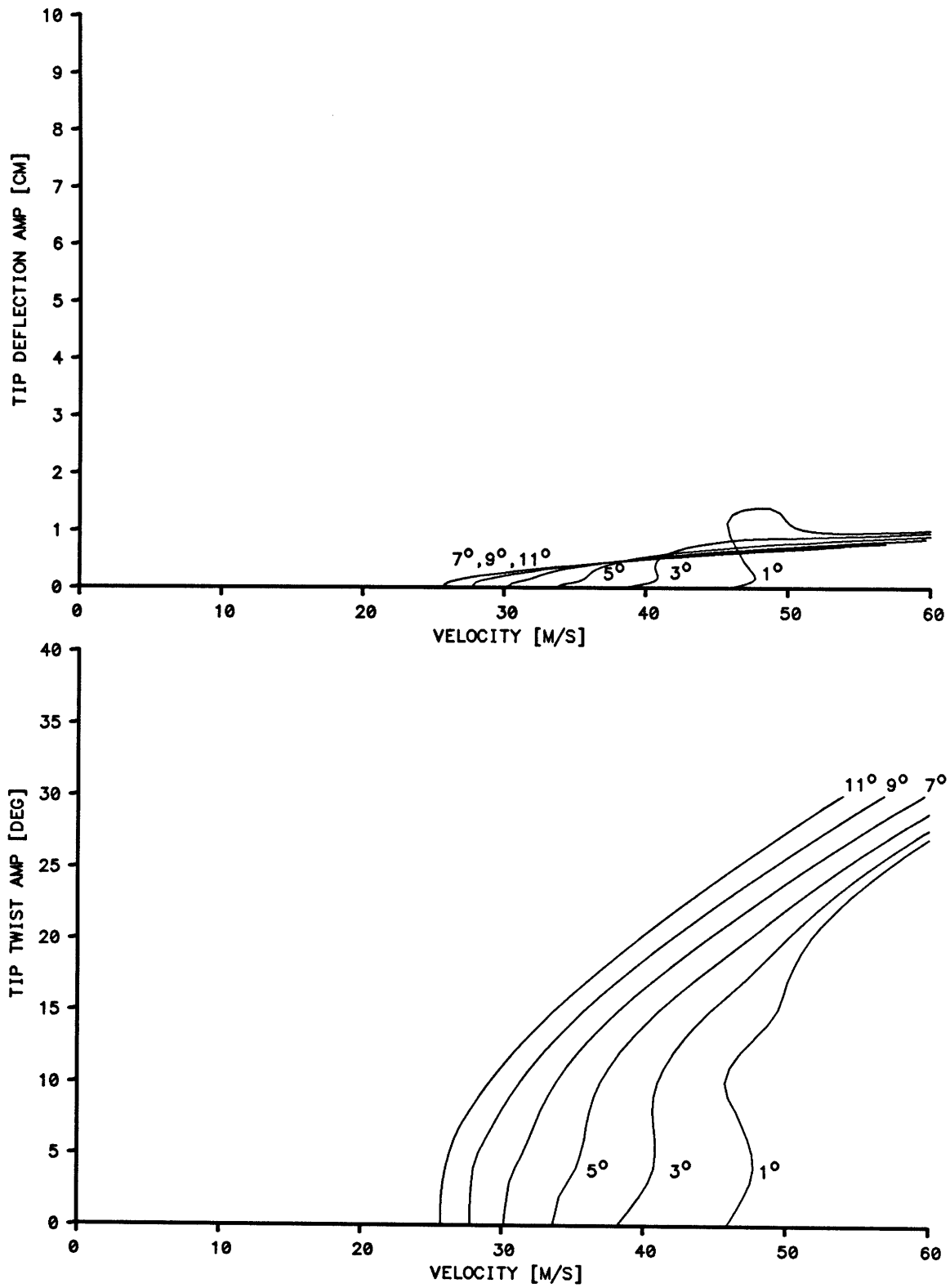
Figure 26c. $[0_2/90]_s$ deflection oscillation amplitudes from nonlinear flutter analysis with cubic stiffening

CHAPTER V
CONCLUSIONS AND RECOMMENDATIONS

An analytic method has been produced to include non-linear structural and aerodynamic effects into a full, 3-dimensional, aeroelastic problem, using the mathematical tools of Fourier analysis, harmonic balance, and the Newton-Raphson method as a numerical solver. The method makes use of the cubic torsional stiffness model together with the ONERA stall flutter model for the aerodynamics. Although in the current investigation the method is used with many simplifications - for example in the simplification of the aerodynamic force curves, in the restricted range of low Reynold's numbers which are considered, and in the low number of harmonics used in the harmonic balance method - the method can easily be extended to implement more complex variations of these factors. The current analysis presents a large step forward from previous linear analyses, and allows for a broader range of nonlinear problems to be considered.

Experimental data have been obtained on a set of aero-elastically tailored wings with varying amounts of bending-torsion coupling. These matched the trends of previous studies [Refs. 1, 2, 3, 4].

As shown in Chapter 4, the current nonlinear aeroelastic analysis predicts well almost all the observed, experimental, nonlinear stall phenomena. Specifically, flutter boundaries have been obtained which decrease with root angle of attack,

limit cycle amplitudes at flutter have been obtained, and the transitions from linear, bending-torsion flutter to torsional stall flutter, and from linear divergence to bending stall flutter, have been predicted analytically.

The advantages of the current analysis are several fold. First and foremost, the method is in such a form that it is generalizable to any type of airfoil and any range of Reynold's number, as long as the structural and aerodynamic characteristics of the airfoil are available. Second, the method is in a simplified form that relieves some of the cumbersomeness inherent in other methods (eg. computational fluid dynamics), and allows the user to choose the number of mode shapes or order of harmonics to suit his particular problem, while retaining the full nonlinearity of the problem. Third, by use of Fourier analysis and the harmonic balance method, the current analysis avoids the need for a time-marching method and avoids any computational time that might be needed in such a method to reach the final flutter limit cycle.

In spite of these advantages, the current analysis poses some problems and requires some further refinement. Although the method is generalizable to any airfoil, the unsteady experimental database for many airfoils does not currently exist. In particular, the semi-empirical coefficients used in the current study are values which had to be gleaned from other low Reynold's number studies, since they are difficult to find for the NACA-0012 airfoil at low Reynold's numbers.

Also, the coefficients could be refined to reflect larger amplitudes where stalling occurs on both sides of the airfoil. The results of the current investigation could be improved by conducting 2-dimensional, low Reynold's number oscillation tests for the NACA-0012 airfoil, or by conducting computational fluid dynamics studies of the airfoil characteristics.

The current investigation also used a simplified, empirical cubic stiffening factor to model the structural nonlinearity. This could be improved through more in-depth analysis, and by using a more general plate theory to model the deflections.

The model does not determine the stability of the limit cycles which it predicts. As already seen in the final section of Chapter 4, because the problem is nonlinear, several solutions are viable. A method to determine the stability of each of these viable solution needs to also be incorporated into the analysis.

Lastly, the current analysis is still in effect a modified strip method, in that it considers no crossflow. These 3-dimensional effects also need to be investigated and, with the other simplifications made, need to be verified against some higher order method, such as computational fluid dynamics.

REFERENCES

1. Hollowell, S.J., and Dugundji, J., "Aeroelastic Flutter and Divergence of Stiffness Coupled, Graphite/Epoxy Cantilevered Plates," Journal of Aircraft, Vol. 21, January 1984, pp. 69-76.

2. Selby, H.P., "Aeroelastic Flutter and Divergence of Rectangular Wings with Bending-Torsion Coupling," Masters Thesis, Department of Aeronautics and Astronautics, M.I.T., January 1982.

3. Landsberger, B., and Dugundji, J., "Experimental Aeroelastic Behavior of Unswept and Forward Swept Graphite/Epoxy Wings," Journal of Aircraft, Vol. 22, August 1985, pp. 679-686.

4. Chen, G.-S., and Dugundji, J., "Experimental Aeroelastic Behavior of Forward-Swept Graphite/Epoxy Wings with Rigid-Body Freedom," Journal of Aircraft, Vol. 24, July 1987, pp. 454-462.

5. Tran, C.T., and Petot, D., "Semi-Empirical Model for the Dynamic Stall of Airfoils in View of Application to the Calculation of Responses of a Helicopter in Forward Flight," Vertica, Vol. 5, No. 1, 1981, pp. 35-53.

6. Dat, D., and Tran, C.T., "Investigation of the Stall Flutter of an Airfoil with a Semi-Empirical Model of 2-D Flow," Vertica, Vol. 7, No. 2, 1983, pp. 73-86.

7. Jacobs, E.N., Ward, K.E., and Pinkerton, R.M., "The Characteristics of 78 Related Airfoil Sections from Tests in the Variable-Density Wind Tunnel," NACA Report No. 460, 1933.

8. Meirovitch, L., Elements of Vibration Analysis, McGraw-Hill, Inc., 1975.

9. Jensen, D.W., "Natural Vibrations of Cantilever Graphite/Epoxy Plates with Bending-Torsion Coupling," Masters Thesis, Department of Aeronautics and Astronautics, M.I.T., August 1981.

10. Crawley, E.F., and Dugundji, J., "Frequency Determination and Non-Dimensionalization for Composite Cantilever Plates," Journal of Sound and Vibration, Vol. 72, No. 1, 1980, pp. 1-10.

11. Peters, D.A., "Toward a Unified Lift Model for Use in Rotor Blade Stability Analyses," Journal of the American Helicopter Society, July 1985, pp. 32-42.

12. Petot, D., and Dat, R., "Unsteady Aerodynamic Loads on an Oscillating Airfoil with Unsteady Stall," 2nd Workshop on Dynamics and Aeroelasticity Stability Modeling of Rotorcraft Systems, Florida Atlantic University, Boca Raton, Florida, November 1987.

13. Petot, D., and Loiseau, H., "Successive Smoothing Algorithm for Constructing the Semi-Empirical Model Developed at ONERA to Predict Unsteady Aerodynamic Forces," NASA TM-76681, March 1982.

14. Jacobs, E.N., and Sherman, A., "Airfoil Section Characteristics as Affected by Variations of the Reynold's Number," NACA Report No. 586, 1937.

15. McAlister, K.W., Pucci, S.L., McCroskey, W.J., and Carr, L.W., "An Experimental Study of Dynamic Stall on Advanced Airfoil Sections Volume 1: Summary of the Experiment," NASA TM-84245, July 1982.

16. McAlister, K.W., Pucci, S.L., McCroskey, W.J., and Carr, L.W., "An Experimental Study of Dynamic Stall on Advanced Airfoil Sections Volume 2: Pressure and Force Data," NASA TM-84245, September 1982.

17. Petot, D., "Dynamic Stall Modeling of the NACA 0012 Profile," Short Note, <u>Recherches Aérospatiales</u>, 1984-6, pp. 55-58.

18. Lagace, P.A., and Brewer, C.B., "TELAC Manufacturing Class Notes," Edition 0-2, Technology Laboratory for Advanced Composites, Department of Aeronautics and Astronautics, M.I.T.

19. Kuo, C.-C., Morino, L., and Dugundji, J., "Perturbation and Harmonic Balance Methods for Nonlinear Panel Flutter," AIAA Journal, Vol. 10, November 1972, pp. 1479-1484.

20. Rainey, G.A., "Preliminary Study of Some Factors Which Affect the Stall-Flutter Characteristics of Thin Wings," NACA TN-3622, March 1956.

APPENDIX A – MATERIAL PROPERTIES

Hercules AS4/3501-6 Graphite/Epoxy properties:

	Extensional	Flexural
Longitudinal modulus, E_L	143 GPa	97.3 GPa[1]
Transverse modulus, E_T	9.7 GPa	6.3 GPa[1]
Shear modulus, G_{LT}	4.9 GPa	5.3 GPa[2]
Poisson's ratio, ν_{LT}	0.30	0.28
Density, ρ	1540 kg/m^3	1540 kg/m^3
Nominal ply thickness, t	0.810 mm	0.810 mm

HD-300, high density styrofoam:

	Nominal	Current Analysis
Longitudinal modulus, E_L	24 MPa	10 MPa[1]
Transverse modulus, E_T	24 MPa	10 MPa[1]
Shear modulus, G_{LT}	15 MPa	10 MPa[1]
Poisson's ratio, ν_{LT}	0.30	0.30
Density, ρ	35 kg/m^3	35 kg/m^3
$Q_{11}^s = Q_{22}^s$	26.37 MPa	10.99 MPa
$Q_{12}^s = Q_{21}^s$	7.91 MPa	3.30 MPa
Q_{66}^s	15.00 MPa	10.00 MPa

(1) Based on static deflection tests

(2) Based on free vibration tests

APPENDIX B – STRUCTURAL AND MODE SHAPE CONSTANTS

Layup	D_{11} (N–m)	D_{22} (N–m)	D_{12} (N–m)	D_{66} (N–m)	D_{16} (N–m)	D_{26} (N–m)	K_{22}^C/K_{22}^L (m^{-2})
$[0_2/90]_s$	4.1811	0.4305	0.0785	0.2347	0.0000	0.0000	6000
$[90/0_2]_s$	1.4806	3.1309	0.0785	0.2347	0.0000	0.0000	9000
$[\pm15/0]_s$	3.8582	0.3301	0.2901	0.4463	0.3942	0.0559	ND*
$[+15_2/0]_s$	3.8582	0.3301	0.2901	0.4463	0.8541	0.1211	6000
$[\pm30/0]_s$	2.7212	0.6208	0.7133	0.8695	0.5589	0.2206	ND*
$[+30_2/0]_s$	2.7212	0.6208	0.7133	0.8695	1.2110	0.4780	ND*

* Not determined

NOTE: K_{22}^L is the <u>flat plate</u> torsion stiffness term

Layup**	β	n	g	f	B_{n1}	B_{n2}	B_{n4}
$[0_2/90]_s$	.02319	1	1.8123	6.8117	−.24029	+.90262	−.24015
		2	5.0371	8.2757	−.38882	+.63903	−.38895
$[90/0_2]_s$	.00821	1	1.7200	11.1672	−.14870	+.96545	−.14870
		2	5.0344	12.1283	−.32787	+.78985	−.32787
$[\pm15/0]_s$	.01126	1	1.7448	9.5856	−.17335	+.95230	−.17334
		2	5.0486	10.6925	−.35105	+.74351	−.35106
$[+15_2/0]_s$	.01126	1	1.7448	9.5856	−.17335	+.95230	−.17334
		2	5.0486	10.6925	−.35105	+.74351	−.35106
$[\pm30/0]_s$	.00408	1	1.6755	15.7544	−.10457	+.98327	−.10457
		2	4.9787	16.4372	−.26563	+.87697	−.26563
$[+30_2/0]_s$	.00408	1	1.6755	15.7544	−.10457	+.98327	−.10457
		2	4.9787	16.4372	−.26563	+.87697	−.26563

** In all cases $B_{n3} = -B_{n1}$

APPENDIX C - STATIC AERODYNAMIC MODELS

Raw data for the static lift curve of the NACA-0012 air-foil is taken from Jacobs and Sherman [Ref. 14] and is empirically fit using the previously described division into polynomial regions. For the current study, the Reynold's number is very low, always below the critical Reynold's number of approximately 340,000. Therefore, no Reynold's number dependence was incorporated for varying free stream velocity. As illustrated in Figure 27, the model of the 3-dimensional lift curve used in this study is divided into three regions and, for simplicity, each region is defined by a straight line: (i) below the stall angle, $\alpha_1 = 10^{\circ}$, the 3-dimensional lift slope is given by $a_{oL} \equiv C_{L\alpha} = 0.8 * 5.9$ rad^{-1} (where the 0.8 factor comes from the finite-span correction), (ii) between 10° and 20° the 3-dimensional lift coefficient drops linearly to 0.75, and (iii) above 20° the 3-dimensional lift coefficient remains constant at 0.75. The 3-dimensional moment coefficient follows the same trend: (i) it remains zero below the stall angle, (ii) drops linearly to -0.108 between 10° and 20°, and (iii) drops linearly to -0.150 between 20° and 37.5°. The two-dimensional profile drag is given by the polynomial,

$$C_{D_O} = 4.923\alpha^3 + .1473\alpha^2 + .042\alpha + .014 \qquad (C-1)$$
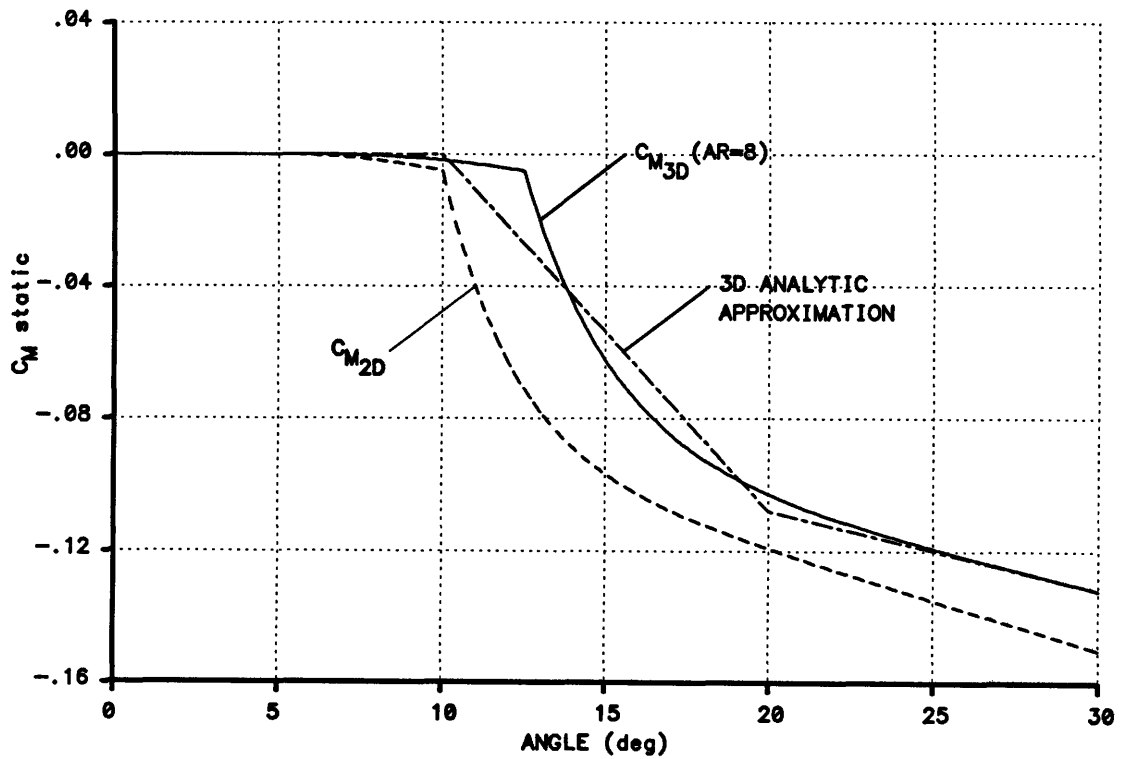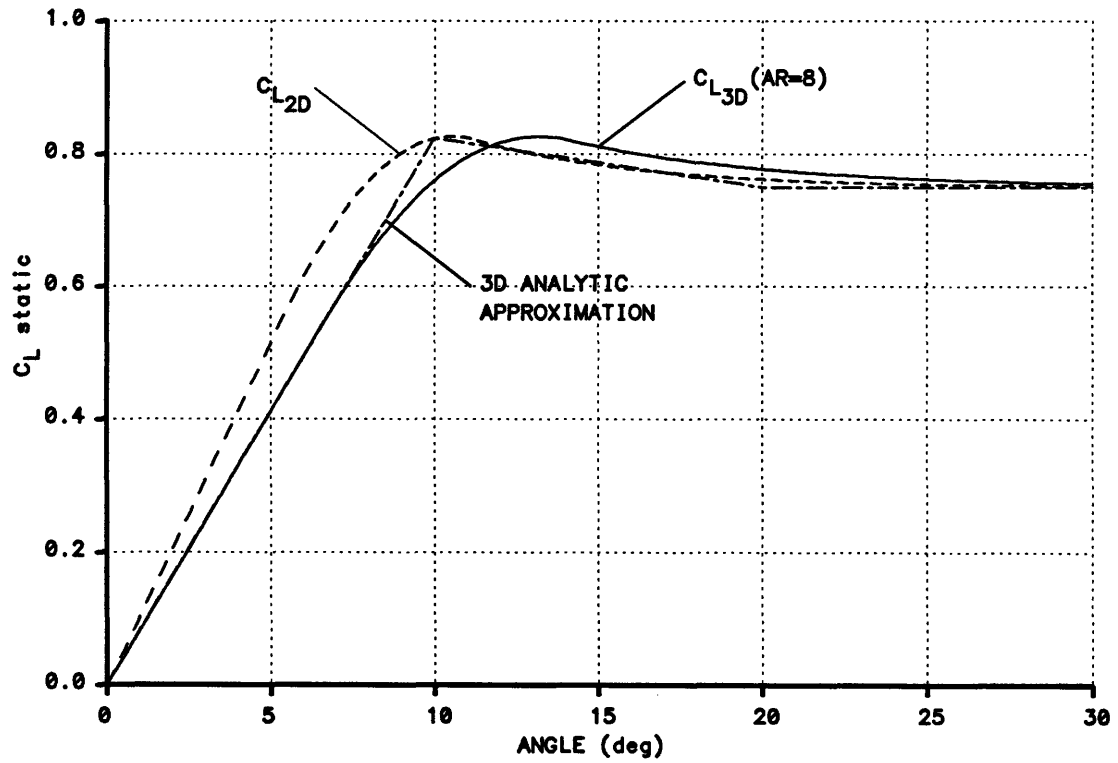
Figure 27. NACA-0012 low Reynold's number lift model

Other 3-dimensional effects are included by adding a span-wise drop. The 2-dimensional curves are already corrected for finite aspect ratio.

$$C_{L_{3D}} = 1.11\left[1 - (\frac{x}{\ell})^9 \right] C_{L_{2D}}(\alpha=\alpha_c) \tag{C-2}$$

where the corrected angle of attack included the finite-span correction,

$$\alpha_c = \frac{1}{1 + \dfrac{a_{oL}}{\pi AR}}\alpha \tag{C-3}$$

The 3-dimensional total drag is found by adding the induced drag to the profile drag,

$$C_D = C_{D_o} + \frac{C_L^2}{\pi AR} \tag{C-4}$$

As is suggested by Petot [Ref. 17], and illustrated in Figure 28, more complex descriptions can be devised, and may be useful for higher Reynold's number flows where the lift drop after stall is more acute. A parabolic fit can be used to describe the slight drop in lift preceding stall. A power series expansion into a high order polynomial can be used to describe the exponential drop immediately following stall (the conversion from exponential form to polynomial form is necessitated by the formulation of the Fourier series in Section 2.9). A flat line can be used to describe the fully decayed exponential for very high angles of attack.

The variables describing the aerodynamic force curves, such as the maximum lift coefficient or the minimum profile

drag, can further be generalized over a wide range of free stream velocities, as suggested by the logarithmic dependence on the Reynold's number described by Jacobs and Sherman [Ref. 14]. Similar fits for the moment coefficient curve can be generated using the data from McCroskey [Ref. 15].
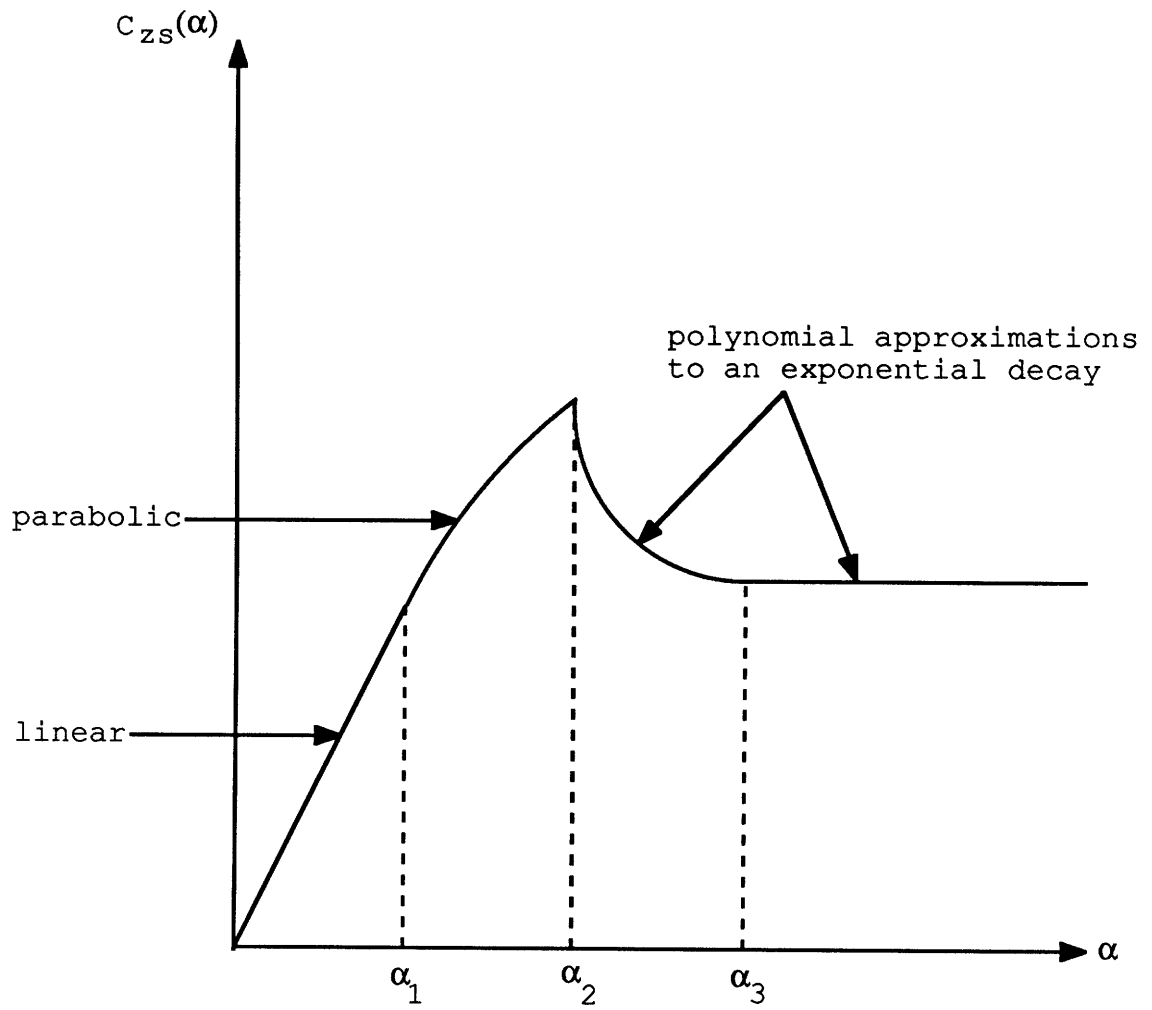
Figure 28. Generalized lift model

APPENDIX D - COEFFICIENTS OF AERODYNAMIC EQUATIONS

The following are the coefficients of the 2-dimensional aerodynamic equations (2-27b) to (2-27d), used for the lift and moment coefficients. It is assumed that there is no hysteresis in the drag coefficient. The linear coefficients (s_L, k_{vL}, λ_L, α_L, σ_L, a_{oM}, s_M, k_{vM}, λ_M, α_M, and σ_M) were taken from standard references with the following exceptions: s_L was taken from Petot [Ref. 17] although a more consistent value could have been $s_L = \pi$; a_{oL} was derived by fitting the NACA-0012 data from Jacobs and Sherman [Ref. 14] although the linear value $a_{oL} = 2\pi$ could have been used. The nonlinear coefficients (a, r, d, w, and e) were taken from Petot [Ref. 17] with corrections for low Reynold's flow guided by similar values given by Petot and Loiseau [Ref. 13].

$$s_L = 0.09*(180/\pi) \text{ rad}^{-1}$$

$$k_{vL} = \pi/2 \text{ rad}^{-1}$$

$$\lambda_L = 0.15$$

$$\alpha_L = 0.55$$

$$\sigma_L = a_{oL} = 5.9 \text{ rad}^{-1}$$

$$a_{oM} = 0$$

$$s_M = -\pi/4 \text{ rad}^{-1}$$

$$k_{vM} = -3\pi/16 \text{ rad}^{-1}$$

$$\lambda_M = 0$$

$$\alpha_M = 1$$

$$\sigma_M = -\pi/4 \text{ rad}^{-1}$$

$$a = 0.25 + 0.1(\Delta C_L)^2 \qquad \text{if } Re > 340{,}000$$

$$= 0.25 + 0.4(\Delta C_L)^2 \qquad \text{if } Re \leq 340{,}000$$

$$r = [0.2 + 0.10(\Delta C_L)^2]^2 \qquad \text{if } Re > 340{,}000$$

$$= [0.2 + 0.23(\Delta C_L)^2]^2 \qquad \text{if } Re \leq 340{,}000$$

$$d = \frac{a}{\sqrt{4r - a^2}}$$

$$w = a/2d$$

$$e = -0.6(\Delta C_L)^2 \qquad \text{if } Re > 340{,}000$$

$$= -2.7(\Delta C_L)^2 \qquad \text{if } Re \leq 340{,}000$$

APPENDIX E - EXAMPLE OF FOURIER ANALYSIS

Equations (2-31) to (2-33) are still applicable:

$$\alpha(\tau) = \alpha_o + \alpha_v \sin(k\tau + \xi) \tag{E-1a}$$

where,

$$\alpha_v = \sqrt{\alpha_s^2 + \alpha_c^2} \tag{E-1b}$$

$$\xi = \sin^{-1}\frac{\alpha_c}{\alpha_v} \tag{E-1c}$$

For a single break point model (see Figure 29), equation (2-29) simplifies to the following equations, where α_Δ is the stall angle and a_{11} is the difference in slopes between the linear region and the nonlinear region,

$$\Delta C_z = a_{11}(\alpha - \alpha_\Delta) \quad \text{for } \alpha \geq \alpha_\Delta$$

$$\Delta C_z = 0 \qquad\qquad \text{for } \alpha \leq \alpha_\Delta \tag{E-2}$$

Equations (2-51) to (2-53) then give that,

$$b_{10} = a_{11}(\alpha_o - \alpha_\Delta) \tag{E-3a}$$

$$b_{11} = a_{11}\alpha_v \tag{E-3b}$$

$$I_{10} = \frac{\pi}{2} - \varphi_\Delta \tag{E-3c}$$

$$I_{11} = \cos\varphi_\Delta \tag{E-3d}$$

$$I_{12} = \frac{1}{2}\sin\varphi_\Delta\cos\varphi_\Delta + \frac{\pi}{4} - \frac{1}{2}\varphi_\Delta \tag{E-3e}$$

where,

$$\varphi_\Delta = \sin^{-1}\left\{\frac{\alpha_\Delta - \alpha_o}{\alpha_v}\right\} \tag{E-4a}$$

and,

$$\varphi_\Delta = \begin{cases} +\dfrac{\pi}{2} & \text{if} \quad \dfrac{\alpha_\Delta - \alpha_o}{\alpha_v} > +1 \\[4mm] -\dfrac{\pi}{2} & \text{if} \quad \dfrac{\alpha_\Delta - \alpha_o}{\alpha_v} < -1 \end{cases} \tag{E-4b}$$

Finally, putting these expressions into the combined mean and oscillatory components of the nonlinear aerodynamic deviations (2-50) and (2-54), we get,

$$\Delta C_{zo} = \frac{a_{11}\alpha_v}{\pi}\left\{-\sin\varphi_\Delta\left[\frac{\pi}{2} - \varphi_\Delta\right] + \cos\varphi_\Delta\right\} \tag{E-5a}$$

$$\Delta C_{zv} = \frac{a_{11}\alpha_v}{\pi}\left\{-\sin\varphi_\Delta\cos\varphi_\Delta + \frac{\pi}{2} - \varphi_\Delta\right\} \tag{E-5b}$$

A symmetric aerodynamic force curve can also be accounted for by including a second stall angle at $-\alpha_\Delta$. This yields expanded versions of equations (E-5a) and (E-5b),

$$\Delta C_{zo} = \frac{a_{11}\alpha_v}{\pi}\left\{-\sin\varphi_\Delta\left[\frac{\pi}{2} - \varphi_\Delta\right] + \cos\varphi_\Delta\right\} + $$
$$\frac{a_{11}\alpha_v}{\pi}\left\{-\sin\overline{\varphi}_\Delta\left[\frac{\pi}{2} + \overline{\varphi}_\Delta\right] - \cos\overline{\varphi}_\Delta\right\} \tag{E-6a}$$

$$\Delta C_{zv} = \frac{a_{11}\alpha_v}{\pi}\left\{-\sin\varphi_\Delta\cos\varphi_\Delta + \frac{\pi}{2} - \varphi_\Delta\right\} + $$
$$\frac{a_{11}\alpha_v}{\pi}\left\{+\sin\overline{\varphi}_\Delta\cos\overline{\varphi}_\Delta + \frac{\pi}{2} + \overline{\varphi}_\Delta\right\} \tag{E-6b}$$

where,

$$\overline{\varphi}_\Delta = \sin^{-1}\left\{\frac{-\alpha_\Delta - \alpha_o}{\alpha_v}\right\} \tag{E-7a}$$

and,

$$\overline{\varphi}_\Delta = \begin{cases} +\dfrac{\pi}{2} & \text{if} \quad \dfrac{-\alpha_\Delta - \alpha_o}{\alpha_v} > +1 \\[4mm] -\dfrac{\pi}{2} & \text{if} \quad \dfrac{-\alpha_\Delta - \alpha_o}{\alpha_v} < -1 \end{cases} \tag{E-7b}$$
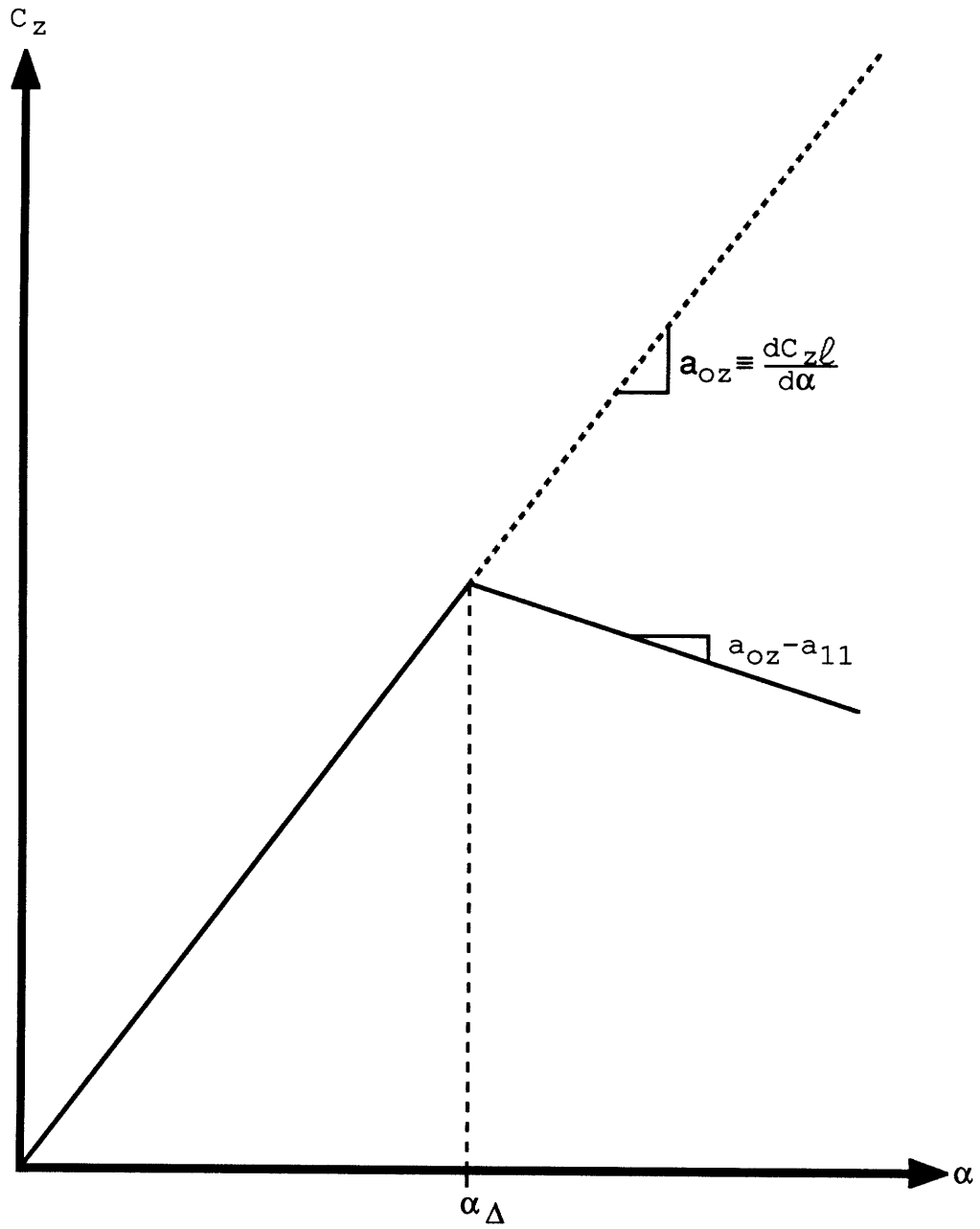
Figure 29. Example of single break point stall model

APPENDIX F – THE NEWTON-RAPHSON METHOD

The Newton-Raphson method is a numerical solver used to find the roots of the implicit vector equation, $\mathbf{f}(\mathbf{x}) = 0$, where $\mathbf{x}$ is the state vector and $\mathbf{f}(\mathbf{x})$ is the vector of residual functions that must be driven to zero. The Newton-Raphson scheme takes an initial guess of the state vector $\mathbf{x}$ and drives the vector $\mathbf{f}(\mathbf{x})$ toward zero by inverting the Jacobian matrix (derivative matrix), and obtaining a correction $\Delta\mathbf{x}$ to the current guess. The process is repeated until the correction $\Delta\mathbf{x}$ becomes negligible and the process is deemed to have converged.

$$\Delta\mathbf{x}^{(n)} = -\left[\frac{d\mathbf{f}}{d\mathbf{x}}\right]_n^{-1} \mathbf{f}(\mathbf{x}^{(n)}) \quad ; \quad \mathbf{x}^{(n+1)} = \mathbf{x}^{(n)} + \Delta\mathbf{x}^{(n)} \tag{F-1}$$

The Newton-Raphson solver is applied in the current analysis by rearranging equation (2-73) as follows;

$$\{\mathbf{f}\} = \begin{bmatrix} [K] & 0 & 0 \\ 0 & -\omega^2[M]+[K] & 0 \\ 0 & 0 & -\omega^2[M]+[K] \end{bmatrix} \begin{bmatrix} \{q_o\} \\ \{q_s\} \\ \{q_c\} \end{bmatrix} - \begin{bmatrix} \{Q_o\} \\ \{Q_s\} \\ \{Q_c\} \end{bmatrix} \tag{F-2}$$

Equation (F-2) comprises $3n$ equations that must be solved in the form $\mathbf{f}(\mathbf{x}) = 0$ and are nonlinear in the aerodynamic dependence of the modal forces Q_i on the modal amplitudes q_i. The state vector $\mathbf{x}$ is comprised of the harmonic components of the modal amplitudes, q_{io}, q_{is}, and q_{ic}, with some minor adjustments to ensure convergence to a non-trivial solution: the sine component of one mode q_i is set to some

small constant to set the amplitude level, while its cosine component is set to zero, since the flutter limit cycle oscillations can start at any arbitrary phase. The mode usually chosen for this substitution is the first torsional mode, since experimentally it is this mode which dominates the oscillatory motion. These sine and cosine components are then dropped from the state vector x and are replaced by the reduced frequency of oscillation, k, and the flutter velocity, U. Because the sinusoidal component of one mode shape has already been set to a non-zero value, the Newton-Raphson scheme does not converge to the trivial steady solution.

Note that the Newton-Raphson solver is not always guaranteed to converge, especially when the initial guess is too far from the ultimate solution or when the derivatives used in the Jacobian matrix are changing abruptly, which often happens with nonlinearities that have discontinuous derivatives. In regions where convergence is difficult (for example near the stall angle where the lift/moment coefficient curves are discontinuous in slope), a relaxation technique, which consists of taking only a fraction of Δx as a correction for each iteration, is more likely to converge. When the Newton-Raphson solver does converge to a solution, it will satisfy the equations, but there is no indication as to whether this solution is unique or not. If other solutions exist, the only way to find them is to start with a different initial state vector.

The Jacobian matrix can be calculated either numerically or analytically. The numerical method involves moving an incremental distance in each direction of the state vector $\mathbf{x}$, finding the resulting incremental change in the residual vector $\mathbf{f}$, and estimating each component of the derivative matrix as $\Delta f_i / \Delta x_j$. The analytic method involves carrying out the entire nonlinear differentiation, which is best carried out by multiple application of the chain rule to the equations of sections 2.9 and 2.10.

Both the numerical and analytic methods have their advantages and disadvantages. The numerical method is easier to code on a computer since it involves using the already existing subroutines which must compute the residual vector. On the other hand, the numerical method is computationally inefficient since it requires recalculating the residual vector for every direction of the state vector. In addition, the numerical method is likely to be inaccurate at points of discontinuity in derivatives, unless the user is careful to choose appropriately small increments in the state vector.

By contrast, the analytic model directly solves for the Jacobian matrix without needing several iterations, and so is computationally faster for higher numbers of mode shapes and harmonics. In addition, the analytic method is always accurate and does not depend on any step size. Unfortunately, the analytic method cannot employ already existing subroutines and requires cumbersome programming for a highly nonlinear problem such as in the current study.

Both the numerical and the analytic methods were used to calculate the Jacobian matrix in the current study and compared well against each other. However, with the large complexity in calculating the modal forces, the numerical method is more likely to have fewer coding errors than the analytic method, despite being computationally slower. For this reason, it was used more extensively for the full flutter analyses.

APPENDIX G - SPECIMEN DIMENSIONS

	t (mm)	w (mm)	ρ (kg/m^3)
nominal	.810	76.20	1540
$[0_2/90]_s$	.802	76.58	1552
$[90/0_2]_s$	.806	76.68	1581
$[+15_2/0]_s$	.766	76.57	1532
$[-15_2/0]_s$	.805	76.53	1570
$[-30_2/0]_s$	.801	76.53	1564

```
C======= FILE: PARAM.INC ===================================================
C
C       "Include" file, PARAM.INC, which describes the general
C       parameters of the stall flutter analysis programs.
C
        IMPLICIT REAL*8 (A-H,O-Z)
        PARAMETER       (PI=3.141592653589793238D0)
        PARAMETER       (RHOA=1.226D0)
        PARAMETER       (RMUA=1.78D-5)
        PARAMETER       (MAXPLIES=20)
        PARAMETER       (MAXMODE=5)
        PARAMETER       (MAXREG=5)
        PARAMETER       (MAXPOW=20)
        INTEGER         GPOINTS
        PARAMETER       (GPOINTS=12)
C
C       RHOA:       Air density in kg/m**3
C       MAXPLIES:   Maximum allowable number of plies in analysis
C       MAXMODE:    Maximum allowable number of mode shapes in analysis
C       MAXREG:     Maximum allowable number of describing regions for
C                   aerodynamic force curves
C       MAXPOW:     Maximum allowable polynomial power for each describing
C                   region for aerodynamic force curves
C       GPOINTS:    Number of integration points used in Gaussian quadrature
C
```

```
C====== FILE: GLBBLK.INC ======
C
C        "Include" file to describe variables used globally
C        by most programs in the stall flutter analysis.
C
         REAL*8      RE,CHORD,LENGTH,LAMBDA,BETA,KT(2),G(2),F(2),B(4,2)
         REAL*8      M(MAXMODE,MAXMODE),K(MAXMODE,MAXMODE),KTT0,KTTCUBE
         INTEGER     NMODES
         LOGICAL     LINEAR,STEADY,REDUC,CORREC,VLINES,LATAN
         CHARACTER   FOIL*5
         COMMON      RE,CHORD,LENGTH,LAMBDA,BETA,KT,G,F,B,M,K,KTT0,KTTCUBE
         COMMON      NMODES,LINEAR,STEADY,REDUC,CORREC,VLINES,LATAN,FOIL
C
C        RE:            Reynold's number
C        CHORD:         Chord length in meters
C        LENGTH:        Half-span in meters
C        LAMBDA:        Sweep angle in degrees
C        BETA,KT,G,F,B: Coefficients of torsional mode shapes
C        M(I,J):        Mass matrix
C        K(I,J):        Stiffness matrix
C        KTT0:          Torsional linear term
C        KTTCUBE:       Torsional cubic factor
C        NMODES:        Number of modes in analysis
C        LINEAR:        Logical variable to tell if linear analysis is conducted
C        STEADY:        Logical variable to tell if steady analysis is conducted
C        REDUC:         Logical variable to tell if finite-span reduction is to
C                       be applied to aerodynamic forces
C        CORREC:        Logical variable to tell if spanwise correction are to
C                       be applied to spanwise integrations
C        VLINES:        Logical variable to tell if constant velocity lines or
C                       constant angle lines are to be calculated by analysis
C        LATAN:         Logical variable to tell if exact angle or small-angle-
C                       approximations are to be applied to angle calculations
C        FOIL:          Character variable that denote airfoil type
C
```

```
C====== FILE : FLUTTER.FOR ============================================
C
        PROGRAM FLUTTER
C
        INCLUDE         'PARAM.INC'
        INCLUDE         'GLBBLK.INC'
        REAL*8          QLIT(MAXMODE,3),QALL(3*MAXMODE),RES(3*MAXMODE)
        REAL*8          DRDQ(3*MAXMODE,3*MAXMODE),DQALL(3*MAXMODE)
        REAL*8          VEL,AOA,FREQ,ATIP(3),HTIP(3)
        INTEGER         IERR,BEN_TOR
        LOGICAL         CONVERGED,DIAGNOSTICS
        CHARACTER       LAYUP*4,ANSWER*1,FILENAME*25,CDUM*7
C
C       QLIT(i,j):      i-th modal amplitude, j-th component (1=mean,
C                       2=sine,3=cosine)
C       QALL:           Augmented state vector
C       RES:            Residual vector
C       DRDQ:           Jacobian matrix, derivatives of residuals (RES)
C                       w.r.t. modal amplitudes (QLIT)
C       DQALL:          Corrections to augmented state vector
C       VEL:            Free stream velocity
C       AOA:            Root angle-of-attack
C       FREQ:           Reduced frequency
C       ATIP:           Components of oscillating tip angle
C       HTIP:           Components of oscillating tip deflection
C
        FOIL = 'NAC12'
C
C       Read in the layup.
C
10      WRITE(6,'(/A,$)') '+Layup : '
        READ(5,'(A4)',ERR=10) LAYUP
C
C       Read in number of mode shapes to be used for the analysis.
C
20      WRITE(6,'(/A,$)') '+Number of modes (2-5) ? '
        READ(5,*,ERR=20) NMODES
        IF ((NMODES.LT.2).OR.(NMODES.GT.5)) GOTO 20
C
C       Create mass and stiffness matrices by calling STATIC subroutine.
C
        CALL STATIC(LAYUP,TRATIO,IERR)
        IF (IERR.NE.0) THEN
            WRITE(6,'(A,I2,A)') ' IOSTAT=',IERR,' error reading data file.'
            GOTO 10
        ENDIF
C
C       Open output file.
C
        FILENAME = '[.'//LAYUP//']'//LAYUP//'WNAV.OUT'
        OPEN(UNIT=2,FILE=FILENAME,STATUS='NEW',FORM='FORMATTED',IOSTAT=IERR)
        IF (IERR.EQ.0) THEN
            WRITE(6,*) 'Analysis results being sent to '//FILENAME
        ELSE
```

```fortran
                WRITE(6,'(A,I2,A)') ' IOSTAT=',IERR,' error opening output file.'
                GOTO 10
           ENDIF
           WRITE(2,'(I2,A)') NMODES,' = number of modes in analysis'
           WRITE(2,'(F5.2,A)') TRATIO,' = NACA airfoil thickness ratio'
C
C       Read in whether to print diagnostics to output file.
C
25         WRITE(6,'(/A,$)') '+Output diagnostics ? '
           READ(5,'(A1)',ERR=25) ANSWER
           DIAGNOSTICS = .FALSE.
           IF ((ANSWER.EQ.'Y').OR.(ANSWER.EQ.'y')) DIAGNOSTICS=.TRUE.
C
C       Read in options for the complexity of the analysis.
C
30         WRITE(6,'(/A,$)') '+  Exact angle calc ? '
           READ(5,'(A1)',ERR=30) ANSWER
           LATAN = .FALSE.
           IF ((ANSWER.EQ.'Y').OR.(ANSWER.EQ.'y')) LATAN=.TRUE.
           IF (LATAN) WRITE(2,'(/A)') ' Exact angle calculation ON'
           IF (.NOT.LATAN) WRITE(2,'(/A)') ' Exact angle calculation OFF'
C
40         WRITE(6,'(/A,$)') '+  Cubic stiffening ? '
           READ(5,'(A1)',ERR=40) ANSWER
           IF ((ANSWER.NE.'Y').AND.(ANSWER.NE.'y')) KTTCUBE=0.D0
           IF (KTTCUBE.NE.0) WRITE(2,*) 'Cubic stiffening ON'
           IF (KTTCUBE.EQ.0) WRITE(2,*) 'Cubic stiffening OFF'
C
50         WRITE(6,'(/A,$)') '+   Non-linear aero ? '
           READ(5,'(A1)',ERR=50) ANSWER
           LINEAR = .TRUE.
           IF ((ANSWER.EQ.'Y').OR.(ANSWER.EQ.'y')) LINEAR=.FALSE.
           IF (LINEAR) WRITE(2,*) 'Aerodynamics LINEAR'
           IF (.NOT.LINEAR) WRITE(2,*) 'Aerodynamics NON-LINEAR'
C
60         WRITE(6,'(/A,$)') '+ Spanwise lift cor ? '
           READ(5,'(A1)',ERR=60) ANSWER
           CORREC = .TRUE.
           IF ((ANSWER.EQ.'N').OR.(ANSWER.EQ.'n')) CORREC = .FALSE.
           IF (CORREC) WRITE(2,*) 'Spanwise lift correction ON'
           IF (.NOT.CORREC) WRITE(2,*) 'Spanwise lift correction OFF'
C
70         WRITE(6,'(/A,$)') '+ Finite span reduc ? '
           READ(5,'(A1)',ERR=70) ANSWER
           REDUC = .FALSE.
           IF ((ANSWER.EQ.'Y').OR.(ANSWER.EQ.'y')) REDUC = .TRUE.
           IF (REDUC) WRITE(2,*) 'Finite span lift reduction ON'
           IF (.NOT.REDUC) WRITE(2,*) 'Finite span lift reduction OFF'
C
80         WRITE(6,'(/A,$)') '+   Steady analysis ? '
           READ(5,'(A1)',ERR=80) ANSWER
           STEADY=.FALSE.
           IF ((ANSWER.EQ.'Y').OR.(ANSWER.EQ.'y')) STEADY=.TRUE.
           IF (STEADY) WRITE(2,*) 'STEADY test case (no flutter)'
```

```
         IF (.NOT.STEADY) WRITE(2,*) 'UNSTEADY test case (flutter)'
C
90       WRITE(6,'(/A,$)') '+Constant vel lines ? '
         READ(5,'(A1)',ERR=90) ANSWER
         VLINES=.TRUE.
         IF ((ANSWER.EQ.'N').OR.(ANSWER.EQ.'n')) VLINES=.FALSE.
         IF (VLINES) WRITE(2,*) 'YES, constant velocity lines'
         IF (.NOT.VLINES) WRITE(2,*) 'NO, constant root angle lines'
C
C        Read in the start & end values and the incremental step size
C        between each line of either (i) constant velocity or
C        (ii) constant root angle of attack.
C
100      IF (VLINES) WRITE(6,'(/A,$)') '+Velocity start, end, & step '//
     &       'size (m/s) ? '
         IF (.NOT.VLINES) WRITE(6,'(/A,$)') '+Root angle start, end, & '//
     &       'step size (deg) ? '
         READ(5,*,ERR=100) DUM1LO,DUM1HI,DUM1INC
         IF ((DUM1LO.LT.0.).OR.(DUM1HI.LT.0.)) GOTO 100
         IF (((DUM1HI-DUM1LO)/DUM1INC).LT.0.) GOTO 100
C
C        Write header.
C
         IF (.NOT.DIAGNOSTICS) THEN
             WRITE(2,'(3(/A))')
     &       '    Vel    AOA    FRQ    H avg    H sin    H cos    '//
     &          'A avg    A sin    A cos',
     &       '   (m/s)  (deg)  (Hz)    (cm)     (cm)     (cm)    '//
     &          '(deg)   (deg)   (deg)',
     &       '   ____   ____   ____    ____     ____     ____    '//
     &          '____    ____    ____'
         ENDIF
C
C        Determine if bending or torsion flutter analysis should be performed
C        (BEN_TOR = 1 for bending, 2 for torsion) in the unsteady case.
C
         BEN_TOR = 2
         IF (.NOT.STEADY) THEN
125          WRITE(6,'(/A,$)') '+[1] bending or [2] torsional flutter ? '
             READ(5,*,ERR=125) BEN_TOR
             IF ((BEN_TOR.NE.1).AND.(BEN_TOR.NE.2)) GOTO 125
         ENDIF
C
C        Loop through each line of either (i) constant velocity or
C        (ii) constant root angle of attack, denoted by the dummy
C        variable DUMMY1.
C
         DO 1000 DUMMY1 = DUM1LO,DUM1HI,DUM1INC
C
C        Set the velocity VEL or the root angle of attack AOA, depending
C        on whether lines of constant velocity or constant angle.
C
         IF (VLINES) VEL = DUMMY1
         IF (.NOT.VLINES) AOA = DUMMY1*PI/180.
```

```
C
          IF (STEADY) THEN
C
C             Initialize to zero the augmented modal amplitude vector QALL,
C             all the modal amplitudes QLIT, and the reduced frequency FREQ.
C
              DO 110 J = 1,3
              DO 110 I = 1,NMODES
                  QLIT(I,J) = 0.D0
                  QALL(NMODES*(J-1)+I) = QLIT(I,J)
110           CONTINUE
              FREQ = 0.D0
C
C             If steady, read in the start & end values and the incremental
C             step size of the root angles/velocities for each corresponding
C             line of constant velocity/root angle.
C
120           IF (VLINES) WRITE(6,'(//A,F5.1,A,$)') '+VEL =',DUMMY1,
     &            ' ; Root angle start, end, & step size (deg) ? '
              IF (.NOT.VLINES) WRITE(6,'(//A,F5.1,A,$)') '+AOA =',DUMMY1,
     &            ' ; Velocity start, end, & step size (m/s) ? '
              READ(5,*,ERR=120) DUM2LO,DUM2HI,DUM2INC
              IF ((.NOT.VLINES).AND.(DUM2LO.LT.0.)) GOTO 120
              IF ((.NOT.VLINES).AND.(DUM2HI.LT.0.)) GOTO 120
              IF ((DUM2HI-DUM2LO)/DUM2INC.LT.0.) GOTO 120
          ELSE
C
C             If unsteady, read in the start & end values and the incremental
C             step size of the amplitude of oscillating twist for each
C             line of constant velocity/root angle.
C
130           IF (BEN_TOR.EQ.1) THEN
                  IF (VLINES) WRITE(6,'(//A,F5.1,A,$)') '+VEL =',DUMMY1,
     &                ' ; Bending amplitude start, end, & step size (cm) ? '
                  IF (.NOT.VLINES) WRITE(6,'(//A,F5.1,A,$)') '+AOA =',DUMMY1,
     &                ' ; Bending amplitude start, end, & step size (cm) ? '
              ELSE
                  IF (VLINES) WRITE(6,'(//A,F5.1,A,$)') '+VEL =',DUMMY1,
     &                ' ; Twist amplitude start, end, & step size (deg) ? '
                  IF (.NOT.VLINES) WRITE(6,'(//A,F5.1,A,$)') '+AOA =',DUMMY1,
     &                ' ; Twist amplitude start, end, & step size (deg) ? '
              ENDIF
              READ(5,*,ERR=130) DUM2LO,DUM2HI,DUM2INC
              IF ((.NOT.VLINES).AND.(DUM2LO.LT.0.)) GOTO 130
              IF ((.NOT.VLINES).AND.(DUM2HI.LT.0.)) GOTO 130
              IF ((DUM2HI-DUM2LO)/DUM2INC.LT.0.) GOTO 130
C
C             Determine if previous values should be used as an initial guess.
C
              ANSWER = 'N'
              IF (DUMMY1.NE.DUM1LO) THEN
135               WRITE(6,'(/A,$)') '+Use previous values as initial guess ? '
                  READ(5,'(A1)',ERR=135) ANSWER
              ENDIF
```

```fortran
              IF ((ANSWER.NE.'Y').AND.(ANSWER.NE.'y')) THEN
C
C                 Initialize the oscillating amplitudes to some fraction
C                 (1/10th) of the first bending/twist amplitude.
C
                  TWIST = DUM2LO*PI/180./10.
                  DEFLC = DUM2LO/100./10.
                  DO 140 J = 2,3
                  DO 140 I = 1,NMODES
                      IF (BEN_TOR.EQ.1) QLIT(I,J) = DEFLEC/FMODE(0,'X',1,1.)/
     &                    FMODE(0,'Y',1,0.)
                      IF (BEN_TOR.EQ.2) QLIT(I,J) = DTAN(TWIST)*CHORD/
     &                    FMODE(0,'X',2,1.)/FMODE(1,'Y',2,0.)
                      QALL(NMODES*(J-1)+I) = QLIT(I,J)
140               CONTINUE
C
C                 Read in the initial guess for root angle AOA, or for
C                 velocity VEL, to be used for the first iteration of the
C                 Newton-Raphson solver for the first corresponding line
C                 of constant velocity/root angle.
C
                  IF (VLINES) THEN
150                   WRITE(6,'(/A,$)') '+Initial root angle guess (deg) ? '
                      READ(5,*,ERR=150) AOA
                      AOA = AOA*PI/180.
                      QALL(NMODES+BEN_TOR) = AOA
                  ELSE
160                   WRITE(6,'(/A,$)') '+Initial velocity guess (m/s) ? '
                      READ(5,*,ERR=160) VEL
                      IF (VEL.LT.0.) GOTO 160
                      QALL(NMODES+BEN_TOR) = VEL**2
                  ENDIF
C
C                 Determine if there is a problem because flutter velocity occurs
C                 above linear divergence velocity, and query user if he wants to
C                 directly input the initial average amplitudes.
C
                  WRITE(6,'(/A,$)') '+Input initial average deflections ? '
                  READ(5,'(A1)') ANSWER
                  IF ((ANSWER.EQ.'Y').OR.(ANSWER.EQ.'y')) THEN
                      DO 165 I = 1,NMODES
162                       WRITE(6,'(/A,I1,A,$)') '+ Mode ',I,' average [m] = '
                          READ(5,*,ERR=162) QLIT(I,1)
                          QALL(I) = QLIT(I,1)
165                   CONTINUE
                  ENDIF
C
C                 Read in the initial guess for reduced frequency FREQ to
C                 be used for the first iteration of the Newton-Raphson solver
C                 for the first line of constant velocity/root angle.
C
170               WRITE(6,'(/A,$)') '+Initial reduced frequency guess ? '
                  READ(5,*,ERR=170) FREQ
                  IF (FREQ.LT.0.) GOTO 170
```

```
               QALL(2*NMODES+BEN_TOR) = FREQ
           ENDIF
C
C          Read in the non-dimensional step size tolerance [maximum
C          delta(X)/X] to be applied to the root angle/velocity and
C          frequency corrections [DQALL(NMODES+BEN_TOR) &
C          DQALL(2*NMODES+BEN_TOR)] in relaxing the Newton-Raphson solver.
C
180        WRITE(6,'(/A,$)') '+Step size tolerance ? '
           READ(5,*,ERR=180) TOL
           IF (TOL.LE.0.) GOTO 180
       ENDIF
C
C      Loop through the appropriate variable, denoted by the dummy variable
C      DUMMY2, for each line of constant velocity/root angle.
C
       DO 1000 DUMMY2 = DUM2LO,DUM2HI,DUM2INC
C
C          Initialize the number of iterations to zero and, for the
C          steady case, extract the appropriate root angle/velocity
C          from the dummy variable DUMMY2.
C
           LOOPS = 0
           IF ((STEADY).AND.(VLINES)) THEN
               AOA = DUMMY2*PI/180.D0
           ELSEIF ((STEADY).AND.(.NOT.VLINES)) THEN
               VEL = DUMMY2
           ENDIF
C
C          Initialize convergence. If zero velocity, automatically set
C          all amplitudes to zero and skip Newton-Raphson solver.
C
           CONVERGED = .FALSE.
           IF ((.NOT.VLINES).AND.(DUMMY2.EQ.0.)) THEN
               DO 190 I = 1,NMODES
                   QLIT(I,1) = 0.
                   QALL(I) = 0.
190            CONTINUE
               CONVERGED = .TRUE.
           ENDIF
C
C          Rescale unsteady, variable amplitudes according to set amplitude.
C
           IF (.NOT.STEADY) THEN
           DO 195 I = 1,NMODES
           DO 195 J = 2,3
               IF ((I.NE.BEN_TOR).AND.(DUMMY2.NE.DUM2LO)) QALL(NMODES*
     &         (J-1)+I)=QALL(NMODES*(J-1)+I)*DUMMY2/(DUMMY2-DUM2INC)
195        CONTINUE
           ENDIF
C
C          Loop through the Newton-Raphson scheme until it is
C          converged to an acceptable limit.
C
```

```
              DO WHILE (.NOT.CONVERGED)
C
C                 Extract the modal amplitudes from
C                 the augmented modal amplitude vector.
C
                  JJ = 3
                  IF (STEADY) JJ = 1
                  DO 200 I = 1,NMODES
                  DO 200 J = 1,JJ
                      QLIT(I,J) = QALL(NMODES*(J-1)+I)
200               CONTINUE
C
C                 If unsteady, extract current values of unknown variables
C                 from the augmented state vector QALL.
C
                  IF (.NOT.STEADY) THEN
C
C                     Extract current value of unknown root angle/velocity
C                     from the augmented state vector QALL, appropriate to lines
C                     of constant velocity or root angle. Set velocity to
C                     zero if Newton-Raphson solver drives VEL**2 below zero.
C
                      IF (VLINES) THEN
                          AOA = QALL(NMODES+BEN_TOR)
                      ELSEIF (QALL(NMODES+BEN_TOR).GT.0.) THEN
                          VEL = DSQRT(QALL(NMODES+BEN_TOR))
                      ELSE
                          QALL(NMODES+BEN_TOR) = 0.
                          VEL = 0.
                      ENDIF
C
C                     Extract current value of the unknown reduced frequency
C                     from the augmented state vector QALL.
C
                      FREQ = QALL(2*NMODES+BEN_TOR)
C
C                     Extract the desired twist oscillating amplitudes from
C                     the dummy variable DUMMY2.
C
                      TWIST = DUMMY2*PI/180.
                      DEFLC = DUMMY2/100.
                      IF (BEN_TOR.EQ.1) QLIT(1,2) = DEFLC/FMODE(0,'X',1,1.)/
     &                    FMODE(0,'Y',1,0.)
                      IF (BEN_TOR.EQ.2) QLIT(2,2) = DTAN(TWIST)*CHORD/
     &                    FMODE(0,'X',2,1.)/FMODE(1,'Y',2,0.)
                      QLIT(BEN_TOR,3) = 0.D0
                  ENDIF
C
                  LOOPS = LOOPS+1
C
C                 Write current values of inputs to residual calculations.
C
                  IF (DIAGNOSTICS) THEN
                      WRITE(2,'(/A,I3,11X,<NMODES>(5X,I1,4X))') ' LOOP =',
```

```fortran
      &              LOOPS,(I,I=1,NMODES)
                WRITE(2,'(A,<NMODES>(1PE10.2))')  ' Avg '//
      &              'modal amp [m] : ',(QLIT(I,1),I=1,NMODES)
                IF (.NOT.STEADY) THEN
                    WRITE(2,'(A,<NMODES>(1PE10.2))')  ' Sin '//
      &                  'modal amp [m] : ',(QLIT(I,2),I=1,NMODES)
                    WRITE(2,'(A,<NMODES>(1PE10.2))')  ' Cos '//
      &                  'modal amp [m] : ',(QLIT(I,3),I=1,NMODES)
                    WRITE(2,'(A,F8.3,A)')  ' VEL =',VEL,' m/s'
                    WRITE(2,'(A,F8.3,A)')  ' AOA =',AOA*180./PI,' degs'
                    WRITE(2,'(A,F8.3)')    '   k =',FREQ
                    OMEGA = FREQ*VEL/(CHORD/2.)/(2.*PI)
                    WRITE(2,'(A,F8.3,A)')  '   w =',OMEGA,' Hz'
                ENDIF
            ENDIF
C
C         Calculate the residuals from subroutine RESIDUAL, which
C         are functions of the velocity VEL, root angle of attack AOA,
C         reduced frequency FREQ, and modal amplitudes QLIT.
C
          CALL RESIDUAL(VEL,AOA,FREQ,QLIT,RES)
C
C         Write current values of residuals.
C
          IF (DIAGNOSTICS) THEN
              WRITE(2,'(/4X,A,<NMODES>(1PE10.2))')  ' Avg '//
      &              'residuals : ',(RES(I),I=1,NMODES)
              IF (.NOT.STEADY) THEN
                  WRITE(2,'(4X,A,<NMODES>(1PE10.2))')  ' Sin '//
      &                  'residuals : ',(RES(I),I=NMODES+1,2*NMODES)
                  WRITE(2,'(4X,A,<NMODES>(1PE10.2))')  ' Cos '//
      &                  'residuals : ',(RES(I),I=2*NMODES+1,3*NMODES)
              ENDIF
          ENDIF
C
C         Calculate the derivative matrix of the residuals wrt the
C         modal amplitudes using subroutine R_REDIV, which is a
C         function of the velocity VEL, root angle of attack AOA,
C         reduced frequency FREQ, and modal amplitudes QLIT. The
C         current values of the residuals RES are also passed since
C         the derivative matrix may be calculated numerically, in
C         which case the current values are needed.
C
          CALL R_DERIV(BEN_TOR,VEL,AOA,FREQ,QLIT,RES,DRDQ)
C
C         Write derivative matrix.
C
          IF (DIAGNOSTICS) THEN
              IF (STEADY) THEN
                  WRITE(2,'(/A)')  ' NUMERIC dR/dq MATRIX :'
                  WRITE(2,'(12X,<NMODES>(6X,I1,3X))') (I,I=1,NMODES)
                  DO 210 J = 1,NMODES
                      WRITE(2,'(5X,A5,I1,A1,<NMODES>(1PE10.2))')
      &                  'dR/dq',J,'o',(DRDQ(I,J),I=1,NMODES)
```

```fortran
210                     CONTINUE
                   ELSEIF (NMODES.LE.2) THEN
                       WRITE(2,'(/A)') ' NUMERIC dR/dq MATRIX :'
                       WRITE(2,'(12X,<3*NMODES>(6X,I1,3X))') (I,I=1,NMODES),
     &                     (I,I=1,NMODES),(I,I=1,NMODES)
                       DO 220 I1 = 1,3
                       DO 220 I2 = 1,NMODES
                           IF (I1.EQ.1) CDUM = 'dR/dq'//CHAR(I2+48)//'o '
                           IF (I1.EQ.2) CDUM = 'dR/dq'//CHAR(I2+48)//'s '
                           IF (I1.EQ.3) CDUM = 'dR/dq'//CHAR(I2+48)//'c '
                           IF ((I1.EQ.2).AND.(I2.EQ.BEN_TOR).AND.
     &                         (VLINES)) CDUM = 'dR/dAOA'
                           IF ((I1.EQ.2).AND.(I2.EQ.BEN_TOR).AND.
     &                         (.NOT.VLINES)) CDUM = 'dR/dV*2'
                           IF ((I1.EQ.3).AND.(I2.EQ.BEN_TOR))
     &                         CDUM = ' dR/dk '
                           J = (I1-1)*NMODES+I2
                           WRITE(2,'(5X,A7,<3*NMODES>(1PE10.2))')
     &                         CDUM,(DRDQ(I,J),I=1,3*NMODES)
220                    CONTINUE
                   ENDIF
               ENDIF
C
C          Apply the Newton-Raphson scheme to figure the appropriate
C          linear correction in the state vector so as to drive the
C          appropriate residuals to zero. For the steady case, only
C          the steady amplitudes need to be corrected.
C
           IF (STEADY) THEN
               CALL SOLVE(DRDQ,RES,DQALL,3*MAXMODE,1,NMODES)
           ELSEIF (.NOT.STEADY) THEN
               CALL SOLVE(DRDQ,RES,DQALL,3*MAXMODE,1,3*NMODES)
           ENDIF
C
C          Write the uncorrected state vector corrections.
C
           IF (DIAGNOSTICS) THEN
               WRITE(2,'(/A,<NMODES>(1PE10.2))') ' DELTA avg '//
     &             'amps [m] : ',(-DQALL(I),I=1,NMODES)
               IF (.NOT.STEADY) THEN
                   IF (BEN_TOR.EQ.1) THEN
                       WRITE(2,'(A,<NMODES>(1PE10.2))') ' DELTA '//
     &                     'sin amps [m] : ',0.D0,-DQALL(NMODES+2),
     &                     (-DQALL(I),I=NMODES+3,2*NMODES)
                       WRITE(2,'(A,<NMODES>(1PE10.2))') ' DELTA '//
     &                     'cos amps [m] : ',0.D0,-DQALL(2*NMODES+2),
     &                     (-DQALL(I),I=2*NMODES+3,3*NMODES)
                   ELSE
                       WRITE(2,'(A,<NMODES>(1PE10.2))') ' DELTA '//
     &                     'sin amps [m] : ',-DQALL(NMODES+1),0.D0,
     &                     (-DQALL(I),I=NMODES+3,2*NMODES)
                       WRITE(2,'(A,<NMODES>(1PE10.2))') ' DELTA '//
     &                     'cos amps [m] : ',-DQALL(2*NMODES+1),0.D0,
     &                     (-DQALL(I),I=2*NMODES+3,3*NMODES)
```

```fortran
                        ENDIF
                        IF (VLINES) WRITE(2,'(A,1PE10.2,A)')
     &                      ' DELTA AOA =',-DQALL(NMODES+BEN_TOR),' deg'
                        IF (.NOT.VLINES) WRITE(2,'(A,1PE10.2,A)')
     &                      ' DELTA V*2 =',-DQALL(NMODES+BEN_TOR),' (m/s)**2'
                        WRITE(2,'(A,1PE10.2)') ' DELTA k   =',
     &                      -DQALL(2*NMODES+BEN_TOR)
                    ENDIF
                ENDIF
C
C
C           Calculate the appropriate factor for relaxation when the
C           correction step size is too large for either the root
C           angle/velocity or reduced frequency.
C
            FACTOR = 1.D0
            IF (.NOT.STEADY) THEN
                DO 230 I = 1,2
                    II = I*NMODES+BEN_TOR
                    IF (QALL(II).NE.0.) THEN
                    IF (ABS(DQALL(II)/FACTOR/QALL(II)).GT.TOL) THEN
                        FACTOR = ABS(DQALL(II)/(TOL*QALL(II)))
                    ENDIF
                    ENDIF
230             CONTINUE
                IF (DIAGNOSTICS) WRITE(2,'(/A,1PE10.2)') ' FACTOR = ',
     &          FACTOR
            ENDIF
C
C
C           Update the augmented state vector, at the same time
C           checking for convergence of the maximum residual and
C           of the relative change in the state vector QALL.
C
            CONVERGED = .TRUE.
            RESMAX = 0.D0
            IMAX = 3*NMODES
            IF (STEADY) IMAX = NMODES
            DO 240 I = 1,IMAX
                QALL(I) = QALL(I)-DQALL(I)/FACTOR
C
C               Check relative change in state vector.
C
                IF (QALL(I).NE.0.) THEN
                    IF (ABS(DQALL(I)/QALL(I)).GT.1.D-5) CONVERGED=.FALSE.
                ENDIF
C
C               Check size of residuals.
C
                IF (ABS(RES(I)).GT.1.D-8) CONVERGED=.FALSE.
                IF (ABS(RES(I)).GT.ABS(RESMAX)) RESMAX=RES(I)
240         CONTINUE
            IF (LOOPS.GE.99) CONVERGED=.TRUE.
C
C           Print current status to screen.
C
```

```fortran
                IF (STEADY) THEN
                    IF (VLINES) THEN
                        WRITE(6,'(A,F6.2,A,I2,A,1PE8.1)') '+STEADY - AOA =',
     &                      DUMMY2,' deg ; Loop',LOOPS,' ; Rmax = ',RESMAX
                    ELSEIF (.NOT.VLINES) THEN
                        WRITE(6,'(A,F6.2,A,I2,A,1PE8.1)') '+STEADY - VEL =',
     &                      DUMMY2,' m/s ; Loop',LOOPS,' ; Rmax = ',RESMAX
                    ENDIF
                ELSE
                    IF (VLINES) THEN
                        WRITE(6,'(A,F6.2,A,I2,A,1PE8.1,A,0PF6.2,A,F5.2)')
     &                      '+AMP =',DUMMY2,' ; Loop',LOOPS,' ; Rmax = ',
     &                      RESMAX,' ; AOA =',QALL(NMODES+BEN_TOR)*180./PI,
     &                      ' deg ; k =',QALL(2*NMODES+BEN_TOR)
                    ELSEIF (.NOT.VLINES) THEN
                        WRITE(6,'(A,F6.2,A,I2,A,1PE8.1,A,0PF6.2,A,F5.2)')
     &                      '+AMP =',DUMMY2,' ; Loop',LOOPS,' ; Rmax = ',
     &                      RESMAX,' ; VEL =',DSQRT(QALL(NMODES+BEN_TOR)),
     &                      ' m/s; k =',QALL(2*NMODES+BEN_TOR)
                    ENDIF
                ENDIF
            END DO
C
C           Extract the modal amplitudes and the velocity and reduced
C           frequency from the final, converged augmented state vector.
C
            DO 250 I = 1,NMODES
            DO 250 J = 1,3
                QLIT(I,J) = QALL(NMODES*(J-1)+I)
                IF ((STEADY).AND.(J.NE.1)) QLIT(I,J) = 0.
250         CONTINUE
            FREQ = 0.
C
C           If unsteady, extract the appropriate root angle/velocity,
C           frequency, and twist oscillating amplitudes from the
C           final, converged augmented state vector.
C
            IF (.NOT.STEADY) THEN
                QLIT(BEN_TOR,3) = 0.D0
                IF (BEN_TOR.EQ.1) QLIT(1,2) = DEFLC/FMODE(0,'X',1,1.)/
     &              FMODE(0,'Y',1,0.)
                IF (BEN_TOR.EQ.2) QLIT(2,2) = DTAN(TWIST)*CHORD/
     &              FMODE(0,'X',2,1.)/FMODE(1,'Y',2,0.)
                IF (VLINES) AOA = QALL(NMODES+BEN_TOR)
                IF (.NOT.VLINES) VEL = DSQRT(QALL(NMODES+BEN_TOR))
                FREQ = QALL(2*NMODES+BEN_TOR)
            ENDIF
C
C           Calculate the midchord tip deflection components and the tip
C           twist components.
C
            DO 270 J = 1,3
                HTIP(J) = 0.D0
                ATIP(J) = 0.D0
```

-178-

```
               DO 260 I = 1,NMODES
                   HTIP(J) = HTIP(J)+QLIT(I,J)*FMODE(0,'X',I,1.)*
     &               FMODE(0,'Y',I,0.)
                   ATIP(J) = ATIP(J)+QLIT(I,J)*FMODE(0,'X',I,1.)*
     &               FMODE(1,'Y',I,0.)/CHORD
260            CONTINUE
C
C              Convert tip deflection to centimeters and tip twist
C              to degrees.
C
               IF (LATAN) ATIP(J) = DATAN(ATIP(J))
               HTIP(J) = HTIP(J)*100.D0
               ATIP(J) = ATIP(J)*180.D0/PI
270        CONTINUE
C
C          Write converged results.
C
           ANG = AOA*180./PI
           OMEGA = FREQ*VEL/(CHORD/2.)/(2.*PI)
           IF (.NOT.DIAGNOSTICS) THEN
               WRITE(2,'(3F7.2,6F9.3)') VEL,ANG,OMEGA,(HTIP(J),J=1,3),
     &             (ATIP(J),J=1,3)
               IF (LOOPS.EQ.99) WRITE(2,*) '   Not converged: '//
     &             'Newton-Raphson solver halted after 100 iterations'
           ELSE
               WRITE(2,'(/A,I3,A)') ' After',LOOPS,' N-R iterations :'
               WRITE(2,'(26X,<NMODES>(5X,I1,4X))') (I,I=1,NMODES)
               WRITE(2,'(A,<NMODES>(1PE10.2))') ' Avg amps [m] : ',
     &             (QLIT(I,1),I=1,NMODES)
               IF (.NOT.STEADY) THEN
                   WRITE(2,'(A,<NMODES>(1PE10.2))') ' Sin amps [m] : ',
     &                 (QLIT(I,2),I=1,NMODES)
                   WRITE(2,'(A,<NMODES>(1PE10.2))') ' Cos amps [m] : ',
     &                 (QLIT(I,3),I=1,NMODES)
               ENDIF
               WRITE(2,'(/A,F7.3,A)') ' AOA =',ANG,' degs'
               WRITE(2,'(A,F7.3,A)')  ' VEL =',VEL,' m/s'
               WRITE(2,'(A,F7.3)')    '   k =',FREQ
               WRITE(2,'(A,F6.3,A)')  '   w = ',OMEGA,' Hz'
           ENDIF
1000   CONTINUE
       CLOSE(2)
C
       STOP
       END
```

```
C━━━━ FILE: MASS.FOR ━━━━━━━━━━━━━━━━━━━━━━━━━━━━━━━━━━━━━━
C
      SUBROUTINE MASS(LO,HI,MPA)
C
C     Subroutine to calculate the components of the flat plate mass matrix.
C
      INCLUDE 'PARAM.INC'
      INCLUDE 'GLBBLK.INC'
      REAL*8  LO,HI,MPA,INTGRL
C
      DO 10 I = 1,NMODES
      DO 10 J = 1,NMODES
         M(I,J) = MPA*CHORD*LENGTH*INTGRL('X',I,0,J,0,LO,HI)*
     &      INTGRL('Y',I,0,J,0,-.5D0,+.5D0)
10    CONTINUE
C
      RETURN
      END
```

```
C=========================================================================
C
      SUBROUTINE QUCON(EL,ET,NULT,GLT,QU11,QU12,QU22,QU66)
C
C     Subroutine to compute the unidirectional elastic constants,
C     the unidirectional Q's, from the ply engineering elastic constants.
C
      IMPLICIT REAL*8 (A-H,O-Z)
      REAL*8   EL,ET,NULT,NUTL,GLT
      REAL*8   QU11,QU12,QU22,QU66
C
      NUTL = ET/EL*NULT
      DENOM = 1.D0-NULT*NUTL
      QU11 = EL/DENOM
      QU12 = NULT*ET/DENOM
      QU22 = ET/DENOM
      QU66 = GLT
      RETURN
      END
C
C=========================================================================
C
      SUBROUTINE QTCON(K,THETA,QU11,QU12,QU22,QU66,QT)
C
C     Subroutine to compute the rotated elastic constants,
C     the Q[theta], for the K-th ply, laid up at an angle theta.
C
      IMPLICIT REAL*8 (A-H,O-Z)
      INTEGER           K
      REAL*8            THETA,QU11,QU12,QU22,QU66
      REAL*8            I1,I2,R1,R2,QT(3,3,*)
C
C     Calculate the invariants
C
      I1 = (QU11 + QU22 + 2.D0*QU12)/4.D0
      I2 = (QU11 + QU22 - 2.D0*QU12 + 4.D0*QU66)/8.D0
      R1 = (QU11 - QU22)/2.D0
      R2 = (QU11 + QU22 - 2.D0*QU12 - 4.D0*QU66)/8.D0
C
      QT(1,1,K) = I1 + I2 + R1*DCOS(2.D0*THETA) + R2*DCOS(4.D0*THETA)
      QT(2,2,K) = I1 + I2 - R1*DCOS(2.D0*THETA) + R2*DCOS(4.D0*THETA)
      QT(1,2,K) = I1-I2 - R2*DCOS(4.D0*THETA)
      QT(3,3,K) = I2 - R2*DCOS(4.D0*THETA)
      QT(1,3,K) = R1*DSIN(2.D0*THETA)/2.D0 + R2*DSIN(4.D0*THETA)
      QT(2,3,K) = R1*DSIN(2.D0*THETA)/2.D0 - R2*DSIN(4.D0*THETA)
      QT(2,1,K) = QT(1,2,K)
      QT(3,1,K) = QT(1,3,K)
      QT(3,2,K) = QT(2,3,K)
C
      RETURN
      END
```

```fortran
C
C===============================================================
C
      SUBROUTINE BEND(NPLIES,ZU,ZL,QT,A,D)
C
C     Subroutine to compute the laminate bending stiffnesses, Aij & Dij.
C
      IMPLICIT REAL*8 (A-H,O-Z)
      INTEGER NPLIES
      REAL*8  ZU(*),ZL(*),QT(3,3,*)
      REAL*8  A(3,3),D(3,3)
C
C     Initialize the A and D matrices.
C
      DO 10 I = 1,3
      DO 10 J = 1,3
          A(I,J) = 0.
          D(I,J) = 0.
10    CONTINUE
C
C     Add the contribution of each ply to the A & D matrices.
C
      DO 30 I = 1,3
      DO 30 J = I,3
      DO 30 K = 1,NPLIES
          A(I,J) = A(I,J) + QT(I,J,K)*(ZU(K)-ZL(K))
          D(I,J) = D(I,J) + QT(I,J,K)*(ZU(K)**3-ZL(K)**3)/3.D0
30    CONTINUE
C
      RETURN
      END
C
C===============================================================
C
      SUBROUTINE STIFF(A,D,LO,HI,Z)
C
C     Subroutine to compute the stiffness matrix, Kij.
C
      INCLUDE 'PARAM.INC'
      INCLUDE 'GLBBLK.INC'
      REAL*8  A(3,3),D(3,3),LO,HI,INTGRL
      REAL*8  Z(MAXMODE,MAXMODE)
C
C     NOTE: INTGRL(XY,I,ID,J,JD,lo,hi) is the function to numerically
C     integrate the XY-variation of the ID-th derivative of the I-th mode
C     with the JD-th derivative of the J-th mode between the interval [lo,hi].
C
      DO 10 I = 1,NMODES
      DO 10 J = 1,NMODES
          Z(I,J) = 0.
          K(I,J) = (CHORD*LENGTH) * (D(1,1)*INTGRL('X',I,2,J,2,LO,HI)*
     &    INTGRL('Y',I,0,J,0,-.5,+.5)/LENGTH**4 + D(2,2)*INTGRL('X',
     &    I,0,J,0,LO,HI)*INTGRL('Y',I,2,J,2,-.5,+.5)/CHORD**4 + 4.D0*
     &    D(3,3)*INTGRL('X',I,1,J,1,LO,HI)*INTGRL('Y',I,1,J,1,-.5,+.5)/
     &    (LENGTH*CHORD)**2 + D(1,2)*(INTGRL('X',I,2,J,0,LO,HI)*
```

```
     &     INTGRL('Y',I,0,J,2,-.5,+.5)+INTGRL('X',I,0,J,2,LO,HI)*
     &     INTGRL('Y',I,2,J,0,-.5,+.5))/(LENGTH*CHORD)**2 + 2.D0*D(1,3)*
     &     (INTGRL('X',I,2,J,1,LO,HI)*INTGRL('Y',I,0,J,1,-.5,+.5)+
     &     INTGRL('X',I,1,J,2,LO,HI)*INTGRL('Y',I,1,J,0,-.5,+.5))/
     &     (LENGTH**3*CHORD) + 2.D0*D(2,3)*(INTGRL('X',I,0,J,1,LO,HI)*
     &     INTGRL('Y',I,2,J,1,-.5,+.5)+INTGRL('X',I,1,J,0,LO,HI)*
     &     INTGRL('Y',I,1,J,2,-.5,+.5))/(LENGTH*CHORD**3))
10       CONTINUE
C
         RETURN
         END
```

```
C═════ FILE : RESIDUAL.FOR ══════════════════════════════════════════
C
      SUBROUTINE RESIDUAL(VEL,AOA,FREQ,QLIT,RES)
C
C     Subroutine to calculate the residuals used in the Newton-Raphson solver.
C
C     INPUT  VARIABLES: velocity VEL, root angle of attack AOA, reduced
C                       frequency FREQ, and modal amplitudes QLIT
C     OUTPUT VARIABLES: residuals RES, non-dimensionalized by
C                       1/2*rho*(V**2)*area
C
      INCLUDE 'PARAM.INC'
      INCLUDE 'GLBBLK.INC'
      REAL*8   VEL,AOA,FREQ,QLIT(MAXMODE,3)
      REAL*8   RES(3*MAXMODE),QBIG(MAXMODE,3)
C
C     Calculate the modal forces QBIG using subroutine MODAL_FORCE, which
C     are functions of the velocity VEL, the root angle of attack AOA,
C     the reduced frequency FREQ, and the modal amplitudes QLIT.
C
      CALL MODAL_FORCE(VEL,AOA,FREQ,QLIT,QBIG)
C
C     Calculate the residuals by including the contributions
C     of the mass and stiffness matrices with the modal forces.
C
      DO 20 J = 1,3
C
C     Calculate the current cubically stiffened torsional stiffness.
C
      IF (J.EQ.1) K(2,2) = KTT0 + KTTCUBE*(QLIT(2,1)**2+1.5*
     &    QLIT(2,2)**2+1.5*QLIT(2,3)**2)
      IF (J.NE.1) K(2,2) = KTT0 + KTTCUBE*(3.*QLIT(2,1)**2+0.75*
     &    QLIT(2,2)**2+0.75*QLIT(2,3)**2)
C
      DO 20 I = 1,NMODES
         II = NMODES*(J-1)+I
         IF ((STEADY).AND.(J.NE.1)) THEN
            RES(II) = 0.
         ELSE
            RES(II) = -QBIG(I,J)
            DO 10 L = 1,NMODES
               RES(II) = RES(II)+K(I,L)*QLIT(L,J)
               OMEGA = FREQ*VEL/(CHORD/2.)
               IF (J.NE.1) RES(II)=RES(II)-OMEGA**2*M(I,L)*QLIT(L,J)
10          CONTINUE
         ENDIF
         RES(II) = RES(II)/(.5D0*RHOA*VEL**2*CHORD*LENGTH)
20    CONTINUE
C
      RETURN
      END
```

```
C═══ FILE: QBIG.FOR ═══════════════════════════════════════════
C
        SUBROUTINE MODAL_FORCE(VEL,AOA,FREQ,QLIT,QBIG)
C
C       Subroutine to calculate the oscillating components of the modal forces.
C
C       INPUT VARIABLES: velocity VEL, root angle of attack AOA, reduced
C                        frequency FREQ, and modal amplitudes QLIT
C       OUTPUT VARIABLE: modal forces QBIG
C
        INCLUDE 'PARAM.INC'
        INCLUDE 'GLBBLK.INC'
        REAL*8  VEL,AOA,FREQ,QLIT(MAXMODE,3),THETA(3),HBAR(3)
        REAL*8  DCL0,CL(5),CM(5),CD(5),QBIG(MAXMODE,3)
C
C       Initialize the modal forces to zero value.
C
        DO 10 I = 1,NMODES
        DO 10 J = 1,3
            QBIG(I,J) = 0.D0
10      CONTINUE
C
C       Loop through Gauss integration points along the span.
C
        DO 60 IGNUM = 1,GPOINTS
C
C           Calculate the non-dimensional 1/4-chord deflection and angle
C           of attack sinusoidal coefficients at the Gauss point
C           spanwise location.
C
            XBAR = (GP(IGNUM)+1.D0)/2.D0
            DO 30 I = 1,3
                HBAR(I) = 0.D0
                THETA(I)= 0.D0
                DO 20 J = 1,NMODES
                    HBAR(I) = HBAR(I) + QLIT(J,I)/(CHORD/2.D0)*
     &                    FMODE(0,'X',J,XBAR)*FMODE(0,'Y',J,+.25)
                    THETA(I) = THETA(I) + QLIT(J,I)/CHORD*
     &                    FMODE(0,'X',J,XBAR)*FMODE(1,'Y',J,+.25)
20              CONTINUE
                IF (LATAN) THETA(I) = DATAN(THETA(I))
                IF (I.EQ.1) THETA(I)=THETA(I)+AOA
30          CONTINUE
C
C           Calculate the lift/moment coefficient sinusoidal coefficients.
C
            CALL AEROF('L',THETA,HBAR,VEL,FREQ,DCL0,CL)
            CALL AEROF('M',THETA,HBAR,VEL,FREQ,DCL0,CM)
C
C           Calculate the profile-drag coefficient contribution using
C           a 3rd-order polynomial fit.
C
            CD(1) = 4.923*ABS(THETA(1))**3 + .1472*THETA(1)**2 + .042*
     &          ABS(THETA(1)) + .014
```

```
          CD(2) = 0.D0
          CD(3) = 0.D0
C
C         Calculate the induced-drag coefficient contribution.
C
          CD(1) = CD(1) + CL(1)**2/PI/(2.*LENGTH/CHORD)
C
          IF (CORREC) DUMMY=SC(XBAR)
          IF (.NOT.CORREC) DUMMY=1.D0
C
C         Add contributions from the lift and moment at the current
C         Gauss point spanwise location to the modal force.
C
          DO 50 I = 1,NMODES
          DO 50 J = 1,3
             QBIG(I,J) = QBIG(I,J)+GW(IGNUM)/2.D0*(.5D0*RHOA*
     &            VEL**2*CHORD*LENGTH)*((CL(J)*DCOS(AOA)+CD(J)*
     &            DSIN(AOA))*FMODE(0,'Y',I,+.25)+CM(J)*
     &            FMODE(1,'Y',I,+.25))*FMODE(0,'X',I,XBAR)*DUMMY
50        CONTINUE
60     CONTINUE
C
       RETURN
       END
```

```
C═════ FILE: AEROF.FOR ════════════════════════════════════════
C
        SUBROUTINE AEROF(LM,THETA,HBAR,VEL,FREQ,DCL0,CZ)
C
C       Subroutine to calculate unsteady, non-linear, oscillatory aero-
C       dynamic coefficients by Fourier decomposition of the oscil-
C       latory, non-linear, stalled static aerodynamic force coefficient.
C
        INCLUDE        'PARAM.INC'
        INCLUDE        'GLBBLK.INC'
C       *** Input variables (LM,THETA,HBAR,VEL,FREQ) and output variables CZ.
        CHARACTER      LM*1
        REAL*8         THETA(*),HBAR(*),VEL,FREQ,DCL0,CZ(*)
C       *** Constants used in non-linear equations.
        REAL*8         ALFA(3),ALF0,ALFV,TC(3),S,KV,LAM,SIG,ALF,W,D,E
C       *** Variables used in linear calculations.
        INCLUDE        'CZ1BLK.INC'
C       *** Variables used in non-linear calculations.
        INCLUDE        'CZ2BLK.INC'
        REAL*8         JCK
C       *** Variables used in plotting routines.
        REAL           XAXIS(2000),YAXIS(2000)
        INTEGER        IOPT(3),NUM(3)
        CHARACTER      TITLE*80,ANSWER*1
        LOGICAL        LPRINT
C
        RE = RHOA*VEL*CHORD/RMUA
C
C       Determine if an output file should be generated.
C
C       IF (LM.EQ.'L') WRITE(*,'(/A,$)') '+Create output file for '//
C    &  'lift trial, AEROF.OUT ? '
C       IF (LM.EQ.'M') WRITE(*,'(/A,$)') '+Create output file for '//
C    &  'moment trial, AEROF.OUT ? '
C       READ (*,'(A1)') ANSWER
C       IF ((ANSWER.EQ.'Y').OR.(ANSWER.EQ.'y')) LPRINT=.TRUE.
        LPRINT = .FALSE.
C
        IF (LPRINT) THEN
            OPEN (UNIT=3,FILE='AEROF.OUT',STATUS='NEW',FORM='FORMATTED')
            WRITE(3,*) ' '
            IF (LM.EQ.'L') WRITE(3,*) 'LIFT TRIAL USING AEROF SUBROUTINE'
            IF (LM.EQ.'M') WRITE(3,*) 'MOMENT TRIAL USING AEROF SUBROUTINE'
            WRITE(3,*) ' '
            WRITE(3,*) 'INPUT VARIABLES:'
            WRITE(3,*) '═══════════════'
            WRITE(3,*) 'Reynold''s Number =',RE
            WRITE(3,*) 'THETA0 =',(THETA(1)*180.D0/PI),' degs'
            WRITE(3,*) 'THETAs =',(THETA(2)*180.D0/PI),' degs'
            WRITE(3,*) 'THETAc =',(THETA(3)*180.D0/PI),' degs'
            WRITE(3,*) ' HBAR0 =',HBAR(1)
            WRITE(3,*) ' HBARs =',HBAR(2)
            WRITE(3,*) ' HBARc =',HBAR(3)
            WRITE(3,*) '  FREQ =',FREQ
```

-187-

```fortran
      ENDIF
C
C     Calculate the perceived angle of attack coefficients [ALFA(i)]
C     and the mean and vibratory amplitudes [ALF0 and ALFV].
C
      ALFA(1) = THETA(1)
      ALFA(2) = THETA(2) + FREQ*HBAR(3)
      ALFA(3) = THETA(3) - FREQ*HBAR(2)
C
      ALF0 = ALFA(1)
      ALFV = DSQRT(ALFA(2)**2+ALFA(3)**2)
      IF (ALFV.EQ.0) ZETA=0.D0
      IF (ALFV.NE.0) ZETA=DASIN(ALFA(3)/ALFV)
      IF (ALFA(2).LT.0) ZETA=-ZETA
C
      IF (LPRINT) THEN
          WRITE(3,*) ' '
          WRITE(3,*) 'ALPHA0 =',(ALF0*180.D0/PI),' degs'
          WRITE(3,*) 'ALPHAs =',(ALFA(2)*180.D0/PI),' degs'
          WRITE(3,*) 'ALPHAc =',(ALFA(3)*180.D0/PI),' degs'
          WRITE(3,*) 'ALPHA~ =',(ALFV*180.D0/PI),' degs'
          WRITE(3,*) ' ZETA  =',(ZETA*180.D0/PI),' degs'
      ENDIF
C
C     Correct effective angle of attack and real angle of attack
C     for finite span.
C
      ALF0 = ALF0/(1.+SLOPE('L')/PI/(2.*LENGTH/CHORD))
      ALFV = ALFV/(1.+SLOPE('L')/PI/(2.*LENGTH/CHORD))
      ALFA(1) = ALFA(1)/(1.+SLOPE('L')/PI/(2.*LENGTH/CHORD))
      ALFA(2) = ALFA(2)/(1.+SLOPE('L')/PI/(2.*LENGTH/CHORD))
      ALFA(3) = ALFA(3)/(1.+SLOPE('L')/PI/(2.*LENGTH/CHORD))
      TC(1) = THETA(1)/(1.+SLOPE('L')/PI/(2.*LENGTH/CHORD))
      TC(2) = THETA(2)/(1.+SLOPE('L')/PI/(2.*LENGTH/CHORD))
      TC(3) = THETA(3)/(1.+SLOPE('L')/PI/(2.*LENGTH/CHORD))
C
      CZ1(1) = SLOPE(LM)*ALF0
C
C     Calculate lowest and highest region in which the alpha
C     oscillation passes through.
C
      LOREG = 0
      HIREG = 0
      AMIN = ALF0 - ALFV
      AMAX = ALF0 + ALFV
      DO 10 I = 1,IREGS(FOIL)
          IF ((TD(I).LE.AMIN).AND.(AMIN.LT.TD(I+1))) LOREG=I
          IF ((TD(I).LT.AMAX).AND.(AMAX.LE.TD(I+1))) HIREG=I
          IF ((-TD(I+1).LT.AMIN).AND.(AMIN.LE.-TD(I))) LOREG=-I
          IF ((-TD(I+1).LE.AMAX).AND.(AMAX.LT.-TD(I))) HIREG=-I
10    CONTINUE
C
      IF (.NOT.STEADY) THEN
C
```

```fortran
C           Calculate coefficients of the linear differential equations.
C
            CALL COEFS_LIN(LM,ALF0,S,KV,LAM,SIG,ALF)
            IF (LPRINT) THEN
                WRITE(3,*) ' '
                WRITE(3,*) '  S =',S,'1/rad'
                WRITE(3,*) ' KV =',KV,'1/rad'
                WRITE(3,*) 'LAM =',LAM
                WRITE(3,*) 'SLP =',SLOPE(LM),'1/rad'
                WRITE(3,*) 'SIG =',SIG,'1/rad'
                WRITE(3,*) 'ALF =',ALF
            ENDIF
C
C           Calculate variables of linear aerodynamic equation.
C
            LS = SLOPE(LM)*ALFA(2)-SIG*FREQ*TC(3)
            LC = SLOPE(LM)*ALFA(3)+SIG*FREQ*TC(2)
            IF (LPRINT) THEN
                WRITE(3,*) ' '
                WRITE(3,*) 'Ls =',LS
                WRITE(3,*) 'Lc =',LC
            ENDIF
C
C           Calculate oscillatory contributions of linear aerodynamics.
C
            CZ1(2) = ((LAM*LAM+ALF*FREQ*FREQ)*LS+LAM*FREQ*
     &          (1.D0-ALF)*LC)/(LAM*LAM+FREQ*FREQ)
            CZ1(3) = ((LAM*LAM+ALF*FREQ*FREQ)*LC-LAM*FREQ*
     &          (1.D0-ALF)*LS)/(LAM*LAM+FREQ*FREQ)
        ENDIF
C
        IF (LPRINT) THEN
            WRITE(3,*) 'C'//LM//'1o =',CZ1(1)
            WRITE(3,*) 'C'//LM//'1s =',CZ1(2)
            WRITE(3,*) 'C'//LM//'1c =',CZ1(3)
        ENDIF
C
C       Calculate the coefficients of CZ2 in time: 1-constant,
C       2-first harmonic sine, 3-first harmonic cosine, 4-second
C       harmonic sine, 5-second harmonic cosine.
C
        IF (((LOREG.EQ.0).AND.(HIREG.EQ.0)).OR.(LINEAR)) THEN
C
C           Set coefficients equal to zero if oscillation
C           never enters the stalled regime or if only considering
C           the linear problem.
C
            DO 220 I = 1,5
                CZ2(I) = 0.D0
220         CONTINUE
        ELSEIF ((STEADY).OR.(ALFV.EQ.0)) THEN
C
C           If steady, calculate steady non-linear coefficient and set
C           unsteady non-linear coefficients to zero.
```

```
C
            CZ2(1) = -DCZS(LM,0,ALF0)
            DO 230 I = 2,5
                CZ2(I) = 0.D0
230         CONTINUE
        ELSE
C
C           Calculate limits of integration for each region for
C           use in the Fourier analysis.
C
            PHI(LOREG) = -PI/2.D0
            PHI(HIREG+1) = PI/2.D0
            IF (LOREG.NE.HIREG) THEN
            DO 240 I = LOREG+1,HIREG
                IF (I.LE.0) THEN
                    PHI(I) = DASIN((-TD(1-I)-ALF0)/ALFV)
                ELSE
                    PHI(I) = DASIN((TD(I)-ALF0)/ALFV)
                ENDIF
240         CONTINUE
            ENDIF
C
            IF (LPRINT) THEN
                WRITE(3,*) ' '
                DO 245 I = LOREG,HIREG+1
                    WRITE(3,*) 'REGION =',I,' PHI =',(PHI(I)*180.D0/PI),' degs'
245         CONTINUE
            ENDIF
C
C           Calculate the coefficients of the polynomial expansion
C           sine series in each region that the oscillation passes thru.
C
            DO 300 I = LOREG,HIREG
                IF (I.EQ.0) GOTO 300
C
C               Calculate constant coefficient.
C
                BB(I,0) = DBLE(SIGN(1,I))*DCZS(LM,0,TD(ABS(I)))
                DO 250 J = 1,JMAX(ABS(I))
                    BB(I,0) = BB(I,0) + DBLE(SIGN(1,I)**(J+1))*
     &              A(LM,ABS(I),J)*(ALF0-DBLE(SIGN(1,I))*TD(ABS(I)))**J
250             CONTINUE
C
C               Calculate higher order coefficients.
C
                DO 280 KK = 1,JMAX(ABS(I))
                    BB(I,KK) = (DBLE(SIGN(1,I)))**(KK+1)*A(LM,ABS(I),KK)*
     &              (ALFV**KK)
                    IF (KK.NE.JMAX(ABS(I))) THEN
                    DO 270 J = KK+1,JMAX(ABS(I))
C
C                       Calculate J-choose-KK.
C
                        JCK = 1.D0
```

```fortran
                      DO 260 L = 1,KK
                          JCK = JCK*DBLE(J-L+1)/DBLE(L)
260                   CONTINUE
C
C                     Add contribution of j-th power to bb(i,kk).
C
                      BB(I,KK) = BB(I,KK) + JCK*(DBLE(SIGN(1,I)))**(J+1)*
     &                A(LM,ABS(I),J)*(ALFV**KK)*((ALF0-DBLE(SIGN(1,I))*
     &                TD(ABS(I)))**(J-KK))
270               CONTINUE
                  ENDIF
280           CONTINUE
C
              IF (LPRINT) THEN
                  WRITE(3,*) ' '
                  WRITE(3,*) 'REGION =',I
                  DO 285 KK = 0,JMAX(ABS(I))
                      WRITE(3,*) 'B(',KK,') =',BB(I,KK)
285               CONTINUE
              ENDIF
C
C             Calculate the integrals of the sine powers in each region
C             using Equation ??? from "???."
C
              INT(I,0) = PHI(I+1) - PHI(I)
              INT(I,1) = DCOS(PHI(I)) - DCOS(PHI(I+1))
              DO 290 KK = 2,JMAX(ABS(I))+2
                  INT(I,KK) = (DCOS(PHI(I))*DSIN(PHI(I))**(KK-1)-
     &            DCOS(PHI(I+1))*DSIN(PHI(I+1))**(KK-1))/DBLE(KK)+
     &            DBLE(KK-1)/DBLE(KK)*INT(I,KK-2)
290           CONTINUE
C
              IF (LPRINT) THEN
                  WRITE(3,*) ' '
                  DO 295 KK = 0,JMAX(ABS(I))+2
                      WRITE(3,*) 'INT(',KK,') =',INT(I,KK)
295               CONTINUE
              ENDIF
300       CONTINUE
C
C         Calculate the polynomial coefficients of the
C         Fourier expansion in the PHI domain.
C
          DCZ0 = 0.D0
          DCZ1 = 0.D0
          DCZ2 = 0.D0
          DO 410 I = LOREG,HIREG
              IF (I.NE.0) THEN
              DO 400 KK = 0,JMAX(ABS(I))
                  DCZ0 = DCZ0 + BB(I,KK)*INT(I,KK)/PI
                  DCZ1 = DCZ1 + BB(I,KK)*INT(I,KK+1)*2.D0/PI
                  DCZ2 = DCZ2 + BB(I,KK)*(INT(I,KK)-2.D0*INT(I,KK+2))*
     &                2.D0/PI
400           CONTINUE
```

```fortran
                ENDIF
410             CONTINUE
C

                IF (LPRINT) THEN
                    WRITE(3,*) ' '
                    WRITE(3,*) 'DC'//LM//'0 =',DCZ0
                    WRITE(3,*) 'DC'//LM//'V1 =',DCZ1
                    WRITE(3,*) 'DC'//LM//'V2 =',DCZ2
                ENDIF
                IF (LM.EQ.'L') DCL0=DCZ0
C
C               Calculate the polynomial coefficients of the Fourier
C               expansion in the OMEGA*TAU domain.
C
                DCZ(1) = DCZ0
                DCZ(2)=DCZ1*ALFA(2)/ALFV
                DCZ(3)=DCZ1*ALFA(3)/ALFV
                DCZ(4)=DCZ2*-2.D0*ALFA(2)/ALFV*ALFA(3)/ALFV
                DCZ(5)=DCZ2*(ALFA(2)**2-ALFA(3)**2)/(ALFV**2)
C
C               Calculate coefficients of the non-linear aerodynamic
C               differential equations. NOTE: this depends on DCL0 having
C               already been calculated, i.e. that the calculations for
C               LM='L' are done before LM='M'.
C
                CALL COEFS_NON(ALF0,DCL0,W,D,E)
                IF (LPRINT) THEN
                    WRITE(3,*) ' '
                    WRITE(3,*) 'W =',W
                    WRITE(3,*) 'D =',D
                    WRITE(3,*) 'E =',E
                ENDIF
C
                CZ2(1) = -DCZ(1)
C
C               Calculate second harmonic coefficients of unsteady aerodynamics.
C
                K1 = 1.D0+D*D-(2.D0*FREQ/W)*(2.D0*FREQ/W)
                K2 = 2.D0*D*(2.D0*FREQ/W)
                K3 = -(1.D0+D*D)*(DCZ(4)-E*2.D0*FREQ*DCZ(5))
                K4 = -(1.D0+D*D)*(DCZ(5)+E*2.D0*FREQ*DCZ(4))
                CZ2(4) = (K1*K3+K2*K4)/(K1*K1+K2*K2)
                CZ2(5) = (K1*K4-K2*K3)/(K1*K1+K2*K2)
C
                IF (LPRINT) THEN
                    WRITE(3,'(/A)') ' Second Harmonic'
                    WRITE(3,*) 'DC'//LM//'s2 =',DCZ(4)
                    WRITE(3,*) 'DC'//LM//'c2 =',DCZ(5)
                    WRITE(3,*) 'K1(2) =',K1
                    WRITE(3,*) 'K2(2) =',K2
                    WRITE(3,*) 'K3(2) =',K3
                    WRITE(3,*) 'K4(2) =',K4
                ENDIF
C
```

```
C          Calculate first harmonic coefficients of unsteady aerodynamics.
C
           K1 = 1.D0+D*D-(FREQ/W)*(FREQ/W)
           K2 = 2.D0*D*(FREQ/W)
           K3 = -(1.D0+D*D)*(DCZ(2)-E*FREQ*DCZ(3))
           K4 = -(1.D0+D*D)*(DCZ(3)+E*FREQ*DCZ(2))
           CZ2(2) = (K1*K3+K2*K4)/(K1*K1+K2*K2)
           CZ2(3) = (K1*K4-K2*K3)/(K1*K1+K2*K2)
C
           IF (LPRINT) THEN
               WRITE(3,'(/A)') ' First Harmonic'
               WRITE(3,*) 'DC'//LM//'0  =',DCZ(1)
               WRITE(3,*) 'DC'//LM//'s1 =',DCZ(2)
               WRITE(3,*) 'DC'//LM//'c1 =',DCZ(3)
               WRITE(3,*) 'K1(1) =',K1
               WRITE(3,*) 'K2(1) =',K2
               WRITE(3,*) 'K3(1) =',K3
               WRITE(3,*) 'K4(1) =',K4
           ENDIF
       ENDIF
       IF (LPRINT) THEN
           WRITE(3,*) ' '
           WRITE(3,*) 'C'//LM//'20  =',CZ2(1)
           WRITE(3,*) 'C'//LM//'2s1 =',CZ2(2)
           WRITE(3,*) 'C'//LM//'2c1 =',CZ2(3)
           WRITE(3,*) 'C'//LM//'2s2 =',CZ2(4)
           WRITE(3,*) 'C'//LM//'2c2 =',CZ2(5)
       ENDIF
C
C      Combine linear, non-linear, and apparent mass terms for
C      total coefficients of full non-linear aerodynamics.
C
       CZ(1) = CZ1(1) + CZ2(1)
       CZ(2) = CZ1(2) + CZ2(2) - S*FREQ*ALFA(3) - KV*FREQ*FREQ*TC(2)
       CZ(3) = CZ1(3) + CZ2(3) + S*FREQ*ALFA(2) - KV*FREQ*FREQ*TC(3)
       CZ(4) = CZ2(4)
       CZ(5) = CZ2(5)
C
       IF (LPRINT) THEN
           WRITE(3,*) ' '
           WRITE(3,*) 'C'//LM//'0  =',CZ(1)
           WRITE(3,*) 'C'//LM//'s1 =',CZ(2)
           WRITE(3,*) 'C'//LM//'c1 =',CZ(3)
           WRITE(3,*) 'C'//LM//'s2 =',CZ(4)
           WRITE(3,*) 'C'//LM//'c2 =',CZ(5)
           CLOSE(3)
       ENDIF
C
       RETURN
       END
```

```
C ════════════════════════════════════════════════════════════════
C
C       "Include" file, CZ1BLK.INC to describe the common variables used
C       in the harmonic balance method applied to the linear lift/moment.
C
        REAL*8  LS,LC,CZ1(3)
        COMMON  /CZ1BLK/LS,LC,CZ1


C ════════════════════════════════════════════════════════════════
C
C       "Include" file, CZ2BLK.INC, to describe the common variables used
C       in the harmonic balance method applied to the non-linear lift/moment.
C
        INTEGER LOREG,HIREG
        REAL*8  PHI(-MAXREG:MAXREG),BB(-MAXREG:MAXREG,0:MAXPOW)
        REAL*8  INT(-MAXREG:MAXREG,0:MAXPOW),DCZ(5),K1,K2,K3,K4,CZ2(5)
        COMMON  /CZ2BLK/LOREG,HIREG,PHI,BB,INT,DCZ,K1,K2,K3,K4,CZ2
```

```
C━━━━ FILE: DRDQ.FOR ━━━━━━━━━━━━━━━━━━━━━━━━━━━━━━━━━━━━━━━━━━━━━━━━━━━
C
      SUBROUTINE R_DERIV(BEN_TOR,VEL,AOA,FREQ,QLIT,RES,DRDQ)
C
C     Subroutine to calculate the Jacobian matrix d(RES)/d(QLIT) by
C     numerical estimation of the derivatives.
C
C     INPUT VARIABLES: velocity VEL, root angle of attack AOA, reduced
C                      frequency FREQ, modal amplitudes QLIT, and
C                      current residuals RES
C     OUTPUT VARIABLE: derivative matrix DRDQ
C
      INCLUDE 'PARAM.INC'
      INCLUDE 'GLBBLK.INC'
      REAL*8   VEL,AOA,FREQ,QLIT(MAXMODE,3),RES(3*MAXMODE)
      REAL*8   VEL2,AOA2,FREQ2,QLIT2(MAXMODE,3),RES2(3*MAXMODE)
      REAL*8   DRDQ(3*MAXMODE,3*MAXMODE)
      INTEGER BEN_TOR
C
C     Loop through each direction of the components of the modal amplitudes,
C     ignoring oscillating components if steady analysis.
C
      MAX = 3
      IF (STEADY) MAX = 1
      DO 30 I1 = 1,NMODES
      DO 30 J1 = 1,MAX
C
C         Skip if looking at components of state vector
C         reserved for angle of attack/velocity and reduced frequency.
C
          IF ((I1.EQ.BEN_TOR).AND.(J1.NE.1)) GOTO 30
C
C         Initialize modal amplitude trial vector.
C
          DO 10 I2 = 1,NMODES
          DO 10 J2 = 1,MAX
              QLIT2(I2,J2) = QLIT(I2,J2)
10        CONTINUE
C
C         Increment desired direction of modal amplitude
C         trial vector by 0.01%
C
          QLIT2(I1,J1) = 1.0001*QLIT(I1,J1)
          IF (QLIT2(I1,J1).EQ.0.) QLIT2(I1,J1)=0.0001
C
C         Calculate new residuals from modal amplitude trial vector.
C
          CALL RESIDUAL(VEL,AOA,FREQ,QLIT2,RES2)
C
C         Calculate numeric derivatives from modal amplitude trial
C         vector QLIT2 and associated residuals RES2.
C
          K1 = NMODES*(J1-1)+I1
          DO 20 I2 = 1,NMODES
```

```fortran
             DO 20 J2 = 1,MAX
                K2 = NMODES*(J2-1)+I2
                DRDQ(K2,K1) = (RES2(K2)-RES(K2))/(QLIT2(I1,J1)-QLIT(I1,J1))
20           CONTINUE
30        CONTINUE
C
C         If steady, skip angle of attack/velocity and frequency derivatives.
C
          IF (STEADY) RETURN
C
C         Increment trial angle of attack/velocity by 0.01% and
C         calculate new residuals.
C
          IF (VLINES) THEN
             AOA2 = 1.0001*AOA
             IF (AOA2.EQ.0.) AOA2=0.0001
             CALL RESIDUAL(VEL,AOA2,FREQ,QLIT,RES2)
          ELSE
             VEL2 = 1.0001*VEL
             IF (VEL2.EQ.0.) VEL2=0.0001
             CALL RESIDUAL(VEL2,AOA,FREQ,QLIT,RES2)
          ENDIF
C
C         Calculate numeric derivatives from trial angle of attack/velocity
C         AOA2/VEL2 and associated residuals RES2.
C
          K1 = NMODES+BEN_TOR
          DO 40 I2 = 1,NMODES
          DO 40 J2 = 1,MAX
             K2 = NMODES*(J2-1)+I2
             IF (VLINES) DRDQ(K2,K1)=(RES2(K2)-RES(K2))/(AOA2-AOA)
             IF (.NOT.VLINES) DRDQ(K2,K1)=(RES2(K2)-RES(K2))/(VEL2**2-VEL**2)
40        CONTINUE
C
C         Increment trial frequency by 0.01% and calculate new residuals.
C
          FREQ2 = 1.0001*FREQ
          IF (FREQ2.EQ.0.) FREQ2=0.0001
          CALL RESIDUAL(VEL,AOA,FREQ2,QLIT,RES2)
C
C         Calculate numeric derivatives from trial frequency FREQ2 and
C         associated residuals RES2.
C
          K1 = 2*NMODES+BEN_TOR
          DO 50 I2 = 1,NMODES
          DO 50 J2 = 1,MAX
             K2 = NMODES*(J2-1)+I2
             DRDQ(K2,K1)=(RES2(K2)-RES(K2))/(FREQ2-FREQ)
50        CONTINUE
C
          RETURN
          END
```

Photo courtesy Christopher J. Andrews

BIOGRAPHY

The author, Peter Dunn, is a native of Canada and was born in Montréal, Québec. He currently resides in Toronto, Ontario. He attended Grades 1 through 13 at the Toronto French School, and is fluent in both French and English, with a smattering of Russian and Latin. He attended the Massachusetts Institute of Technology as an undergraduate, completing Bachelors of Science in Aeronautics & Astronautics and in Applied Mathematics in 1985. During his years as an undergraduate he worked as teaching assistant for the Aero-Astro Department's Unified Engineering class. Upon graduation he was awarded the Henry Webb Salisbury award from the MIT Aero-Astro Department.